The American Mineralogist

Journal of the Mineralogical Society of America

VOL. 43 NOVEMBER–DECEMBER 1958 Nos. 11 and 12

Contents

System $CaO-Al_2O_3-SiO_2-H_2O$ IV; phase equilibria in the high-lime portion of the system $CaO-SiO_2-H_2O$ . . . . D. M. Roy 1009
Isogyres in interference figures . . . . W. Barclay Kamb 1029
Sassolite from the Kramer borate district, California . . . . G. L. Smith, H. Almond and D. L. Sawyer 1068
Differential thermal analysis of pyrite and marcasite . . . . O. C. Kopp and P. F. Kerr 1079
Eskolaite, a new chromium mineral . . . . O. Kouvo and Y. Vuorelainen 1098
Ajoite, a new hydrous aluminum copper silicate . . . . W. T. Schaller and A. C. Vlisidis 1107
Copper vermiculites from northern Rhodesia . . . . W. A. Bassett 1112
Heinrichite and metaheinrichite, hydrated barium uranyl arsenate minerals . . . . E. B. Gross, A. S. Corey, R. S. Mitchell and K. Walenta 1134
First known occurrence of inyoite in a playa, at Laguna Salinas, Peru . . . . Siegfried Muessig 1144
Phosphate minerals of the Borborema pegmatites: II—Boqueirão . . . . J. Murdoch 1148
Mineralogical applications of electron diffraction . . M. Ross and C. L. Christ 1157
Optical properties of heated plagioclases . . . . J. R. Smith 1179
Synthetic cuspidine . . . . A. Van Valkenburg and G. F. Rynders 1195
Notes and News: Eskolaite in "merumite" from British Guiana . . . . C. Milton and E. C. T. Chao 1203
New occurrences of sassolite in the United States . . . . R. L. Smith 1204

(Continued on Cover 2)

UNIVERSITY OF ILLINOIS
LIBRARY
JAN 19 1959
CHICAGO

EDITOR: LEWIS S. RAMSDELL
BOARD OF ASSOCIATE EDITORS:
CHARLES L. CHRIST
ROBERT GARRELS
D. JEROME FISHER
E. WM. HEINRICH (1957–58)
JOSEPH MURDOCH (1957–59)
GEORGE T. FAUST (1958–60)

Published bi-monthly by the Society

(*Contents continued*)

Natrojarosite from near the Montana-Wyoming line .... R. S. Mitchell and W. F. Giannini 1205
X-ray data for dolomite and ankerite .... R. A. Howie and F. M. Broadhurst 1210
Book Reviews 1217
New Mineral Names 1219
Index to volume 43; Title Page; Table of Contents 1226

Mineralogical Society of America

ASSOCIATED WITH THE GEOLOGICAL SOCIETY OF AMERICA

President: George E. Goodspeed, University of Washington, Seattle 5, Washington.
Vice-President: Ralph E. Grim, University of Illinois, Urbana, Illinois.
Secretary: C. S. Hurlbut, Jr., Harvard University, Cambridge 38, Massachusetts.
Treasurer: Marjorie Hooker, U. S. Geological Survey, Washington 25, D. C.
Editor: Lewis S. Ramsdell, University of Michigan, Ann Arbor, Michigan.
Councilors: Leonard G. Berry, Queen's University, Kingston, Ontario, Canada.
Chester B. Slawson, University of Michigan, Ann Arbor, Michigan.
Alfred O. Woodford, Pomona College, Claremont, California.
Samuel S. Goldich, University of Minnesota, Minneapolis 14, Minnesota.
Brian H. Mason, American Museum of Natural History, New York 24, New York.
Richard H. Jahns, California Institute of Technology, Pasadena, California.
Charles Milton, U. S. Geological Survey, Washington 25, D. C.
D. Jerome Fisher, University of Chicago, Chicago 37, Illinois.

The enlarged issues of this journal for 1958 are made possible by a grant from the Penrose Fund of the Geological Society of America.

The American Mineralogist—Journal of the Mineralogical Society of America

The journal, containing articles on mineralogy, crystallography, and allied sciences, is issued every two months. Contributions are invited.

The general conduct of the journal is in the hands of the editor, Lewis S. Ramsdell, Department of Mineralogy, University of Michigan, to whom all manuscripts should be submitted. To assist the editor, the Council of the Society has appointed the following Board of Associate Editors:

Charles L. Christ, U. S. Geological Survey, Washington 25, D. C.
E. Wm. Heinrich, Department of Mineralogy, University of Michigan, Ann Arbor, Michigan.
Robert M. Garrels, Harvard University, Cambridge 38, Massachusetts.
Joseph Murdoch, University of California at Los Angeles, Los Angeles, California.
D. Jerome Fisher, University of Chicago, Chicago 37, Illinois..
George T. Faust, U. S. Geological Survey, Washington 25, D. C.

Authors are requested to submit two copies of each manuscript, typewritten on standard size paper, 8½×11 inches. Photographs submitted for cuts should be glossy prints.

Beginning with Vol. 43, 1958, authors are entitled to 50 free reprints, without covers, of each article published.

Sent to all members and fellows of the Mineralogical Society of America. Membership dues $4.00 annually, fellowship dues $5.00 annually, which includes receipt of the American Mineralogist and GeoTimes, which is published by the American Geological Institute. Subscriptions for libraries, colleges, institutions, companies and similar organizations $6.00 annually.

Entered as second class matter at the post office at Menasha, Wis., under Act of March 3, 1879. Acceptance for mailing at the special rate of postage provided for in section 1103, Act of Oct. 3, 1917, paragraph 4 section 429 P. L. & R. authorized March 13, 1922.

Notice of change of address, orders, and remittances should be sent to Mineralogical Society of America, Marjorie Hooker, Treasurer, c/o U. S. Geological Survey, Washington 25, D.C.

Printed by the George Banta Company, Inc., Menasha, Wisconsin
Printed in the United States of America

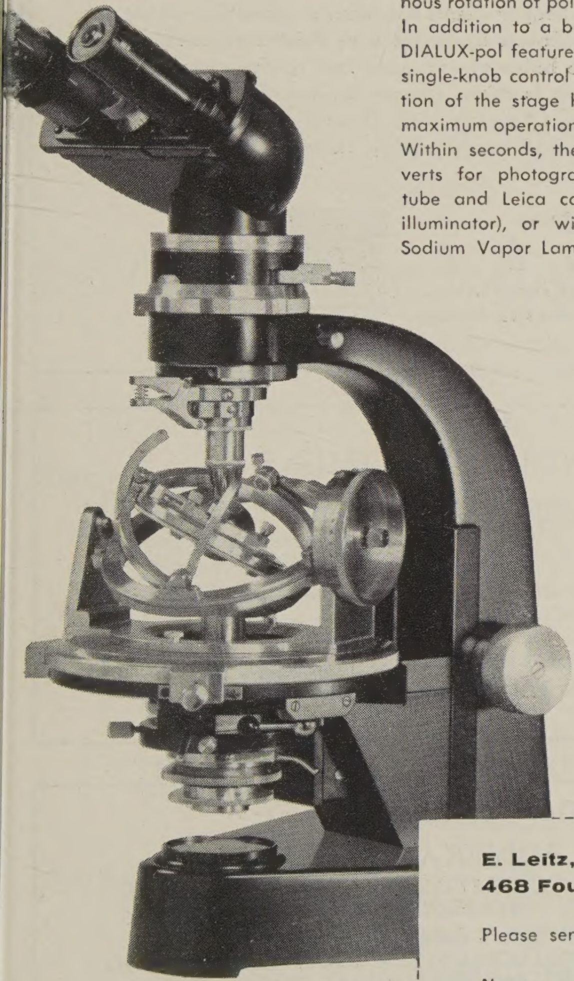Leitz®

SATISFIES THE MOST EXACTING REQUIREMENTS

RESEARCH POLARIZING MICROSCOPE

DIALUX-POL

The new *LEITZ* DIALUX-pol is the most advanced, universal polarizing research microscope ever manufactured. It was designed for the geologist, minerologist, petrographer, paleontologist, and the industrial research microscopist.

The DIALUX-pol maintains the principle of interchangeability, famous with all *LEITZ* precision instruments, so that it is readily used for transmitted light as well as for reflected-polarized light. With the simple addition of a connecting bar, it provides synchronous rotation of polarizer and analyzer.

In addition to a built-in light source and condenser system, the DIALUX-pol features many other operational advantages: unique single-knob control of both coarse and fine adjustment by alteration of the stage height (and not the tube), thus focusing with maximum operational ease.

Within seconds, the DIALUX-pol, through *LEITZ* accessories, converts for photography (through combined monocular-binocular tube and Leica camera), for ore microscopy (through vertical illuminator), or will accommodate the *LEITZ* Universal Stage, Sodium Vapor Lamp, and other facilities.

- monocular or binocular vision
- combination tube FS for photography
- synchronous polarizer-analyzer rotation upon request
- dual coarse and fine focusing
- built-in light source; 6-volt, 2.5-amp, variable intensity
- vertical illumination for ore microscopy
- polarizing filters or calcite prisms
- adaptable to all universal stage methods

Send for the DIALUX-pol information bulletin—then see and examine this fine instrument for yourself.

E. Leitz, Inc., Department AM-12
468 Fourth Ave., New York 16, N. Y.

Please send me the *LEITZ* DIALUX-pol brochure.

Name ____________________

Street ____________________

City ____________ Zone ______ State ______

25158

E. LEITZ, INC., 468 FOURTH AVENUE, NEW YORK 16, N. Y.
Distributors of the world-famous products of
Ernst Leitz G. m. b. H., Wetzlar, Germany—Ernst Leitz Canada Ltd.
LEICA CAMERAS · LENSES · MICROSCOPES · BINOCULARS

New American

PEAT AND MARL SAMPLER

The instrument embodies the essential features of a design by Professor Davis of the Geographical Survey. It consists of a jacketed plunger with a sharpened end. As the instrument is pressed into the ground, it remains closed. When the proper depth has been reached for taking the sample, the instrument is drawn up about 6 or 8 inches; at this point an internal locking device holds the plunger fast in the upper part of the jacket. This instrument is again forced downward, cutting and retaining the desired sample. Complete with illustrated head, 9 four foot lengths of extension rod and case; catalog number 76-432 sells for $80.00.

Eberbach SCIENTIFIC INSTRUMENTS & APPARATUS CORPORATION
ANN ARBOR, MICH. ESTABLISHED 1843

MINERAL SPECIMENS

Large variety of crystals, crystal groups, rare minerals, and ore minerals for collectors, universities and museums.

1958 Mineral Catalog 25¢, or sent free when requested on official letterhead.

Filer's are interested in buying or exchanging for good quality minerals, especially from foreign countries. Correspondence is invited.

FILER'S
P. O. Box 372, Redlands, California

Our Specialty is

SELECTED MINERAL SPECIMENS
FROM WORLD-WIDE LOCALITIES FOR COLLECTORS AND MUSEUMS

we also carry a complete line of
MINERALIGHTS, DETECTRON GEIGER COUNTERS, ESTWING PROSPECTOR PICKS, MINERALOGICAL BOOKS, ETC.

Send for free current bulletin

SCHORTMANN'S MINERALS
6 McKinley Avenue Easthampton, Massachusetts

For Mineralogists:

Index of Refraction Liquids

Range: 1.35 to 2.11 index; available in sets of limited range, or in sets with various intervals, or in any selection. Note that liquids 2.01 to 2.11 are now available.

See detailed price list of index liquids in our three-page advertisement in the July-August and September-October issues of the American Mineralogist. Or, write for Price List Nd-AM

Allen Reference Sets for Microscopical Studies in Mineralogy and Petrology

Six sets of Authentic materials for use as standards for refractive index, for standard materials mounted in balsam to be compared with unknowns, and for demonstration of typical optical characteristics under microscopical study.

Write for descriptive material A-AM

Text: Practical Refractometry by Means of the Microscope

By ROY M. ALLEN, D.SC.

Describes the technique of the immersion method of microscopy, with particular reference to the identification of minerals. Written primarily for elementary instruction, but this text will be very useful also to advanced workers. Price $1.00. Copy will be sent on approval.

Heavy Liquids

Formulated especially for determination of specific gravity of minerals, but special formulations are being made to order for various procedures. If you have any special problem in this field of separation of minerals or other materials by differences in specific gravity, please write us about your problem. Or, just write for leaflet HL-AM.

Lovins Field Finder

For re-locating any point of interest on microscope slide. Same size as a 3″ x 1″ microscope slide; has 1012 1mm. squares, each square numbered and lettered, with sides graduated into tenths. A beautiful example of micro-photography.

Write for Leaflet LFF-AM

Gems, Testing For Identity and For Defects

The CARGILLE-ALLEN GEM TESTING SET is the title of our new book describing the properties of gems and also the equipment for certain identification of gems by a new simple procedure. Price $1.00; this amount applicable to purchase price of any of the items listed in the book.

R. P. Cargille Laboratories, Inc.
117 Liberty St., New York 6, N.Y.

SCOTT J. WILLIAMS
Mineralogist
offers
NEW MINERAL CATALOG 25¢
Specializing in Specimens for
Collections, Museums, Research and Teaching Purposes
Specimens for Sale or Exchange
2346 S. Scottsdale Road Scottsdale, Arizona, U.S.A.

ULTRA VIOLET LAMPS FOR QUALITY FLUORESCENCE

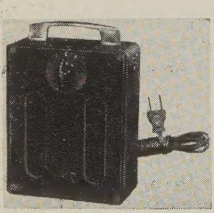

"Most powerful small lamps available"—Dr. H. C. Dake.
For the mineralogist, laboratory or school.
Compact—Rugged—Versatile
7 models available, priced from $14.50
(Model SL-1, combination sw-lw dual unit, illustrated, only $47.50) Write for brochure.
Radiant Ultra Violet Products-Manufacturers
Cambria Heights 11, L.I., New York

d. m. organist
PETROGRAPHIC
LABORATORY
BOX 176 • NEWARK, DELAWARE

THIN SECTIONS OF
ROCKS, MINERALS, ORES, CERAMICS
PREPARED ROCK SECTIONS FOR STUDENT USE
GRAIN COUNTS • PETROGRAPHIC ANALYSIS

THE AMERICAN MINERALOGIST

JOURNAL OF THE MINERALOGICAL SOCIETY OF AMERICA

Vol. 43 NOVEMBER-DECEMBER 1958 Nos. 11 and 12

STUDIES IN THE SYSTEM $CaO-Al_2O_3-SiO_2-H_2O$ IV; PHASE EQUILIBRIA IN THE HIGH-LIME PORTION OF THE SYSTEM $CaO-SiO_2-H_2O$*

Della M. Roy, *The Pennsylvania State University*
University Park, Pennsylvania.

Abstract

Phase equilibria in the high-temperature portion of the system $CaO-SiO_2-H_2O$ were determined by the use of hydrothermal quenching techniques. Three previously unidentified phases, designated X, Y, and Z, having the probable compositions $8CaO \cdot 3SiO_2 \cdot 3H_2O$, $6CaO \cdot 3SiO_2 \cdot H_2O$ and $9CaO \cdot 6SiO_2 \cdot H_2O$ were found to be stable to temperatures above 800° C. at moderate water pressures. *X*-ray diffraction patterns, optical properties and infra-red absorption spectra were obtained, and are diagnostic for the various phases.

The equilibrium temperature for the reaction $C_8S_3H_3$** $=\alpha' Ca_2SiO_4$ (bredigite) $+CaO+H_2O$ increases from 820° C. at 2000 psi to 870° C. at 15,000 psi. The curve for $C_6S_3H=\alpha' Ca_2SiO_4+H_2O$ ranges from 790° C. at 7,500 psi to 810° C. at 15,000 psi; and the reaction $C_9S_6H=$rankinite$+H_2O$ varies from 807° C. at 2000 psi to 820° C. at 15,000 psi. C_3SH_2 is in equilibrium with $X(C_8S_3H_3)+Ca(OH)_2$ at 505° C. at 10,000 psi and 520° C. at 15,000 psi. Afwillite decomposes at about 215° C. at 15,000 psi.

X is apparently a calcium analogue of chondrodite (Taylor, personal communication), and a related phase X* formed from compositions near the C_2S ratio at low pressures may be another member of the chondrodite-type series. Attempts made to synthesize members of the chondrodite series in the $MgO-SiO_2-H_2O$ system for comparison were largely unsuccessful. Possible applications of the results to the study of cement materials and mineral associations are discussed.

Introduction

The stability relationships of phases in the system $CaO-SiO_2-H_2O$ have been important to mineralogists and cement chemists alike for many years; and, while a great deal of the work done in the past has been concerned with equilibria under atmospheric conditions, newer techniques in recent years have made possible more extensive investigations at elevated temperatures and pressures. The present study has been directed toward obtaining information on the stability relations of calcium silicate hydrates under hydrothermal conditions. It was hoped that new data obtained under conditions of higher pressure and temperature at which equilibrium is readily attained would indicate the ultimate direction in which lower temperatures non-equilibrium reactions tend to proceed. The high-lime portion of the system was selected, inasmuch as phase equilibrium data in this region could eventually give information leading to the understanding of the behavior of cement clinker components such as $3CaO \cdot SiO_2$ and $2CaO \cdot SiO_2$ under conditions of hydration, and of the natural hydrous and anhydrous mineral counterparts.

---

* Contribution No. 57-64, College of Mineral Industries, The Pennsylvania State University, presented at the 1956 Annual Meetings of the Mineralogical Society of America, Minneapolis, Minnesota; see Roy (1956_b).

** Throughout the paper the customary cement chemists' abbreviations $C=CaO$, $S=SiO_2$, and $H=H_2O$ are used for the molecular formulae of the compounds.

While the total composition of hydrated cement is high in CaO content, tobermorite (ideally $4CaO \cdot 5SiO_2 \cdot 5H_2O$) or poorly crystallized structurally related hydrates are now believed to form the basis of the binder in concrete and high-temperature insulating materials (Taylor, 1950, 1952; Kalousek, 1954, 1955). A summary of conditions of formation, properties, and apparent stabilities of various lime-silica hydrates has been given by Bogue (1955, Chap. 22), Bernal (1952), Taylor (1952_a), and Kullerud (1953), and a list of properties by Heller and Taylor (1956). It would appear from these data and from the work of Flint, McMurdie and Wells (1938) and of other recent investigators that in the high CaO portion of the system the minerals afwillite, hillebrandite, foshagite, possibly a high-temperature hydrate (such as $C_2SH(D)$) corresponding to the $2CaO:SiO_2$ ratio, and C_3SH_2 would be stable in the "hydrothermal" range. A systematic study should yield more accurate information on the stability limits of these phases.

Buckner and Roy (1955) in their study of the join $CaSiO_3$-H_2O found that tobermorite of the $CaO:SiO_2$ ratio 1:1 was stable as high as 220° C. at 15,000 psi water pressure, and that an intermediate phase was formed for a small interval (40° C.) above this temperature before giving rise to the less hydrous phase xonotlite. Recently the stability relations of dicalcium silicate and related compositions were determined under hydrothermal conditions (Roy, 1958. In press). The present study was directed toward obtaining information on hydrates in the high-lime portion of the system CaO-SiO_2-H_2O and as such is an extension of the previous study to lower temperatures. Of particular interest was the determination of the upper stability limits of hydrated phases where they are in equilibrium with anhydrous compounds such as rankinite, larnite or bredigite.

A composition diagram of a portion of the ternary system on which are plotted most of the well established phases is given in Fig. 1, and naturally occurring minerals are given by name. Cross-hatched lines are drawn to suggest solid solution; the variation in H_2O content and $CaO:SiO_2$ ratio in the tobermorite series is described in detail by Taylor (1950, 1952_a, 1952_b). Compositions from $3CaO \cdot 2SiO_2$ to $3CaO \cdot SiO_2$ were in-

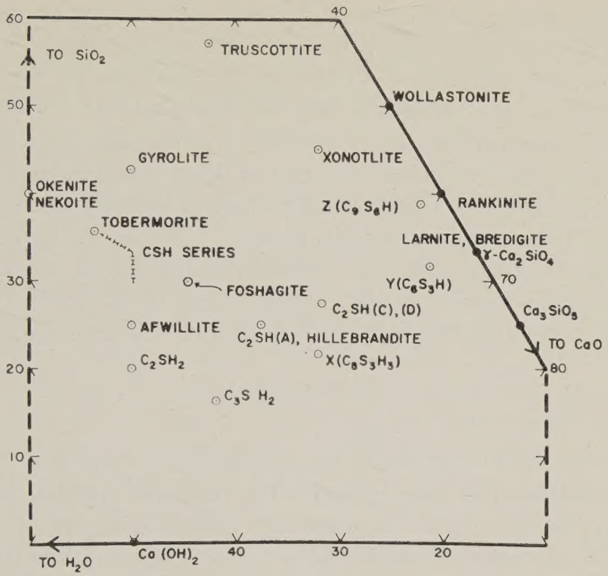

FIG. 1. A portion of the composition diagram for the ternary system CaO-SiO_2-H_2O. Established phases are indicated as well as the new phases X, Y and Z found in the present study; compositions are given in molar ratios $CaO:SiO_2:H_2O$.

vestigated by hydrothermal techniques, using a variety of starting materials.

EXPERIMENTAL METHODS

Equipment Used

The hydrothermal quenching apparatus used was essentially that described by Roy, Roy and Osborn (1950). Samples were held in gold or platinum envelopes or sealed silver, gold or palladium tubes. In order to avoid hydration during initial heating of the pressure vessel, in a number of cases the pressure was introduced after the bomb had reached the desired temperature. Powder x-ray diffraction patterns were obtained on a GE XRD-3 diffractometer and on a Norelco Wide Range diffractometer using filtered Cu radiation. Many samples were examined under the petrographic microscope, and a few infra-red absorption spectra were obtained on a Perkin-Elmer model 21 double beam spectrometer, using on one side a pressed KBr disc "blank" and the other a KBr disc containing about 0.67% of sample.

Starting Materials

The starting materials included natural minerals, mixtures fired to make the anhydrous compounds rankinite, γCa_2SiO_4 and tricalcium silicate; "gels" essentially amorphous to x-ray prepared by the method described by R. Roy (1956); and hydrated phases crystallized hydrothermally from gels, anhydrous compounds or mixtures of SiO_2 gel and $Ca(OH)_2$. The products obtained were not analyzed, but reasonable confidence in the compositions was established by checking the homogeneity of the high-temperature phases obtained on firing the samples. During the hydrothermal quenching runs possible change in composition of the material was checked by comparing the product obtained from an ordinary run in a gold envelope with that obtained under similar conditions in a sealed tube which does not permit transfer of any of the material. No substantial difference could be found in the results with most compositions.

RESULTS

New Phases Synthesized

At least three new compounds were formed in the high-CaO portion of the system at elevated temperatures. The probable compositions of the three phases designated X, Y and Z are indicated in Fig. 1. Proposed formulae of these compounds are based on the composition of the starting material and weight loss on ignition of a small sample at 1400° C after drying at 110° C, inasmuch as insufficient material was synthesized to permit accurate analysis. A small amount of CO_2 was no doubt part of the loss under ignition, particularly in X. The new phases are relatively low in H_2O content, and they were found to be stable to remarkably high temperatures, which is consistent with this observation. An additional needle-shaped phase was formed at temperatures around 700° C at high pressures, but insufficient data have been obtained to fully describe this phase and its stability limits at the present time. Refractive indices are: $n_\gamma = 1.612$, $n_\alpha = 1.598$; extinction parallel or very nearly so, +elongation. Principal x-ray diffraction lines are: 7.4w, 3.68mw, 3.28s, 2.89vs, 2.58vw, 2.318vw, 2.027mw, 1.622vw.

Optical Properties

X phase ($C_8S_3H_3$) occurs generally as low birefringent crystals with poorly developed crystal faces. Very low birefringent crystal sections have an olivine-like shape with, however, inclined extinction of about 18°, negative elongation. Refractive indices are: $n_\gamma = 1.636$, $n_\alpha = 1.630$; interference figure is probably biaxial positive with a very small 2V. Y phase (C_6S_3H) occurs as moderately low birefringent plates or prisms with $n_\alpha = 1.650$, $n_\beta = 1.661$, $n_\gamma = 1.664$, biaxial negative, 2V smaller than 30°, negative elongation with extinction angle 15°. The symmetry is apparently not higher than monoclinic. The optical properties easily distinguish this phase from β and γ Ca_2Sio_4. Z phase (C_9S_6H) is difficult to distinguish optically from rankinite, having approximately the same index of refraction ($n_\gamma = 1.654$ and $n_\alpha = 1.649$), and the crystals are seldom well enough formed to enable accurate determination of the indices. However, it is easily identified by its x-ray diffraction pattern.

X-ray Diffraction Data

X-ray diffraction patterns for the phases X, Y, and Z are given in Table I. These were obtained on a Norelco wide range diffractometer using filtered Cu radiation. The patterns are diagnostic for each of the phases and are easily distinguished from those of the established lime-silica hydrates. Certain reflections of the X-phase are also characteristic of calcite, and the latter phase frequently occurs as impurity in high-CaO products; however, the pattern of X is sufficiently complex to distinguish it from a mixture of calcite and another lime silicate phase. Taylor (personal communication, 1958) has recently synthesized a phase of apparent composition C_5S_2H, the properties of which agree well with those of X. This will be discussed further in a later section. Dent and Taylor in dehydration studies of afwillite have also encountered a poorly crystallized phase similar to Z (Dent, 1957).

Infra-red Spectra

Infra-red absorption spectra obtained for the compounds X, Y, and Z previously dried at 110° C. are given in Fig. 2. The spectrum of Y-phase is distinct from those of β and γCa_2SiO_4 (see Roy, 1958) having two very small absorption bands present in the $OH\text{-}H_2O$ region, at 2.81 and 2.91 microns, which is consistent with the minor H_2O content in the proposed formula $3Ca_2SiO_4 \cdot H_2O$. Z-phase showed even smaller absorption maxima at 2.82 and 2.91 microns, in agreement with the proposed formula $3Ca_3Si_2O_7 \cdot H_2O$. The spectra of Z and Y are rather complex at longer wave lengths, and no interpretations are made of these, except that they do demonstrate the unique character of each phase. X-Phase ($8CaO \cdot 3SiO_2 \cdot 3H_2O$), in contrast to Y and Z, showed a greater intensity of absorption at 2.82 and 2.90 microns. Possible absorption due to $CO_3^{=}$ is present at 6.9 microns, but this is probably the spectrum of calcite, which is frequently present as impurity in high-lime mixtures, and which was identified optically in a small quantity in the particular sample used for the spectrum. It cannot be maintained that CO_2 is essential to the formation of X-phase, inasmuch as the compound forms from anhydrous Ca_3SiO_5 (heated to 1400° C.) as well as from gels formed at lower temperatures which would be more likely to contain adsorbed CO_2.

Other Phases Present

Crystals of C_3SH_2 were well-formed needles or laths, the optical properties and x-ray diffraction pattern agreeing with those reported by Mc-

Table 1. Powder X Ray Diffraction Data on New Calcium Silicate Hydrates*

$X(C_8S_3H_3)$ No. 940		$Y(C_6S_3H)$ No. 509		$Z(C_9S_6H)$ No. 948		$CaCO_3$** Calcite		$Ca(OH)_2$***	
d(Å)	I/I_0	d(Å)	I/I_0	d(Å)	I/I_0	d(Å)	I/I_0	d(Å)	I/I_0
8.45	.25			5.10	.2				
		6.90	.25	4.76	.1			4.90	.74
5.435	.7			4.18	.1				
4.351	.2	4.61	.1	3.970	.2				
4.220	.6			3.758	.1	3.86	.12		
4.020	.2	3.435	.7	3.670	.1				
3.832	.45	3.349	.25	3.559	.4				
3.708	.1	3.293	.2						
3.346	.55	3.258	.25						
3.143	.05	3.209	.05						
3.043	.65	3.067	.5	3.057	.75	3.035	1.00	3.112	.23
2.950	.35	2.986	.4						
2.920	.6	2.890	.25	2.883	1.0				
2.815	.25	2.860	.15	2.840	.3	2.845	.03		
2.781	.45	2.823	.35						
2.716	.6	2.736	.10	2.733	.1				
2.582	.25	2.718	.20						
2.561	.35	2.634	.15	2.673	.75			2.628	1.00
2.526	.3	2.594	.02						
2.498	.25	2.556	.25	2.549	.2				
2.481	.1	2.488	.02	2.481	.2	2.495	.14		
2.372	.1	2.473	.02	2.424	.3			2.447	.03
2.326	.1	2.290	1.0	2.350	.15				
2.144	.1	2.270	.05	2.264	.05	2.285	.18		
2.110	.05	2.243	.02						
2.026	.1	2.135	.05			2.095	.18		
1.914	.55	2.002	.10	1.964	.3				
1.901	.25	1.936	.05	1.902	.15	1.927	.05	1.927	.42
1.875	.05					1.913	.17		
1.855	.05					1.875	.17		
1.829	.15			1.833	.3				
1.811	.55							1.796	.36
1.783	.05								
1.727	.05	1.725	.02	1.749	.2				
1.700	.15	1.716	.25						
1.690	1.0			1.692	.1			1.687	.21
1.665	.25	1.635	.02			1.626	.04	1.634	.01
						1.604	.08		
1.558	.1			1.570	.05				
						1.587	.02	1.557	.03
1.461	.05			1.489	.05	1.525	.05		

* Filtered Cu radiation using Norelco Wide Range Diffractometer; spacings considered accurate to ±0.002 A at 3.3 Å.

** Calcite data from H. Swanson and R. Fuyat, Standard X-Ray Diffraction Patterns, Natl. Bur. Stand. Circular 539, Vol. II, 52–53 (1953).

*** $Ca(OH)_2$ data from H. Swanson, E. Tatge, *ibid.*, Vol. I, 59 (1953).

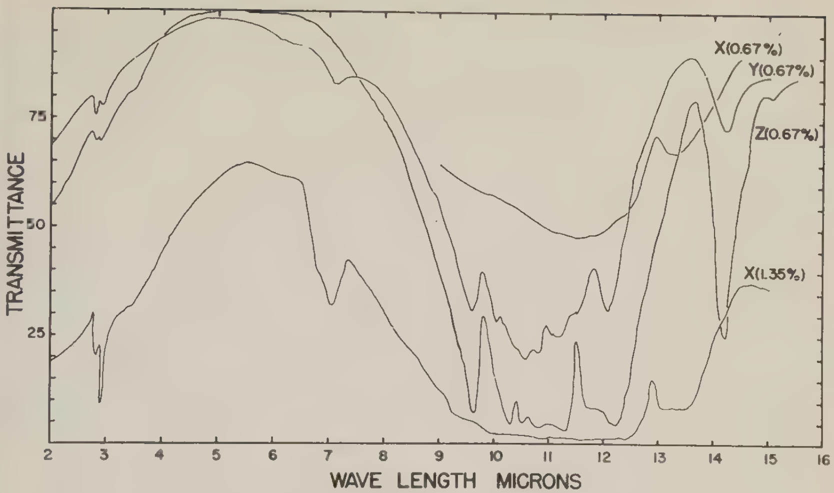

FIG. 2. Infra-red absorption spectra for $X(C_8S_3H_3)$, $Y(C_6S_3H)$ and $Z(C_9S_6H)$ using KBr method.

Murdie and Flint (1943). *X*-ray patterns of γ and βCa_2SiO_4 are consistent with earlier data (Roy, 1956_a). Rankinite crystallized hydrothermally formed small very low birefringent crystals, with $n_\beta = 1.644$. The *x*-ray diffraction patterns of rankinite formed in the present study, both hydrothermally and "dry" at elevated temperatures differ slightly from previous data (Clark, 1946; Heller and Taylor, 1956), and therefore typical patterns of hydrothermal and "dry" rankinite are given in Table II. The comparison between the two is quite good, with, however, some differences in the intensity pattern of the reflections.

Foshagite, although apparently not a stable phase in the composition range studied ($CaO:SiO_2$ ratios of from 3:1 to 3:2) was formed in trial runs in which excess SiO_2 was added to the 3:2 composition, and also in an occasional run of long duration from 3:2 $CaO:SiO_2$ mixture, in which CaO was believed to be leached out, leaving a CaO-poor mixture. Approximate conditions of formation were 450° C., 15,000–30,000 psi, although no attempts were made to define a region of stability. These observations, however, suggest that the formula proposed by Gard and Taylor (1958) having a $CaO:SiO_2$ ratio of 4:3 is more correct than the previous approximation 5:3 (Eakle, 1935).

Hydrothermal Phase Equilibria

Hydrothermal quenching data used to determine the p-T curves of Fig. 3 are summarized in Table III. In all cases more than one type of

TABLE 2. POWDER X-RAY DIFFRACTION DATA ON RANKINITE

Rankinite 1385° 24 hrs.		Rankinite 850°, 20,000 psi 3 days		Rankinite 1385° 24 hrs.		Rankinite 850°, 20,000 psi 3 days	
d(Å)	I/I_0	*d*(Å)	I/I_0	*d*(Å)	I/I_0	*d*(Å)	I/I_0
		6.4	.02	2.281	.1	2.278	.05
		5.62	.1			2.228	.05
5.43	.3	5.44	.2	2.193	.2	2.198	.05
		5.19	.1	2.166	.3	2.167	.2
4.48	.4	4.49	.3	2.134	.1	2.139	.1
4.10	.3	4.09	.15	2.110	.1	2.110	.05
3.84	.4	3.84	.5	2.047	.1	2.039	.05
3.786	.4	3.79	.5	1.998	.1	1.987	.1
		3.58	.15	1.968	.8	1.970	.2
3.382	.2	3.380	.2	1.963	.6	1.964	.1
3.238	.2			1.958	.5	1.958	.05
3.198	.3	3.200	.6	1.922	.8		
3.174	.6	3.177	.7	1.916	.3	1.919 br	.05
3.013	1.0	3.019	1.0			1.886	.05
		2.990	.1	1.864	.1	1.864	.2
2.903	.2	2.906	.6	1.832	.3	1.835	.1
		2.791	.1	1.828	.3	1.828	.05
2.780 br	.3	2.770	.15	1.819	.4	1.820	.2
2.746	.9	2.750	.2	1.800	.05	1.802	.02
2.719	.9	2.718	.8	1.761	.2	1.743	.05
2.714						1.738	.05
2.607	.5	2.609	.1			1.734	.05
		2.594	.3			1.730	.05
2.592		2.580	.3	1.632	.02	1.635	.1
2.578	.5	2.542	.1	1.611	.2	1.611	.05
2.522	.4	2.523 br	.3			1.599	.05
2.508	.1			1.588	.1		
2.366	.1						
2.300	.05						

starting material was used in the hydrothermal runs, to provide a reasonable check on the attainment of equilibrium. For example, for curve IV, when C_3S, $X+Ca(OH)_2$ and crystalline C_3SH_2 all yield the same product it is clear that equilibrium has been attained. It was fairly easy to reverse the equilibria involving C_3SH_2, X, Y, C_2S, and C_3S for curves I, III, and IV (i.e., phases above and below a particular p-T curve could be converted readily to the other assemblage). Rankinite, however, was not readily hydrated, and curve II is based on results from decomposed afwillite and more than one gel. Afwillite was not synthesized sufficiently

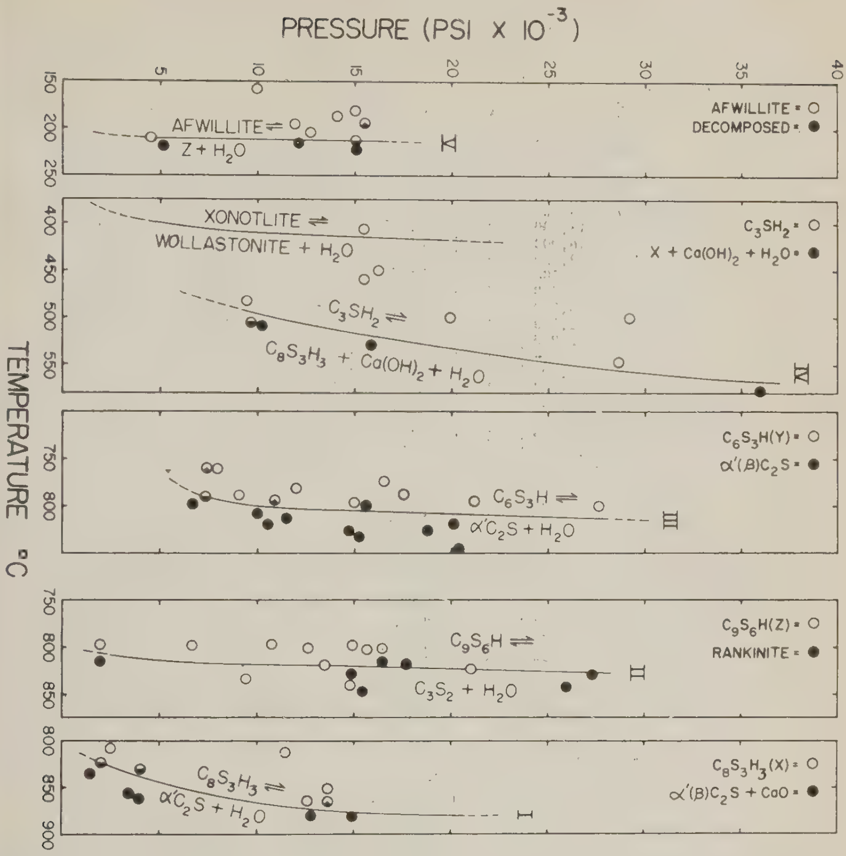

FIG. 3. Pressure-Temperature equilibrium curves for reactions in the system CaO-SiO_2-H_2O. Xonotlite⇌Wollastonite+H_2O is from Buckner and Roy (1955).

free from other phases to enable use as a starting material, so the results for curve V are based on results of the decomposition of two different samples of natural afwillite, which gave closely similar results.

The temperature for the reaction $X = \alpha' Ca_2SiO_4$ (βC_2S on quench) $+ CaO + H_2O$ (curve I) varies from about 820° C. at 2,000 psi to about 875° C. at 15,000 psi. Curve II for Z = rankinite + H_2O does not show a significant variation with pressure, which is not surprising in terms of the low H_2O content of Z, and the optical properties which would suggest not very different densities for Z-phase and rankinite. The best value on the curve seems to be about 820° C. at 15,000 psi. Y-phase is in equilibrium with $\alpha' Ca_2SiO_4 + H_2O$ at 803° C. and 10,000 psi, and 815° C. at 15,000 psi. Attempts made to obtain points at pressures of 30,000 psi or greater

TABLE 3. HYDROTHERMAL QUENCHING DATA FOR THE SYSTEM CaO-SiO_2-H_2O

Composition Mol %		Run No.	Temp. ° C.	Press. psi	Time days	Remarks (Starting Material)	Phases Present
CaO	SiO_2						
						Curve I	
75	25	540	880	15,000	1	CS-15(Xln C_3S)	β C_2S largely
75	25	593	880	12,800	1	CS-15(Xln C_3S)	β C_2S largely
75	25	571	869	13,700	1	CS-15(Xln C_3S)	X phase+β
75	25	568	854	13,700	1	CS-15(Xln C_3S)	X phase largely
75	25	723	761	16,000	1	CS-29(Xln C_3S)	X+l $Ca(OH)_2$
75	25	592	880	12,800	1	CS-19(C_3S gel)	β C_2S 1. CaO
75	25	581	812	11,500	3	CS-19(C_3S gel)	X largely
75	25	541	880	15,000	1	CS-5 (C_3S gel)	β C_2S largely
75	25	572	869	13,700	1	CS-5 (C_3S gel)	X+l β C_2S
75	25	214	807	2,500	1	CS-5 (C_3S gel)	X largely
75	25	227	825	2,000	1	CS-5 (C_3S gel)	β+X+CaO
75	25	222	835	1,500	1	CS-5 (C_3S gel)	β+CaO
75	25	234	832	4,000	1	CS-5 (C_3S gel)	β+X+CaO
75	25	245	857	3,500	1	CS-5 (C_3S gel)	β+l X+CaO
75	25	257	862	4,000	2	CS-5 (C_3S gel)	β+CaO
71	29	594	880	12,800	1	CS-18(C_5S_2 gel)	β C_2S largely
71	29	582	812	11,500	3	CS-18(C_5S_2 gel)	X+β C_2S
						Curve II	
60	40	321	800	2,000	1	gel CS-7	Z phase
60	40	93	815	2,000	5	gel CS-7	Rankinite
60	40	826	799	6,700	1	mixture CS-32	Z
60	40	747	810	16,500	1	mixture CS-32	Z+l Woll
60	40	754	818	16,500	1	mixture CS-32	Rank+l Woll
60	40	1206	799	10,800	1	gel CS-31	Z phase
60	40	937	803	12,700	3	gel CS-31	Z
60	40	934	820	13,600	1	gel CS-31	Z
60	40	1226	833	9,400	1	gel CS-31	Z
60	40	931	834	14,900	1	gel CS-31	Z
60	40	924	845	15,200	3	gel CS-31	Rank
60	40	963	824	21,000	1	gel CS-31	Z
60	40	939	829	27,300	1	gel CS-31	Rank
60	40	943	842	26,000	2	gel CS-31	Rank
60	40	512	800	15,000	8	gel CS-7	Z
60	40	621	803	15,500	1	gel CS-7	Z
60	40	629	820	17,700	1	gel CS-7	Rank
60	40	578	828	14,800	1	gel CS-7	Rank
						Curve III	
67	33	824	760	7,500	1	$Ca(OH)_2$+qtz reacted (CS-33)	Y phase largely
67	33	764	790	7,300	1	$Ca(OH)_2$+qtz reacted (CS-33)	Y largely
67	33	1193	791	9,000	5	CS-17 gel	Y phase
67	33	603	790	17,500	3	CS-17 gel	Y largely
67	33	1209	799	10,800	1	CS-17 gel	Y phase+l β C_2S
67	33	619	803	15,500	1	CS-17 gel	β largely
67	33	1213	805	10,000	1	CS-17 gel	β+l X
67	33	583	812	11,500	3	CS-17 gel	β+l X
67	33	529	685	4,000	13	CS-14 (γ C_2S)	Y largely
67	33	825	760	7,500	1	CS-14 γ C_2S	β C_2S+Y
67	33	763	790	7,300	1	CS-14 γ C_2S	β C_2S+l γ
67	33	828	799	6,700	1	CS-14 γ C_2S	β C_2S
67	33	564	781	12,000	3	CS-14 γ C_2S	Y phase largely
67	33	584	812	11,500	3	CS-14 γ C_2S	Y C_2S+β C_2S
67	33	727	774	16,500	1	CS-14 γ C_2S	Y phase
67	33	638	810	22,500	19	CS-14 γ C_2S	β+l γ?+Y?
67	33	576	828	14,800	1	CS-14(γ C_2S)	β+l γ
67	33	509	800	15,000	8	CS-11(γ C_2S)	Y phase
67	33	496	830	15,000	10	CS-11 (γ C_2S)	β C_2S
67	33	1192	791	9,000	5	1045 (γ C_2S)	Y phase
67	33	1268	799	10,800	1	1045 (γ C_2S)	β C_2S+l Y
67	33	1212	805	10,000	1	1045 (γ C_2S)	β C_2S+l X
67	33	1222	815	10,300	1	1045 (γ C_2S)	β C_2S
67	33	1194	791	9,000	5	865 (Y phase)	Good Y
67	33	955	798	21,200	1	866 (β C_2S)	Y phase
67	33	958	804	27,500	3	866 (β C_2S)	Y phase
67	33	951	815	20,100	1	866 (β C_2S)	β largely

Abbreviations: X = crystalline; $\beta=\beta$ C_2S; Woll = Wollastonite; Rank = rankinite; qtz = quartz; Cc = calcite; l = little; decomp = decomposition.

Where wollastonite was formed it agrees with the pattern of Heller and Taylor (1955) but is undistinguished from para-wollastonite.

TABLE 3 (*Continued*)

Composition Mol %		Run No.	Temp. ° C.	Press. psi	Time days	Remarks (Starting Material)	Phases Present
CaO	SiO_2						
67	33	949	826	18,750	1	866 (β C_2S)	β largely
67	33	946	850	20,400	3	866 (β C_2S)	β C_2S
						Curve IV	
75	25	676	231	12,000	4	C_3SH_2 (No. 666)	C_3SH_2
75	25	702	410	15,500	3	C_3SH_2 (No. 666)	C_3SH_2 largely
75	25	711	454	15,900	3	C_3SH_2 (No. 666)	C_3SH_2 largely
75	25	725	460	15,500	5	C_3SH_2 (No. 666)	$X+C_3SH_2$
75	25	1220	483	9,400	1	C_3SH_2 (No. 666)	$C_3SH_2+X+Ca(OH)_2$
75	25	1197	500	29,200	1	C_3SH_2 (No. 666)	C_3SH_2+l X
75	25	1189	504	20,000	1	C_3SH_2 (No. 666)	C_3SH_2+X+l $Ca(OH)_2$
75	25	1225	507	9,800	1	C_3SH_2 (No. 666)	C_3SH_2+some X+CC+$Ca(OH)_2$
75	25	700	525	15,900	1	C_3SH_2 (No. 666)	X largely+$Ca(OH)_2$
75	25	1186	580	36,000	1	C_3SH_2 (No. 666)	X+l calcite+l $Ca(OH)_2$
75	25	1230	507	10,000	2	C_3SH_2 (No. 666)	X+Cc+$Ca(OH)_2$
75	25	712	454	15,900	3	$X+Ca(OH)_2$(CS-35)	$X+C_3SH_2$+some $Ca(OH)_2$
75	25	1219	483	9,400	1	$X+Ca(OH)_2$(CS-35)	$X+Ca(OH)_2+C_3SH_2$
75	25	744	485	12,700	5	$X+Ca(OH)_2$(CS-35)	$X+Ca(OH)_2$
75	25	1196	500	29,200	1	$X+Ca(OH)_2$(CS-35)	C_3SH_2+X+l $Ca(OH)_2$
75	25	1188	504	20,000	1	$X+Ca(OH)_2$(CS-35)	$X+C_3SH_2+Ca(OH)_2$
75	25	1224	507	9,800	1	$X+Ca(OH)_2$(CS-35)	$X+Ca(OH)_2$
75	25	1229	507	10,000	2	$X+Ca(OH)_2$(CS-35)	$X+Ca(OH)_2$+l Cc
75	25	1185	580	36,000	1	$X+Ca(OH)_2$(CS-35)	$X+Ca(OH)_2$+l Calcite
75	25	666	204	12,400	4	Ca_3SiO_5 (CS-22)	C_3SH_2
75	25	677	297	1,500	1	Ca_3SiO_5 (CS-22)	C_3SH_2
75	25	682	386	6,400	1	Ca_3SiO_5 (CS-22)	C_3SH_2
75	25	703	410	15,500	3	Ca_3SiO_5 (CS-22)	$C_3SH_2+X+Ca(OH)_2$
75	25	724	460	15,500	5	Ca_3SiO_5 (CS-22)	$C_3SH_2+X+Ca(OH)_2$
75	25	743	485	12,700	5	Ca_3SiO_5 (CS-22)	$X+Ca(OH)_2$
75	25	701	525	15,900	1	Ca_3SiO_5 (CS-22)	$X+Ca(OH)_2$
75	25	1218	483	9,400	1	Ca_3SiO_5 (1044)	$X+Ca(OH)_2$
75	25	1195	500	29,200	1	Ca_3SiO_5 (1044)	C_3SH_2+X
75	25	1187	504	20,000	1	Ca_3SiO_5 (1044)	C_3SH_2+X+l $Ca(OH)_2$
75	25	1223	507	9,800	1	Ca_3SiO_5 (1044)	$X+Ca(OH)_2$
75	25	1228	507	10,000	2	Ca_3SiO_5 (1044)	$X+Ca(OH)_2$
75	25	1184	580	36,000	1	Ca_3SiO_5 (1044)	$X+Ca(OH)_2$+l Calcite
						Curve V	
60	40	850	157	10,000	7	Afwillite-Crestmore	Afwillite
60	40	835	188	15,000	8	Afwillite-Crestmore	Afwillite
60	40	818	190	14,200	1	Afwillite-Crestmore	Afwillite
60	40	814	194	15,200	1	Afwillite-sealed tube	Decomp; Z beginning?
60	40	797	218	15,000	5	Afwillite-sealed tube	Partly decomp
60	40	771	291	11,500	1	Afwillite-sealed tube	Z phase largely
60	40	627	200	12,000	1	Afwillite-Megaw	Afwillite
60	40	669	204	12,400	4	Afwillite-Megaw	Afwillite
60	40	647	215	12,200	15	Afwillite-Megaw	Decomp
60	40	656	214	15,000	1	Afwillite-Megaw	Some decomp?
60	40	635	212	12,000	1	Afwillite-Megaw	Some decomp?
60	40	643	211	4,500	1	Afwillite-Megaw	Afwillite
60	40	663	219	5,100	4	Afwillite-Megaw	Decomp

were beyond the practical limit of the apparatus at such high temperatures except for short runs. However, it was doubtful that equilibrium was attained under such conditions, inasmuch as the results thereby obtained were not consistent.

C_3SH_2 was in equilibrium with $X+Ca(OH)_2$ (curve IV) at temperatures ranging from about 505° C. at 10,000 psi to 520° C. at 15,000 psi to 570° C. at 30,000 psi. The reaction was fairly easily reversible, although there was some indication of persistence of C_3SH_2 above the curve in short runs. C_3SH_2 was formed as low as 200° C. in the present study. The curve for the equilibrium xonotlite = wollastonite + H_2O is taken from Buckner and Roy (1955). Curve V was obtained using two samples of afwillite,* one from Scawt Hill and the other from Crestmore. Both samples gave closely comparable decomposition temperatures, about 210° C. at 15,000 psi. The decomposition product just above the curve was difficult to identify, but at about 300° C. or higher the decomposition product compared well with the Z-phase which is formed from gels at temperatures up to 830° C.

DISCUSSION

Stability of X-phase and Variability in Composition

The phase designated X (suggested composition: $8CaO \cdot 3SiO_2 \cdot 3H_2O$) formed throughout a wide range of conditions of temperature and pressure (see Table IV). Since in most of the runs at lower temperatures anhydrous C_3S was used as the starting material, X was formed from these runs (in equilibrium with $Ca(OH)_2$) only above the upper stability limits of C_3SH_2. It is possible that $C_8S_3H_3$ from its own composition would be stable to much lower temperatures.

X is a well crystallized phase, and was mentioned earlier (along with the synthesis of Y and Z) in connection with studies on dicalcium silicate (Roy, $1956_{a,b}$ and 1958.). No difference in the spacings nor the intensity pattern of the reflections was observed at high temperatures where it was in equilibrium with $\alpha' Ca_2SiO_4$ (from $C_{2.2}S$ and $C_{2.5}S$ compositions) or CaO (from C_3S compositions). Therefore, at least in the approximate range 700–850° C. the phase X is considered to be a unique well crystallized material showing no measurable solid solution. Taylor (personal communication, 1958) has recently synthesized an essentially identical phase having a structure analogous to chondrodite, which he calls "calciochondrodite," $2Ca_2SiO_4 \cdot Ca(OH)_2$. If a calcium analogue of chondrodite is stable it is reasonable to expect one or more of the homologues norbergite, humite or clinohumite (see W. H. Taylor and J. West, 1928, 1929, for structures of chondrodite series) to be formed. In the previously mentioned studies a phase resembling X was formed below about 600° C. at low pressures (Roy, $1956_{a,b}$ and 1958) at the expense of γCa_2SiO_4, the olivine structure. (The apparently unrelated phase Y formed alternatively at high pressures.) A comparison of the *x*-ray diffraction pattern of X with a typical pattern of the phase formed from dicalcium silicate, designated X* is given in Table V. Many of the stronger lines of X are present in X*, but a variation in the intensity pattern of the lines is observed, and several lines are absent, notably the 001 and 002 (of "calcio-chondrodite" based on Taylor's indexing). These absences would strongly suggest that X* is another of the "calcio-chondro-

---

* The generosity of Dr. H. Megaw and of Col. C. M. Jenni in contributing the samples from Scawt Hill and Crestmore, is greatefully acknowledged.

TABLE 4. HYDROTHERMAL QUENCHING RUNS DESCRIBING STABILITY OF X PHASE

Run No.	Temp. ° C.	Press. psi	Time days	Phases Present
Ca_3SiO_5 Composition				
540	880	15,000	1	β C_2S largely
571	869	13,700	1	X+some β
222	835	1,500	1	β C_2S+CaO
214	807	2,500	1	X largely
206	775	2,000	1	X+CaO
724	460	15,500	5	C_3SH_2+X+$Ca(OH)_2$
682	386	6,400	1	C_3SH_2
597	290	1,000	2	X+$Ca(OH)_2$
666	204	12,400	4	C_3SH_2
2.5(CaO)(SiO_2) Composition				
582	812	11,500	3	X+l β C_2S
586	772	15,500	6	X+some Y
2.2(CaO)(SiO_2) Composition				
246	857	3,500	1	β C_2S+l CaO
235	832	4,000	1	β C_2S+X
508	800	15,000	8	X+Y
207	775	2,000	1	X+β C_2S
521	630	10,500	8	X+Y
201	665	2,000	3	γ C_2S+X
182	640	20,000	1	X+Y
249	528	2,000	1	X*
514	433	13,500	6	Y+X*?
2(CaO)(SiO_2) Composition				
325	750	20,000	2	Y
334	744	2,000	1	β C_2S
328	670	2,000	3	γ C_2S+some X*
262	650	3,500	1	γ C_2S+some X*
288	640	20,000	3	Y
159	590	3,500	3	γ C_2S+X*
271	490	2,000	2	X*
300	500	20,000	3	Y
466	475	15,000	7	Y
242	472	1,500	1	X*
515	433	14,200	6	Y
294	420	20,000	1	unknown
277	320	1,000	1	X*
598	290	1,000	2	X*

Abbreviations X=X phase ($C_8S_3H_3$)
X*=poorly crystallized phase similar to X, see Table IV
Y=Y phase (C_6S_3H)
C_2S=Ca_2SiO_4, l=little

TABLE 5. COMPARISON OF THE *X*-RAY DIFFRACTION DATA ON THE PHASES X AND X*

X* No. 271 formed from Ca_2SiO_4		X formed from C_8S_3		
d(A°)	I/I$_0$	*d*(A°)	I/I$_0$	*hkl* (Taylor's)
		8.45	.25	001
		5.435	.7	200, 20$\bar{1}$
4.37	.05	4.351	.2	
		4.220	.6	002
4.06	.1	4.020	.2	201, 20$\bar{2}$
3.829	.3	3.832	.45	111
		3.708	.1	210, 21$\bar{1}$
3.349	.2	3.346	.55	331
		3.143	.05	
3.045	1.0	3.043	.65	31$\bar{1}$
2.950	.1	2.950	.35	310
2.917	.15	2.920	.6	202, 20$\bar{3}$
2.840	.2	2.815	.25	40$\bar{1}$
2.784	.1	2.781	.45	31$\bar{2}$
2.698	.2	2.716	.6	400, 40$\bar{2}$
2.629	.05	2.582	.25	311
2.556	.1	2.561	.35	11$\bar{3}$
2.525	.2	2.526	.3	211, 21$\bar{3}$
		2.498	.25	41$\bar{1}$
2.481	.15	2.481	.1	120, 12$\bar{1}$
		2.372	.1	401, 40$\bar{3}$
		2.326	.1	
		2.144	.1	
		2.110	.05	
1.949	.02	2.026	.1	402, 40$\bar{4}$
1.913	.5	1.914	.55	222, 22$\bar{3}$
1.899	.2	1.875	.05	
		1.855	.05	420, 42$\bar{2}$
		1.829	.15	511
		1.811	.55	600, 60$\bar{3}$
		1.783	.05	
		1.727	.05	
		1.700	.15	
1.689	.2	1.690	1.0	(005)
1.667	.2	1.665	.25	
1.556	.1	1.558	.1	
		1.461	.05	

dite" series. Unexplained are absences of *h*00 spacings, although sufficient *hk*0 spacings are present to suggest the same general type of framework. Furthermore, the line 1.689 is present, though diminished in intensity, which would correspond to the interlayer distance between successive oxygen (or hydroxyl) sheets characteristic of the chondrodite type structures containing Ca.

The poorly crystallized nature of this phase (X*) makes tentative the suggestions outlined. There is the problem of reconciling possible formulae with the composition of the starting material $2CaO \cdot SiO_2$; however, the material, being poorly crystallized might contain amorphous SiO_2. It is an additional problem to determine what is the stable phase under these conditions. The phase Y is apparently stable at higher pressures at least as low as 475° C., and X*, though formed reproducibly, may be only metastable.

Chondrodite in the MgO-SiO_2-H_2O System

The stable hydrothermal formation of a calcium analogue of chondrodite was unexpected, inasmuch as chondrodite had never been encountered in the studies of the system MgO-SiO_2-H_2O (Bowen and Tuttle, 1949) or MgO-Al_2O_3-SiO_2-H_2O (Roy and Roy, 1955). Three alternatives would immediately come to mind to explain failure to achieve synthesis of the chondrodite series: (1) F^- is essential to the *stability* (not only formation) of the structures, (2) chondrodite is stable with a deficiency of H_2O in the region where the assemblage serpentine+brucite is stable with excesss H_2O (under the hydrothermal experimentation conditions), or (3) chondrodite is actually only a metastable phase.

Inasmuch as the previous work (Bowen and Tuttle, 1949; Roy and Roy, 1955) only incidentally provided information on stable assemblages involving forsterite, serpentine and brucite, it was decided to make a few more exploratory runs in this region. Gels of the compositions $2.5 MgO \cdot SiO_2$ and $3MgO \cdot SiO_2$ and a sample of natural chondrodite from Orange Co., New York* were used as starting materials. Runs were made in the temperature interval immediately below the decomposition of brucite, roughly 430–650° C. at pressures of from 5,000 to 35,000 psi for periods of time varying from 15 minutes to 10 days.

The results obtained were somewhat inconclusive. Although the shorter runs did not bring about decomposition of chondrodite, in most cases the 001 and 002 spacings were diminished or absent, and other changes in the *x*-ray powder pattern took place, especially reinforcement of the 200 line.

No positive evidence for synthesis of chondrodite (or norbergite) from gels was obtained, and in most cases the final product was a mixture of brucite+forsterite. In some of the shorter runs at low pressures weak lines at ca. 7.4 and 3.72 Å were observed which could possibly correspond to 001 and 002 of chondrodite, but more than likely correspond to 001 and 002 of poorly crystallized serpentine formed during the few minutes of heating up to temperature.

---

* F. A. Genth collection, No. 415.12, College of Mineral Industries, The Pennsylvania State University.

Other Observations on Chondrodite Stability

In view of the failure to achieve synthesis of chondrodite and other members of the homologous series in the system MgO-SiO_2-H_2O, the presence of a stable chondrodite structure in the calcium silicate hydrates was unexpected. The high stability temperature of X (875° C at 15,000 psi) was a further surprise inasmuch as $Ca(OH)_2$ decomposes much lower (about 742° C. at 15,000 psi: Majumdar and Roy, 1956). Natural occurrences of the chondrodite series suggest that the usual mode of formation is alteration of olivine, or retrograde metamorphism where the H_2O pressure would be low, usually associated with limestone. The further alteration of the chondrodite to serpentine is observed, probably at lower temperatures and higher water pressures.

The converse seems to be true in the calcium silicate instance, where the lime olivine γCa_2SiO_4 is stable only below about 675° C. at moderately low pressures (Roy. In press.) and is "up-graded" through the formation of the chondrodite phase Ca^{++} is present in six-fold coordination in γCa_2SiO_4, and apparently in calcio-chondrodite and $Ca(OH)_2$, while the more dense forms of Ca_2SiO_4 in which Ca^{++} is present in a higher coordination state with respect to oxygen are stable above 675° C. The combination of the olivine and $Ca(OH)_2$ layers to form the chondrodite structure apparently enhances the stability of the six-coordinated polyhedra, and the combination structure is stable to a higher temperature than either of the components.

The Role of H_2O in the Structures of the Hydrates

The proposed formula for X-phase, $C_8S_3H_3$ suggests a higher H_2O content than that of Taylor (C_5S_2H). The formula $C_8S_3H_3$ is based on total ignition loss, and it is recognized that a small amount of $CaCO_3$ is present, which may well explain the difference. Infra-red absorption spectra, however, show two maxima in the "water-band" region, and a second type of "water" may be present in addition to the hydroxyls of the $Ca(OH)_2$ layer (Fig. 2).

The infra-red absorption spectra of the phases Y and Z, respectively, show diminishing amounts of "H_2O," and similarly have two separate maxima in this region. The poorly crystallized phase resembling Z obtained by Dent from the decomposition of afwillite (Dent, 1957) appears to be anhydrous; however, this is not surprising, in view of the fact that any number of pseudo-phases may be cited, particularly clays, micas, etc., in which the water has been almost totally removed and yet essentially the same *x*-ray pattern persists. The low H_2O content of Z and similarity in the refractive indices to those of rankinite, suggest not too different densities and probably similar coordination of the calcium ions in the two phases; and the formation of Z-phase seems to be a logical step on the way to the formation of rankinite.

Y-phase appears to be unrelated to any of the known hydrates, and thus far has not been formed at low pressures (below about 5,000 psi). Having relatively high refractive indices, it appears to be more closely related to the structures of the higher temperature polymorphs of Ca_2SiO_4, α' or β; it converts readily to the latter on heating "dry" at temperatures of about 800° C. or higher.

It has been generally accepted that the H_2O content of C_3SH_2 is variable, and no attempt was made in the present study to determine the actual composition—the optical properties and *x*-ray diffraction pattern were sufficient to establish the identity of the phase with the phase previously described by Flint, McMurdie and Wells (1938) and others. No positive evidence was obtained for more than one step in the process of breakdown of the C_3SH_2 structure, i.e., the optical and *x*-ray data were consistent up to the temperature of decomposition. A temperature interval over which the three phases C_3SH_2, X and $Ca(OH)_2$ coexist was found, but this may be the result of leaching out of some CaO to change the total composition. A few runs in sealed tubes in which the total composition of the sample cannot change suggest that this is the explanation. Therefore, the maximum temperature at which C_3SH_2 was formed was taken as the upper stability limit.

The hydrothermal decomposition of afwillite similarly failed to reveal more than one step in the process. The optical properties and *x*-ray diffraction pattern remained those characteristic of well crystallized afwillite up to the temperature of the decomposition curve. The fact that hydrothermal decomposition takes place nearly 100° C. lower than dehydration at atmospheric pressure (about 300° C., Parry and Wright, 1925) is not surprising, inasmuch as the hydrothermal decomposition is believed to be an equilibrium reaction. Dent (1957) has pointed out the fact that during dehydration at atmospheric pressure a steady gradual weight loss is observed, and the weight loss curves are based on extent of dehydration during a "reasonable" length of time.

Natural Occurrences

The apparent formation of the three phases X, Y and Z throughout a wide temperature range was surprising inasmuch as none of the three are known to occur naturally. Four possible explanations for their absence in known calcium silicate localities might be proposed:

1. The deposits are formed at high temperatures above about 800° C.
2. The deposits were formed at high or intermediate temperatures in the absence of sufficient H_2O to give rise to hydrates.
3. Reaction was dominated by CO_2 from limestone, and silicate-carbonates were formed.
4. Reaction to form calcium silicates took place at high temperatures, and later low temperature hydrothermal alteration gave rise to comparatively low temperature hydrates such as afwillite, hillebrandite or perhaps foshagite.

A combination of 2, 3 and 4 appears to be the case at Crestmore (Burnham, 1954). The results of the present study, however, may not be strictly applicable where MgO is a component. Monticellite is stable under water pressure of about 15,000 psi as low as 475° C., and merwinite as low as 625° C., though not as low as 475° C. (Roy, 1956a).

Wollastonite is by far the most common of the anhydrous calcium silicates. Although other factors have also to be considered, wollastonite would be expected to be relatively abundant in contrast to hydrate minerals, from the comparatively low decomposition temperature of the $CaSiO_3$-hydrate stable to highest temperatures, xonotlite—decomposing at about 420° C. at 15,000 psi (Buckner and Roy, 1955).

While tobermorite type structures undoubtedly play the dominant role in the binder of portland cement, it would be worthwhile to examine various poorly crystallized cement materials for the presence of X or Z. These phases are apparently formed stably at low pressures—although probably not at ordinary temperatures, but steam cured or autoclaved materials might provide sufficiently high temperatures. The phase Y formed only at moderate or high pressures and would not be expected under similar conditions as X and Z; and cement phases having the ratios $2CaO \cdot SiO_2$ would be more likely to contain a mixture of X and Z.

ACKNOWLEDGMENT

This study was supported by National Science Foundation Grants, NSF G-1000 and NSF G-4648. The author is grateful to her husband, Dr. Rustum Roy for advice and discussion, and for reading the manuscript.

In the course of preparation of the manuscript, Dr. H. F. W. Taylor visited the laboratories, and Dr. Lesley Dent arrived as a visiting scientist. Comparison of results and discussion with Drs. Taylor and Dent proved to be of considerable mutual benefit.

References

Bernal, J. D. (1952), "The Structures of Cement Hydration Compounds," Proceedings of the Third International Symposium on the Chemistry of Cement. Cement and Concrete Association, 52 Grosvenor Gardens, London, SW1. Paper 9, 216–260.

Bogue, R. H. (1955), "The Chemistry of Portland Cement," Second Edition. Reinhold Publishing Company, 430 Park Avenue, New York, Chapter 22.

Bowen, N. L. and Tuttle, O. F. (1949), "The System MgO-SiO_2-H_2O," *Bull. Geol. Soc. Amer.*, **60**, 439 460.

Buckner, D. A. and Roy R. (1955), "The System $CaSiO_3$-H_2O and the Influence of Sr^{++} in Solid Solution," *Bull. G.S.A.*, **66**, 1536.

Burnham, C. W. (1954), "Geology of Southern California, VII. Mineralogy and Petrology, 7. Contact Metamorphism at Crestmore, California," *Bull.* **170**, Calif. Div. of Mines, San Francisco.

Clark, C. B. (1946), *J. Am. Cer. Soc.*, **29**, 25.

Dent, Lesley (1957), "Crystallographic Studies on the Dehydration of Hydrates of Calcium Silicates and Aluminates," Ph.D. Thesis, University of Aberdeen, Old Aberdeen, Scotland.

Eakle, A. S. (1925), *Am. Mineral.*, **10**, 97.

Flint, E. P., McMurdie, H. W. and Wells, L. S. (1938), "Formation of Hydrated Calcium Silicates at Elevated Temperatures and Pressures," *J. Res. Natl. Bur. Stand.*, **21**, 617–638.

Gard, J. A. and Taylor, H. F. W. (1958), "Foshagite: Composition, Unit Cell and Dehydration," *Am. Mineral.*, **43**, 1–15.

Heller, L. and Taylor, H. F. W. (1951), "Hydrated Calcium Silicates, II. Hydrothermal Reactions of Mixtures of Lime: Silica, Molar Ratio 1:1," *J. Chem. Soc., London*, 2397–2401.

——— (1952a), "Hydrated Calcium Silicates, III. Hydrothermal Reactions of Mixtures of Lime:Silica, Molar Ratio 3:2," *J. Chem. Soc., London*, 1018–1020.

——— (1952b), "Hydrated Calcium Silicates, IV. Hydrothermal Reactions: Lime:Silica, Ratios 2:1 and 3:1," *J. Chem. Soc., London*, 2535–2541.

——— (1956), "Crystallographic Data for the Calcium Silicates," Dept. of Scientific and Industrial Research; Her Majesty's Stationery Office, London.

Kalousek, G. L. (1954), "Studies on Cementitious Phases of Autoclaved Concrete Products Made of Different Raw Materials," *J. Am. Concrete Inst.*, **25**, 365–378.

——— (1955), "Tobermorite and Related Phases in the System CaO-SiO_2-H_2O," *J. Am. Concrete Inst.*, **26**, 989–1011.

Kullerud, G. (1953), "Systemet CaO-SiO_2-H_2O," *Saertrykk Norsk geol. tids.*, **33**, 197–218.

Majumdar, A. J. and Roy R. (1956), "Phase Equilibria in the System CaO-Al_2O_3-SiO_2-H_2O, I. The System CaO-Al_2O_3-H_2O," *J. Am. Ceram. Soc.*, **39**, 434–442.

McMurdie, H. E. and Flint, E. P. (1943), "X-ray Patterns of Hydrated Calcium Silicates," *J. Res. Natl. Bur. Stand.*, **31**, 225–228.

Parry, J. and Wright, F. E. (1925), "Afwillite, a New Hydrous Calcium Silicate from Dutoitspan Mine, Kimberley, South Africa," *Min. Mag.*, **20**, 277–285.

Roy, D. M. and Roy, R. (1955), "Synthesis and Stability of Minerals in the System MgO-Al_2O_3-SiO_2-H_2O," *Am. Mineral.*, **40**, 147–178.

Roy, D. M. (1956a), "Subsolidus Data for the Join Ca_2SiO_4-$CaMgSiO$, and the Stability of Merwinite," *Min. Mag.*, **31**, 188–194.

——— (1956b), "Portion of the System CaO-SiO_2-H_2O," *Bull. G.S.A.*, **67**, 1729 (Abst.).

——— (1958), "Studies in the System CaO-Al_2O_3-SiO_2-H_2O, III. New Data on the Polymorphism of Ca_2SiO_4 and Its Stability in the System $CaO\text{-}SiO_2\text{-}H_2O$," *J. Amer. Ceram. Soc.*, **41**, 293–299.

Roy, R., Roy, D. M. and Osborn, E. F. (1950), "Compositional and Stability Relationships Among the Lithium Aluminosilicates: Eucryptite, Spodumene and Petalite," *J. Am. Ceram. Soc.*, **33**, 152–159.

Roy, R. (1956), "Aids in Hydrothermal Experimentation, II." *J. Amer. Ceram. Soc.*, **39**, 145–146.

Taylor, H. F. W. (1950), "Hydrated Calcium Silicates: I. Compound Formation at Ordinary Temperatures," *J. Chem. Soc.* (*London*), **1950**, 3682–3690.

——— (1952a), "Hydrothermal Reactions in the System $CaO\text{-}SiO_2\text{-}H_2O$," *Proc. International Symposium on Reactivity of Solids*, 677–682.

———, (1952b), "Identification of Cementing Material in a Lightweight Sand-Lime Block," *J. Appl. Chem.* (*London*), **2**, 3–5.

——— and Buckle, E. R. (1958), "A Calcium Analogue of Chondrodite," *Am. Mineral.*, **43**, 818–823.

Taylor, W. H. and West, J. (1928), "Crystal Structure of Chondrodite," *Proc. Roy. Soc.* **A117**, 517.

——— (1929), "Crystal Structure of Norbergite," *Z. Krist.*, **70**, 461.

Manuscript received March 1, 1958.

THE AMERICAN MINERALOGIST, VOL. 43, NOVEMBER-DECEMBER, 1958

ISOGYRES IN INTERFERENCE FIGURES

W. Barclay Kamb, *California Institute of Technology, Pasadena, Calif.**

Abstract

The use of skiodromes in interpreting interference figures of crystal plates leads to both qualitative and quantitative errors, and should be abandoned. The theory of isogyre patterns is correctly developed by considering the effect on isogyre position of "rotation" of the polarization plane by the optical system. Although the amount of the rotation may be 10°–15°, its effect on isogyre position is found to be small because the effects of rotation above and below the crystal plate work in opposite directions. An analysis, based on this conclusion, of the uniaxial flash figure, acute and obtuse bisectrix figures, and optic normal figure leads to isogyre equations from which can be calculated the angle of rotation of the stage (from extinction) required to disperse the isogyres from the field. The formulas are simple and convenient, and are verified experimentally by comparison with values measured upon oriented thin sections. They provide a means of measuring $2V$ in *Bxo* figures and in *Bxa* figures of large $2V$, and in particular a means of distinguishing between *Bxa* and *Bxo* figures. The corresponding formulas given by the skiodrome theory and the theory of Michel-Lévy are not satisfactory. An analysis of the optic axis figure reveals that 45° isogyre curves derived by Wright upon seemingly unsound assumptions are in fact surprisingly accurate. Replacements for the skiodromes currently in use are mentioned.

1. *Introduction*

The theory of interference figures in crystal optics was developed mainly between about 1900 and 1925. Most of the results and methods of this early work have fallen into disuse. In explaining the origin and form of isogyres, recent textbooks (Wahlstrom, 1951; Burri, 1950) make use exclusively of the skiodrome, a device introduced originally by Becke (1904). The skiodrome is, however, an incorrect representation of interference phenomena. It is physically unsatisfactory, and leads to incorrect predictions as to the positions and shapes of isogyres.

With the hope of correcting this situation, the present paper advances a coherent theory of the positions of isogyres in interference figures. The theory is subjected to practical test with the petrographic microscope, and its predictions are compared directly with the predictions of the skiodrome theory and other representations of interference phenomena. As a result of these tests (aside from the reasoning behind the theory) one may conclude that the theory here developed accounts correctly for the positions of isogyres, and that the older theories do not. On the basis of the theory a practical means for distinguishing between *Bxa* and *Bxo* figures can be established, and a method given for measuring $2V$ in figures of either kind.

---

* Division of Geological Sciences, contribution No. 865.

2. History of isogyre theory

A survey of the literature on the isogyre problem reveals three main lines of development: (1) a protracted dispute (1904–1923) between F. Becke and F. E. Wright over the proper method of measuring $2V$ from interference figures; (2) introduction of the skiodrome theory by Becke, and its subsequent interpretation and development by Johannsen, and others; (3) formulation and application of approximate isogyre equations by Michel-Lévy and Wright.

The dispute between Becke and Wright arose from the following question. Suppose that at a given point in the interference field of the conoscope, the direction of vibration (direction of electric displacement $\boldsymbol{D}$) of light reaching the observer's eye is known. What is the direction of $\boldsymbol{D}$ of the corresponding ray of light while traversing the crystal plate under observation? Becke and Wright proposed different constructions (in stereographic projection) for the solution of this problem, and in the years 1904-1925 disputed the correctness of one another's methods (Becke, 1904; Wright 1907; Becke, 1909; Wright, 1911; Kaemerer, 1913; Souza-Brandao, 1914; Wright, 1923). A review of the course of the dispute can be found in Wright's 1923 paper (pp. 807-809). In this paper Wright concluded that the correct construction is unknown, and that there is in general an uncertainty equal roughly to the difference between the Becke and Wright methods in translating the position of isogyres in an interference figure into conditions in the crystal plate that produce the figure. The interpretation of interference figures is, he concluded, inherently approximate at best.

This conclusion was probably responsible for the lack of further development of the theory of interference figures. Discrediting the older "exact" methods of analyzing interference figures, it was probably responsible for the abandonment of these methods and the reliance instead exclusively on the skiodrome theory, a theory developed along lines quite different from those of the "exact" methods, but one which led to convenient diagrams and easily visualized conclusions.

The skiodrome actually had been introduced by Becke in 1904. Whether it was intended as an exact theory or simply a handy tool is difficult to judge from the original article, but in the hands of others it was treated as an exact theory and developed in considerable detail to give isogyre equations for various types of interference figure. A detailed development of the skiodrome theory can be found in Johannsen's textbook (1918, pp. 429–440).

Nowadays the skiodrome theory seems to be used mainly as a device for demonstrating qualitatively to students the origin and general pattern of isogryes. The exact numerical development of the theory seems largely to be disregarded. Neverthless, the emphasis placed on the skiodrome theory suggests that it should provide a more accurate description of isogyres if such a description were needed.

An accurate description was, in fact, required by Michel-Lévy in an early work (1888) in which he proposed a method for determining $2V$ from bisectrix figures. For this purpose he developed an equation for the isogyres in bisectrix figures, by treating the interference phenomena as though they took place in a plane and applying the planar analog of the law of Biot and Fresnel. Wright (1905) rederived his formula but pointed out (1907, p. 341) that it did not seem to give trustworthy results and recommended that it not be used. Nevertheless, he applied the same type of analysis to the optic axis figure, obtaining an equation for the isogyre in the 45° position, from which he calculated the isogyre curves that have been reproduced in almost every optical mineralogy textbook.

Present day teaching and practice in interference figure interpretation are outgrowths of these three unrelated lines of approach to the isogyre problem. In this paper I want to show that the skiodrome theory is patently incorrect and should be discarded. A theory to replace it can be formulated when it is shown that the dispute between Becke and Wright failed to recognize the factors that actually determine the position of isogyres. The application of the new theory to bisectrix and flash figures provides a test of the theory against the predictions of the skiodrome theory and the theory of Michel-Lévy. Finally, the new theory can be applied to the optic axis figure and the result compared, for the 45° position, with the equation and curves given by Wright (1905).

3. *The skiodrome theory*

The skiodrome theory consists of two distinct elements: (1) definition and details of construction of the skiodrome corresponding to a given interference figure; (2) interpretation of the skiodrome in terms of the positions and shapes of isogyres, and justification of this interpretation.

A skiodrome of a given crystal plate is an orthographic projection of curves of constant wave index of refraction ("isotaques") plotted on the surface of a sphere, which may be called the "reference sphere" for the crystal under consideration.* The details of this construction are given in most textbooks.

Interpretation of the skiodrome is based on an analogy with the phenomenon of extinction in orthoscopic light: the isogyres are said to be located at those points in the interference field where the allowed directions of $\boldsymbol{D}$ in the crystal coincide with the directions transmitted by the polarizer or analyzer. If one were to start from this assumption, he would need to determine what direction of $\boldsymbol{D}$ in the crystal plate corresponds to an observed direction of $\boldsymbol{D}$ at a given point in the interference field. This is exactly the question disputed by Becke and Wright. Becke's and Wright's methods of determining $2V$ from the isogyre patterns are based, in fact, on the above assumption and on the separate constructions which the two men proposed as the solution of the resulting problem.

---

* Evans (1907), who first introduced the theory into the English language, called the individual projected isotaques "skiodroms." Nowadays the term "skiodrome" is used confusingly both for the individual curves, and for the entire figures which they compose. I shall use the term only for the entire figure.

The skiodrome theory, however, presents an entirely different solution to the problem, because it asserts in effect that the allowed directions of $\boldsymbol{D}$, as seen in the interference field, correspond to the tangents (and normals?) to the projected equirefringence curves in the skiodrome. This construction leads to predicted directions of $\boldsymbol{D}$ that differ by as much as 90° from the directions given by the Becke or Wright constructions.

It is difficult to see why Becke, who proposed the skiodrome approach to the isogyre problem, should have thereby chosen a method which gives predictions so greatly different from his own "exact" solution of the $\boldsymbol{D}$-direction construction. The only justification for the skiodrome method, as far as I can see, is that the interference phenomena do take place in effect on the focal sphere of the hemispherical objective lens, and this focal sphere, when observed from the distance of the ocular, is for practical purposes projected onto a plane perpendicular to the microscope axis—a fact that is responsible for the validity of Mallard's law. The fact that the focal sphere is observed in orthographic projection does not necessarily mean that the directions of $\boldsymbol{D}$ on the focal sphere are orthographically projected when viewed from the ocular, and I shall in fact show that this is definitely not the case.

Consider the allowed directions $\boldsymbol{D}_1$ and $\boldsymbol{D}_2$ corresponding to a given wave normal direction $\boldsymbol{n}$ in a crystal, shown in stereographic projection in Fig. 1. The pole of the projection is the microscope axis. When the waves 1 and 2, having wave normal $\boldsymbol{n}$ in the crystal, have been refracted by the objective lens so as to travel up the microscope tube their directions of $\boldsymbol{D}$ are now $\boldsymbol{D}_1'$ and $\boldsymbol{D}_2'$, if determined from the Becke construction, or $\boldsymbol{D}_1''$ and $\boldsymbol{D}_2''$, if determined from the Wright construction. In the Becke construction, the directions are rotated about the horizontal axis N until they are horizontal, N being the intersection of plane $\boldsymbol{D}_1\boldsymbol{D}_2$ (which is normal to $\boldsymbol{n}$) with the horizontal plane. (By "horizontal" is meant "parallel to the microscope stage.") Thus $\boldsymbol{D}_1'$ and $\boldsymbol{D}_2'$ lie on the small circles, drawn about N as center, that pass through $\boldsymbol{D}_1$ and $\boldsymbol{D}_2$. In the Wright construction, the "vibration planes" $\boldsymbol{D}_1\boldsymbol{n}$ and $\boldsymbol{D}_2\boldsymbol{n}$ are intersected with the horizontal plane to find the final directions of $\boldsymbol{D}$. Thus

D_1'' and D_2'' lie at the ends of the great circles passing respectively through D_1 and n and through D_2 and n.

The skiodrome construction gives final directions D_1''' and D_2'''. These are derived by orthographic projection of the vectors D_1 and D_2. Since azimuthal directions are the same in orthographic or stereographic projection of a sphere, D_1''' and D_2''' evidently lie at the ends of radii from the pole of the projection, passing respectively through D_1 and D_2.

The geometry of small circles and great circles in stereographic projection requires that D_1' and D_1'' always lie on the same side of D_1''', except in the case that D_1 lies at C or N, in which event the three points D_1', D_1'', and D_1''' coincide. This fact can be justified in detail but is obvious without detailed proof. Hence the skiodrome point D_1''' always lies *outside* the range of directions between D_1' and D_1'', and a similar statement applies to D_2'''. The one certain conclusion from the Becke-Wright controversy is, however, that a correct construction would place the final direction of D between D_1' and D_1'', and between D_2' and D_2''. Thus the skiodrome construction cannot possibly give the correct D directions except for points on the reference sphere where D is either horizontal, or lies in a vertical plane containing n. For all other points the skiodrome construction is wrong.

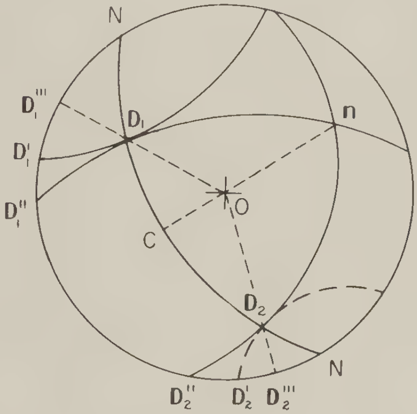

FIG. 1. Stereographic projection to illustrate the Becke, Wright, and Skiodrome constructions for finding the D vector in the interference field from the D vector in the crystal. n is a wave normal in the crystal, and D_1, D_2, the associated directions allowed for D. o is the microscope axis.

This objection is fundamental, but another objection can be raised independently. For all except the centered uniaxial optic axis skiodrome, and at all points on the skiodromes except the center and in some cases points on the edge, the orthographically projected equirefringence curves are not orthogonal, so that the allowed $\boldsymbol{D}$ directions given by the skiodrome are not perpendicular when they reach the interference field of the microscope. The skiodrome theory takes account of this circumstance in a clever but puzzling way. It asserts that there are, in fact, always two isogyres, one in which the projected meridianal equirefringence curves are parallel to the directions of $\boldsymbol{D}$ transmitted either by the polarizer or the analyzer (which we will henceforth regard as NS and EW respectively), called the meridianal isogyre, and one in which the projected equatorial curves are parallel to NS or EW, called the equatorial isogyre. The two isogyres are superposed to form the isogyre actually observed, and since a doubling, even faintly, of the isogyre is never observed, the theory supposes that the two isogyres are broad and overlap to such an extent that the actual isogyre appears simply as a "broad brush" where the two separate significantly, an interpretation that correlates qualitatively with the observed features of isogyres.

Even if a qualitative explanation were adequate for all purposes, the skiodrome theory would have to be discarded, because its predictions are qualitatively wrong for at least one type of figure, the biaxial optic normal figure. The skiodrome for this case predicts that the meridianal and equatorial isogyres should lie in adjacent quadrants of the interference field. As the crystal plate is rotated away from the extinction position, in which the isogyres form a centered cross, the cross should break up into four hyperbolic isogyres which move out into the four quadrants of the field. The meridianal isogyres move into the quadrants into which the acute bisectrix also moves, and the equatorial isogyres move into the other two quadrants. The equatorial isogyres disappear from the field more rapidly than the meridianal isogyres. For $2V=90°$ the stage must still be rotated about 4° before the isogyres (which in this case move out equally fast in all four quadrants) reach the edge of the field.

One need only examine an appropriate thin section, however, to see that the optic normal cross breaks up into only two isogyres, and these move into the quadrants into which the acute bisectrix moves. As $2V$ approaches 90°, the figure becomes less and less distinct, and the isogyres leave more and more rapidly, until for $2V=90°$ the dark field simply vanishes as the stage is rotated from the extinction position, without breaking up clearly into hyperbolic curves at all.

If the skiodrome theory fails qualitatively, its quantitative applications can hardly be of much value. One example had already been given the angle of rotation of the crystal plate required to bring the optic normal isogyres for $2V=90°$ to the edge of the interference field. For a conoscope of numerical aperture 0.85 the calculated angle is about 4°, which is actually close to the observed angle for the isogyres in a uniaxial flash figure. Thus, if the skiodrome theory were correct, optic normal figures for which $2V=90°$ would resemble uniaxial flash figures quite closely, except that there would be four isogyres instead of two.

In most cases it is difficult to propose a quantitative test of the skiodrome theory, because the theory provides no method by which the two types of isogyre should be combined to get the actual isogyre. Such a method cannot be found, because the theory has no physical meaning which would enable one to calculate the amount of light transmitted by the analyzer for a given point in the interference field with a given configuration of projected equirefringence curves. In short, a theory that defies the laws of optics is difficult to interpret quantitatively.

Nevertheless, there is one interference figure that provides a quantitative test of the skiodrome theory, the uniaxial flash figure. The skiodrome for this case shows that there will be no equatorial isogyres, but instead a uniform change in illumination of the field as the crystal plate is rotated. Thus the isogyres in the uniaxial flash figure must be solely the meridianal ones of the skiodrome theory, for which a definite position can be calculated. The calculation (section 6) shows that the predicted isogyres leave the field exactly half as rapidly as actually observed. This is a decisive test and shows definitely that the skiodrome theory is wrong, even when applied only to the inner portion of the interference field.

4. The effect of "rotation," and the "isotropic cross"

Because the effects that produce the "isotropic cross" are important in determining the location of isogyres, it is necessary to discuss them.

Whenever a light wave passes through a refracting surface, a certain fraction of the energy is transmitted and a certain fraction reflected. If the light wave is plane polarized with $\boldsymbol{D}$ in the plane of incidence, a greater fraction of the incident energy is transmitted than if the wave is polarized with $\boldsymbol{D}$ perpendicular to the plane of incidence (i.e., $\boldsymbol{D}$ parallel to the refracting surface).

A plane polarized light wave with $\boldsymbol{D}$ intermediate in orientation between the incident plane and its normal will therefore suffer a greater diminution of the component perpendicular to the incident plane than of the component parallel to the incident plane, in passing through the refracting surface. This relative decrease in the perpendicular component of the $\boldsymbol{D}$ vector is responsible for a "rotation" of the vector away from the orientation that would be calculated by Becke's method.

The amount of this rotation can be calculated from the electromagnetic theory. A different derivation was given by Wright (1923, pp. 796–797), but his method lacks a physical basis. Moreover, there are misstatements and misprints in the derivation and his final result is wrong; it is valid for a wave travelling in the direction opposite to the one assumed in the derivation.

Suppose that the $\boldsymbol{D}$ vector amplitude of the incident plane polarized wave, moving in a medium of index n_i, has components $D_i^{\parallel}$ in the incident plane and component $D_i^{\perp}$ perpendicular thereto. The incident wave normal $\boldsymbol{n}_i$ makes an angle θ_i with the normal to the refacting surface. $\boldsymbol{D}_i$ is of course perpendicular to $\boldsymbol{n}_i$. The refracted wave, in medium of index n_t, then has components

$$D_t^{\parallel} = D_i^{\parallel} \frac{2n_t \cos \theta_i}{\sqrt{n_t^2 - n_i^2 \sin^2 \theta_i} + \dfrac{n_t^2}{n_i} \cos \theta_i}$$

$$D_t^{\perp} = D_i^{\perp} \frac{2n_i \cos \theta_i}{\sqrt{n_t^2 - n_i^2 \sin^2 \theta_i} + n_i \cos \theta_i}.$$

The derivation of these results can be found in works on electromagnetic theory. From these equations, and with the help of Snell's law,

$$n_i \sin \theta_i = n_t \sin \theta_t$$

the value of the ratio $D_t^{\perp}/D_t^{\parallel}$ is found (after some manipulation) to be simply

$$\frac{D_t^{\perp}}{D_{t\parallel}} = \frac{D_i^{\perp}}{D_{t\parallel}} \cos (\theta_i - \theta_t). \tag{1}$$

The decrease in the ratio $D^{\perp}/D^{\parallel}$ is thus independent of the sign of $\theta_i - \theta_t$. The situation is depicted in stereographic projection in Fig. 2. In terms of the angles ν_i and ν_t, (1) can be written

$$\tan \nu_t = \cos (\theta_i - \theta_t) \tan \nu_i, \tag{2}$$

a formula first obtained by Fresnel.

It can be shown that (2) leads to the conclusion that $\boldsymbol{D}_i$ and $\boldsymbol{D}_t$ lie on a great circle through $\boldsymbol{n}_i$, as shown in Fig. 2. This conclusion is the basis for Wright's construction, mentioned previously.

Note that if it were true that $\nu_t = \nu_i$, then $\boldsymbol{D}_i$ and $\boldsymbol{D}_t$ would lie on a small circle centered at N, the normal to the incident plane. This is Becke's construction. Actually $\nu_t < \nu_i$, so that the $\boldsymbol{D}$ vector is "rotated" toward the incident plane by the amount $\delta = \nu_i - \nu_t$.

In an interference figure, the only light that reaches the observer's eye is light that has travelled almost straight up the microscope axis from each point on the interference sphere (focal sphere of the objective lens). Thus, the only light that is seen from a given point P on the interference sphere is light that has been refracted through the optical system in a plane of incidence always containing the microscope axis and P.

At the corresponding point P in the interference figure (Fig. 3), the

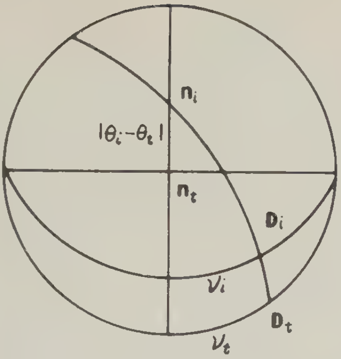

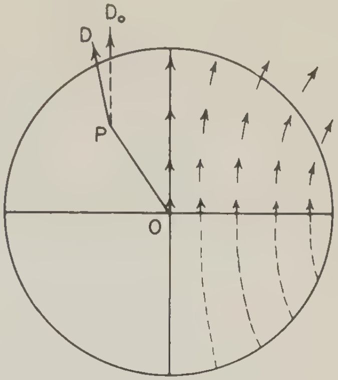

FIG. 2 (left). Stereographic projection to illustrate the "rotation" of the ***D*** vector caused by refraction of plane polarized light. $\boldsymbol{n}_i$ is the incident wave normal, which is refracted to $\boldsymbol{n}_t$. $\boldsymbol{D}_i$ and $\boldsymbol{D}_t$ are the corresponding directions of ***D***. The orientation of the refracting surface is not plotted.

FIG. 3 (right). Pattern of ***D***-vectors in the interference field of the conoscope. The pattern, shown in the NE quadrant, can be extended symmetrically to the rest of the field, as suggested.

light would have ***D***-direction PD_o if ν_t were equal to ν_i at every refraction in the lens system. But in fact the component of PD_o perpendicular to OP is reduced relative to the component parallel to OP, so that the actual direction of ***D*** at P is rotated toward OP (prolonged), to some orientation such as PD. The resulting directions of ***D*** in the interference field form the pattern shown in the NE quadrant of Fig. 3, in which it is assumed that the polarizer is set to transmit ***D*** accurately NS. Such a pattern was described by Wright (1923).

The pattern shown in Fig. 3 is responsible for the isotropic cross, and can be verified by rotating the polarizer (or analyzer) of the microscope. The cross breaks up into two hyperbolic curves. If the ***D*** direction transmitted by the polarizer, which will be called the polarization direction, is rotated into the NW–SE quadrants of the field, the hyperbolae move into the NE and SW quadrants, and vice versa. By rotating the polarizer, the amount of "rotation" δ at any point in the field can be measured. The maximum value for the lens system alone (without any plate inserted between the condenser and objective) is about 6° or 7° for most microscope lens combinations of half-aperture close to 60° (in air).

The isotropic cross described above is produced without birefringence or path differences, as can be tested with the gypsum plate. Johannsen (1918, p. 416), however, refers to the cross as having "weakly uniaxial positive character." In this statement he confuses the above isotropic cross with a second "cross" that can be observed when the microscope is adjusted improperly. The first cross, described above, is observed when the cone of light coming directly from the light source, converged by the condensing system, fills the field of the conoscope, so that the image of the light source, seen in the interference field, fills the entire field. If the microscope tube is then raised, the image of the light source shrinks rapidly. Superposed upon the image of the upper face of the condenser, which does not shrink so rapidly, can be seen a second "cross." It can better be observed by substituting a small bright light source for the usual diffuse one—for example, by removing the blue diffusing plate used in most lamps. A gypsum plate shows that path differences are associated with this cross (in some microscopes). If the cross were interpreted as uniaxial, its sign would be +, as noted by Johannsen. When the polarizer is rotated, the cross of the second kind behaves very differently from the cross of the first kind, as shown in Fig. 4 (row II).

Upon raising the microscope tube further, so that the image of the condenser face shrinks down into the center of the field, a third kind of cross can be observed in the remainder of the field. It can also be seen simply by swinging the movable substage condenser out of the optical train. It has no "uniaxial" character. Upon rotating the polarizer the cross breaks up into a pair of hyperbolae that move slowly out into the same quadrants as the direction of polarization does, as shown in Fig. 4, row III.

The crosses of the second and third kinds are produced by light that has been twice or more *reflected* at lens surfaces in the optical train. If a beam of perfectly parallel light enters the condensing system from below, the light reflected by the lens surfaces from rays that do not travel exactly along the condenser axis forms, after a second reflection that sends the light in a general upward direction again, a broad weak cone of light diverging at all angles from the main light cone. The light in this cone is polarized with $\boldsymbol{D}$ nearly perpendicular to the plane of incidence, because the perpendicular component is preferentially reflected. That portion of the twice reflected light that has been reflected at the polarizing angle will have $\boldsymbol{D}$ exactly perpendicular to the incident plane. The twice (or more) reflected light from the condenser forms the cross of the second kind, and light similarly reflected in the objective forms the cross of the third kind.

A plot of the expected direction of $\boldsymbol{D}$ after *one* reflection is shown in Fig. 5. The plot is qualitative only. Radial distance is angle of incidence plotted stereographically. The solid circle is drawn at the polarizing angle. The polarizer is set NS. To determine the directions of $\boldsymbol{D}$ expected in the multiple reflected light from the actual lens combinations requires a knowledge of the paths of the reflected rays, and hence a detailed knowledge of the lens system design. However, it can be shown rather simply

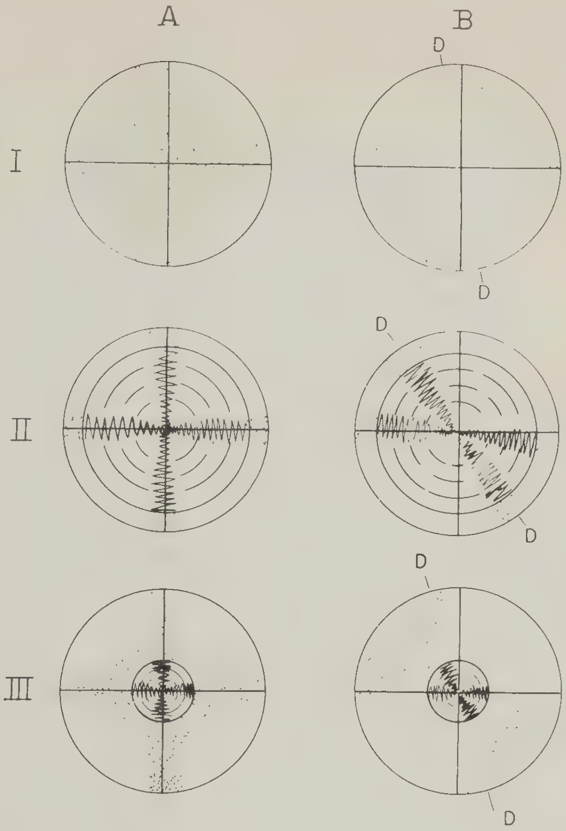

FIG. 4. The three types of "isotropic cross" seen in the conoscope field. Column A shows the centered cross seen when the polarizer is set NS and the analyzer EW. When the polarizer is turned to the position DD, the cross breaks up into the form shown in column B. The circular object within the field in rows II and III is the image of the upper face of the substage condenser.

that the twice reflected light from the objective which appears at a given point in the interference field can have been reflected at an angle of incidence at most equal to the angle, in glass, corresponding to the distance of the given point from the center of the field. At the edge of the field this angle is about 30°, much less than the polarizing angle (56° for $n=1.50$), so that a distribution of vectors roughly similar to that shown inside the solid circle in Fig. 5 may be expected for the cross of the third kind. This conclusion is in agreement with the behavior of the cross upon rotation of the polarizer. Thus, if the analyzer transmits in the direction *AA* in Fig. 5, a dark curve would be expected to follow the heavy dotted line shown.

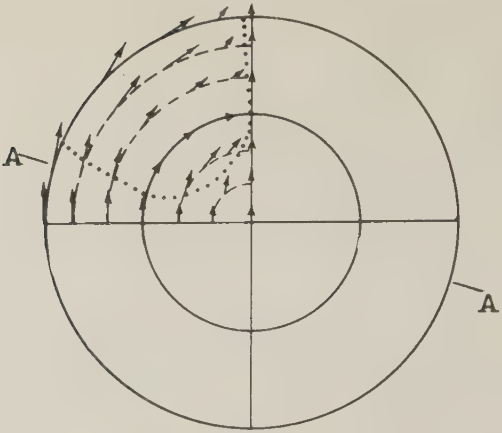

FIG. 5. Direction of ***D*** after one reflection of plane polarized light. The directions are shown as short arrows stereographically projected into the plane of the drawing from their actual position in space. The incident light is polarized in such a way that before reflection all the arrows would have been NS. Radial distance is angle of incidence plotted stereographically. The diagram is qualitative only. The solid inner circle corresponds to the polarizing angle.

The cross of the second kind behaves in a way appropriate to the outer portion of Fig. 5. I do not know the exact reason for this, but it appears that the light must have been reflected several times.*

A more exact analysis of the crosses of the second and third kinds would be interesting, but it is unnecessary for a discussion of interference figures, which are observed in the strong direct beam of light from the light source, to which the discussion leading to Fig. 3 applies. It is reasonable to assume that the weak light responsible for the crosses of the second and third kinds, which are always superposed on the interference field of the direct light, will have a negligible effect on the appearance of the interference figure. This is evident in observing the behavior of the isotropic cross of the first kind, which blots out the other two crosses.

5. *Location of the isogyres*

The isogyres are regions in the interference figure where the light inten-

---

* The path differences exhibited by the cross of the second kind are doubtless due to strain birefringence caused by internal stresses in the lenses of the substage condenser. In all internally stressed lenses that I have examined, the birefringence has radially-slow character, as observed in the cross of the second kind. All Leitz microscopes that I have examined show the presence of these internal stresses. The new Zeiss research and student models, however, have stress-free substage condensers, and the cross of the second kind in these microscopes shows no path differences.

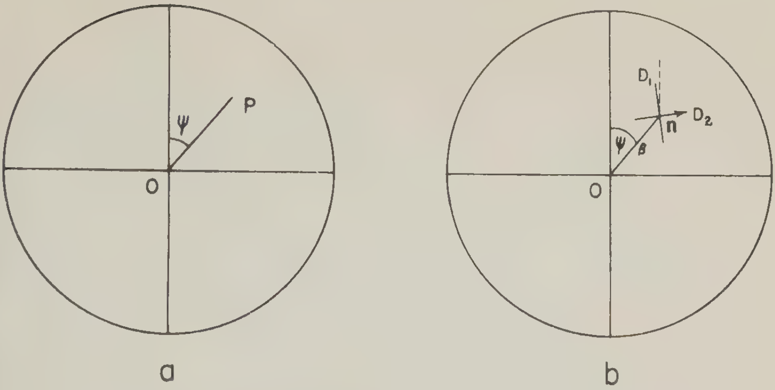

FIG. 6. Diagrams to illustrate the factors that determine isogyre position. 6*a*, orthographic projection; 6*b*, stereographic projection.

sity transmitted by the analyzer is locally a minimum. We therefore ask, for a given point P in the interference field (Fig. 6*a*), what orientation of the allowed directions of $\boldsymbol{D}$ for the corresponding wave normal in the crystal will minimize the light intensity from P transmitted by the analyzer? The allowed directions are shown as a small cross in the stereographic projection of Fig. 6*b*. Note that a stereographic projection of the cross is equivalent to rotating the cross from the reference sphere into the horizontal plane by Becke's construction, that is, about a horizontal axis perpendicular to OP at P.

Figures 7*a* and 7*b* are magnifications of a small region about $\boldsymbol{n}$ and P in Fig. 6*b* and 6*a*. The vector $\boldsymbol{D}$ of the plane polarized light wave that enters the base of the crystal plate is resolved into two components $\boldsymbol{D}_1$ and $\boldsymbol{D}_2$. The birefringence is assumed small enough that $\boldsymbol{D}_1$ and $\boldsymbol{D}_2$ can be considered to lie in the same plane, so that $\boldsymbol{D}_1$ and $\boldsymbol{D}_2$ are perpendicular. The dashed axes lie NS and EW. If there were no "rotation" of the $\boldsymbol{D}$ vector in passing from the polarizer to the crystal plate via the condensing system, $\boldsymbol{D}$ would lie along NS. Instead, it has been rotated an amount δ_1 toward On. ξ defines the orientation of the allowed directions of $\boldsymbol{D}$. At the top of the crystal plate the resolved waves 1 and 2 can be written

$$\begin{aligned} D_1' &= D \cos(\xi + \delta_1) e^{-i\omega t} \\ D_2' &= D \sin(\xi + \delta_1) e^{-i\Phi - i\omega t} \qquad (3) \end{aligned}$$

where a phase shift Φ between the two waves is produced in traversing the crystal plate.

Next the effect of rotation in the remainder of the optical system must be accounted for. We suppose that ξ is small enough that the rotations of the plane polarized waves D_1' and D_2' are the same as for waves with

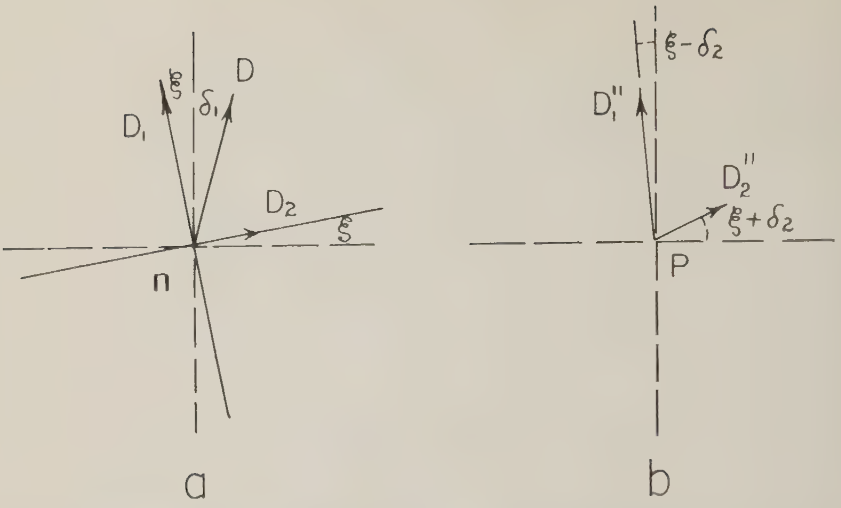

FIG. 7. Enlargements of portions of Fig. 6. 7*a* represents the region around ***n*** in Fig. 6*b*. 7*b* shows the ***D*** vectors in the light that reaches the analyzer from the point *P* in Fig. 6*a*.

$\xi=0$. The condition for this is $\xi \ll \psi$, which we will verify *a posteriori* to be satisfied, because when $\psi \sim 45°$, $\xi \sim 1°$ at most. It will develop later that the amount of rotation for D_1 varies as $\sin 2\psi$, and is therefore equal for ψ and $\pi/2-\psi$, so that D_1' and D_2' are rotated by equal amounts δ_2, both toward the incident plane *On*, as shown in Fig. 7b. It can be shown that if δ_2 is small the two waves are attenuated by nearly the same factor C owing to the energy carried away by the reflected light, so that we can write for the amplitudes D_1'' and D_2'' of the waves that arrive at the analyzer:

$$D_1'' = C\kappa_1 D_1', \qquad D_2'' = C\kappa_2 D_2' \tag{4}$$

where C is a constant factor independent of ξ, κ_1 and κ_2 are functions of ψ and δ_2 and can be shown to be

$$\kappa_1 = 1 - \delta_2 \tan\psi + \cdots, \qquad \kappa_2 = 1 - \delta_2 \cot\psi + \cdots$$

to the first order in δ_2. Note that $\kappa_1=\kappa_2$ for $\psi=\pi/4$. The first order terms $\delta_2 \tan\psi$ and $\delta_2 \cot\psi$ remain small for any value of ψ, because of (10), below.

The amplitude of the wave transmitted by the analyzer (set EW) is

$$D_A = -D_1'' \sin(\xi-\delta_2) + D_2'' \cos(\xi+\delta_2). \tag{5}$$

The intensity I of the light seen at P is obtained by combining (3), (4), and (5):

$$\frac{I}{C^2 I_o} = \frac{|D_A|^2}{C^2 |D|^2} = \kappa_2^2 \sin^2(\xi+\delta_1)\cos^2(\xi+\delta_2) + \kappa_1^2 \cos^2(\xi+\delta_1)\sin^2(\xi-\delta_2)$$
$$- 2\kappa_1\kappa_2 \sin(\xi+\delta_1)\cos(\xi+\delta_1)\ \sin(\xi-\delta_2)\cos(\xi+\delta_2)\cos\Phi \tag{6}$$

where I_o is the intensity of light entering the crystal plate at the bottom.

In keeping with the assumption that ξ, δ_1 and δ_2 are small angles (all less than about 5° in the field of the conoscope), (6) may be expanded to lowest order in powers of these quantities to obtain

$$\frac{I}{C^2I_o} = 2\xi^2 + \delta_1^2 + \delta_2^2 + 2\xi(\delta_1 - \delta_2) - 2[\xi^2 + \delta_1\delta_2 + \xi(\delta_1 - \delta_2)]\cos\Phi. \tag{7}$$

To find the condition that P lie on an isogyre, we minimize (7) with respect to ξ:

$$[2\xi + (\delta_1 - \delta_2)](1 - \cos\Phi) = 0. \tag{8}$$

Φ applies, of course, to a given wavelength of light. Cos Φ is equal to 1 only for certain select wavelengths, so that the term $1-\cos\Phi$ does not in general vanish for white light (for monochromatic light it locates the dark fringes). Thus the isogyre passes through points in the interference field where

$$\xi = \tfrac{1}{2}(\delta_2 - \delta_1). \tag{9}$$

This shows that the effects of rotation in the condenser and objective tend to cancel in determining the position of the isogyre. The protagonists in the Becke-Wright controversy had assumed in effect that $\xi = \delta_2$, evidently a serious error if δ_1 and δ_2 are of roughly the same size. The "correct" construction envisaged by Wright (1923) would have required ξ to be about 6° (about one half δ_{l+p} in Table 1), whereas, as we shall see below, ξ is almost certainly less than 1° in practice.

Note that the condition (9) for location of the isogyre is based on two important assumptions: (1) the birefringence of the crystal plate is small; (2) the variation of C with position in the interference field is not large enough to be significant.

To assess the size of ξ, consider first the application of (2) to the rotation produced in the microscope. If the angles of rotation are small, $\nu \cong \psi$, so that we may write for the rotation δ produced in one reflection

$$\tan(\psi - \delta) = \cos\Delta\theta \tan\psi$$

which when expanded for δ small gives

$$\delta = \sin 2\psi \sin^2\frac{\Delta\theta}{2}\cdot \tag{10}$$

TABLE 1

Series	I	II	III	Average
δ_{l+p}	11.4°	12.5°	11.1°	11.7°
δ_l	6.1	7.5	7.1	6.9
δ_p	5.3	5.0	4.0	4.8

For the complete rotation in the microscope

$$\delta_1 + \delta_2 = \sin 2\psi \sum_i \sin^2 \frac{\Delta\theta_i}{2} \tag{11}$$

where $\Delta\theta_i$ is the change of direction of the ray at the i'th refracting surface.

The applicability of (10) can be tested in the following way. A clean glass slide of known index of refraction is placed on the stage, and the angle of rotation for light in the interference field is measured by rotating the polarizer. In view of (10), the maximum rotation, δ max, occurs at $\psi = 45°$. δ max. is easily measured, because it requires setting the polarizer so that the center of the dark hyperbolic shadow in Fig. 4 (IB) is just tangent to the edge of the interference field. Call the rotation measured in this way δ_{l+p}. The glass slide is then removed and the rotation δ_l due to the lens system alone is measured. The difference $\delta_{l+p} - \delta_l$ is the rotation produced by the plate. Since there are two refractions of amount $\Delta\theta$ in passing through the plate, and since the rotation is measured at $\psi = 45°$, (10) predicts

$$\delta_{l+p} - \delta_l = \delta_p = 2 \sin^2 \frac{\Delta\theta}{2} \tag{12}$$

where

$$\Delta\theta = \left| \theta_i - \theta_r \right| = \theta_m - \sin^{-1} \frac{\sin \theta_m}{n} . \tag{13}$$

θ_m is the half-aperture (in air) of the conoscope, and is a constant for a given objective lens; n is the index of the glass plate.

The results of three series of measurements are shown in Table 1. The objective used is a Leitz achromatic, No. 7 (N.A. 0.85). The glass plate has $n = 1.516$, measured by the immersion method. Each measured δ value given in the table is the average of four or five individual measurements. The scatter of the results indicates the inaccuracy of such measurements. The inaccuracy arises from the diffuseness of the hyperbolic shadow. There seems also to be a personal bias in judging when the center of the shadow is set at the edge of the field, and this bias varies unpredictably from one series of measurements to another. Nevertheless, there is a general consistency in the results, and the average, $\delta_p = 4.8°$, agrees exactly with the value calculated from (12) and (13) with the assumption $\theta_m = 57.6°$, which is the value derived from isogyre measurements (section 7), for the particular objective used. The exact agreement is, of course, fortuitous, but verifies the correctness of (12).

Wright (1923, p. 802) gave a more elaborate series of measurements of the same kind, although he did not explain exactly what he measured, and he described the results rather vaguely as "positions of extinction of different points in the interference field." He did not compare his results with the predictions of a theory of the effect. The position $\psi=45°$, $\theta_m=57.6°$ at which I have measured δ_l corresponds to small circle coordinates $N=36.6°$, $E=36.6°$, as used by Wright; interpolating in his table (1923, p. 802), I find that he measured $\delta_l=6.8°$, which is remarkably close to the average in Table 1.

To estimate ξ note that the effects of rotation due to equal refraction angles $\Delta\theta_i$ above and below the crystal plate under examination cancel, so that rotation produced by refraction at the surfaces of the crystal plate does not affect ξ, nor does the rotation produced by the glass slide and cover glass, if the two have the same index n. Moreover, since the front surface of the front objective lens element is plane, as is also the upper surface of the upper lens of the condenser, the effects of rotation at these two surfaces also cancel if the two lenses have the same index. If this index is about 1.5, the contribution of these surfaces to δ_l is close to δ_p. If there is a difference between δ_1 and δ_2, its maximum value is evidently

$$|\delta_2-\delta_1| \leq \delta_1+\delta_2-\delta_p=\delta_l-\delta_p \cong 2°.$$

Hence ξ is certainly no larger than about 1°, and very likely it is smaller, because it seems obvious that all of the remaining rotation is not produced solely in the objective or solely in the condenser. In section 8 it will be shown that ξ can be measured by means of interference figures, and the conclusion that ξ is less than 1° verified experimentally.

In the theory that follows (except in section 8) I shall assume that $\xi=0$. When a given lens combination produces a significant value of ξ, the resulting effect on the position of the isogyres can be obtained by an obvious extension of the theory developed. For any point in the interference field

$$\xi=\frac{1}{2}(\delta_2-\delta_1)=\frac{1}{2}\sin 2\psi\left\{-\sum_{i=1}^{n_1}\sin^2\frac{\Delta\theta_i}{2}+\sum_{i=n_1+1}^{n_1+n_2}\sin^2\frac{\Delta\theta_i}{2}\right\}. \tag{14}$$

To the first approximation we can write

$$\Delta\theta_i=K_i\theta \tag{15}$$

where θ is the inclination in the crystal plate of the wave normal corresponding to a point P in the interference field with coordinates (θ,ψ). K_i is a constant for the i'th refracting surface. There are n_1 refracting surfaces in the condenser and n_2 in the objective. To the same approximation to which (15) is valid, $\sin^2\Delta\theta_i/2=(\Delta\theta_i/2)^2$ so that (12) becomes

$$\xi=\frac{1}{2}\sin 2\psi\frac{\theta^2}{4}\left[-\sum_{1}^{n_1}K_i^2+\sum_{n_1+1}^{n_1+n_2}K_i^2\right].$$

The distribution of ξ values in the interference field is therefore, to the first approximation in θ,

$$\xi(\theta, \psi) = \xi_m \sin 2\psi \cdot \frac{\theta^2}{\theta_m{}^2} \tag{16}$$

ξ_m is the maximum value of ξ, the quantity estimated above.

Based on the assumption that ξ is 0, the isogyre theory I shall apply is contained in the following principle. At each point P in the interference field, imagine a cross to be drawn in the orientation given by a stereographic projection of the allowed directions of $\boldsymbol{D}$ drawn as a small cross on the reference sphere at the point corresponding to P. An isogyre passes through those points at which the crosses are aligned parallel to the NS and EW crosshairs of the microscope.

Note that Becke's construction would have given the same method of finding the position of the isogyres, if he had applied it in this way, instead of relying on the skiodrome theory. However, the assumption *behind* Becke's construction would *not* lead to the correct method. It is a case where an incorrect assumption and an incorrect construction lead to the correct conclusion.

6. *Uniaxial flash figures*

It is worthwhile to make a detailed application of the principle stated in the last section to the uniaxial flash figure, because for this figure the predictions of the theory can be compared precisely with the predictions of the skiodrome theory.

In applying the principle, it is easier and more direct to work with the reference sphere than to carry out the stereographic projection specifically. Fig. 8*a* is an orthographic view of the reference sphere, showing a point P defined by coordinates ϕ and $\rho = \sin\theta$, where θ is the inclination in the crystal plate of the wave normal $\boldsymbol{n}$ corresponding to P. PD_1 and PD_2 are drawn parallel to the arms of the stereographically projected $\boldsymbol{D}_1$, $\boldsymbol{D}_2$ cross corresponding to P. Fig. 8*b* is a stereographic projection of the same sphere. For a uniaxial crystal with optic axis emerging at A, the allowed directions of $\boldsymbol{D}$ at $\boldsymbol{n}$ are parallel and perpendicular, at $\boldsymbol{n}$, to the great circle $A\boldsymbol{n}$. In stereographic projection the angle γ, on the sphere, between $O\boldsymbol{n}$ (prolonged) and $\boldsymbol{n}A$ is preserved, because the stereographic projection is angle-true and the great circle $O\boldsymbol{n}$ projects as a line with the same azimuth ϕ. Thus in Fig. 8*a* the angle γ between PD_1 and OP (prolonged) can readily be calculated from spherical triangle $O\boldsymbol{n}A$ in Fig. 8*b*:

$$\cos\theta \cos\left(\frac{\pi}{2} - \phi\right) = -\sin\left(\frac{\pi}{2} - \phi\right) \cot(\pi - \gamma). \tag{17}$$

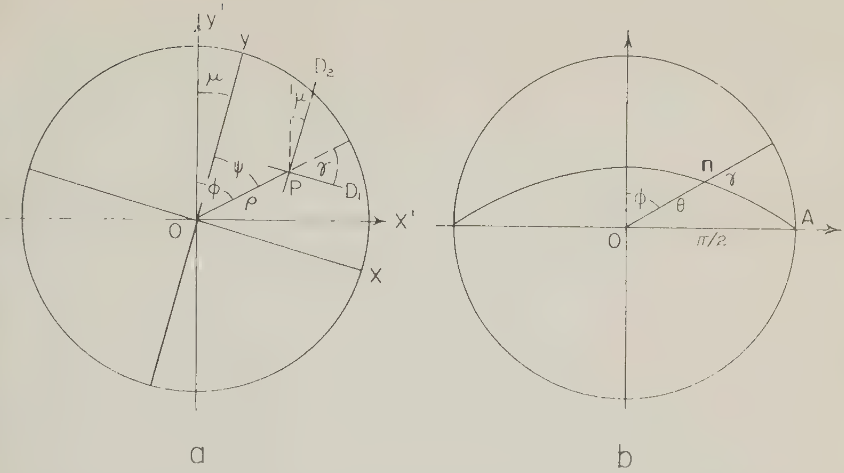

FIG. 8. Diagrams for analysis of the uniaxial flash figure. 8*a* represents the interference field (orthographic projection), and 8*b* is a stereographic projection of the interference hemisphere.

Now a given isogyre is traced out by all points P having a given inclination μ of the stereographically projected axes D_1, D_2 to the axes x', y':

$$\phi - \mu = \frac{\pi}{2} - \gamma. \tag{18}$$

Combining (17) and (18) we have for the equations of the isogyres

$$\tan(\phi - \mu) = \cos\theta \tan\phi \tag{19}$$

where μ is constant for a given isogyre.

(19) is written in coordinates (θ, ϕ) measured with respect to axes x', y' fixed in the crystal plate. If, as in most microscopes, the plate is rotated and the nicols remain fixed, it is more appropriate to describe the isogyres in terms of coordinates (θ, ψ) defined by the NS and EW cross hairs, which, for an isogyre passing through P, must be the x, y axes of Fig. 8*a*, so that

$$\psi = \phi - \mu \tag{20}$$

and the isogyre equation is

$$\tan(\psi + \mu) = \frac{\tan\psi}{\cos\theta}\cdot \tag{21}$$

μ is the angle through which the crystal has been rotated from extinction.

To translate (21) into an equation describing the isogyre seen in the flash figure, it is necessary to introduce a relation between θ and radial distance ρ' from the center of the figure. If Mallard's law is valid, ρ' is

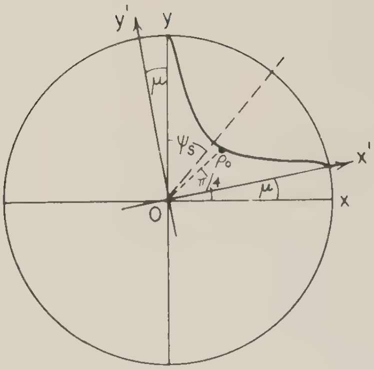

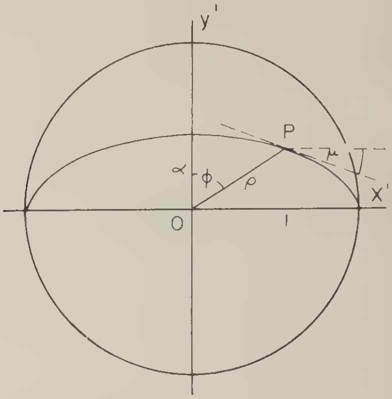

Fig. 9 (left). Form of the isogyre (heavy curve) in the uniaxial flash figure. The diagram is an orthographic projection of the entire interference hemisphere, of which only the inner part is visible in the conoscope. μ is exaggerated in the drawing.

Fig. 10 (right). Diagram for calculating the position of meridianal isogyres from the skiodrome theory for the uniaxial flash figure. The meridianal skiodrome passing through P is shown.

proportional to $\sin\theta$ and hence to ρ in Fig. 8*a*, the proportionality constant depending, of course, on the microscope objective and the index of refraction of the crystal plate. I shall write the isogyre equations in terms of θ or ρ, realizing that these can always be converted to radial distance ρ' in the interference figure when needed.

The main features of an isogyre defined by equation (21) are plotted approximately in Fig. 9, which is an orthographic projection similar to Fig. 8*a*. The isogyre has a roughly hyperbolic shape. It passes through the optic axis at $x'=1$ and through the cross hair axis y at the edge of the sphere. The curve is mirror symmetric about the line $\psi=\psi_s=\pi/4-\mu/2$. Its closest approach to the center is along this line, and the derivative $d\rho/d\psi$ vanishes at the point of closest approach. $d\rho/d\psi$ is zero where the curve meets the edge of the sphere, but this affects only a small portion of the curve, as shown in Fig. 9. These features can be verified from equation (21).

Consider the shape of the isogyre near the center of the field for small angles of rotation μ. (21) can then be expanded:

$$(\tan\psi + \mu\sec^2\psi)(1 - \tfrac{1}{2}\rho^2) = \tan\psi$$

or

$$\rho^2 \sin 2\psi = 4\mu. \tag{22}$$

(22) is the equation of a rectangular hyperbola, as can be verified by substituting

$$x = \rho \sin \psi,$$
$$y = \rho \cos \psi.$$

As a quantitative test of eqn. (21), I shall use the angle μ_o required to bring the isogyre out to the edge of the interference field, defined by some angle θ_o and corresponding distance ρ_o. The isogyre actually disappears from the field along the line $\psi = \pi/4 - \mu/2$, but since μ_o is about 5° in practice this differs little from $\psi = \pi/4$. The distance ρ_o of the isogyre along $\psi = \pi/4$ is obtained by substituting this value in (21). After some simple reduction it is found to be given exactly by

$$2 \sin 2\mu_o = \frac{{\rho_o}^2}{1 - \frac{1}{2}{\rho_o}^2} \cdot \tag{23}$$

Note that (22) agrees with (23) in the limiting case in which ρ_o and μ_o are small. The difference between θ_o calculated from (23) and θ_o' measured along $\psi = \pi/4 - \mu/2$ can be shown from (21) to be 0.05°, which is imperceptible. The change in μ required to move the isogyre from the position where it touches the edge of the field along $\psi = \pi/4$ to the position where it touches along $\psi = \pi/4 - \mu/2$ is 0.014°.

For comparison with (21), (22), and (23), the corresponding results for the meridianal isogyre given by the skiodrome theory will now be derived. The orthographically projected sphere is taken to have radius 1, as before. The meridianal skiodroms are ellipses, as shown in Fig. 10. α is a parameter defining the particular ellipse that passes through P. We have

$$x'^2 + \frac{y'^2}{\alpha^2} = 1$$

$$\tan p\mu = -\frac{dy'}{dx'} = \frac{x'}{y'} \alpha^2 = \alpha^2 \tan \phi.$$

Now put

$$x' = \rho \sin \phi$$
$$y' = \rho \cos \phi.$$

Then

$$\rho^2 \sin^2 \phi + \frac{\rho^2 \cos^2 \phi}{\tan \mu} \tan \phi = 1$$

or

$$\tan \mu = \frac{\rho^2 \sin 2\phi}{2(1 - \rho^2 \sin^2 \phi)} \cdot$$

To write the result in cross hair coordinates, substitute (20) to get

$$\tan \mu = \frac{\rho^2 \sin 2(\psi + \mu)}{2(1 - \rho^2 \sin^2 (\psi + \mu))} \cdot \tag{24}$$

(24) is the skiodrome equivalent of (21). Near the center of the field, where ρ is small, and μ must be small for the isogyre to be visible, (24) reduces to

$$2\mu = \rho^2 \sin 2\psi, \tag{25}$$

a rectangular hyperbola that is to be compared with (22). The meridianal isogyre reaches a given point in the interference field only after a rotation μ twice as great as the isogyre described by (22). Thus even at the center of the field the predictions of the two theories differ by a factor of 2.

For $\psi = \pi/4 - \mu$ (24) reduces to

$$2 \tan \mu_o = \frac{\rho_0^2}{1 - \frac{1}{2}\rho_0^2}. \tag{26}$$

(26) is also very nearly true for $\psi = \pi/4$, so that it is the skiodrome equivalent of (23).

A test between the two theories can best be made on the basis of (23) and (26). Note that (24) predicts a slightly larger value of μ_o than does (26), so that it accentuates the difference between the values of μ_o given by (23) and (26).

The results of a series of measurements of μ_o for flash figures in oriented mineral sections is given in Table 2. Each value reported is the mean of about 30 measurements for a given point in a given thin section. The "limit of error" values do not represent estimated standard errors of the mean, but rather the maximum scatter of μ_o values obtained in each set of about 30 measurements. The means scatter more than one would have estimated from the scatter of the individual measurements, probably because of subjective effects of the kind mentioned in section 5, and also because of an effect discussed in section 8.

TABLE 2. SUMMARY OF FLASH FIGURE MEASUREMENTS
CONOSCOPE OF HALF APERTURE $\theta_m \cong 55°$

Mineral	n	μ_o values
Quartz	1.55	4.4±0.6, 5.0±0.6, 4.8±0.6 (av.) 4.7
Beryl	1.56	3.7±0.3, 4.6±0.6, 4.0±0.7, 3.8±0.3, 5.7±0.8, 4.9±0.7, 4.6±0.6, 5.2±1.2 (av.) 4.6
Apatite	1.64	4.3±0.4, 3.5±0.4, 4.4±1.1, 4.3±0.8 (av.) 4.1
Tourmaline	1.64	4.5±1.7, 4.4±2.1, 3.5±1.1, 4.5±2.1 (av.) 4.2

The measurements are made in the following way. Only nearly centered figures are measured. The azimuthal setting of the stage required to place the isogyre at the edge of the field in each quadrant of the field is then measured five or six times, for rotation from a given extinction position. Finally several measurements are made of the azimuthal setting that produces the centered cross. The μ_o values are obtained afterwards, by difference. This procedure tends to eliminate advanced bias as to how the values should turn out. The final μ_o value, obtained by averaging the values from each equadrant, tends to eliminate the effects of slight misorientation of the section.

In making the measurements, the object is to set the center of the isogyre at the edge of the field. This is made difficult and somewhat uncertain by the fact that when set properly, only one edge of the isogyre can be seen. It is necessary to swing the stage back and forth through the correct position in order to make sure where the center of the isogyre is. The flash figure isogyre is rather diffuse, so that the settings cannot be made very accurately. It might be preferable to make the settings for a ρ_o value within the field of the conoscope, as could be done with an ocular provided with a circular reference hair. Such an ocular was not available, but in addition I considered it desirable to make the measurements at the largest possible value of ρ_o, for which the μ_o values predicted by (23) and (26) differ most.

Before beginning the measurements, I estimated from standard *Bxa* slides that the conoscope used (see section 5) has a half-aperture in air, which I will call θ_m, of about 55°. For a mineral with index $n=1.56$, the interference sphere can therefore be seen out to $\theta_o=31.9°$, and for $n=1.64$, $\theta_o=30.0°$. Equations (23) and (26) then predict the μ_o values shown in Table 3.

TABLE 3. COMPARISON OF CALCULATED AND OBSERVED μ_0 VALUES FOR FLASH FIGURES. $\theta_m=55°$

n	μ_o (23)	μ_o (26)	μ_{obs} (av.)
1.56	4.6°	9.1°	4.6°, 4.7°
1.64	4.1°	8.1°	4.1°, 4.2°

The observed values are the averages from Table 2 for each of the four minerals. It is clear that (23) accounts for the observed values and (26) does not. To obtain agreement between (26) and the observed values it would be necessary to assume $\theta_m=37.8°$, whereas the isogyres in 45° position in a centered *Bxa* figure of muscovite, with $E=39°$, are well within the field of the conoscope.

The measurements of *Bxa* and *Bxo* figures, given in the next section, suggest that the correct value of θ_m for the conoscope used is about

57.6°, slightly larger than the value used in Table 3. The numerical aperture 0.85 of the objective, stated by the manufacturer, corresponds to $\theta_m = 58.2°$. This value gives calculated μ_o values somewhat larger than those listed in Table 3 (e.g., $\mu_o(23) = 5.1°$ for $n = 1.55$). Students who have made flash figure measurements for me generally find somewhat higher μ_{obs} values also, for lenses of the same rated N.A. as the one I used.

At first I was cautious not to rely on the accuracy of the conoscopic angles and numerical apertures stated by lens manufacturers, but the close agreement between μ_o values actually measured and μ_o values calculated from the theory by assuming the correctness of the rated numerical apertures shows that this caution is unnecessary. Several examples of the agreement will be seen in sections 7 and 8. For any lens for which the numerical aperture in air,

$$\text{N.A.} = n_{\text{air}} \sin \theta_m \cong \sin \theta_m = \rho_m,$$

is accurately known, isogyre calculations can be readily made by taking

$$\rho_o = \frac{\rho_m}{n}$$

where n is the index of refraction of the crystal plate.

7. *Acute and Obtuse Bisectrix Figures*

The analysis of *Bxa* and *Bxo* figures can be carried out by the methods used in the last section, with the help of Fig. 11. Angles α_1, α_2 and γ can be introduced as shown, and the inclination μ calculated from the law of Biot and Fresnel. I shall not write down the details of the derivation, but simply state the result, converted to cross-hair coordinates θ and ψ, as defined by (20):

$$\cot 2\psi \sin 2(\psi + \mu) \cos \theta + \sin^2 (\psi + \mu)(2 - \sin^2 \theta) = 1 + \sin^2 \theta \cot^2 V. \quad (27)$$

The result is cumbersome, but can be simplified in two ways. If we suppose that θ is small enough that to a sufficiently good approximation

$$\cos \theta = 1 - \tfrac{1}{2}\rho^2$$

then one can show, after some calculation, that (27) reduces to the simple form

$$\frac{\rho_1^2}{1 - \frac{1}{2}\rho_1^2} \sin 2\mu = \frac{\rho^2}{1 - \frac{1}{2}\rho^2} \sin 2\psi, \quad (28)$$

where

$$\rho_1 = \sin V$$

and, as before,

$$\rho = \sin \theta.$$

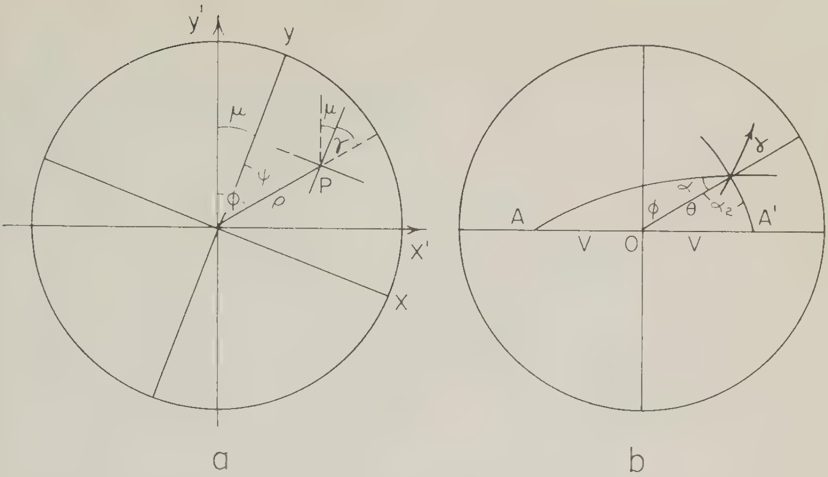

FIG. 11. Diagrams for analysis of centered *Bxa* and *Bxo* figures. In 11*b* the optic axes project to the points *A* and *A'*. 11*a* represents the interference field (orthographic projection), and 11*b* is a stereographic projection of the interference hemisphere.

(28) describes a curve that approaches the shape of a rectangular hyperbola for small ρ. Its closest approach to the center is along the line $\psi = \pi/4$.

A second simplification is to evaluate (27) for $\psi = \pi/4$. It then reduces exactly to

$$\frac{\rho_1^2}{1 - \frac{1}{2}\rho_1^2} \sin 2\mu_o = \frac{\rho_0^2}{1 - \frac{1}{2}\rho_0^2} \cdot \tag{29}$$

Note that (28) yields (29) when $\psi = \pi/4$, and that (29) reduces to (23) when $\rho_1 = 1$ (uniaxial flash figure). Since the exact shape of the isogyre, as given by (27), is not important in practice, I will make use only of (29) in applications of the theory.

The relationship between (28) and (29) makes possible a fairly simple evaluation of the deviation of (27) from (28). The two curves evidently intersect at $\rho = \rho_o$, $\psi = \pi/4$. The slope $d\theta/d\psi$ at this point is found to be

$$\frac{d\theta}{d\psi} = \frac{2 \cos 2\mu_o}{\cos \theta_o(1 + \sin 2\mu_o + 2 \cot^2 V)} \cdot (1 - \tfrac{1}{2}\rho_0^2 - \sqrt{1 - \rho_0^2}).$$

The slope is greatest for the uniaxial flash figure (for which it is 0.036), and decreases steadily as V decreases and μ_o increases, becoming zero for $\mu_o = 45°$ ($V = \theta_o$). This conclusion seems to violate what is observed in practice, that for figures with μ_o about 15° or greater, the slope $d\theta/d\psi$ of the isogyre at $\psi = \pi/4$ appears to become noticeable. However, I think the apparent slope is exaggerated by the rapid fanning out of the isogyre near the optic axes, which are near the edge of the field in such figures.

Because of the importance of $\rho^2/1-\frac{1}{2}\rho^2$ in (28) and (29), the function is plotted againt θ in Fig. 12. In Fig. 13 are shown curves giving μ_o as a function of V, from (29), for various values of the mean index n of the crystal plate. The conoscope half aperture θ_m is assumed to be 57.6° in the calculation of these curves. Each curve corresponds to a given value of θ_o, as shown in Table 4, so that the curves can be adapted to conoscopes of different aperture by using the relation (Snell's Law)

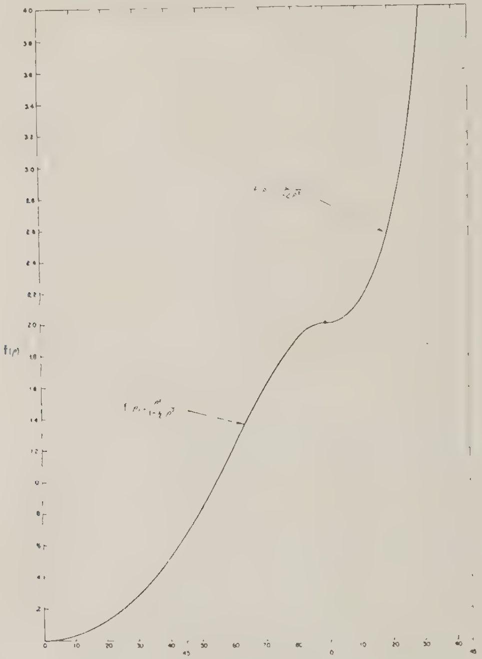

FIG. 12. The functions $f(\rho)=\rho^2/1-\frac{1}{2}\rho^2$ and $f(\rho)=2/1-2\rho^2$ plotted against θ.

$$n \sin \theta_o = \sin \theta_m. \tag{30}$$

Equation (29) and the curves of Fig. 13 provide a means of measuring

TABLE 4. PARAMETERS FOR THE CURVES IN FIG. 13

Curve	1	2	3	4	5
θ_0	33.1°	31.9°	30.8°	29.8°	28.8°
$\rho_0^2/1-\frac{1}{2}\rho_0^2$	.351	.326	.302	.281	.261
n	1.55	1.60	1.65	1.70	1.76

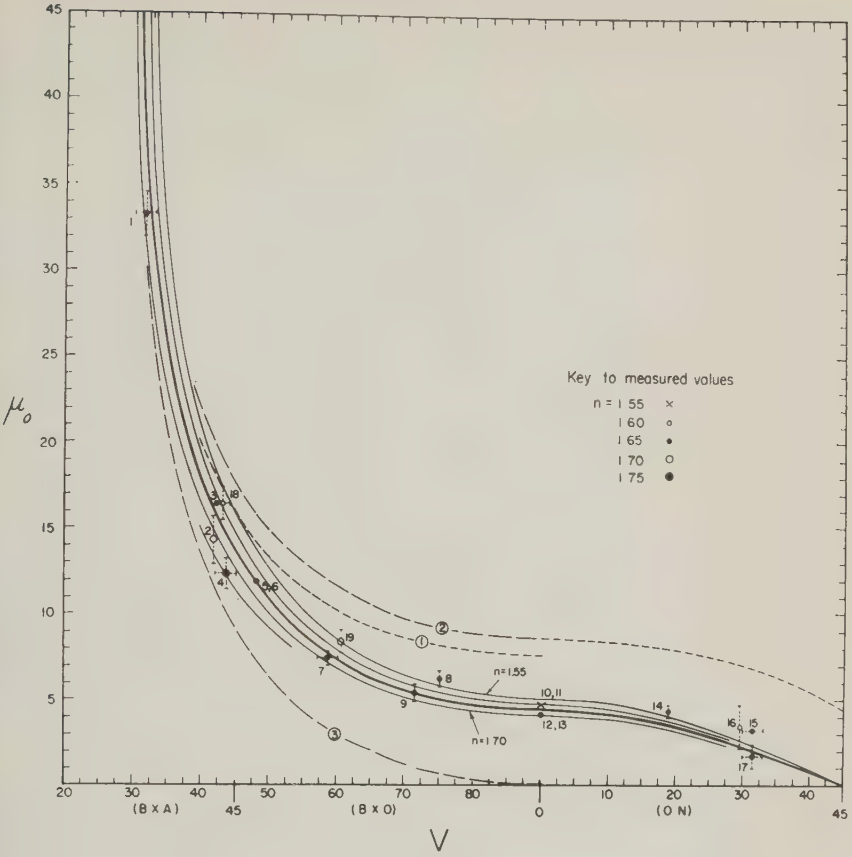

FIG. 13. Comparison of theoretical curves of μ_0 as a function of V with measured μ values from oriented thin sections. Conoscope is assumed to have half aperture $\theta_m = 57.6°$ (N.A. 0.845) for the theoretical curves, which are calculated for crystal plate indices of refraction varying from 1.55 to 1.70 in intervals of 0.05. The curve for $n = 1.65$ is drawn with a heavy line, and is to be compared with dashed curve (1), given by the theory of Michel-Lévy for the same index and aperture, and with curves (2) and (3), from the skiodrome theory. The plotted points are identified by number in Table 5, and by index in the key on the figure.

V in *Bxa* and *Bxo* figures, and in particular a means of distinguishing between *Bxa* and *Bxo* figures. The method was first proposed by Michel-Lévy (1888) but his theoretical treatment of the method was not satisfactory. Curve 1 (dashed) in Fig. 13 shows the angles μ_o given by his theory for $n = 1.65$. $\theta_m = 57.6°$. The curve is calculated from the isogyre equation

$$\rho^2 \sin 2\psi = \rho_1{}^2 \sin 2\mu \tag{31}$$

by putting $\psi = \pi/4$, $\rho = \rho_o$, $\mu = \mu_o$.

A derivation of (31) can be found in Wright's paper (1905, p. 288) or in Johannsen's text (1918, p. 441).

Curves 2 and 3 are derived from the isogyres of the skiodrome theory. The calculation of skiodrome isogyre shapes is cumbersome, but simplifies for $\psi=\pi/4$ to the relationships

$$\rho_1{}^2 = \frac{\rho_o{}^2}{\sin 2\mu_o[1 - \frac{1}{2}\rho_o{}^2(1 - \tan \mu_o)]} \tag{32a}$$

$$\rho_1{}^2 = \frac{\rho_o{}^2}{\sin 2\mu_o[1 + \frac{1}{2}\rho_o{}^2(\cot \mu_o - 1)]} \,. \tag{32b}$$

(32*a*) gives curve 2, which corresponds to the meridianal isogyre for $V>45°$, while (32*b*) gives curve 3 (Fig. 13).

To test the various theories, I have measured angles μ_o for a number of *Bxo* figures, and *Bxa* figures of large $2V$, obtained from oriented thin sections. The points are plotted in Fig. 13. The measurements were made in the way described in section 6 for uniaxial flash figures. Values of V are averages of data given by Winchell (1951) and Tröger (1956). I have avoided minerals for which a wide range of V is reported. Note that the points in Fig. 13 are identified by index n and by a reference number, which refers to the summary in Table 5. Rough "limit of error" brackets have been added to those points in Fig. 13 for which the uncertainty in measured μ_o values or in V values quoted in the literature is important.

The measurements confirm the applicability of (29). Best overall agreement with the calculated curves is obtained by taking $\theta_m=57.6°$. Points 14–17 were omitted in the comparison.

The averages of the μ_o values given by curves 2 and 3 in Fig. 13, for given values of V, reproduce rather closely the μ_o values calculated from (29). In this sense the skiodrome theory is "on the average" correct, which can be understood from the way the $\boldsymbol{D}_1$, $\boldsymbol{D}_2$ cross behaves when orthographically projected. Nevertheless, the skiodrome theory itself has no means of predicting what sort of averaging of the μ_o values should give the correct result, and the use of (32) and (33), with averaging, is, of course, more cumbersome than direct application of (29).

In Fig. 14 are given curves of μ_o against V calculated from (29) for values of n ranging from 1.45 (curve 1) to 1.80 (curve 8). The curves 1 to 8 are for an objective of N.A. 0.85, and the curves a to h for N.A. 0.65, these being the numerical apertures of standard objectives used in conoscopic work. The larger aperture is clearly advantageous. For example, the reliability with which a figure can be distinguished as *Bxa* or *Bxo* increases with the (magnitude of) the slope of the μ_o vs. V curve at $V=45°$.

It is advisable before using the curves of Fig. 14 to check the N.A. of the objective used. This can conveniently be done, and the applicability

TABLE 5. MEASURED DATA PLOTTED IN FIG. 13. LIMIT OF ERROR IS (ROUGHLY) ESTIMATED STANDARD DEVIATION OF MEAN. OBJECTIVE OF N.A. 0.85 (Leitz No. 7)

Point Ref. No.	Mineral	Sec.	n	μ_0 (measured)	V (lit.)
1	Topaz	*Bxa*	1.63	33.2±1.3	30 –33
2	Kyanite	*Bxa*	1.72	14.3±1.4	41.7
3	Andalusite	*Bxa*	1.64	16.4±0.1	41.5–42.5
4	Staurolite	*Bxa*	1.75	12.3±0.9	42 –45
5	Andalusite	*Bxo*	1.64	11.8±0.1	41.5–42.5
6	Andalusite	*Bxo*	1.64	11.9±0.3	41.5–42.5
7	(F−) Topaz	*Bxo*	1.63	7.4±0.4	30 –33
8	Sillimanite	*Bxo*	1.67	5.9±0.5	12.5–15
9	Barite	*Bxo*	1.64	5.4±0.5	18.7
10	Quartz	flash	1.55	4.7±0.2	0
11	Beryl	flash	1.56	4.6±0.2	0
12	Apatite	flash	1.64	4.1±0.2	0
13	Tourmaline	flash	1.64	4.2±0.2	0
14	Barite	o.n.	1.64	4.3±0.4	18.7
15	Topaz	o.n.	1.63	3.2±0.2	30 –33
16	Augite	o.n.	1.70	3.4±1.3	29.5
17	Topaz	o.n.	1.63	1.7±0.7	30 –33
18	Tremolite	*Bxa* (poorly centered)	1.61	16.4±1.0	42? –44
19	Augite	*Bxo*	1.69	8.2±0.7	29.5

of the theory also tested, by measuring μ_o for *Bxa* and *Bxo* figures of andalusite ($V=42°$ and $48°$), plotting the measured points on Fig. 14, and checking that they fall at places appropriate to $n=1.64$. If the objective has numerical aperture (ρ_m) other than 0.85 or 0.65, the curves of Fig. 14 can be adapted to it by assigning new values of n by the relation (30). The ρ_o values for the curves of Fig. 14 are given in Table 6. If ρ_m for an objective is unknown, it can be determined by reversing the above procedure, or also, of course, by using a stage apertometer.

8. *The effect of non-zero* ξ

Although ξ (section 5) is small, so that the isogyre equations for $\xi=0$ give a good representation of observed interference figures, an actual non-zero value of ξ has a small but definite effect on the μ_o values measured. It can be seen from Fig. 11, or from diagrams of the kind shown in Fig. 19, that if μ_o is measured by rotating the crystal plate from the extinction position where the optic plane is NS, then a positive value of ξ, as defined in eqn. (9) and Fig. 7*a*, tends to reduce the measured μ_o value from the value predicted for $\xi=0$. Call the μ_o value measured in this way μ_V, and call the value measured about the extinction position with the optic plane EW μ_H. If ξ is positive, then μ_V is less than μ_o, the value expected for $\xi=0$, but μ_H is greater than μ_o. A detailed analysis of this situation would be required if ξ were large. Instead, since

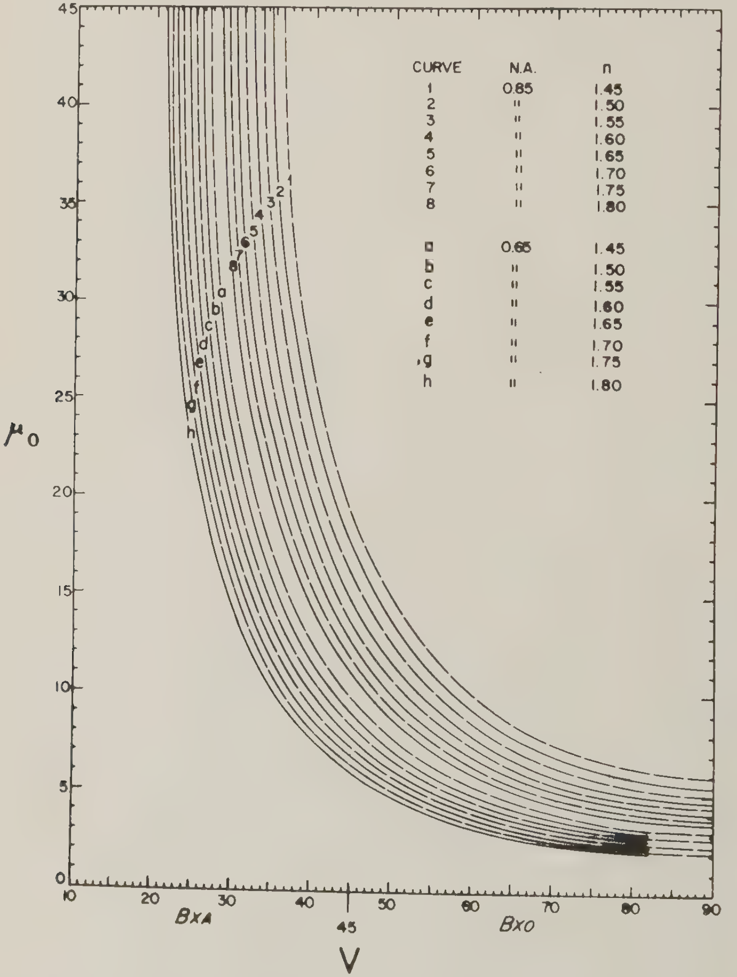

FIG. 14. Theoretical curves of μ_0 against V for conoscopes of N.A. 0.85 (numbered curves) and N.A. 0.65 (lettered curves). The curves are calculated for crystals of mean index of refraction ranging from 1.45 to 1.80 at intervals of 0.05, as indicated.

ξ is small, then if μ, regarded as a function of ψ for constant $\theta=\theta_o$ in eqn. (27), varies much less rapidly than ψ itself, as is true for the *Bxa* and *Bxo* figures considered above, we may write (to first order in ξ_m)

TABLE 6. DATA FOR CURVES OF FIGURE 14

N.A.	Curve	n	θ_0	ρ_0	$\frac{\rho_0^2}{1-\frac{1}{2}\rho_0^2}$
0.85	1	1.45	35.9°	0.586	0.415
	2	1.50	34.5	.566	.382
	3	1.55	33.3	.548	.354
	4	1.60	32.1	.531	.328
	5	1.65	31.0	.515	.306
	6	1.70	30.0	.500	.285
	7	1.75	29.1	.486	.267
	8	1.80	28.2	.472	.251
0.65	*a*	1.45	26.6	.448	.223
	b	1.50	25.7	.433	.207
	c	1.55	24.8	.419	.193
	d	1.60	24.0	.406	.180
	e	1.65	23.2	.394	.168
	f	1.70	22.5	.382	.158
	g	1.75	21.8	.371	.148
	h	1.80	21.2	.361	.139

$$\begin{aligned}\mu_V &= \mu_o - \xi_m \\ \mu_H &= \mu_o + \xi_m\end{aligned} \tag{33a}$$

where ξ_m is the value of ξ at $\psi=\pi/4$, $\theta=\theta_o$ (eqn. (16)).

Thus for a given figure μ_o and ξ_m can be determined by measuring μ_V μ_H:

$$\mu_o = \tfrac{1}{2}(\mu_V + \mu_H) \tag{33b}$$

$$\xi_m = \tfrac{1}{2}(\mu_H - \mu a) \tag{33c}$$

To test the above conclusions, I have made a careful series of measurements on three figures: andalusite *Bxa*, andalusite *Bxo*, and quartz flash, for which the data are given in Table 7. The figures were measured with a Zeiss model GFL668-666 petrographic microscope, using objective "Pol 50/0.85" of N.A. 0.85. The scatter in ξ_m values calculated from (33c) is probably mainly random, though ξ_m may be affected by the slides themselves, if slide and cover glass have different indices. Evidently ξ_m is about $-0.7°$ for the lens combination used. The measured μ_o values, obtained from (*33b*), agree excellently with the values calculated from the theory (eqn. (29)) by assuming $\rho_m=0.85$ and assuming $V=42°$ for andalusite. I consider the data of Table 7 to be the most definitive test of the theory, because the measurements reported in Tables 2 and 5 were made before I was aware of the proper way to take a nonzero ξ into account, and they were made with an inferior microscope.

TABLE 7. INTERFERENCE FIGURE MEASUREMENTS WITH ZEISS MODEL GFL668-666, OBJECTIVE "Pol 50/0.85," OF N.A. 0.85

Extinction setting	Optic plane set	Isogyre in quadrant	Andalusite Bxa		Andalusite Bxo		Quartz Flash	
			μ_V	μ_H	μ_V	μ_H	μ_V	μ_H
1	NS	1	16.3	—	12.7	—	5.6	—
		2	15.7	—	11.0	—	6.7	—
		3	18.0	—	12.7	—	5.0	—
		4	15.7	—	14.7	—	6.8	—
2	EW	1	—	15.2	—	9.8	—	3.8
		2	—	14.3	—	11.5	—	4.9
		3	—	16.0	—	11.9	—	4.8
		4	—	16.1	—	11.6	—	4.4
3	NS	1	18.5	—	13.3	—	5.1	—
		2	16.3	—	14.0	—	5.7	—
		3	15.9	—	14.0	—	5.4	—
		4	16.3	—	10.8	—	6.3	—
4	EW	1	—	15.7	—	12.1	—	4.9
		2	—	16.9	—	11.6	—	4.2
		3	—	15.7	—	10.2	—	3.7
		4	—	13.4	—	10.5	—	4.7
Average μ_V and μ_H			16.6	15.4	12.9	11.1	5.8	4.4
ξ_m from (33*c*)			−0.6		−0.9		−0.7	
μ_0 from (33*b*)			16.0		12.0		5.1	
μ_0 from (29)			16.1		12.0		5.1	

The important conclusion to be drawn is that in measuring *Bxa* and *Bxo* figures, the effect of a small non-zero ξ is eliminated by averaging μ_V and μ_H.

9. *Optic Normal Figures*

Equations of the optic normal isogyres can be obtained with the help of Fig. 15. The rather unwieldy result is

$$2 \cot 2\psi \cos \theta \sin 2(\psi - \mu) - (2 - \sin^2 \theta) \cos 2(\psi - \mu) + \sin^2 \theta \cos 2V = 0 \quad (34)$$

(34) simplifies for $\psi = \pi/4$ to

$$2 \sin 2\mu_0 = \frac{\rho_0^2}{1 - \frac{1}{2}\rho_0^2} \cos 2V$$

or

$$\frac{2}{1 - 2\rho_1^2} \sin 2\mu_0 = \frac{\rho_0^2}{1 - \frac{1}{2}\rho_0^2} \cdot \tag{35}$$

Note that when $\rho_1 = 0$ (uniaxial flash figure), (35) reduces to (32).

In Fig. 13 (35) is plotted as a continuation of the μ_o vs. V curves, with a new origin for the V coordinate. The angle μ_o for a "neutral" figure with $2V = 90°$ is 0, meaning that the cross does not break up into hyperbolae as the crystal is rotated from extinction.

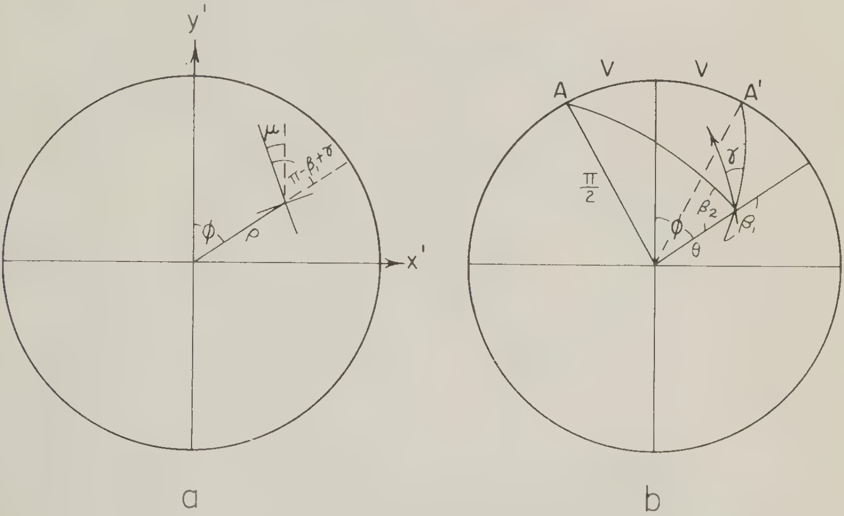

FIG. 15. Diagrams for analysis of optic normal figures. 15*a* represents the interference field (orthographic projection), and 15*b* is a stereographic projection of the interference hemisphere.

Most of the measured μ_o values for optic normal figures lie above the curves of Fig. 13. The figures are difficult to measure with any accuracy because the isogyres are so diffuse, and it therefore seems that a detailed comparison with the other theories is not of much value over this range. Michel-Lévy's equation cannot logically be extended to optic normal figures. I have bothered to analyze the skiodrome theory only for $V = 45°$, where it predicts two points at an equal distance above and below the $\mu_o = 0$ axis, corresponding to the continuation of curves 2 and 3 of Fig. 13. The predicted value of μ_o is given exactly by

$$\frac{\tan \mu_o}{1 - \tan^2 \mu_o} = \frac{\rho_o^2}{4(1 - \frac{1}{2}\rho_o^2)} \tag{36}$$

Since μ_o is small, the value given by (36) is just half the value predicted by the skiodrome theory for uniaxial flash figures, eqn. (26). It is plotted as a point in Fig. 13, and curve 2 is connected across schematically from $V=0$ to $V=45°$.

10. Optic Axis Figures

As a last application of the theory, it is interesting to compare its predictions with those of Wright (1905, 1907) for optic axis figures. In the 1905 paper Wright gave a series of curves showing the appearance of the optic axis isogyres in the 45° position. The curves were computed from the equation

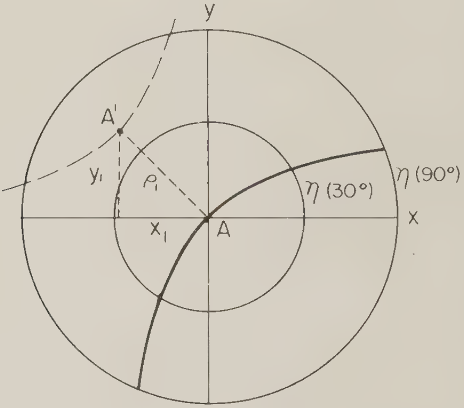

FIG. 16. Orthographic projection of the interference hemisphere for the optic axis figure. The optic axis is at A, and the heavy line shows the position of the isogyre in the 45° setting. The second optic axis is shown schematically at A', as envisaged in Wright's derivation of the isogyre equation.

$$xy + \tfrac{1}{2}x_1(y - x) = 0 \tag{37}$$

where x, y are coordinates (in the interference field) of points on the isogyre and x_1 is the x-coordinate of the second optic axis, which may or may not be in the interference field, as shown in Fig. 16 (note that $x_1 = y_1$). (37) is derived by applying a planar analog of the law of Biot and Fresnel to the plane of Fig. 16, and is thus the optic axis figure analog of Michel-Lévy's equation, (31). To be consistent, one would assume that the points (x, y) and (x_1, y_1) represent an orthographic projection of the interference sphere. However, Wright assumed the projection to be gnomonic in calculating his isogyre curves. The only justification for such an assumption, as far as I can see, is that it gives the correct type of isogyre (a straight line) for $2V=90°$, which an orthographic projection would not.

In his 1907 paper, Wright superseded the earlier curves with a new set, apparently determined from the skiodrome theory. Nevertheless, the older curves have found their way into optical mineralogy texts and the newer ones not, perhaps because the newer curves do not look much like the isogyres actually seen in interference figures.

The present theory may be applied by using Fig. 17. Written in coordinates (θ, ψ) measured with respect to the cross-hair axes x, y, the isogyre equation is

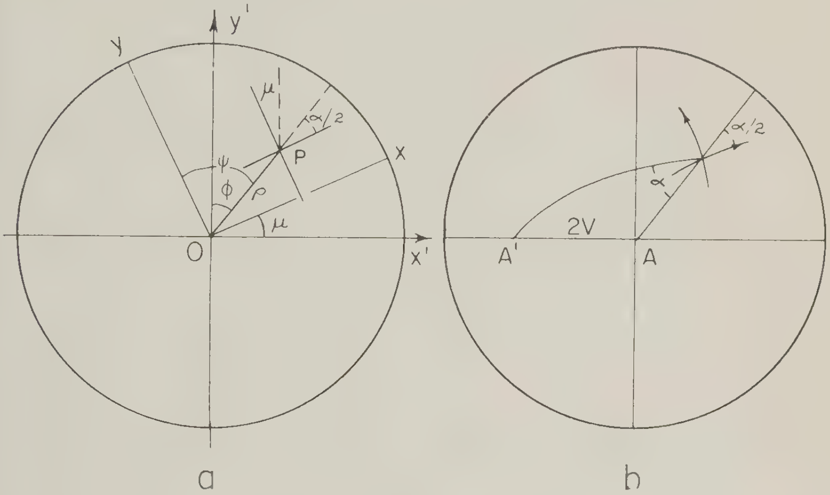

FIG. 17. Diagrams for analysis of optic axis figures. 17*a* represents the interference field (orthographic projection), and 17*b* is a stereographic projection of the interference hemisphere.

$$\sin\theta \cot 2V + \cos\theta \sin(\psi - \mu) - \cot 2\psi \cos(\psi - \mu) = 0. \tag{38}$$

For the isogyre in the 45° position, put $\mu = \pi/4$ in (38); the isogyre then has the form shown by the solid curve in Fig. 16. A good test of Wright's curves (1905, p. 291) is to compare the angle η (Fig. 16) at the periphery of the field (which Wright chose as $\theta_o = 30°$) with the corresponding values calculated from (38).

Since $\eta = \pi/2 - \psi$, (38) becomes

$$\tan 2V = \frac{\sin\theta}{\cot 2\eta \cos\left(\frac{\pi}{4} - \eta\right) - \cos\theta \sin\left(\frac{\pi}{4} - \eta\right)} \tag{39}$$

from which values of V can be calculated for a series of η values, at a given value of θ. A curve for $\theta = 30°$ is plotted in Fig. 18. Note that, to a

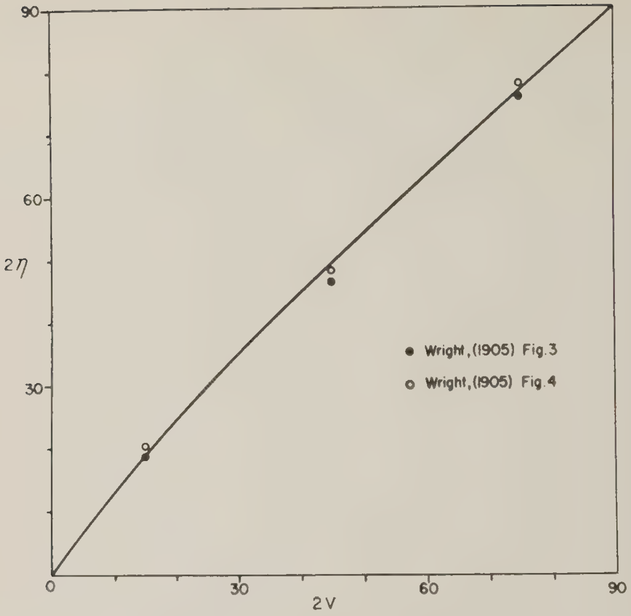

FIG. 18. Curve showing 2η (30°) as a function of $2V$, from equation (39). For comparison are plotted values measured from Wright's isogyre curves (1905, Figs. 3 and 4).

good approximation, $\eta \cong V$, a fact that may be convenient to remember. Plotted also in Fig. 18 are points measured from Wright's (1905) Fig. 3 and Fig. 4. The agreement is remarkably close, certainly well within the accuracy needed for practical work.

This unexpected agreement has an interesting explanation. If we suppose the interference sphere to be orthographically projected, so that

$$x = \rho \sin \psi, \qquad y = \rho \cos \psi,$$
$$x^2 + y^2 = \rho^2, \qquad \rho = \sin \theta,$$

then (38) becomes, in cartestian coordinates, and with $\mu = \pi/4$:

$$(x^2 - y^2)(x + y) - 2\sqrt{2}\rho^2 xy \cot 2V - 2\sqrt{1 - \rho^2}(x - y)xy = 0 \tag{40}$$

(40) is to be compared with Wright's equation, (37).
In case ρ is small enough that we can write

$$\sqrt{1 - \rho^2} = 1 - \tfrac{1}{2}\rho^2$$

then (40) reduces to

$$(x - y)(1 + xy) - 2\sqrt{2}\, xy \cot 2V = 0. \tag{41}$$

This is of the same form as (37), except for the factor $(1+xy)$. The factor is always near 1 for points in the conoscope field, where xy has a maximum value of 1/4. Hence (41) is approximated by

$$xy + \frac{\tan 2V}{2\sqrt{2}}(y - x) = 0 \tag{42}$$

which is a rectangular hyperbola passing through the origin.

Now if (37) were a plot in gnomonic projection, with the plane of projection tangent to the unit sphere about the projection point, presumably this would mean taking

$$x_1 = \rho_1 \sin \psi = \frac{\tan 2V}{\sqrt{2}}$$

and this substitution makes (37) and (42) identical. This is the reason for the close agreement between Wright's curves and the predictions of (39). It seems remarkable that the gnomonic projection of a sphere that should be orthographically projected, combined with the planar analog of a law that applies to the surface of a sphere, should yield a result so nearly correct. It seems unlikely that there is anything specially suitable about the gnomonic projection, because the substitution $\rho_1 = \tan V$ in Michel-Levy's equation, (31), does not yield the correct result, (28).

11. Summary and Conclusion

The most useful result obtained with the present theory is a relation from which $2V$ can be measured in centered *Bxa* figures of large $2V$, and in centered *Bxo* figures. One measures the angle of stage rotation μ_o required to disperse the isogyres from a centered cross (extinction) to the edge of the interference field of radius

$$\rho_o = \sin \theta_o = \frac{\sin \theta_m}{n} = \frac{\rho_m}{n}$$

where θ_m is the half-aperture of the conoscope in air and n is the average index of refraction of the mineral examined. ρ_m is the numerical aperture of the objective lens. μ_o is then related to $\rho_1 = \sin V$ by

$$\frac{\rho_o^2}{1 - \frac{1}{2}\rho_o^2} = \frac{\rho_1^2}{1 - \frac{1}{2}\rho_1^2} \sin 2\mu_o$$

which is plotted in Fig. 14 for N.A. 0.85 and 0.65, and various values of n. Experimental verification of this relation is considered a verification of the theory here used. The relation does not depend on the validity of Mallard's law. It provides in particular a means for distinguishing between *Bxa* and *Bxo* figures.

An important practical feature of the theory is that, although the effect on isogyre position of the much-debated "rotation" of the polarization plane in the conoscope is small but definite, it can be entirely eliminated from the measurements simply by averaging the μ_o values obtained by turning from the two extinction positions (optic plane NS or EW).

An application of the theory to the optic axis figure shows that the 45° isogyre curves derived by Wright (1905) are very nearly correct, quite good enough for practical work. This seems remarkable, in view of the peculiar assumptions made in Wright's derivation of the curves.

The skiodrome theory gives incorrect isogyres, significantly incorrect even near the center of the field. Stereographic projection of the reference sphere would give a much better representation of the isogyre pattern. If the stereographic projection is carried out by the relation

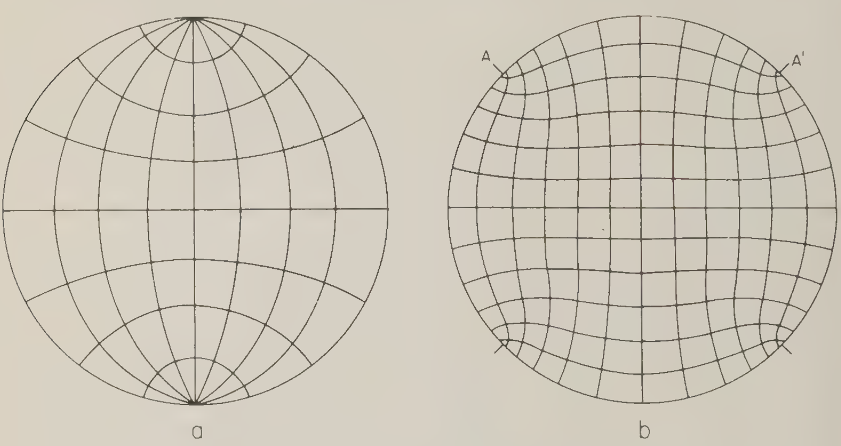

FIG. 19. "Extinction direction nets" for uniaxial flash figure (a) and optic normal figure with $2V=90°$ (b).

$$\rho' = 1.945 \tan \theta/2$$

the radial distance ρ' will differ little from the radial distance

$$\rho = \sin \theta$$

for orthogonal projection of the interference sphere, within the field of practical conoscopes ($\theta < 30°$). The outer portion of the stereographically projected pattern would be enlarged, but this part is never seen anyway.

The main advantage of the skiodrome is that the projected isotaques are easily calculated, at least when projected on the principal planes, where they are ellipses or hyperbolae. The same advantage probably will not accure to the stereographically projected curves. In principal it is possible to calculate the two orthogonal sets of curves of a net which would correctly represent the isogyres in the orthogonally projected interference sphere, according to the theory here developed. However, for quantitative purposes the direct approach used in this paper is more useful, and for qualitative purposes, as in teaching, a diagram can be drawn from qualitative considerations that shows all the features that are important, without the need of resorting to exact calculation of the net. Thus Fig. 19*a* represents the "extinction direction net" for the uniaxial flash figure—it rather resembles a stereographic projection of the reference sphere—and Fig. 19*b* represents the net for an optic normal figure of $2V=90°$.

ACKNOWLEDGMENTS

I wish to thank Prof. George Tunell and Prof. A. E. J. Engel for helpful advice and discussion. I am grateful to Prof. Horace Winchell for valuable suggestions and criticism of the manuscript.

REFERENCES

BECKE, F. (1904), *Denk. Akad. Wiss. Wien, Math.-Naturw. Klasse*, **75**.
——— (1905), *Tsch. Min. Pet. Mitt.*, **24**, 1–34.
——— (1909), *Tsch. Min. Pet. Mitt.*, **28**, 290–293.
BURRI, C. (1950), *Das Polarisationsmikroskop:* Basel.
EVANS, J. W. (1907), *Min. Mag.*, **14**, 276–280.
JOHANNSEN, A. (1918), *Manual of Petrographic Methods:* N. Y.
KAEMMERER (1913), *Fort. d. Min.*, **3**, 141–158.
MICHEL-LÉVY, A. (1888), *Les Minéraux d. Roches*, 94–95.
SOUZA-BRANDAO (1914), *Z. Krist.*, **54**, 113–119.
TRÖGER, W. E. (1956), *Optische Bestimmung der gesteinsbildenden Minerale:* Stuttgart.
WAHLSTROM, E. E. (1951), *Optical Crystallography:* N. Y.
WINCHELL, A. N. AND WINCHELL, H. (1951), *Optical Mineralogy*, Part II: N. Y.
WRIGHT, F. E. (1905), *Am. J. Sci.* (4), **20**, 285.
——— (1907), *Am. J. Sci.* (4), **24**, 317.
——— (1911a), *Am. J. Sci.* (4), **31**, 157–211.
——— (1911b), *Carnegie Inst. Wash. Pub.*, **158**, 75–76.
——— (1923), *J. Opt. Soc. Amer.*, **7**, 779–817.

THE AMERICAN MINERALOGIST, VOL. 43, NOVEMBER–DECEMBER, 1958

SASSOLITE FROM THE KRAMER BORATE DISTRICT, CALIFORNIA*

George L. Smith and Hy Almond,† *U. S. Geological Survey, Menlo Park California*, and Dwight L. Sawyer, *Trona, California*

Abstract

Sassolite (H_3BO_3), previously unreported from the Kramer Borate District, California, was found near the base of the borate-bearing shales underlying the ore body. Probertite, ulexite, colemanite, borax, and kernite, all found within the borate body, produce alkaline borate solutions (pH values of 8.3 to 9.2) when dissolved in water. Thus the presence of sassolite, which forms in an acidic environment, is distinctly anomalous.

Sodium, borate, and sulfate form the major portions of the water-soluble materials in the sassolite-bearing rocks; calcium and iron form lesser concentrations. Efflorescences of copiapite, mirabilite, sassolite, ulexite, borax and a little calcite and halite confirm the presence of their constituents in the wall rocks. The phase relationships between Na_2SO_4-$Na_2B_4O_7$-H_3BO_3-H_2O thus approximate the limiting conditions under which the sassolite probably formed. It is concluded that after lithification, sulfuric acid was formed by oxidation of iron sulfides by groundwater; this reacted with earlier formed borates to form acidic borate solutions, and from these sassolite was deposited at some temperature below about 35°.

The optical properties and x-ray patterns of sassolite and copiapite are given; an analysis of the copiapite shows it to contain iron, sulfate, and minor copper and phosphate.

Introduction

Sassolite, not previously reported from the Kramer Borate District, was found by two of the writers in the mine of the California Borate Company. Sassolite is normally the product of an acidic environment. In rocks characterized by borates that form strongly alkaline solutions, the presence of this acidic mineral is striking. The purpose of this paper is to describe the occurrence and properties of the mineral and to speculate briefly on its origin.

Sassolite has been reported previously in California from efflorescences around Siegler Springs in Lake County and Tuscan Springs in Tehama County (Bailey, 1902), from The Geysers, Sonoma Co. (R. L. Smith, this issue, page 1204), and from Death Valley (Allen and Kramer, 1957). It has also been found in spring deposits at Steamboat Springs, Nevada, and Yellowstone National Park (R. L. Smith, this issue). Several Italian, and Tibetan localities, some of which have been worked commercially for sassolite, are noted by Palache, Berman, and Frondel (1944).

Geology

Kramer Borate District

The Kramer ore body, located in southern California (Fig. 1), is the

---

* Publication authorized by the Director, U. S. Geological Survey.

† Present address: 3642 West 135th St., Hawthorne, Los Angeles County, California.

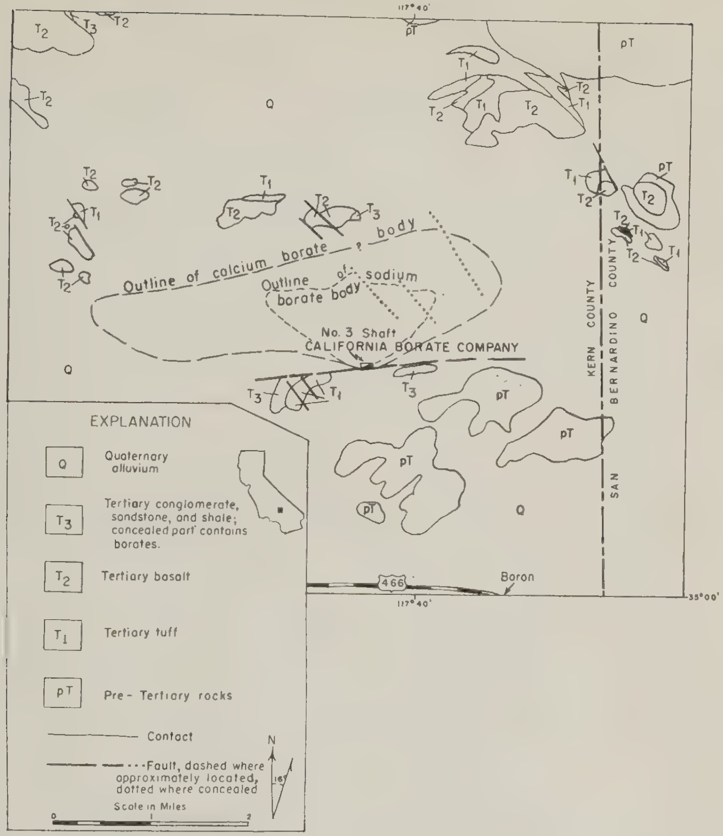
117°40'
pT
T2
T3
T1
Q
Outline of calcium borate body
Outline of sodium borate body
No. 3 Shaft
CALIFORNIA BORATE COMPANY
KERN COUNTY
SAN BERNARDINO COUNTY
Boron
466
35°00'
EXPLANATION
Q Quaternary alluvium
T3 Tertiary conglomerate, sandstone, and shale; concealed part contains borates.
T2 Tertiary basalt
T1 Tertiary tuff
pT Pre-Tertiary rocks
Contact
Fault, dashed where approximately located, dotted where concealed
N
16°
Scale in Miles
0
1
2

FIG. 1. Index map showing the location of the Kramer Borate District and the No. 3 Shaft of the California Borate Company. Geology and outline of the borate bodies after Gale (1946).

largest known deposit of sodium borates in the world. As described by Gale (1946), the sodium borate ore body, consisting chiefly of borax and kernite, occurs as a lenticular bed up to 250 feet thick which lies at depths varying from 300 to 1000 feet below the surface of the alluvial basin. The ore is surrounded by shales containing smaller percentages of calcium and sodium-calcium borates. The northern two-thirds of the borate body is underlain by basalt; the southern one-third is underlain by arkosic sandstone and conglomerate. Sandstone and conglomerate overlie the borate body at all places.

The matrix rock of the Kramer ore body is chiefly shale or clay, some of which appears to be beidellite (Schaller, 1930). Chemical analyses of the clay indicate an unusual concentration of lithium (Anon., 1956). Some beds of clay have notable concentrations of carbonaceous material.* Quartz, feldspar, and mica form the bulk of the coarser detritus; some beds contain fine-grained pyroclastics.

Schaller (1930) and Gale (1946) report the following borate minerals: borax and kernite form the bulk of the ore minerals; in the shale surrounding the ore body, probertite, ulexite, colemanite, and howlite are found. Lesserite and inderite have been described (Frondel, Morgan, and Waugh, 1956; Frondel and Morgan, 1956). Searlesite is locally abundant (R. C. Erd, written communication). The non-borate minerals listed by Schaller and Gale are pyrite(?), stibnite, realgar, chert, and calcite (or aragonite). Gerstleyite was described by Frondel and Morgan (1956). Unidentified iron sulfides and beds of analcime crystal sand are also found (R. C. Erd, written communication).

Sassolite locality

The chief sassolite locality occurs in the part of the D-level of the California Borate Company mine (the "Western Borax mine" of Gale's (1946) report) shown in Fig. 2a. This part of the mine is about 25 feet from the southernmost edge of the ore body, and stratigraphically in the northeast-dipping rocks underlying the ore. Traveling toward the north in this drift is equivalent to passing up through the section which underlies the ore. Figure 2b shows the approximate extent of the borate minerals. The solid lines indicate the ranges of the largest mineral concentrations, the dashed lines indicate the range of visible but smaller concentrations.

The largest concentrations of sassolite are in units 6 and 8 where the mineral is concentrated in rocks underlain by a trough of fault gouge. It is closely associated with probertite, searlesite, analcime, and a little gypsum. Here, the sassolite abundance increases back into the wall for a depth of at least six inches. Sassolite is also found in small amounts north and south of the main exposures in units 6 and 8, and throughout the rest of the mine where the rocks underlying the ore are penetrated.†

Sassolite very possibly existed prior to the opening of the mine. The chief mineral localities are along a mine drift that was enlarged several feet within the last few years. Other occurrences, along the underlying E-level, were noted only a few days after the workings were developed. Although the rocks throughout the mine are brecciated, there is no evi-

---

* A partial analysis (by H. Almond) of one such bed, at the base of unit 3 shown in figure 2b, shows the following percentages: $P_2O_5=0.06$, inorganic $CO_2=1.3$, organic C $=8.9$, total S as $SO_4=0.66$, As$=0.008$, Ge$=0.005$.

† Sassolite was subsequently found as an efflorescence at the exposed contact of shale and basalt in the Pacific Coast Borax Company mine during a visit by one of the writers.

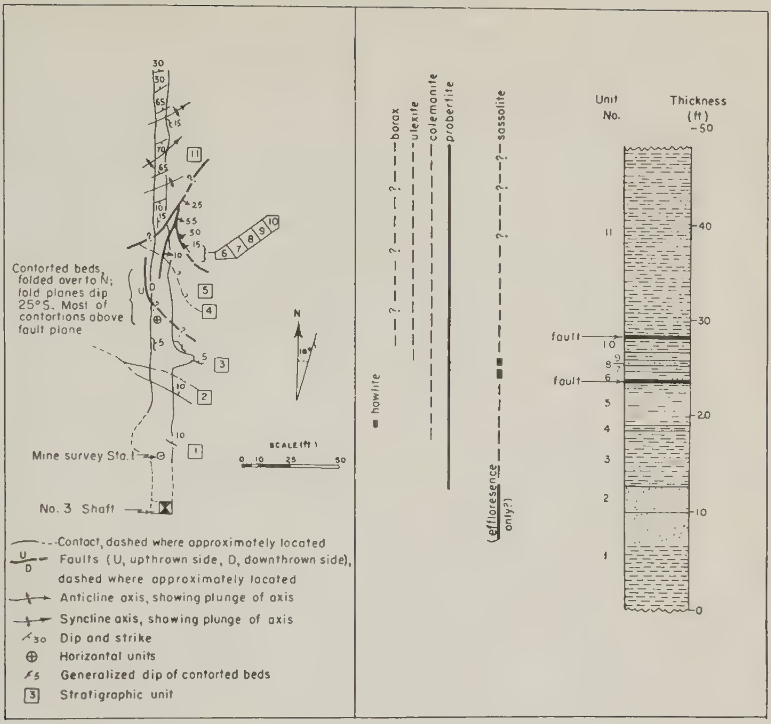
30
30
65
15
70
65
11
25
55
50
15
10
15
10
?
6
7
8
9
10
Contorted beds, folded over to N; fold planes dip 25°S. Most of contortions above fault plane
U
D
5
4
5
3
10
2
10
1
N
18°
Mine survey Sta. 1
SCALE (ft)
0 10 25 50
No. 3 Shaft
Contact, dashed where approximately located
Faults (U, upthrown side, D, downthrown side), dashed where approximately located
Anticline axis, showing plunge of axis
Syncline axis, showing plunge of axis
30 Dip and strike
Horizontal units
5 Generalized dip of contorted beds
3 Stratigraphic unit
borax
ulexite
colemanite
probertite
sassolite
howlite
(efflorescence only?)
Unit No.
Thickness (ft)
50
40
30
20
10
0
11
fault
10
9
8
7
6
fault
5
4
3
2
1

a. b.

FIG. 2a. Geologic map of a portion of the D-level of the California Borate Company mine, Kramer Borate District, California. Stratigraphic unit numbers refer to those shown in Fig. 2b. Mapped October, 1956.

FIG. 2b. Stratigraphic units exposed in the portion of the mine shown in Fig. 2a north of Mine Survey Station 1; also shown are the approximate stratigraphic ranges of the borate minerals present, the solid and dashed lines indicating major and minor amounts respectively. The lithologic symbols for sandstone, siltstone, and shale are those commonly used.

dence at most sassolite localities, or in thin sections, for the introduction of solutions since the workings were made.

The probertite probably formed later than the host rock (Schaller, 1930, p. 139) which consists of clastics, searlesite, analcime, and iron sulfides. The sassolite, in turn, was formed later than the probertite as it forms coatings on the surfaces of the probertite clusters. Consequently, these sassolite crystals, if also formed at depth, are unique. All other known deposits of sassolite were formed at or near the surface.

In moist parts of the mine, especially the upper part of unit 1 and unit 2, efflorescences occur on the mine walls and along cracks and joints within the rocks. The mineralogy of these is significant because they consist of the water-soluble materials in the wall rocks, and some of them are not detectable in the dry parts of the mine. The following efflorescent minerals have been found: mirabilite, copiapite, sassolite, ulexite, borax, and a little calcite and halite (R. C. Erd, written communication). The exact relationships between these minerals has not been determined, but apparently the first three tend to coexist to the exclusion of the others. The presence of copiapite and mirabilite shows that water-soluble sulfates exist within the rocks, although a little gypsum is the only sulfate mineral detected in the dry parts of the mine.

Mineral Descriptions

Sassolite

The sassolite crystals occur most abundantly as small flexible flakes which fill numerous fractures within the shale beds. Most of the crystals are 0.5 mm. or less in diameter, but some are as large as 5 mm. Several are about 5 microns thick. In the most abundant patches, sassolite flakes appear to cover as much as 75 percent of the hand specimen area; more commonly, however, they form only enough of the surface area to furnish a pearly "sparkle." In thin section, the mineral is seen to form the entire filling of lenticular veins that cut through the host rock. Individual veins range in size up to 0.3 mm. thick and 20 mm. long and commonly taper gradually to a featheredge.

Individually, the crystals are very thin colorless wafers, commonly with several edges conforming to a pseudohexagonal pattern. In reflected light, many flakes show interference colors ("Newton's rings"), mostly red or green. There is generally no preferred orientation of the individual crystals in hand specimen or thin section. The crystals show a fair to good pseudohexagonal parting.

Crystals lying on the basal plate or cleavage are nearly isotropic, β and α being nearly identical. The indices of refraction, determined in sodium light, are $\gamma' = 1.454 \pm 0.003$, $\alpha = 1.337 \pm 0.005$. The α index was measured in a mixture of acetone and water saturated with H_3BO_3, the mixture having a known refractive index. The apparent optic angle $(-2E)$ is very small and slightly variable. Dispersion is not apparent. Some crystals are faintly zoned(?) parallel to the pseudohexagonal faces. Polysynthetic twinning is found in most crystals; the twin law was not determined. An x-ray pattern of one sample gave the results shown in Table 1.

Copiapite and mirabilite

Neither copiapite nor mirabilite has been previously reported from the Kramer Borate District. Both occur as efflorescences and, for this reason,

TABLE 1. *X*-RAY POWDER DATA FOR BORIC ACID (C.P.), SASSOLITE, AND COPIAPITE

Fe/Mn radiation λ = 1.9373 Å

Boric acid[1] (C.P.)		Sassolite[2] (Kramer Borate District)		Copiapite[3] (Kramer Borate District)	
d Å	I	*d* Å	I	*d* Å	I
6.06	1	6.1	2	10.49	10
5.90	<1	5.9	1	8.90	<1?
4.80	<1	4.8	<1	8.01	1
4.60?	<1	4.60	<1	7.18	<1
4.21	1	4.27	<1	6.87	3
4.06	<1	4.05	<1	6.40	1
3.51	1	3.52	2	5.96	2
3.19	10	3.19	10	5.47	1
3.03	<1	3.04	<1	5.32?	1
2.96	<1	2.97	1	5.12	2
2.92	<1	2.92	1	4.92	2
2.84	<1	2.85	1	4.80	1
2.72	<1	2.73	<1	4.58	2
2.65	1	2.65	2	4.39	1
2.56	<1	2.57	1	4.15	3
2.50	<1	2.50	1	3.87	<1
2.30	<1	2.29	<1	3.75	1
2.25	<1	2.27	<1	3.66	3
2.23	<1	2.23	1	3.59	<1
2.17	<1	2.17	<1	3.43	4
2.10	<1	2.10	1	3.24	1
2.07	<1	2.07	<1	3.16	1
2.04	<1	2.05	<1	3.06	4
—		1.992	<1	3.01	<1
1.695	<1	1.697	<1	2.92	1
1.674	<1	1.674	<1	2.82	1
1.648	<1	1.654	<1	2.72	4
—		1.636	<1	2.64	1
1.593	1	1.598	1	2.57	2
				2.54	<1
				2.47	2
				2.41	3
				2.29	1
				2.18	<1
				2.09	1
				2.05	2
				1.992	2
				1.923	2
				1.873	1
				1.815	1
				1.786	3
				1.762	<1
				1.662	1
				1.621	<1
				1.600	1
				1.580	2
				1.510	2
				1.466	<1
				1.452	<1
				1.225	<1
				1.144	<1

---

[1] Sample ground for 1½ hours, scanned on diffractometer at rate of 1°/min., over the range 5° to 80°.

[2] Sample picked and ground slightly, mounted on glass fiber. Lines from glass have been omitted.

[3] Sample crushed but not ground. (On previous attempts, sample was ground and the pattern consisted of lines at 4.11 Å (10), 3.71 Å (5), 2.49 A (1), and a broad dark zone between 8–12 Å).

have only secondary importance in this paper. For the benefit of future workers, however, the habits and data for these minerals are given below.

The best copiapite efflorescences form as yellow balls, 0.1 to 0.5 mm. across. The most dense blooms cover the surface of the rock. Microscopically, the efflorescent material is a very fine-grained aggregate of crystals which have a faint yellow color. The optical properties are as follows (R. C. Erd, written communication):

$$\text{Opt.}(+)\qquad \begin{aligned} \alpha' &= 1.512 \pm 0.002 \\ \beta &= 1.534 \pm 0.002 \\ \gamma &= 1.576 \pm 0.002 \end{aligned}$$

The mineral is pleochroic with Y = colorless, Z = greenish yellow; 2V is about 70°. It is present as lath-shaped individuals flattened into "books" along $\{010\}$ and giving rise to radiating aggregates. Two distinct cleavages are visible. Extinction, parallel to one of them, gives an anomalous blue color. An *x*-ray pattern for this sample of copiapite is given in Table 1.

An analysis of 10 mg. of the same sample gives the following (H. Almond, analyst):

Fe = 27.0 percent
Cu = 0.5–0.6 percent
P_2O_5 = 0.15 percent
SO_4 = 46 percent
H_2O = 26 percent (by difference)

Tests for Mg and Ca were negative.

Mirabilite is found in small patches as a white "fuzz" where moisture has seeped through the mine walls. Individual fibers are commonly 5 to 10 mm. long. When collected and brought to the surface, the fibers collapsed and the mineral rapidly altered to thenardite.

ORIGIN OF SASSOLITE

On the basis of the field relationships, we conclude that the sassolite formed by the reaction of ground water on the earlier-formed sodium and calcium borates, iron sufides, and their host rocks. To further test this conclusion, two additional lines of evidence are considered: 1) the phase relationships between the associated minerals, and 2) the composition of the water-soluble portion of the sassolite-bearing rocks. It is reasoned that analyses of the water-soluble extract from these rocks should report the same constituents that were present in the sassolite-forming solutions, although the relative amounts of the constituents may be different. This premise may be wrong for solutions that deposit many minerals, but with a very soluble material (sassolite) as one of the precipitates, only a small number of still more soluble compounds could have passed through the rock without leaving a trace. All equally or less soluble

TABLE 2. PARTIAL COMPOSITION OF WATER SOLUBLE EXTRACT. ANALYSIS BY H. ALMOND

	Sample			
	Unit 8a	Unit 8b	Unit 6	Unit 2
BO_3	3.5 (6)	9.3 (16)	5.0 (8)	0.15 (0.3)
SO_4	2.4 (2)	2.3 (2)	2.9 (3)	1.0 (1)
Na	0.89 (4)	2.8 (12)	2.4 (10)	0.24 (1)
Ca	0.18 (0.4)	0.84 (2)	0.44 (1)	0.09 (0.2)
Fe	—	nil	nil	0.0025
pH	8.5	7.12	6.85	6.49

Values are in weight percents; parenthetical values are moles$\times 10^2$.

The sample numbers refer to those defined by Fig. 2b.

Unit 8a was digested with cold water; all others were digested with boiling water.

Qualitative tests on the solutions for chloride, carbonate, bicarbonate, phosphate, and nitrate were negative.

All pH values are of a slurry of ground-up sample and distilled water allowed to stand for 1.5 hours.

compounds will be represented in the analysis. Those only partly dissolved by the excess-water extraction will tend to exceed their original relative concentrations.

Table 2 shows the composition of the water-soluble portions of the sassolite-bearing rocks. Disregarding the calcium content, the system Na_2SO_4-$Na_2B_4O_7$-H_3BO_3-H_2O can be used to approximate the mineral and chemical environment found here. The relationships within this system are shown in Fig. 3. The pH values for these mixtures have been observed experimentally for the points bordering the sassolite field and are added to the diagrams. This figure shows three things of interest: 1) With increasing temperature, the sassolite field diminishes in size, and, if extrapolated linearly, ceases to exist above 35° C. 2) The stable associated sodium borate is $Na_2B_{10}O_{16}\cdot 10H_2O$, a form not known to occur naturally; this borate may exist in the vicinity of the sassolite deposists.* 3) All of

---

* Since this manuscript was written, this mineral has been found and named sborgite. C. cipriani, Un nuovo minerale fra i produtti boriferi di Larderello: *Atti accad. nazl. Lincei, Rend. classe sci. fis., mat. e nat.* **22,** 519–525, (1957).

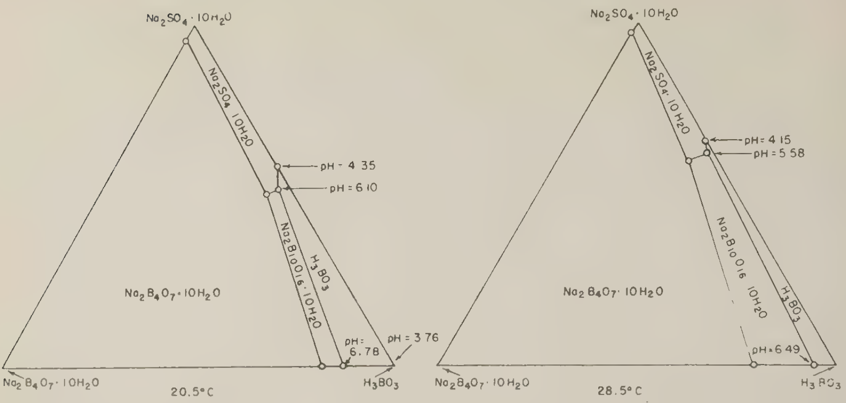

FIG. 3. The system Na_2SO_4-$Na_2B_4O_7$-H_3BO_3-H_2O at 20.5° C. and 28.5° C. The solid phases are borax ($Na_2B_4O_7 \cdot 10H_2O$), mirabilite ($Na_2SO_4 \cdot 10H_2O$), sassolite (H_3BO_3), and the synthetic sodium pentaborate. Analytical data recalculated from Teeple (1929, system XXI), pH values by H. Almond.

the solutions of this system which will precipitate sassolite are acidic.

In this borate body, circulating water is normally alkaline. Table 3 lists the pH values of solutions in contact with samples of the sodium, sodium-calcium, and calcium borates known to exist in the Kramer ore body. Solutions of kernite or tincalconite would resemble borax: howlite is not present in significant amounts. Sassolite cannot be deposited from solutions such as these.

Consequently, the problem of the origin of the sassolite is one of finding a source of acidifying solutions. The presence of the sulfates, gypsum, copiapite, and mirabilite, indicate sulfuric acid solutions in particular.

TABLE 3. THE pH OF SLURRIES OF CRUSHED BORATE MINERALS AND WATER

Sample	pH		
	1	2	3
ulexite	8.88	8.88	8.98
probertite	8.31	8.41	8.69
colemanite	8.94	8.93	9.10
borax (0.1N)	9.2		

1. The pH after standing 1.5 hours at 19° C.
2. The pH after standing 4.5 hours at 21.5° C.
3. The pH after standing 7 hours at 60° C.

The figure for borax is taken from the Handbook of Chemistry and Physics, 30th edition; other pH values by H. Almond.

The most probable explanation is as follows: Neutral ground water penetrated the lower part of the borate section, oxidized the unidentified iron sulfides found throughout the section, and produced sulfuric acid; this, in turn, reacted with the pre-existing borates and formed sassolite.

Reactions of sulfuric acid with the available borates might be as follows:

$$3H_2SO_4+\overset{\text{(probertite)}}{2CaNaB_5O_9\cdot 5H_2O}+14H_2O=$$

$$\overset{\text{(gypsum)}}{2CaSO_4\cdot 2H_2O}+\overset{\text{(mirabilite)}}{Na_2SO_4\cdot 10H_2O}+\overset{\text{(sassolite)}}{10H_3BO_3}$$

$$H_2SO_4+\overset{\text{(borax)}}{Na_2B_4O_7\cdot 10H_2O}+5H_2O=\overset{\text{(mirabilite)}}{Na_2SO_4\cdot 10H_2O}+\overset{\text{(sassolite)}}{4H_3BO_3}$$

$$2H_2SO_4+\overset{\text{(colemanite)}}{Ca_2B_6O_{11}\cdot 5H_2O}+4H_2O=\overset{\text{(gypsum)}}{2CaSO_4\cdot 2H_2O}+\overset{\text{(sassolite)}}{6H_3BO_3}$$

Reactions with ulexite, tincalconite, or kernite would differ only in the balance of water molecules. If calcite, aragonite, or the easily leached constituents of biotite were added to the reactions, additional sulfates would appear in the products. As written, each reaction produces sassolite and sodium or calcium sulfate, with three or more moles of sassolite being produced for each mole of the sulfate. Some corroboration of these reactions is found in the analyses for units 6 and 8 listed in Table 2 which have a BO_3 to SO_4 mole ratio of the correct order of magnitude. Furthermore, sassolite is abundant enough to be visible to the naked eye on the mine walls, whereas the coproducts, except for a little gypsum, are found only where they are concentrated as an efflorescence.

One problem remains: the manner in which water permeated the shale and clay. At present, groundwater penetrates only to the base of unit 3, whereas sassolite, which resulted from the oxidizing reactions of such water, is present in traces throughout the entire section shown in Fig. 2b. This excessive penetration may have resulted from greater hydrostatic pressures while buried at greater depth, from penetration before the sediments had reached their ultimate compaction, or from some unsuspected mechanism. More detailed work on the entire mining district is needed to supply this answer.

ACKNOWLEDGMENTS

The writers would like to thank the members of the California Borate Company for the thorough cooperation which was extended during this study. In particular, Messrs. George D. Dub, Kenneth Richmond, Blair Stewart, and Ralph Struve have made special efforts to help. Additional data and suggestions by R. C. Erd, of the U. S. Geological Survey, have improved the paper.

References

Allen, R. D. and Kramer, H. (1957), Ginorite and sassolite from Death Valley, California: *Am. Mineral.*, **42,** 56–61.

Anon. (1956), Lithium compounds: California State Div. Mines, Mineral Inf. Service, **9,** no. 9, 1–4.

Bailey, G. E. (1902), Saline deposits of California: Calif. State Mining Bureau Bull. **24.**

Frondel, C. and Morgan, V. (1956), Inderite and gerstleyite from the Kramer Borate District, Kern County, California: *Am. Mineral.*, **41,** 839–843.

Frondel, C., Morgan, V. and Waugh, J. L. T. (1956), Lesserite, a new borate mineral: *Am. Mineral.*, **41,** 927–928.

Gale, H. S. (1946), Geology of the Kramer Borate District, Kern County, California: *Calif. Jour. Mines and Geol.*, **42,** 325–378.

Palache, C., Berman, H. and Frondel, C. (1944), Dana's System of Mineralogy, 7th ed., v. 1, John Wiley & Sons, New York.

Schaller, W. T. (1930), Borate minerals from the Kramer District, Mohave Desert, California: U. S. Geol. Survey Prof. Paper **158,** 137–170.

Teeple, J. E. and Associates of A. P. & C. C. (1929), The industrial development of Searles Lake brines with equilibrium data: The Chemical Catalog Company, Inc., New York.

Manuscript received March 6, 1958.

THE AMERICAN MINERALOGIST, VOL. 43, NOVEMBER–DECEMBER, 1958

DIFFERENTIAL THERMAL ANALYSIS OF PYRITE AND MARCASITE

OTTO C. KOPP AND PAUL F. KERR, *Columbia University, New York, N. Y.*

ABSTRACT

Pyrite and marcasite were investigated by differential thermal analysis using a modification of a technique described by Kopp and Kerr (1957). Distinctive curves were obtained for both species. The initial oxidation peak of pyrite occurs at about 538° C. for a 50 mg. sample (125–149 micron fraction). Under the same conditions the initial oxidation peak of marcasite is noted at about 460° C. The writers believe that the lower peak temperature reflects the relative instability of marcasite in contrast to pyrite.

The thermal reaction products at 1000° C. are hematite and sulfur dioxide for both pyrite and marcasite. During the analysis pyrrhotite and other iron oxides may form as intermediate products. These may include maghemite and magnetite. At the completion of the oxidation reactions an endothermic reaction marks the Curie point.

Peak temperatures of both pyrite and marcasite are lowered by a decrease in grain size. The initial oxidation peak of marcasite merges with an adjacent higher peak for samples consisting of grains finer than 74 microns and only an inflection in the curve is noted.

Peak areas increase with increase in sample weight in a relatively uniform manner and greater detail is obtained for samples weighing more than 30 milligrams. Minor reactions which occur with increasing sample weight may result from oxygen depletion of the sample atmosphere. The heat evolved from the same weight of several pyrite and marcasite samples is found to be essentially the same.

INTRODUCTION

The differential thermal behavior of pyrite was briefly investigated during a preliminary study using a new apparatus designed for the analysis of minerals containing corrosive elements such as sulfur and arsenic (Kopp and Kerr, 1957). Subsequent work on sphalerite (Kopp and Kerr, 1958) has emphasized the importance of controlled conditions. A similar detailed study of pyrite and marcasite was undertaken in an attempt to enlarge fundamental data through use of the differential thermal method.

The chemical relationship of pyrite and marcasite has long been a subject of interest. Buerger (1934) states that, "The control of the precipitation of pyrite and marcasite by chemical environment suggests that these two minerals are not a dimorphous pair in the usual sense of the term, but rather that they are chemically distinct compounds. A critical study of all available analyses indicates that pyrite corresponds very closely to ideal FeS_2, but marcasite is definitely sulfur-low."

Hiller and Probsthain (1956), in their DTA investigations of the sulfides in an inert atmosphere, studied a group of Cu-Fe-S minerals including pyrite and marcasite. They note a small exothermic reaction for marcasite at about 520° C. Debye-Scherrer powder diagrams of material heated to about 500° C. produced only marcasite lines, but at 630° C.

the material yielded a true pyrite pattern. The authors conclude that under the conditions of differential thermal analysis a monotropic inversion from marcasite to pyrite occurs, and the Buerger equation may hold only for the formal character of pyrite and marcasite.

ACKNOWLEDGMENTS

The authors are indebted to Dr. Martin J. Buerger of the Massachusetts Institute of Technology and Dr. Edwin Roedder of the U. S. Geological Survey for their helpful discussions of the pyrite-marcasite relationship.

PROCEDURE

The method used is a modification of the technique previously described (Kopp and Kerr, 1957). Heating rate, grain size and sample weight were controlled within critical limits. The effect upon the peak parameters of sphalerite by changes in these factors has been noted (Kopp and Kerr, 1958). It was considered desirable in this study to determine whether heating rate, grain size and sample weight would influence the DTA curves of pyrite and marcasite in a similar way. Here peak temperatures appear to decrease with grain size as noted for sphalerite. However, sphalerite produced only one peak which increased in intensity with sample weight, but pyrite and marcasite exhibit additional peaks with increasing weight.

Samples were screened and those portions in the size range 125–149 microns were selected for analysis. Grain size ranges from >297 to <44 microns were also tested to ascertain the effect of size upon peak parameters. Sample weights of 50 ± 1 and 10 ± 1 mg. were used for analysis. Samples were mixed with alumina powder (250 microns) in glass vials and transferred directly to the sample well. The heating rate was kept at 12° to 13° C. per minute. No correction appeared necessary since all peaks were formed with this heating rate. All analyses were made at an amplification of 20×.

DIFFERENTIAL THERMAL BEHAVIOR OF PYRITE

Pyrite from Bingham, Utah (sample K-1) was crushed, sieved and the resulting grain size distributions subjected to differential thermal analysis. The effect of grain size was studied by testing various size fractions using the same sample weight (50 ± 1 mg.). The effect of sample weight was observed for 5 to 50 mg. samples of the 125–149 micron fraction.

The Effect of Grain Size

Several grain size fractions between 149–297 microns and <44 microns were analyzed under standard conditions. The results (Table 1 and Fig.

1) indicate a general decrease in temperature with grain size for the several oxidation peaks.

In general a decrease in peak temperature corresponds to a decrease in grain size, especially below 44 microns. With finer sizes certain peaks are not distinct, and only an inflection in the curve is observed. The final endothermic reaction at about 670° C. is small and may escape detection. This peak appears as two endothermic peaks for material finer than 44 microns. The first is almost negligible compared to the larger peak at 673° C.

TABLE 1. EFFECT OF GRAIN SIZE ON PEAK TEMPERATURE, PYRITE, BINGHAM, UTAH (SAMPLE K-1)

Sieve No. Range	Diameter Range (Microns)	Peak Temperatures (° C. ± 5° C.)					
50–100	149–297	(555 ↑)	595 ↓	602 ↑	—	—	—
100–120	125–149	(537 ↑)	578 ↓	600 ↑	—	—	—
120–200	74–125	540 ↑	582 ↓	600 ↑	—	—	—
200–325	44– 74	(530 ↑)	580 ↓	605 ↑	—	—	668 ↓
>325	<44	(512 ↑)	554 ↓ –574 ↑		605 ↓	628 ↑	673 ↓

540 ↑ Exothermic; 582 ↓ Endothermic; 554 ↓ –574 ↑ Inflection; (555 ↑) Estimated temperature for peak off record.

Discussion

The effect of grain size upon the shift in peak temperature is of interest. The temperature of the first exothermic peak decreases with grain size (see Table 1 and Fig. 1). This is because of the increased surface area available for oxidation as the grain size decreases. The intensity of the second exothermic peak ranges, and for material finer than 44 microns only an inflection between 553°–574° C. is observed. The intensity of the second peak indicates the amount of pyrite or other unoxidized material which remains after the initial supply of oxygen is depleted.

The 44–74 micron fraction yields a small endothermic peak at about 668° C. The thermal curve for the fraction finer than 44 microns shows an endothermic peak at about 673° C. several times as intense as that for the 44–74 micron fraction. Also, it is preceded by a minor endothermic peak. The cause of this peak at about 670° C. was investigated. It should be noted that before the reaction, at about 600° C., the material is magnetic, although outwardly appearing to be hematite. According to Mason (1943):

> "Confusion is especially marked with respect to the magnetic properties of α-Fe_2O_3. It has mostly been described as paramagnetic, the ferromagnetism reported by some workers

being put down to the presence of intermixed magnetite or other ferrites. However, other investigators have positively stated that α-Fe_2O_3 even when quite free from Fe_3O_4 is ferromagnetic; thus Chaudron and Forestier even determined the Curie point of α-Fe_2O_3 and found that it was at 675°, considerably higher than that of magnetite (590°). This might be considered to settle the question, were it not for the recent experiments by Michel on γ-Fe_2O_3 stabilized by the addition of small amounts of sodium ferrite. He found that the (extrapolated) Curie point for γ-Fe_2O_3 was exactly at 675°. The supposed ferromagnetic character of α-Fe_2O_3 is thus very doubtful, since a small amount of γ-Fe_2O_3 in the material investigated by Chaudron and Forestier would suffice to explain their results very well without the necessity of ascribing ferromagnetic properties to α-Fe_2O_3."

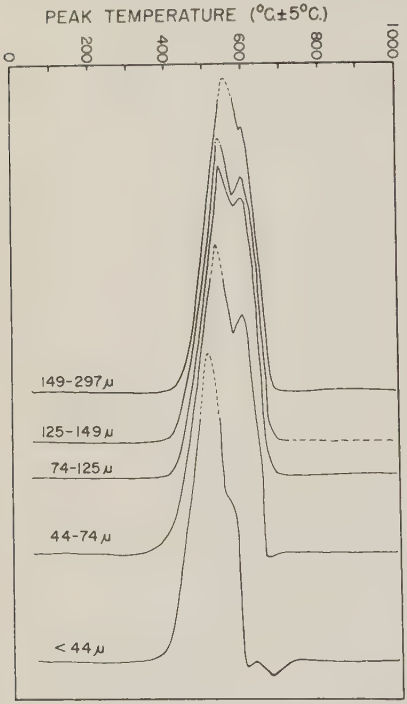

FIG. 1. The effect of grain size on peak temperature. Pyrite (sample K-1), 50 milligram samples.

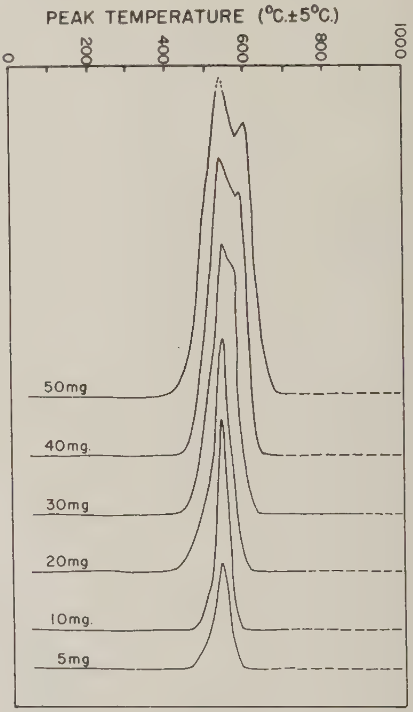

FIG. 2. The effect of sample weight on the peak parameters. Pyrite (sample K-1) 125–149 microns.

Schmidt and Vermaas (1955) investigating the differential thermal properties of magnetite report, "The temperature of 580° C. where the second reaction begins, remains absolutely constant for all samples examined and is preceded by a very small endothermic peak, the intensity of which is depressed by the second exothermic reaction. It is interesting to note that the so-called Curie point, where the ferromagnetism of magnetite changes to paramagnetism occurs at 590° C."

It appears then that the Curie point may be recognized by differential thermal analysis. The endothermic peak determined for pyrite at about 670° C. appears to be somewhat high compared to the Curie point of magnetite at 590° C. Maghemite (γ-Fe_2O_3) is also ferromagnetic, and as pointed out by Mason (1943), the extrapolated Curie point of γ-Fe_2O_3 is about 675° C.

Pyrite (sample K-1; less than 44 microns, 50 milligrams) was heated in air to 610° C. at which time the furnace was removed and the material allowed to cool in air. The resulting material was ferromagnetic. An *x*-ray powder diagram of this material contained lines which do not belong to hematite. At least one of these lines at 2.87 Å may result from either magnetite or maghemite. This spacing is slightly low compared to the 2.97 Å line of magnetite or the 2.95 Å line of maghemite. However, a similar pattern of marcasite at 620° C. has a less intense line at about 2.99 Å. The spacing and intensity of this line may vary during the oxidation process. A weak line at about 2.04 Å corresponds closely with the strongest line of α-Fe (Swanson, *et al.*, 1955).

The interplanar spacings and their intensities for pyrite heated to 610° C. are listed in Table 2.

The intensity of the endothermic reaction appears to increase with decreasing grain size. It is also apparent (Figs. 1 and 3) that the intensity of the corresponding peak for marcasite is much greater than that of pyrite, and this endothermic reaction is observed for all the grain size ranges of marcasite tested, whereas it is only observed for fractions finer than 74 microns for pyrite. The peak temperature of the endothermic peak appears to increase with decreasing grain size for both pyrite and marcasite.

The following interpretation for the thermal reactions of pyrite varying with grain size is based upon the differential thermal curves and *x*-ray study of the material. The peak temperature of the first oxidation reaction decreases with grain size as a result of the increased surface area available for oxidation. The second oxidation peak varies somewhat in intensity and reflects the amount of unoxidized material still present after the first peak. The second peak is inhibited until sufficient oxygen becomes available for oxidation to proceed. The endothermic reaction at about 670° C. represents the Curie point of the ferromagnetic material formed during the oxidation reaction. This is only apparent for the finer grain sizes. Since the finer grain sizes oxidize more rapidly and produce sulfur dioxide more rapidly, there is a greater possibility that incomplete

TABLE 2. REACTION PRODUCTS OF PYRITE (SAMPLE K-1)
HEATED IN AIR TO 610° C.

Pyrite (K-1)[1] At 610° C.		Hematite[2]		Magnetite[3]		Maghemite[4]	
d(Å)	I	*d*(Å)	I	*d*(Å)	I	*d*(Å)	I
—	—	—	—	—	—	5.90	2
—	—	—	—	4.86	30	4.82	5
—	—	—	—	—	—	4.18	1
3.66	20	3.68	70	—	—	3.73	5
—	—	—	—	—	—	3.41	2
2.87	30	—	—	2.97	60	2.95	34
—	—	—	—	—	—	2.78	19
2.68	100	2.69	100	—	—	—	—
2.51	80	2.51	80	2.530	100	2.52	100
—	—	—	—	2.425	10	2.41	1
—	—	—	—	—	—	2.32	6
2.20	30	2.20	70	—	—	—	—
2.07	5	2.07	10	2.097	50	2.08	24
2.04	10	—	—	—	—	—	—
1.834	40	1.837	70	—	—	1.87	0.5
1.691	60	1.691	80	1.714	40	1.70	12
—	—	1.634	10	—	—	—	—
1.597	30	1.596	40	1.615	60	1.61	33
—	—	—	—	—	—	1.55	0.5
—	—	—	—	—	—	1.53	1
1.483	40	1.484	70	1.484	70	1.48	53

[1] Copper radiation, Debye-Scherrer camera, 11.46 cm. diameter.

[2] Rooksby, H. P., (1951), X-ray Identification and Crystal Structure of Clay Minerals, G. W. Brindley, ed., Mineralogical Society, London, p. 264.

[3] *Ibid.*, p. 264.

[4] A.S.T.M. *X*-ray Powder Data File, Card No. 4-0755 (original reference unobtainable).

oxidation will occur. For material finer than 44 microns the larger peak is preceded by a smaller endothermic reaction. The peak at 670° C. may represent the Curie point of the maghemite present while the preceding peak that of magnetite or other partially oxidized iron present.

The Effect of Sample Weight

Samples of pyrite from Bingham, Utah (sample K-1) were analyzed to determine the effect of weight on the peak parameters (temperature and area). Since composite peaks result for samples weighing more than 30 milligrams, peak heights and widths were not measured. However, the peak areas were measured with a polar planimeter to the nearest 0.1 inch. Peak temperatures and areas for pyrite weighing from 5 to 50 milligrams were determined. These data are presented in Table 3 and illustrated in Fig. 2. For samples weighing less than 30 milligrams, only one peak (at about 540° C) appears in the thermal record. At about 30 milligrams an inflection in the curve is first noted, and for samples weighing 40 milligrams or more a second exothermic peak appears.

TABLE 3. THE EFFECT OF SAMPLE WEIGHT ON THE PEAK PARAMETERS, PYRITE, BINGHAM, UTAH (SAMPLE K-1)

Sample Weight	Peak Temperatures			Total Area Under Peaks
(±1 mg.)	(° C. ±5° C.)			(In.^{2}, Planimetric)
5	544 ↑	—	—	0.5
10	538 ↑	—	—	1.2
20	541 ↑	—	—	2.3
30	541 ↑	563 ↓	– 573 ↑	3.7
40	538 ↑	580 ↓	588 ↑	4.7
50	(537 ↑)	578 ↓	600 ↑	5.9 est.

544 ↑ Exothermic; 580 ↓ Endothermic; 563 ↓ –573 ↑ Inflection; (537 ↑) Estimated temperature for peak off record.

Discussion

Earlier curves for the same material (Kopp and Kerr, 1957) also show two exothermic peaks for the oxidation reaction for a sample to inert filler ratio of about 1:15. At this time it was stated that the two peaks might result from two exothermic reactions, or that they might result from the effect of the reaction products which "will alter the reaction rate and peak temperatures, and may even introduce secondary reactions by surrounding the material with an atmosphere other than air."

Hiller and Probsthain (1956) working in an atmosphere of nitrogen, determined that under these conditions of differential thermal analysis, pyrite did not dissociate into FeS, but rather to pyrrhotite (Fe_7S_8). To determine the nature of the second peak pyrite (sample K-1; 44–74 microns, 50 mg.) was heated in air to 580° C. and then cooled rapidly in carbon dioxide. The resulting material was analyzed by *x*-ray powder photography with the Debye-Scherrer camera. The results (Table 4) indicate that the major reaction product is hematite.

The strongest line of pyrite at 1.6332 Å appears to be absent, indicating that almost all of the pyrite has been oxidized. A small amount, sufficient

TABLE 4. REACTION PRODUCTS OF PYRITE (SAMPLE K-1) HEATED TO 580° C.

Pyrite at 580° C. Sample K-1[1]		Hematite[2]		Pyrite[3]	
d(Å)	I	*d*(Å)	I	*d*(Å)	I
3.70	40	3.68	70	—	—
—	—	—	—	3.128	36
2.70	100	2.69	100	2.709	84
2.52	80	2.51	80	—	—
—	—	—	—	2.423	66
2.20	30	2.20	70	2.2118	52
—	—	2.07	10	—	—
—	—	—	—	1.9155	40
1.839	50	1.837	70	—	—
1.693	50	1.691	80	—	—
—	—	1.634	10	1.6332	100
1.598	20	1.596	40	—	—
—	—	—	—	1.5640	14
—	—	—	—	1.5025	20
1.483	40	1.484	70	1.4479	24

[1] Copper radiation, Debye-Scherrer camera, 11.46 cm. diameter.

[2] Rooksby, H. P., (1951), *X*-ray Identification and Crystal Structure of Clay Minerals, G. W. Brindley, ed., Mineralogical Society, London, p. 264.

[3] Swanson, H. E., Gilfrich, N. T. and Ugrinic, G. M. (1955), Standard *X*-ray Diffraction Powder Patterns: NBS Circ. 539, v. V, p. 30.

to produce the second exothermic peak might not be observed by the *x*-ray powder method. The strong pattern of hematite may mask the presence of other iron compounds. For example, the two strongest lines of maghemite (γ-Fe_2O_3) occur at 2.52Å and 1.48 Å (A.S.T.M. Card No. 4-0755). Magnetite's strong lines are 2.530 Å and 1.484 Å (Rooksby, 1951). Pyrrhotite has its most intense line at 2.06 Å (Harcourt, 1942). Minor amounts of any of these compounds might escape detection. Also, since several reactions may be taking place during the oxidation, some of the products may not attain sufficient size to reflect the *x*-ray beam.

Based on the thermal pattern observed and *x*-ray study of the material obtained before the reaction has gone to completion, the following interpretation is given for the reaction: small amounts of pyrite when subjected to differential thermal analysis in air are oxidized essentially to hematite (this material is magnetic until heated to about 700° C.). Small amounts of pyrite may remain, and the presence of other iron compounds may be masked by the large amount of hematite formed. Although Hiller and Probsthain (1956) noted that pyrite was converted to pyrrhotite when heated in nitrogen, pyrrhotite was not detected in the x-ray study of the material heated in air. Apparently, the relatively large amount of sulfur dioxide formed by a sample of pyrite weighing more than 30 mg., impedes the reaction until sufficient oxygen becomes available for the reaction to continue. With the supply of additional oxygen the small amount of remaining pyrite (or possibly the small amount of pyrrhotite formed under non-oxidizing conditions) then oxidizes causing the second exothermic peak. This peak increases in intensity and peak temperature as the amount of sample increases.

Differential Thermal Behavior of Marcasite

Marcasite from Ottawa County, Oklahoma (sample K-11) was crushed and sieved. The resulting grain size distributions were analyzed to determine the effect of grain size and sample weight under standard conditions.

The Effect of Grain Size

Several grain size fractions from >297 microns to <44 microns were tested using a sample weight of 50 ± 1 mg. The results (Table 5 and Fig. 3) indicate a general decrease in temperature with grain size for the several oxidation peaks.

A general decrease in peak temperature for the oxidation reactions is noted with decreasing grain size, especially below 44 microns. The first exothermic peak gradually coalesces with the second exothermic peak as the grain size decreases. The peak temperature of the final endothermic peak appears to increase with decreasing grain size. Also, this peak appears to subdivide into a few smaller peaks besides the major peak as the grain size decreases. The intensity of the final endothermic peak from about 645°–692° C. appears to increase with decreasing grain size.

Discussion

The effect of grain size for 50 ± 1 mg. samples of marcasite was determined. The peak temperatures of the exothermic peaks decrease with grain size (see Table 5 and Fig. 3). The initial peak temperature decreases from about 462° C. for material larger than 297 microns to an inflection between 410–422° C. for material finer than 44 microns. The second exothermic peak decreases from about 562° C. for material larger than 297 to about 475° C. for material finer than 44 microns. The major endothermic reaction increases in peak temperature from about 645° C. for material larger than 297 microns to 692° C. for material finer than 44 microns. There is also a marked increase in intensity for this endothermic

Table 5. Effect of Grain Size on Peak Temperature, Marcasite, Ottawa County, Oklahoma (sample K-11)

Sieve No. Range	Diameter Range (Microns)	Peak Temperatures (° C. ± 5° C.)									
<50	>297*	462↑	492↓		(562↑)		—	—	—	—	645↓
50-100	149–297	456↑	482↓		(550↑)		—	—	—	—	652↓
100–120	125–149	440↑	482↓	530↑	564↓	575↑	—	—	—	—	655↓
120–200	74–125	445↑	472↓	525↑	556↓–565↑		—	—	—	—	662↓
200–325	44– 74	422↑	– 437↓		(495↑)		—	—	585↓	626↑	673↓
>325	<44	410↑	– 422↓		(475↑)		548↓	565↑	597↓	628↑	692↓

* 38 ± 1 mg. sample.

462↑ Exothermic; 492↓ Endothermic; 555↓–565↑ Inflection; (562↑) Estimated temperature for peak off record.

peak as the grain size decreases. One or two additional minor endothermic peaks are observed for material finer than 125 microns. X-ray powder photographs of marcasite (sample K-11; 44–74 microns, 50 mg.) heated in

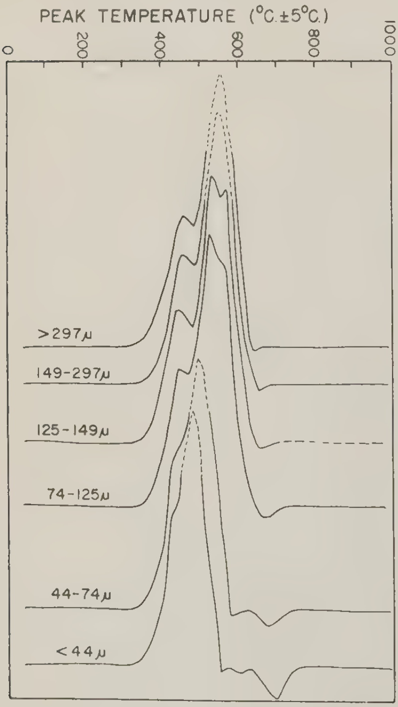

Fig. 3. The effect of grain size on peak temperature. Marcasite (sample K-11), 50 milligram samples.

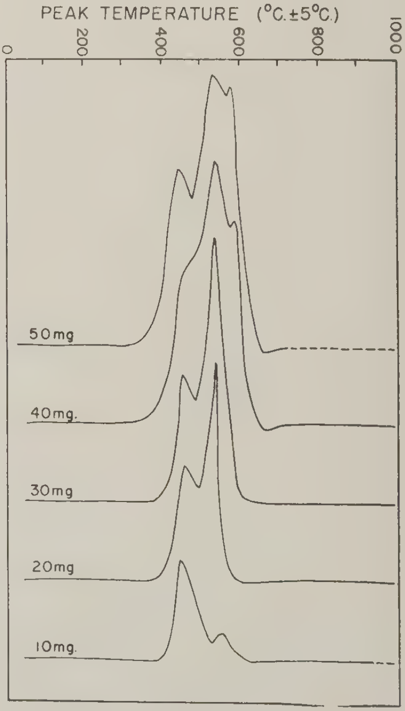

Fig. 4. The effect of sample weight on the peak parameters. Marcasite (sample K-11), 125–149 microns.

Table 6. Reaction Products of Marcasite (sample K-11) Heated to 620° C.

Marcasite at 620° C.[1]		Hematite[2]		Maghemite[3]		Magnetite[4]	
d(Å)	I	*d*(Å)	I	*d*(Å)	I	*d*(Å)	I
—	—	—	—	5.90	2	—	—
—	—	—	—	4.82	5	4.86	30
—	—	—	—	4.18	1	—	—
3.65	30	3.68	70	3.73	5	—	—
—	—	—	—	3.41	2	—	—
2.99	10	—	—	2.95	34	2.97	60
—	—	—	—	2.78	19	—	—
2.70	100	2.69	100	—	—	—	—
2.52	80	2.51	80	2.52	100	2.530	100
—	—	—	—	2.41	1	2.425	10
—	—	—	—	2.32	6	—	—
2.20	20	2.20	70	2.23	0.5	—	—
—	—	2.07	10	2.08	24	2.097	50
1.836	30	1.837	70	1.87	0.5	—	—

[1] Copper radiation, Debye-Scherrer camera, 11.46 cm. diameter.

[2] Rooksby, H. P. (1951), *X*-ray Identification and Crystal Structure of Clay Minerals, G. W. Brindley, ed. Mineralogical Society, London, p. 264.

[3] A.S.T.M. *X*-ray Powder Data File, Card No. 4-0755 (original reference unobtainable).

[4] Rooksby, *op. cit.*, p. 264.

air to 630° C. indicate that maghemite and magnetite may be present. These data are listed in Table 6.

The interpretation for the variation in thermal reactions of marcasite with grain size is based upon the differential thermal curves and *x*-ray study of the material. The peak temperatures of the oxidation reactions decrease with grain size as a result of the increased surface area available for oxidation. The initial peak occurs at a lower temperature than for pyrite under the same test conditions (see Tables 1 and 5, and Figs. 1 and 3). This is thought to reflect the relative instability of marcasite compared with pyrite. The second exothermic reaction occurs at about the same temperature as the initial pyrite reaction, and may indicate that a transformation to pyrite occurs at the surfaces of the unoxidized marcasite. This pyrite would be oxidized rapidly to hematite and the magnetic iron oxides. The endothermic reaction (Curie point) which occurs at about 650-690° C. increases in peak temperature with decreasing grain size. As the grain size decreases, oxidation will proceed more rapidly. This in turn produces sulfur dioxide more rapidly, allowing the reaction to proceed in a reducing rather than an oxidizing environment. Under these conditions, maghemite or the partially oxidized iron compounds may form.

Effect of Sample Weight

The peak parameters for marcasite (sample K-11) were determined for samples weighing 10 to 50 mg. These data are presented in Table 7 and illustrated in Fig. 4. An initial exothermic peak at about 450° C. is observed for all samples. A second exothermic peak at about 535° C. also occurs, and for samples weighing more than 30 mg. two peaks are noted in a manner similar to pyrite. A final minor peak (endothermic) occurs at about 655° C. for samples weighing more than 30 mgs.

Table 7. The Effect of Sample Weight on the Peak Parameters, Marcasite, Ottawa County, Oklahoma (sample K-11)

Sample Weight (±1 mg.)	Peak Temperatures (° C. ±5° C.)						Total Area Under Peaks (In.^{2}, Planimetric)
10	445 ↑	520 ↓	540 ↑	—	—	—	1.1
20	455 ↑	492 ↓	535 ↑	—	—	—	2.5
30	449 ↑	484 ↓	535 ↑	—	—	—	3.5
40	452 ↑	–482 ↓	534 ↑	573 ↓	582 ↑	655 ↓	5.0
50	440 ↑	482 ↓	530 ↑	564 ↓	575 ↑	655 ↓	5.9

445 ↑ Exothermic; 520 ↓ Endothermic; 452 ↑ –482 ↓ Inflection.

Discussion

The initial exothermic reaction of marcasite (125–149 microns) heated in air occurs at about 450° C. or about 90° C. below the corresponding initial exothermic reaction of pyrite. The intensity of this first peak increases slightly with increased sample weight, but not proportionally. The second exothermic peak occurs at about 535° C. and increases rapidly in intensity. For samples weighing more than 30 milligrams this peak becomes two peaks as was observed for pyrite. The close correspondence of the second exothermic peak of marcasite at 535° C. with the first exothermic peak of pyrite at about 540° C. suggests that a transformation from marcasite to pyrite may have occurred. However, *x*-ray powder photographs of marcasite (sample K-11; 125–149 microns, 50 mg.) heated to 480° C. and cooled rapidly in carbon dioxide indicate that hematite is the major reaction product. Some marcasite remains, and the presence of pyrite at this stage is doubtful since the strongest line of pyrite at 1.6332 Å is not present. The results are presented in Table 8.

Hiller and Probsthain (1956) working in an inert atmosphere noted a small flat exothermic peak for marcasite at a temperature of about 520° C. Above this temperature the thermal curve corresponds to that of pyrite. (They also state that the same inversion point has been found by ordinary thermal analysis to be 520-535° C.) *X*-ray photographs of material heated to 500° C. produced only marcasite lines, while a test of material heated to 630° C. yielded a true pyrite pattern.

TABLE 8. REACTION PRODUCTS OF MARCASITE (SAMPLE K-11) HEATED TO 480° C.

Marcasite at 480° C.[1] Sample K-11		Hematite[2]		Marcasite[3]		Pyrite[4]	
d(Å)	I	*d*(Å)	I	*d*(Å)	I	*d*(Å)	I
3.67	10	3.68	70	—	—	—	—
3.43	5	—	—	3.44	60	—	—
—	—	—	—	—	—	3.1280	36
2.96	5	—	—	2.96	40	—	—
2.70	100	2.69	100	2.70	100	2.7088	84
2.52	60	2.51	80	2.55	20	—	—
2.41	10	—	—	2.41	70	2.4281	66
2.30	10	—	—	2.31	70	—	—
2.20	10	2.20	70	—	—	2.2118	52
—	—	2.07	10	2.10	20	—	—
—	—	—	—	2.05	20	—	—
—	—	—	—	1.94	40	—	—
1.908	10	—	—	1.91	60	1.9155	40
1.834	20	1.837	70	1.87	10	—	—
1.755	20	—	—	1.76	90	—	—
—	—	—	—	1.72	30	—	—
1.691	20	1.691	80	1.69	50	—	—
—	—	—	—	1.67	40	—	—
—	—	1.634	10	—	—	1.6332	100

[1] Copper radiation, Debye-Scherrer camera, 11.46 cm. diameter.

[2] Rooksby, H. P. (1951), *X*-ray Identification and Crystal Structures of Clay Minerals, G. W. Brindley, ed., Mineralogical Society, London, p. 264.

[3] A.S.T.M. *X*-ray Powder Data File, Card No. 2-0908 (original references unobtainable).

[4] Swanson, H. E., Gilfrich, N. T. and Ugrinic, G. M. (1955), Standard *X*-ray Diffraction Powder Patterns: NBS Circ. 539, v. V, p. 30.

A small endothermic reaction at about 655° C. occurs for samples weighing more than 30 mg. (125–149 microns). As in the case of pyrite this endothermic reaction is believed to represent the Curie point of the ferromagnetic material formed during the oxidation.

Based on the thermal records produced and *x*-ray study of the material obtained before the reaction has gone to completion, the following interpretation is given for the reactions: marcasite, when heated in air starts to oxidize at a lower temperature than pyrite. At the completion of this first peak, hematite and marcasite appear to be the major components. Pyrite is not detected. The reaction may produce this initial peak either as a result of the early depletion of oxygen, or the initial peak may represent the surficial oxidation of marcasite to hematite. As the temperature is raised the transformation of marcasite to pyrite may take place at the surfaces of the remaining marcasite, and this "nascent" pyrite is oxidized rapidly producing the second exothermic reaction. As the sample weight is increased a small endothermic peak is observed at about 655° C. which represents the Curie point of the ferromagnetic material formed during the oxidation.

A COMPARISON OF SEVERAL PYRITES AND MARCASITES

Four additional samples of pyrite and three of marcasite were analyzed to determine the variations in peak parameters for different samples. Samples weighing 10 and 50 mg. were analyzed. The grain size used was 125–149 microns. The sample localities are listed in Table 9.

TABLE 9. SAMPLE LOCALITIES

Sample Number	Locality
Pyrite	
K-1	Bingham, Utah
K-2	Yak Mine, Leadville, Colorado
K-3	Isle of Elba
K-4	Brazil
K-10	Saratoga Mine, Central City, Colorado
Marcasite	
K-11	Ottawa County, Oklahoma
K-12	Joplin, Missouri
K-13	Brux, Bohemia
K-14	Pitcher, Oklahoma

Thermal curves for these samples are illustrated in Fig. 5 and 6. The peak parameters are listed in Tables 10 and 11.

Under equivalent conditions (sample weight, heating rate and grain size) several samples of pyrite appear to agree closely in the general appearance of thermal curves and peak parameters. In general for a 10 mg. sample only one exothermic peak is observed at 543° C. ± 5° C. For a 50 mg. sample, two exothermic peaks are observed, the first at 538° C.

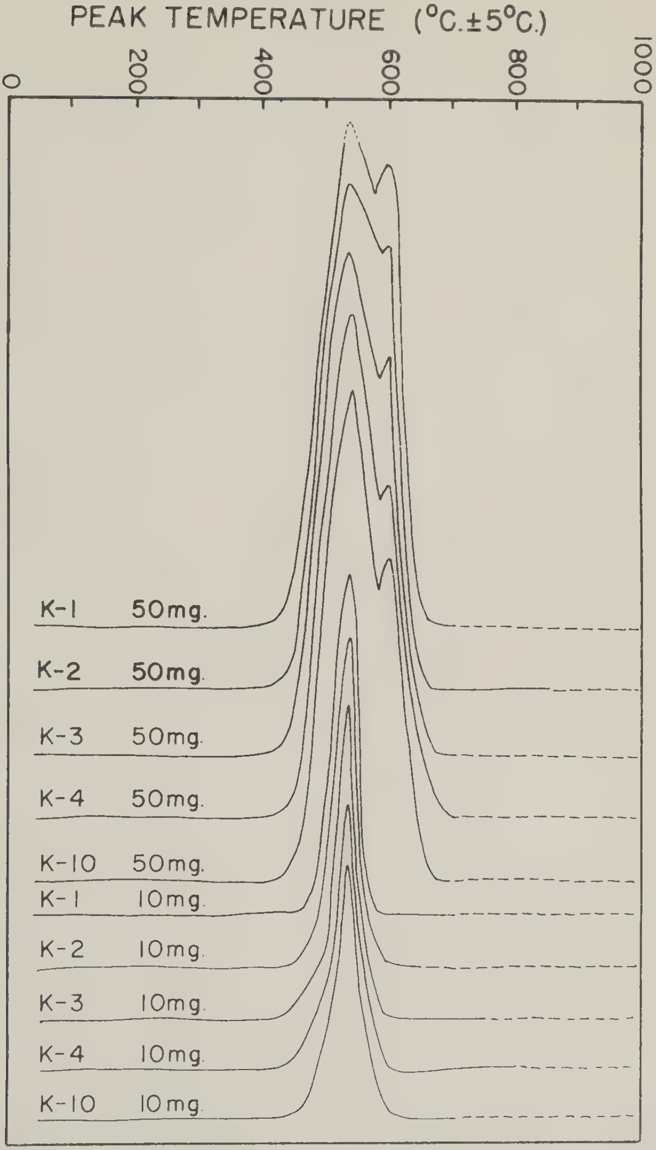

FIG. 5. Selected pyrite DTA curves. 125–149 micron fraction, 10 and 50 milligram samples.

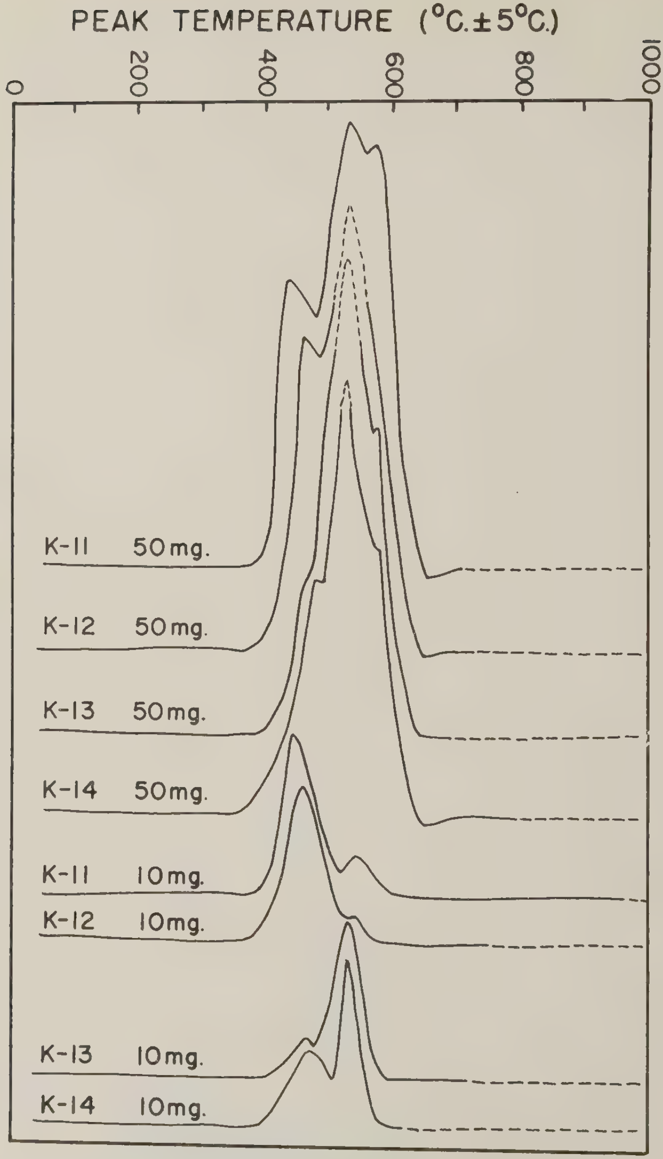

FIG. 6. Selected marcasite DTA curves. 125–149 micron fraction, 10 and 50 milligram samples.

TABLE 10. PEAK PARAMETERS FOR SEVERAL PYRITES (125–149 MICRONS) (10± MILLIGRAM SAMPLES)

Sample Number	Peak Temperatures (° C. ± 5° C.)			Peak Areas (In.^{2}, Planimetric)
K-1	538 ↑			1.2
K-2	544 ↑			1.2
K-3	545 ↑			1.4
K-4	548 ↑			1.1
K-10	542 ↑			1.0
	(50 ± 1 Milligram Samples)			
K-1	(537 ↑)	578 ↓	600 ↑	5.9 est.
K-2	(538 ↑)	590 ↓	598 ↑	6.2 est.
K-3	535 ↑	585 ↓	608 ↑	5.9
K-4	540 ↑	585 ↓	600 ↑	6.0
K-10	(541 ↑)	581 ↓	600 ↑	6.2 est.

535 ↑ Exothermic; 578 ↓ Endothermic; (537 ↑) Estimated peak temperature for peak off record.

TABLE 11. PEAK PARAMETERS FOR SEVERAL MARCASITES (125–149 MICRONS) (10 ± 1 MILLIGRAM SAMPLES)

Sample Number	Peak Temperatures (° C. ± 5° C.)						Peak Areas (In.^{2}, Planimetric)
K-11	445 ↑		520 ↓		540 ↑		1.1
K-12	462 ↑		528 ↓		538 ↑		1.1
K-13	465 ↑		475 ↓		528 ↑		1.3
K-14	470 ↑		504 ↓		529 ↑		1.0
	(50 ± 1 Milligram Samples)						
K-11	440 ↑	482 ↓	530 ↑	564 ↓	575 ↑	655 ↓	5.9
K-12	465 ↑	488 ↓	(532 ↑)	—	—	655 ↓	6.4 est.
K-13	455 ↑	– 480 ↓	(530 ↑)	580 ↓	583 ↑	—	6.2 est.
K-14	480 ↑	490 ↓	(535 ↑)	585 ↓	595 ↑	658 ↓	6.2 est.

440 ↑ Exothermic; 482 ↓ Endothermic; 455 ↑ –480 ↓ Inflection; (532 ↑) Estimated temperature for peak off record.

± 5° C. and the second at 603° C. ± 5° C. The peak areas agree closely, the area for a 50 mg. sample being approximately 6.1 in.^{2} and the area for a 10 mg. sample about 1.2 in.^{2}

Several samples of marcasite under the same test conditions also have the same general thermal curves and peak parameters. However, the agreement is not as close as for pyrite. This may be attributed to the relative instability of marcasite compared with pyrite. For a 10 mg. sample two exothermic peaks are observed. The first occurs at 458° C. ± 13° C and the second at 534° C. ± 6° C. For a 50 mg. sample two exothermic reactions are also observed for all samples, the first at 460° C. ± 20° C. and the second at 532° C. ± 3° C. A third exothermic peak may be observed at 585° C. ± 10° C., and an endothermic reaction may be observed at about 655° C. It is of interest to note that the peak showing the widest variation in peak temperature is the initial oxidation peak of marcasite which is believed to represent the instability of marcasite compared with pyrite. The peak areas agree closely with each other and also with the peak areas of pyrite. The measured peak areas for 50 mg. samples average about 6.2 in.^{2} and for 10 mg. samples approximately 1.1 in.^{2}.

CONCLUSIONS

Pyrite and marcasite analyzed under standard conditions of heating rate, grain size and sample weight yield distinctive differential thermal curves. The initial oxidation peak of marcasite occurs at about 460° C. for a 50 mg. sample (125–149 micron fraction) while under the same conditions the initial oxidation peak of pyrite does not occur until about 538° C. Marcasite appears to oxidize at a lower temperature because of its relative instability compared with pyrite.

The inversion of marcasite to pyrite was not observed for samples heated in air. Upon completion of the initial oxidation reaction, X-ray powder patterns indicate the presence of a mixture of hematite and marcasite.

Oxidation peak temperatures decrease with grain size for both species. The peak temperature of the Curie point (endothermic) which is observed for pyrite finer than 74 microns and for the entire size range of marcasite tested (>297 to <44 microns; 50 ± 1 mg. samples) appears to increase with decreasing grain size. Peak areas for both pyrite and marcasite increase in an essentially linear manner with sample weight and under standard conditions of grain size and sample weight do not differ significantly.

The final reaction products for both pyrite and marcasite are hematite and sulfur dioxide. When the sulfur dioxide produced during the oxidation depletes the sample atmosphere of oxygen, pyrrhotite and other iron oxides including magnetite and maghemite may form as intermediate products.

REFERENCES

American Society for Testing Materials X-ray Powder Data File, Card No. 2-0908.
American Society for Testing Materials X-ray Powder Data File, Card No. 4-0755.

Buerger, M. J. (1934), The pyrite-marcasite relation: *Am. Mineral.*, **19,** 37–61.

Harcourt, G. A. (1942), Tables for the identification of ore minerals by *x*-ray powder patterns: *Am. Mineral.*, **27,** 63-113.

Hiller, J. E. and Probsthain, K. (1956), Differentialthermoanalyse von Sulfidmineralen: *Geologie (Berlin)*, **5,** 607-616.

Kopp, O. C. and Kerr, P. F. (1957), Differential thermal analysis of sulfides and arsenides: *Am. Mineral.*, **42,** 445–454.

Kopp, O. C. and Kerr, P. F. (1958), Differential thermal analysis of sphalerite: *Am. Mineral.*, **43,** 732–748.

Mason, B. (1943), Mineralogical aspects of the system FeO-Fe_2O_3-MnO-Mn_2O_3: *Geol. För. Förh. Stockholm*, **65,** 97–180.

Rooksby, H. P. (1951), *X*-ray Identification and Crystal Structure of Clay Minerals, G. W. Brindley, ed., Mineralogical Society, London, 345 p.

Schmidt, E. R. and Vermaas, F. H. S. (1955), Differential thermal analysis and cell dimensions of some natural magnetites: *Am. Mineral.*, **40,** 422–431.

Swanson, H. E., Fuyat, R. K. and Ugrinic, G. M. (1955), Standard *X*-ray diffraction powder patterns: *NBS Cir.* **539, IV.**

Swanson, H. E., Gilfrich, N. T. and Ugrinic, G. M. (1955), Standard *X*-ray diffraction powder patterns: *NBS Cir.* **539, V.**

Manuscript received March 11, 1958

THE AMERICAN MINERALOGIST, VOL. 43, NOVEMBER–DECEMBER, 1958

ESKOLAITE, A NEW CHROMIUM MINERAL

OLAVI KOUVO AND YRJÖ VUORELAINEN, *Department of Geological Exploration, Outokumpu Co., Outokumpu, Finland*

ABSTRACT

A new mineral was discovered at the Outokumpu mine in Finland. Its formula is $(Cr_{1.90}, V_{0.09}, Fe_{0.01}) O_3$ from chemical analysis. *X*-ray studies of single crystals and powders, as well as optical examination in reflected light, show the mineral to be isostructural with Cr_2O_3, the crystal structure of which, determined by Zachariasen (1928), has type $D5_1$ and space group $R\bar{3}c$. The cell dimensions are not measurably affected by the substitution of Fe^{+++} and V^{+++} for Cr^{+++}. The habit ranges from long prismatic to platy.

The new mineral was found by Yrjö Vuorelainen, and it is named in honor of Professor Pentti Eskola of the University of Helsinki.

INTRODUCTION

The compounds Fe_2O_3, Cr_2O_3 and Al_2O_3 are isostructural, having the hematite structure. The end members of the series have been synthesized in the laboratory, but Cr_2O_3 has not been found in nature.

The oxide of trivalent chromium, Cr_2O_3, is known by many names because of its color: green oxide of chromium, chrome ocher, ultramarine green, green cinnabar, green rouge etc. The known physical and chemical properties of this chromium compound are summarized by Udy (1957). The data given include the melting point (about 2435° C.), the boiling point (3000° C.), the heat capacity, the magnetic, thermal expansion, and oxygen expansion data, the heat content and the entropy, the thermal conductivity, resistivity and emissivity, the index of refraction (2.5), and the chemical properties. *X*-ray powder data for pure Cr_2O_3 are given by Jay and Wilde (1947), and by Swanson, Gilfrich, and Ugrinic (1955). The Curie point has been reported to be 305° K. and 320° K. by different investigators. Greenwald and Smart (1950) have found a change in crystal structure at 318° K. which first becomes apparent as a very slight broadening of the 422 reflection. At 307° K. the line is a distinct doublet, and the separation increases rapidly as the temperature is lowered.

A complete series of solid solutions formed between Cr_2O_3 and Fe_2O_3 has been described by Hamelin (1950). In addition, the formation of Cr_2O_3 in chromium spinel in heating experiments has been discussed by Karyakin, Pyatikop and Sukharevskiĭ (1956, 1957). Hamelin (1950) has pointed out that the presence of aluminum favors the formation of spinels.

OCCURRENCE

The mineral later identified as the natural counterpart of the artificial compound Cr_2O_3 was first observed by Yrjö Vuorelainen in the summer of 1949 at the Outokumpu mine, Finland. The mineral characteristically occurred in fresh, well developed hexagonal prisms and plates, 1–5 mm. in size (Fig. 1), in chromium-bearing tremolite skarn.

The geology of the Outokumpu mine is described by Veikko O. Vähätalo (1953). Although the Outokumpu ore is a copper ore consisting of about one million tons of metallic copper, there are in the ore field, according to Eskola's estimation (Eskola, 1953), about seven million tons of metallic chromium in the numerous serpentine and skarn rocks. In an earlier work he (Eskola, 1933, p. 43) describes a number of chromium-bearing minerals in different rocks associated with serpentine-rock, which is itself very poor in chromium and only seems to contain chromite in the form of pigment-like secondary products. The other chrome-bearing minerals and rocks are: (1) fuchsite in quartzite, which also contains streaks and patches of chrome-diopside and -tremolite, and uvarovite; (2) the latter three minerals, especially diopside, forming skarn deposits associated with dolomite; (3) chromite in dolomite; (4) picotite, kämmererite, and chromite in anthophyllite-cordierite rock; (5) uvarovite and tawmawite with some chromite in quartzose copper sulfide ore, and finally (6) the most remarkable occurrence of veins composed of uvarovite, tawmawite, chrome-tremolite with sulfides, mostly pyrrhotite, and also containing chrome-diopside and chromite. The chromite, as well as all the other chromium-bearing minerals of this locality, is in all probability of hydrothermal origin. The occurrence of chromium at Outokumpu illustrates the ability of this element to migrate and to take part in metasomatic replacements.

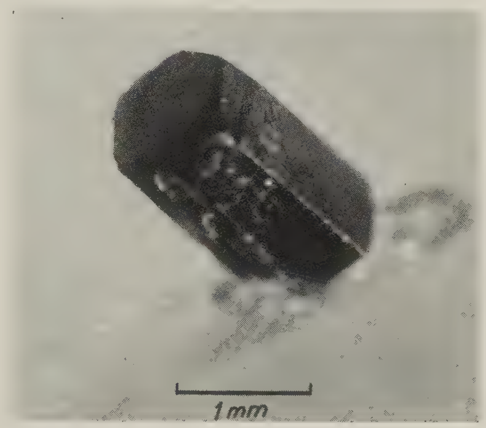

FIG. 1. Crystal of eskolaite from Outokumpu, Finland. Photo: W. S. Starks.

The specimens most abundant in the new chromium mineral were as follows:

1. Chromium-bearing tremolite skarn, rich in calcite, from contact with the ore. Mineral habit: long hexagonal prisms (up to 5 mm.). Associated minerals: pyrrhotite, pentlandite, chalcopyrite, chromium tremolite, uvarovite, tawmawite, calcite, and talc.
2. Quartzite from the foot wall of the ore. The specimen is from a cavity in a vein of milky quartz. Mineral habit: long prismatic (up to 1.5 mm.). Associated minerals: uvarovite, chromium bearing tremolite, calcite, and pyrite (pentagonal dodecahedron).
3. Veins of pyrrhotite. Mineral habit: platy (up to 6–7 mm.). Associated minerals: pyrrhotite, chromium-bearing tremolite, and chromium tourmaline. In some cases the mineral occurs as thin sheets on the surface of quartz.
4. Skarn ore rich in pyrrhotite. Mineral habit: short prismatic. Associated minerals: chromium-bearing tremolite, uvarovite, chromium tourmaline, chromium spinel, pyrrhotite, pyrite (octahedron), and chalcopyrite.
5. Chlorite seams. Mineral habit: thin platy. Associated minerals: chlorite, pyrite, chalcopyrite, pyrrhotite, and chromium spinel.

The mineral has not been found to occur with chromium diopside.

A further sample, weighing about eight kilos, was selected for separation. The concentration of the new mineral from rock samples was done by means of standard techniques. A Denver-Wilfley laboratory concentration table was adapted for treating the crushed sample. The heavy fraction was cleaned with bromoform, and then leached with a large quantity of hot hydrochloric and nitric acid to remove the soluble sulfides. The residue was further divided by centrifuging in Clerici solution. The heavy portion was passed through the Frantz isodynamic separator at the highest magnetic flux available to isolate the new mineral from the other constituents of higher magnetic susceptibility, especially from the abundant chromium spinel. The sample that was analyzed was determined by grain counts to contain less than 1% impurity, principally chromium spinel and tremolite.

Subsequent spectrographic, *x*-ray, and chemical analyses of the final sample of 1.5 grams established the mineral to be a new anhydrous chromium oxide expressed by the formula Cr_2O_3.

PHYSICAL AND OPTICAL PROPERTIES

The new mineral is lustrous black in color in crystals, and light green in finely divided material.

The specific gravity of 5.18 gm.cm.$^{-3}$ was obtained by using an ASE Torsion-Type Balance and suspension in toluene and in bromoform. The determinations were made on a number of grains weighing between 6 and 20 mg. The grains were too small to guarantee high accuracy and from the invariable presence of tiny inclusions and cavities it might be inferred that the values would tend to be too low. A measured specific gravity of 5.215 is given for pure Cr_2O_3 (Donnay, et al., 1954).

The absorption is so strong that in thin sections the mineral is opaque. In fragment mounts the thin grain edges are dark green with evident anisotropism, and with pleochroism from emerald green to olive green. It was not found to be pleochroic in polished sections.

On polished surfaces the mineral is gray. It is usually euhedral and strongly anisotropic with polarization colors as follows:

1. In air	Nicols completely crossed:	gray blue greenish gray
	Nicols not completely crossed:	dark violet blue light greenish gray
2. In oil	Nicols completely crossed:	gray brownish gray
	Nicols not completely crossed:	brownish gray greenish gray

Internal reflections are emerald green (also on borders against gangue). A clear red glint can be seen at the edges of small holes, which give a green reflection from the bottom.

Tests with chemical reagents gave the following results:

1:1	HNO_3	neg.	Aq. reg.	neg.
1:1	HCl	neg.	CrO_3+HCl	neg.
20%	$FeCl_3$	neg.	HF	neg.
20%	KCN	neg.	70% $HClO_4$	neg.
40%	KOH	neg.	$KMnO_4$	neg.
5%	$HgCl_2$	neg.		

The microhardness (Vickers) was found to be about 3200 kg/mm^2 (cassiterite: 1900–2000 kg/mm^2 and chromite: 1800 kg/mm^2).

The reflectivity in air as compared to that of hematite is:

	green	orange	red
eskolaite	22%	21%	20%
hematite	(26%)	(25%)	(21%)

A photomicrograph of a polished surface of the mineral is shown in Fig. 2.

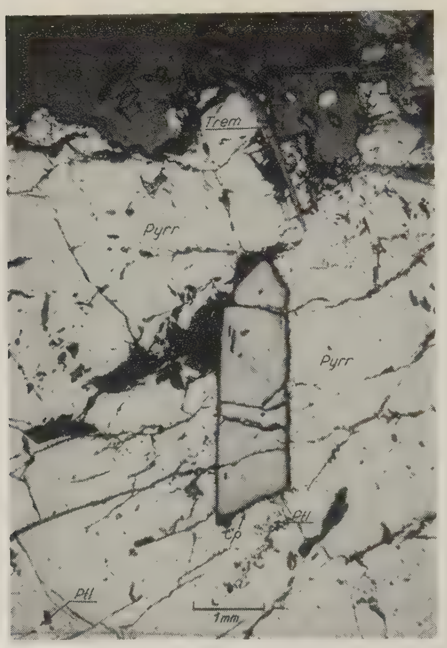

FIG. 2. Photomicrograph of a polished surface of eskolaite, Cr_2O_3, from Outokumpu, Finland. Pyrrhotite—Pyrr; chalcopyrite—Cp; pentlandite, PH; tremolite—Trem; and carbonate—Crb. Photo: Erkki Halme.

CHEMICAL COMPOSITION

A chemical analysis was made by Mr. Jorma Kinnunen, on material containing less than 1% impurities, mainly chromium spinel and tremolite. Results are given in Table 1.

The mineral sample was decomposed by means of Na_2O_2 fusion in an Alsint crucible (pure alumina). Chromium+vanadium were titrated with ferrous ammonium sulphate using diphenyl amine sulfonate as indicator. Vanadium was titrated after removal of chromium by means of a mercury cell. Iron was separated from chromium and vanadium in alkaline carbonate solution and determined photometrically by means of salicylic acid. Aluminum, manganese, magnesia, silica, copper, and nickel were estimated spectrographically.

The above figures represent an average corresponding to the chemical composition of all samples collected. It seems reasonable to assume that for solid solutions the lattice constants and specific gravity would vary as a function of chemical composition from grain to grain. Small inclusions and cavities in grains were found to cause differences which overlapped the possible real differences in specific gravity between the

TABLE 1. CHEMICAL ANALYSIS OF ESKOLAITE FROM OUTOKUMPU, FINLAND
Analyst: Jorma Kinnunen

	Weight per cent	Number of moles multiplied by 10,000
Cr_2O_3	94.13±0.20	6191
Fe_2O_3	0.55	34
V_2O_3	4.58	305
Al_2O_3	0.19*	18
MgO	0.03*	7
MnO	0.03*	4
SiO_2	0.20*	33
H_2O (total)	0.10	
Total	99.81	

* Based on a spectrographic analysis:	O.X	Al, Si	(about 0.1)
	O.OX	Mg, Mn	(about 0.02)
	tr.	Cu, Ni	

Formula: $(Cr_{1.90}, V_{0.09}, Fe_{0.01}) O_3$.

grains. On the other hand the specific gravities of Cr_2O_3 and Fe_2O_3 are very close together. The determinations on the lattice dimensions did not show any remarkable differences. The total quantity of this mineral available for study was quite limited and did not allow several chemical analyses. A semiquantitative recast of the analysis on a different sample did not show any serious differences.

CRYSTALLOGRAPHY

The mineral usually forms in hexagonal prisms and thick plates, and gives a green streak. The calculated density obtained from the analysis given in Table 1 and from the cell dimensions given in Table 3, is 5.218 $gm.cm.^{-3}$

Powder patterns were obtained using filtered copper, iron, and chromium radiation. The data for the interplanar spacings were calibrated with a silicon standard mixed with the sample. The results are given in Table 2, column 2, together with the data for synthetic Cr_2O_3 and hematite.

The structural identity of the new mineral with the synthesized Cr_2O_3 and hematite is evident. The x-ray powder pattern of hematite is similar, but it differs chiefly in having d-spacings corresponding to a larger unit cell than those of both the chromium compounds, although small differences in intensities were also noted. Intensity measurements were made by the flat-plate reflection method of the diffractometer.

In addition to the powder diffraction patterns shown in Fig. 3, the

TABLE 2. COMPARATIVE POWDER DIFFRACTION DATA FOR SYNTHETIC Cr_2O_3 (SWANSON, GILFRICH AND UGRINIC, 1955), FOR ESKOLAITE, AND FOR HEMATITE (HARCOURT, 1942)

hkil	Cr_2O_3		Eskolaite		Hematite	
	d(Å)	I	*d*(Å)	I	*d*(Å)	I
$01\bar{1}2$	3.633	74	3.630 ±.024	96	3.66	1
$10\bar{1}4$	2.666	100	2.665 ±.011	97	2.69	7
$11\bar{2}0$	2.480	96	2.479 ±.009	94	2.51	4
0006	2.264	12	2.269 ±.008	w	—	—
$11\bar{2}3$	2.176	38	2.174 ±.007	48	2.18	2
2022	2.048	9	—	—	—	—
$02\bar{2}4$	1.816	39	1.8146±.0034	58	1.835	3
$11\bar{2}6$	1.672	90	1.6746±.0039	100	1.68	5
$10\bar{1}8$	—	—	1.6139±.0032	w	—	—
$21\bar{3}2$	1.579	13	1.5782±.0030	w	1.58	0.5
$21\bar{3}4$	1.465	25	1.4656±.0024	32	1.485	1
$30\bar{3}0$	1.4314	40	1.4331±.0019	47	1.44	2
$1.0.\bar{1}.10$	1.2961	20	1.2971±.0025	12	1.30	0.5
$22\bar{4}0$	1.2398	17	1.2440±.0014	w	1.255	0.3

single crystal photographs were taken with Cu Kα radiation on the Buerger precession camera using the crystal shown in Fig. 1. These studies establish that the diffraction aspect is $R{*}c$. All dimensions obtained from these films are given in Table 3. The morphology of the crystals obeys the rhombohedral lattice criterion, as the prism is $\{11\bar{2}0\}$ rather than $\{10\bar{1}0\}$, and $\{11\bar{2}3\}$ is observed, not $\{11\bar{2}1\}$. The forms $\{01\bar{1}2\}$ and $\{1014\}$ should be dominant, however, and their absence is anomalous.

The cell edges were also calculated from the *d*-values 3.630±.001 Å (0112) and 2.479±.001 Å $(11\bar{2}0)$ obtained by means of a Norelco high-

TABLE 3. COMPARISON OF CRYSTAL DATA OF ESKOLAITE, V_2O_3, Cr_2O_3 AND Fe_2O_3 (DONNAY ET AL., 1954)

	V_2O_3	Cr_2O_3	Eskolaite		Fe_2O_3
			powder data	single crystal data	
Lattice dimensions					
a_0	4.933 kX	4.94 kX	4.958± .002 Å	4.973± .015 Å	5.025 kX
c_0	13.940 kX	13.57 kX	13.60 ± .01 Å	13.57 ± .04 Å	13.735 kX
c/a	2.826	2.748	2.743	2.730	2.733
Cell volume	—	—	289.45 Å^3	290.6 Å^3	—
G	5.04	5.25	5.218	5.20	5.25

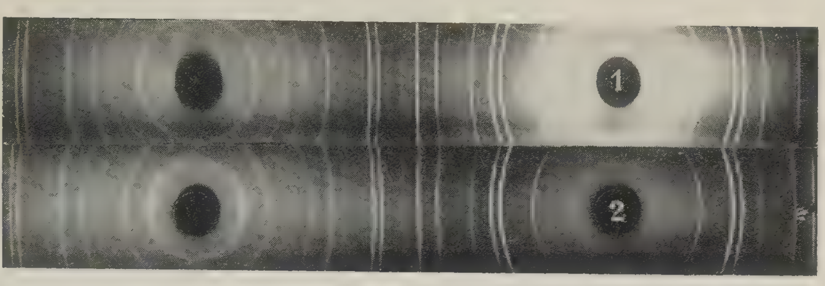

FIG. 3. Comparison of x-ray powder photographs: (1) eskolaite from Outokumpu, Finland; (2) hematite. Cr-radiation, V filter.

angle X-ray Spectrometer and using the sample mounting technique suggested by Holland (Holland et al., 1955).

The crystallographic data of eskolaite are given in Table 3 together with those of Cr_2O_3, V_2O_3, and Fe_2O_3.

NOMENCLATURE

On the evidence adduced above, the existence in nature of a chromium oxide corresponding in composition to Cr_2O_3 and isostructural with hematite and corundum, is proposed.

The mineral is named in honor of Professor Pentti Eelis Eskola of the University of Helsinki in recognition of Professor Eskola's many fundamental contributions to mineralogy and petrology during the past half century.

By analogy with hematite and corundum, the name eskolaite should be appropriate for the pure end member.

ACKNOWLEDGMENTS

The authors are indebted to the Outokumpu Co. for permission to undertake the work and to publish the results.

The facilities of the Department of Geology, Princeton University, of the Geophysical Laboratory, Carnegie Institution of Washington, and of the Geological Survey of Finland have been placed at the authors' disposal. The writers wish to thank all these institutions for their valuable aid.

Thanks are due also to Dr. Gabrielle Donnay for a critical reading of the manuscript, as well as for information and assistance regarding the single crystal studies with the Buerger precession camera.

To Mr. Jorma Kinnunen, M.A., from the Outokumpu Co., the authors would like to extend their thanks for the chemical analyses.

NOTE: A second occurrence of eskolaite is reported on page 1203 of this issue.

REFERENCES

DONNAY, J. D. H. AND NOWACKI, WERNER (1954), Crystal Data. Geol. Soc. Amer. Memoir **60.**

ESKOLA, PENTTI (1933), On the chrome minerals of Outokumpu: *Compt. rend. Soc. géol. Finlande,* **7**; *Bull. Comm. gêol. Finlande,* **103,** 26.

ESKOLA, PENTTI (1953), Malmien synnystä: Vuoriteollisuus—Bergshanteringen **11,** p. 13.

GREENWALD, SELMA AND SMART, J. SAMUEL (1950), Deformations in the crystal structures of anti-ferromagnetic compounds: *Nature,* **166,** 523.

HAMELIN, M. (1950), Reactions á l'état solide á haute température de mélanges d'oxydes réfractaires des systémes: Cr_2O_3-MgO-FeO, Al_2O_3-TiO_2, Cr_2O_3-TiO_2. Revue de Metallurgie XLVII, p. 324.

HARCOURT, G. ALAN (1942), Tables for the identification of ore minerals by x-ray powder patterns: *Amer. Mineral.,* **27,** 63.

HOLLAND, H. D., HEAD, W. B., III, WITTER, G. G., JR., AND HESS, G. B. (1955), A new method for mounting samples for powder x-ray spectrometry: *Am. Mineral.,* **40,** 761.

JAY, A. H. AND WILDE, W. T. (1947), The lattice parameters of α-alumina and chromic oxide: *Mineral. Mag.,* **27,** 56.

KARYAKIN, L. I., PYATIKOP, P. D. AND SUKHAREVSKIĬ, B. YA. (1956), Changes and reactions between chromium spinel and magnesioferrite during heating (In Russian). *Doklady Akad. Nauk S.S.S.R.,* **109,** 1009; *Chemical Abstracts,* **51,** 4219.

SWANSON, HOWARD E., GILFRICH, NANCY T., AND UGRINIC, GEORGE M. (1955), Standard X-ray Diffraction Powder Patterns. Chromium (III) oxide, Cr_2O_3 (hexagonal). *U. S. National Bureau of Standards Circular* **539,** Vol. **V,** p. 22.

UDY, MURRAY C. (1957), The physical and chemical properties of compounds of chromium. Chromium I. Reinhold Publ. Co., New York, p. 113.

VÄHÄTALO, VEIKKO O. (1953), On the geology of the Outokumpu ore deposit in Finland: *Bull. Comm. geol. Finlande,* **164.**

ZACHARIASEN, W. H. (1928), Untersuchungen über die Kristallstruktur von Sesquioxyden und Verbindungen ABO_3: *Skrifter Norske Videnskaps-Akad. Oslo,* **I.** *Nat.-Naturv. Kl.* No. 4.

Manuscript received April 14, 1958.

THE AMERICAN MINERALOGIST, VOL. 43, NOVEMBER–DECEMBER, 1958

AJOITE, A NEW HYDROUS ALUMINUM COPPER SILICATE*

W. T. Schaller and Angelina C. Vlisidis, *U. S. Geological Survey, Washington 25, D. C.*

Abstract

Ajoite is a new bluish-green hydrous aluminum copper silicate from Ajo, Pima County, Arizona. It was collected by Harry Berman in 1941 and recognized by him at that time as probably a new mineral. Mostly massive, a few cavities contain platy crystals or laths elongated parallel to *c* and flattened parallel to {010}. It is biaxial positive with indices of refraction $\alpha = 1.565$, $\beta = 1.590$, $\gamma = 1.650$, $+2V = 68°$, $X = b$, $Z \wedge c = 15°$. The specific gravity is 2.96. The *x*-ray powder pattern could not be related to that of any other copper silicate. The strongest lines are: 12.4 (100), 3.34 (25), 6.19 (9), 4.12 (9), 3.09 (9). Examination with an *x*-ray diffractometer showed that neither medmontite nor any montmorillonite group mineral can be present. Chemical analysis yielded the formula $Al_2O_3 \cdot 6CuO \cdot 10SiO_2 \cdot 5\frac{1}{2}H_2O$. Ajoite is not related to any of the several impure mixtures of copper silicates and aluminum minerals.

Introduction

Specimens of a bluish-green copper aluminum silicate, named ajoite† after the locality Ajo in northwestern Pima County, Arizona, were collected by Harry Berman of Harvard University, in August 1941 together with specimens of dark blue shattuckite. Preliminary examination by him, chiefly optical, indicated that the greenish mineral was probably a new species. It had been planned by Berman and Schaller to collaborate on the study of this new mineral and possibly to extend such a collaborative investigation so as to include all the known copper silicate minerals, a plan nullified by Berman's untimely death in 1944. It is a tribute to Berman's keen perception that his earlier prediction of a new mineral has been borne out.

The two gram sample of massive ajoite prepared for analysis by Berman was further purified by hand-picking the few remaining small spherulites of blue shattuckite enclosed in the greenish ajoite. The resulting purified sample was analyzed by Angelina C. Vlisidis after a pycnometer determination of the specific gravity and a preliminary spectrographic analysis.

Later, the entire collection of these specimens was forwarded by Prof. Clifford Frondel (Harvard University) for completion of the study. A second small sample of massive ajoite was prepared from these samples for the several qualitative tests made, checking the optical determinations, and taking additional *x*-ray powder-diffraction patterns.

---

* Publication authorized by the Director, U. S. Geological Survey.

† Pronounced ah′hō-ite.

ASSOCIATION

Most of the ajoite is compact massive, resembling some deeper colored chrysoprase in color and specimen structure, and is intimately mixed with dark blue shattuckite and white massive quartz. Occasional small cavities contain aggregates of elonaged plates of ajoite, a millimeter and less in length. Other less abundant associated minerals observed are minute pearly scales of sericite, white powdery quartz, pyrite, very pale blue altering shattuckite, limonitic stains, and on one specimen massive conichalcite. Berman (letter to W. T. Schaller, dated June 12, 1942) also noted the presence of this mineral (he referred to it as "higginsite") perched on the new copper silicate.

As observed in a thin section, the relation between ajoite and shattuckite seems rather indefinite, but, in general, the greenish ajoite appears to have replaced the shattuckite, as noted by Berman. On the other hand, the presence of small seams of shattuckite, grading down in size to isolated minute spherulites, suggests to one of us (W.T.S.) that shattuckite may be forming at the expense of the ajoite and later than it.

PHYSICAL AND OPTICAL PROPERTIES

In color ajoite approaches very closely Ridgway's Venice green, Plate VII, 41. BB-G, about 75 per cent green and 25 per cent blue.

A letter, dated June 12, 1942, from Berman to Schaller, stated that the light green, lathlike ajoite found replacing the shattuckite is monoclinic, elongated parallel to *c* and flattened parallel to {010}. Berman determined the indices of refraction to be $\alpha = 1.565$, $\beta = 1.590$, $\gamma = 1.650$, with a birefringence of 0.085. From these indices 2V is calculated to be 68°. Optically positive, $X = b$, $Z \wedge c = 15°$. These values have been confirmed by Schaller.

The specific gravity of the analyzed sample is 2.96 (pycnometer).

X-RAY POWDER-DIFFRACTION DATA

X-ray powder-diffraction patterns (films 5759, 12557, and 12559) of the massive analyzed material are identical with those taken of the better crystallized material (films 5757 and 5757A) on which Berman made his optical determinations. The measured powder data listed in Table 1 were obtained from a pattern (film 12559) taken by Mary E. Mrose, U. S. Geological Survey, with a Debye-Scherrer camera (114.59 mm. diameter) using the Straumanis technique, with CuKα radiation (Ni filter), $\lambda = 1.5418$ Å. Film 12557 is reproduced in Fig. 1.

COMPOSITION

The analysis of the small sample of ajoite first purified by Berman and later by Schaller, guided by prior spectrographic examination,

TABLE 1. *X*-RAY POWDER-DIFFRACTION DATA FOR AJOITE FROM AJO, ARIZONA
(analyzed material; film 12559)
CuKα (Ni filter), λ=1.5418Å
Camera diameter 114.59 mm.; cutoff at 17.7 Å
Corrected for shrinkage (by M. E. Mrose)

I[1]	*d*(meas.)	I	*d*(meas.)	I	*d*(meas.)
100	12.4	1	2.37	1	1.577
4	9.98	3	2.30	1	1.555
9	6.19	3	2.28	2	1.540
1	5.19	3	2.26	1	1.527
1	4.99	1	2.21	1	1.506
3	4.53	1	2.16	1	1.489
3	4.25	1	2.12	2	1.480
9	4.12	1	2.08	2	1.449
1	3.87	1	2.02	1	1.416
1	3.73	1	2.00	1	1.384
4	3.48	1	1.978	1	1.373
2	3.40	1	1.949	2	1.347
25	3.34	1	1.862	1	1.333
9	3.09	1	1.841	1	1.309
5	2.93	3	1.818	1	1.296
6	2.79	1	1.802	1	1.278
3	2.66	1	1.775	1	1.268
2	2.59	1	1.752	1	1.250
3	2.55	2	1.672	1	1.228
4	2.51	1	1.642	1	1.198
6	2.46	1	1.617	1	1.184
1	2.43	1	1.595	1	1.181
			Plus many more weak lines		

[1] Intensities were obtained by visual comparison with a calibrated intensity strip based on log $\sqrt{2}$.

showed that ajoite is a hydrous aluminum copper silicate with the formula $Al_2O_3 \cdot 6CuO \cdot 10SiO_2 \cdot 5\frac{1}{2}H_2O$.

The spectrographic analysis by K. J. Murata, U. S. Geological Survey, showed:

XO Si, Cu
X Al, As, Ba
O.X Ca, Fe, Mg, Mn, Ti
O.OX Na
O.OOX B
Not found: P, Pb, V, Sn, Be, Bi, Cr, Ge, Li, Sb, Zr, Zn

The results of the chemical analysis are given in Table 2. The formula derived therefrom is $Al_2O_3 \cdot 6CuO \cdot 10SiO_2 \cdot 5\frac{1}{2}H_2O$.

Ajoite is readily decomposed by acids, leaving a coherent white mass

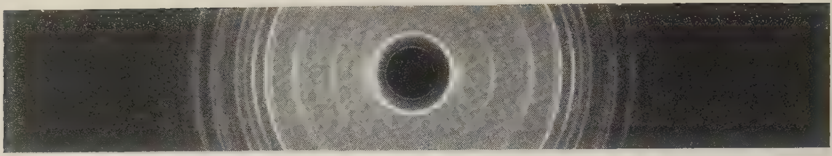

FIG. 1. *X*-ray powder-diffraction pattern of ajoite. Cu Kα, Ni filter.

of hydrated silica with small unattacked particles of blue shattuckite scattered through it. At room temperature, with 1:1 HCl, decomposition takes place overnight. In 1:1 NHO_3 several days are required. When the mineral was treated with NH_4OH at room temperature overnight, no reaction was noticed.

The role of arsenic and barium in the mineral is not definitely known, but the arsenic is considered as due to admixed conichalcite and the barium to barite as the ratios of BaO (0.0033) and SO_3 (0.0029) are very close. Based on the determined percentages of As_2O_5 and of BaO, 3 per cent of conichalcite and 0.76 per cent of barite are deducted as impurities. The value given for FeO is for total iron.

TABLE 2. ANALYSIS OF AJOITE
(by A. C. Vlisidis)

Analysis		Deducting conichalcite and barite	Remainder Ajoite	Ratios		
SiO_2	45.90	—	45.90	0.7642	0.7642	10.10
						10 ×1.01
CuO	33.90	0.92	32.98	.4146		
FeO	.78	—	.78	.0109		
MnO	.10	—	.10	.0014	.4494	5.94
						6 ×0.99
MgO	.66	—	.66	.0164		
CaO	.99	.65	.34	.0061		
BaO	.50	.50	—	—		
Al_2O_3	7.30	—	7.30	.0716		0.97
					.0736	1 ×0.97
TiO_2	.16	—	.16	.0020		
As_2O_5	1.33	1.33	—	—		
SO_3	.23	.23	—	—		
H_2O^-	2.55	—	2.55	.1415		5.49
					.4151	5½×1.00
H_2O^+	5.03	.10	4.93	.2736		
	99.43	3.73	95.70			
G	2.96					

Determinations of the water content of ajoite were repeated on two other small samples of the material, (1) a second small sample prepared by Berman and (2) a small sample prepared by Schaller. The results obtained are:

	(1)	*(2)*	*Analyzed sample*
H_2O^-	1.85	1.92	2.55
H_2O^+	5.69	6.34	5.03
Total H_2O	7.54	8.26	7.58

If the values of (2) are substituted for those given in the analysis, then the ratio of the total H_2O becomes 5.96, very close to 6.

Relations to Other Copper Silicates

John C. Hathaway of the U. S. Geological Survey examined ajoite with an *x*-ray diffractometer using both air-dried and ethylene glycol saturated samples and was unable to detect any montmorillonite group mineral. *X*-ray examination of ajoite heated at 400° C. showed no collapse in the structure. These results demonstrate that neither medmontite, a copper-bearing (20.96 per cent CuO) clay of the montmorillonite group, nor any other montmorillonite group mineral can be present.

Ajoite is not closely related to any of the several described hydrous copper aluminum silicates such as traversoite, a light blue "new variety of chrysocolla" with 21.84 per cent Al_2O_3 and 32.84 per cent H_2O, believed to be a mixture of chrysocolla and gibbsite; or pilarite with 16.9 per cent Al_2O_3 and 21.7 per cent H_2O, or to similar material from Utah with 10.78 per cent Al_2O_3 and 25.76 per cent H_2O, the alumina being ascribed to admixed allophane; or to any of the several probably impure bluish chrysocollas with small amounts of Al_2O_3. A mixture of chrysocolla and alunite (or natroalunite) has also been described. Most of these chrysocollas containing appreciable amounts of alumina are probably mixtures of typical chrysocolla (essentially $CuO \cdot SiO_2 \cdot 2H_2O$) with other copper free minerals. Alumina is commonly present in these mixtures as hydrate, phosphate, sulfate, or silicate. All these mixtures contain much more water than is present in ajoite.

Acknowledgments

Our appreciation is expressed to Mary E. Mrose for powder-diffraction work, to K. J. Murata for the spectrographic analysis, and to John C. Hathaway for his kind assistance.

Manuscript received March 12, 1958.

THE AMERICAN MINERALOGIST, VOL. 43, NOVEMBER-DECEMBER, 1958

COPPER VERMICULITES FROM NORTHERN RHODESIA

WILLIAM A. BASSETT, *Columbia University, New York, New York.*

ABSTRACT

Vermiculite has been identified as the chief copper bearing mineral in samples of micaceous material from the copper belt of Northern Rhodesia. These samples range from 2% to 7% copper which is carried in the exchange position of the vermiculite. For comparison, copper vermiculite was synthesized from magnesium vermiculite and from biotite by simple base exchange procedures. The resultant materials give *x*-ray diffraction patterns with intensities for the 7 Å, 4.7 Å, and 3.5 Å reflections greater than those of a magnesium vermiculite, indicating that copper has entered the exchange position of the vermiculite lattice. The natural samples give *x*-ray diffraction patterns having a similar distribution of intensities. In some of the natural samples this intensity distribution must be attributed to the presence of chlorite but in others it is due to copper in the exchange position. Vermiculite has been distinguished from chlorite on the basis of differential thermal analysis, direct weight measurements of H_2O loss on heating, continuous *x*-ray diffraction during heating on the thermal increment diffractometer, and by exchanging large univalent ions for small bivalent ions in the exchange position. Copper appears to be firmly fixed in the vermiculite lattice and no simple base exchange procedure was found for its removal from either the natural or the synthetic material.

INTRODUCTION

Samples from the Roan Antelope mine of Northern Rhodesia were sent to the mineralogy laboratory at Columbia University for investigation. The samples consisted of micaceous material from the oxidation zone and had been found to contain up to 7% copper which was not recoverable by conventional methods of treatment. Later a bulk sample of similar material from the Banded Sandstone in the Nchanga mine of Northern Rhodesia was examined. The problem was similar to that encountered in the Roan Antelope samples.

The lack of ordinary copper minerals in an amount adequate to account for the copper content suggested the possibility that the copper might be carried in the micaceous material itself. The nature and extent of this association has formed the basis of a detailed mineralogical and *x*-ray study.

GENERAL DESCRIPTION OF THE ROAN ANTELOPE SAMPLES

Samples RA5, RA6, RA7, and G1 from the oxidation zone of the Roan Antelope deposit range from 2% to 7% copper (Table 1). Of these only one, RA5, has recognizable normal copper mineralization which is in the form of brochantite and constitutes about 1% of the sample. The chief constituents of all the samples examined are micaceous minerals. In RA5 the micaceous material is light green and represents about 90% of the sample. About 50% of RA6 is a light brown micaceous mineral. In RA7 light brown micaceous minerals constitute 65% of the sample, while G1 consists of nearly 95% colorless to light brown micaceous material. The optical properties of these micaceous minerals are variable even within the individual samples. The refractive indicies range from 1.575 to 1.605. All the flakes are biaxial negative but the axial angle ranges from 0° to 30° with a large majority of measurements in the range from 5° to 10°.

Quartz, tremolite, hematite, goethite, and limonite occur as secondary minerals in all the samples. The quartz appears as angular fragments ranging from less than 1% in G1 to nearly 20% in RA7. White tremolite needles range from less than 1% in RA5 to 40% in RA6. Hematite, goethite, and limonite are found both as discrete fragments and as inclusions in the micaceous minerals.

TABLE 1. COPPER CONTENT OF THE SAMPLES STUDIED

Sample	%Cu (*X*-ray spectrometer)
Nchanga	1.5
RA5	7.2
RA6	2.6
RA7	2.4
G1	3.8
Synthetic Copper Vermiculite	10.0

GENERAL DESCRIPTION OF THE MATERIAL FROM NCHANGA

This material is granular with fragments that range from 28 mesh to fine dust. About 65% consists of micaceous minerals with optical properties similar to those of the Roan Antelope samples. Quartz, which is largely euhedral, constitutes about 25% of the sample. Recognizable copper mineralization consists of malachite, brochantite and chalcopyrite which together represent about 0.1% of the sample. A black iron-manganese wad-like material accounts for about 2% of the sample and carries a minor amount of copper. Accessory minerals are anthophyllite, apatite, and zircon.

When all the normal copper mineralization is considered, there is still far too little to account for the 1.5% copper content of the material. However, small red and yellow inclusions in the micaceous minerals offered a possible explanation for the copper content (Fig. 1). It had been suggested in an Anglo American Technical paper that the red inclusions might be cuprite. These inclusions are also present to a lesser extent in the other samples. Thus, a positive identification of the inclusions became desirable.

The red inclusions are round or irregularly shaped, range from 1 mm to submicroscopic, and are deep red. Under crossed nicols they show wavy extinction and sometimes yield false interference figures. This behavior under crossed nicols suggests that the inclusions are aggregates of elongate anisotropic crystals with a radial orientation. The individual crystals are not distinguishable under the highest power. The refractive index of the red inclusions is above that of the highest available refractive index media (sulfur and selenium; $n=2.7$).

The final identification of the red inclusions was accomplished by a recently developed x-ray technique for dealing with particularly small quantities of material. This technique is the micro x-ray camera. With this camera specimens 10–100 μ in diameter may be identified. The camera is mounted on a Norelco basic unit and is used with characteristic radiation.

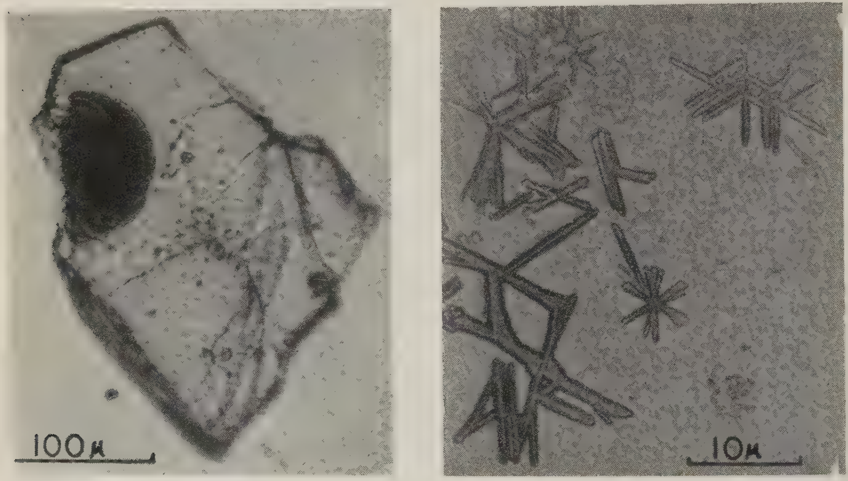

(a) (b)

FIG. 1. (a) Photomicrograph of a vermiculite flake containing a semicircular inclusion of hematite; (b) Photomicrograph of yellow snowflake-like inclusions of goethite in a vermiculite flake.

The micro x-ray camera was well suited for the identification of the red inclusions since the inclusions consist of an aggregate of minute crystals with a large range of orientations resulting from the radial structure. With such a wide range of orientations, a single inclusion acts as if it were a powder having a random orientation. Three flakes containing red inclusions were hand picked under the polarizing microscope. These were first placed on a glass slide, then a drop of Duco cement was smeared over the fragments. When the Duco cement had dried it was easily floated off in water as a plastic sheet containing the fragments, which were then transferred to the camera.

The red inclusions in the flakes were exposed to characteristic copper radiation in the micro *x*-ray camera for six hours. The photographs show spots resulting from Laue type reflections produced by a single flake of micaceous material. Superimposed on the Laue pattern are rings characteristic of a powder type picture produced by the multi-oriented crystals of the red inclusions. The diameters of the rings were measured and the *d*(Å) values calculated by means of a nomogram provided with the microcamera. The values obtained are given in Table 2, where they are shown to compare favorably with the accepted values for hematite.

An exhaustive search was made in an effort to find red inclusions not showing birefringence which might be identified as cuprite. Only one such inclusion was found among the hundreds examined. It was too small to give a useful *x*-ray photograph and was probably a single crystal of hematite oriented in such a way as to show no birefringence.

Table 2. Micro *X*-ray Camera Data

Red Inclusions		Hematite		Yellow Inclusions		Goethite	
d(Å)	Int.	*d*(Å)	Int.	*d*(Å)	Int.	*d*(Å)	Int.
3.7	2	3.68	2	2.70	2	2.70	4
2.7	10	2.69	10	2.60	1	2.58	2
2.52	9	2.51	8	2.45	10	2.45	8
2.22	1	2.20	2	2.25	1	2.25	1
1.85	1	1.84	6	1.80	1	1.80	1
1.72	1	1.69	6	1.74	1	1.72	4
				1.55	1	1.56	3

Yellow inclusions are a little more abundant than the red ones but are less noticeable due to their lighter color. They occur in three forms within the flakes of micaceous material.

1. As layers of fairly continuous yellow material sometimes showing needle-like crystals along the edges.
2. As snowflake-like aggregates (Fig. 1). Each "snowflake" is made up of six or more single crystals all of which have parallel extinction and are length slow. Occasionally red inclusions are found at the centers of these aggregates.
3. As rounded forms showing good false figures. None of the inclusions were observed to be more than 0.1 mm in diameter. These aggregates also are sometimes found intimately associated with the red material.

The index of refraction of the yellow inclusions was found to be above 2.00.

Micro x-ray photographs were taken of the yellow inclusions which seemed to show the largest number of crystals having different orientations. The resulting pictures yielded data comparing favorably with goethite (Table 2).

Thus scrutiny of the inclusions reveals iron minerals rather than copper. By a process of elimination, the existence of the copper in the micaceous material itself affords the most logical explanation. The diffraction and dehydration data which follow are offered as further proof

DIFFRACTION DATA

The diffraction diagrams (Fig. 2) reveal the quartz and tremolite observed under the microscope. Nchanga, RA7, and G1 show the 10 Å reflections of biotite. All of the diagrams have 14 Å, 7 Å, 4.7 Å, and 2.8 Å reflections which may be attributed to either vermiculite or chlorite or both. Broad peaks at 12 Å, 8.5 Å, 4.85 Å, and 3.4 Å indicate interstratified biotite and 14 Å minerals. This corresponds to Gruner's hydrobiotite when the layers are biotite and vermiculite (Gruner, 1934).

Vermiculite may be distinguished from chlorite by the intensities of the x-ray reflections. Vermiculite has an intense 14 Å reflection and a weak 7 Å reflection, while chlorite has a 7 Å reflection which is about twice as intense as the 14 Å reflection (Fig. 3). RA5, RA6, and G1 give reflections with intensities intermediate between these two extremes (Nchanga and RA7 are complicated by mixed layer structure). The difference in structure between vermiculite and chlorite which is responsible for the distribution of intensities is to be found in the intersilicate magnesium. Because the intersilicate magnesium in chlorite (i.e. the brucite layer) is hydrated with OH^- ions, a high density of magnesium (approximately 3 ions per 10 oxygens) obtains, providing a high electron density at $z=0.5$ in the unit cell.

Vermiculite (Fig. 4), on the other hand, has an intersilicate layer (the exchange position) of magnesium hydrated with H_2O which permits only a relatively low density of magnesium (approximately 0.5 ion or less per 10 oxygen atoms) and hence a low electron density at $z=0.5$. The electron density of the intersilicate layer has a strong effect on the relative intensities of the 14 Å and the 7 Å reflections due to the fact that at $z=0.5$, $\cos 2\pi lz$ equals -1 for the 14 Å reflection and $+1$ for the 7 Å reflection.

When a material gives a diffraction pattern with intensities intermediate between those of vermiculite and chlorite, the material has an average electron density at $z=0.5$ intermediate between that found in vermiculite and that found in chlorite. This intermediate electron density in the intersilicate layer may result from four different circumstances:

1. A mechanical mixture of vermiculite and chlorite, (Weiss and Rowland, 1956).

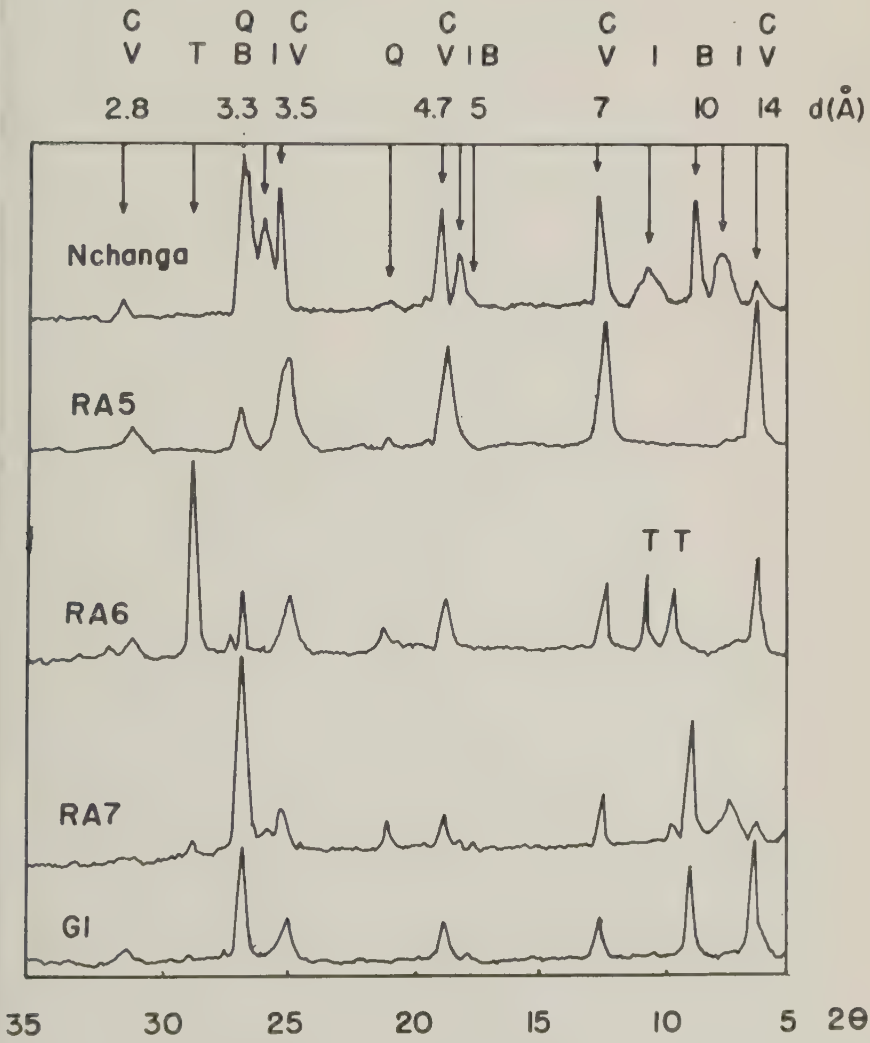

FIG. 2. *X*-ray diffraction diagrams of five copper-bearing micaceous samples from Northern Rhodesia. V=vermiculite, C=chlorite, B=biotite, I=interstratified 10 Å–14 Å material, Q=quartz, T=tremolite.

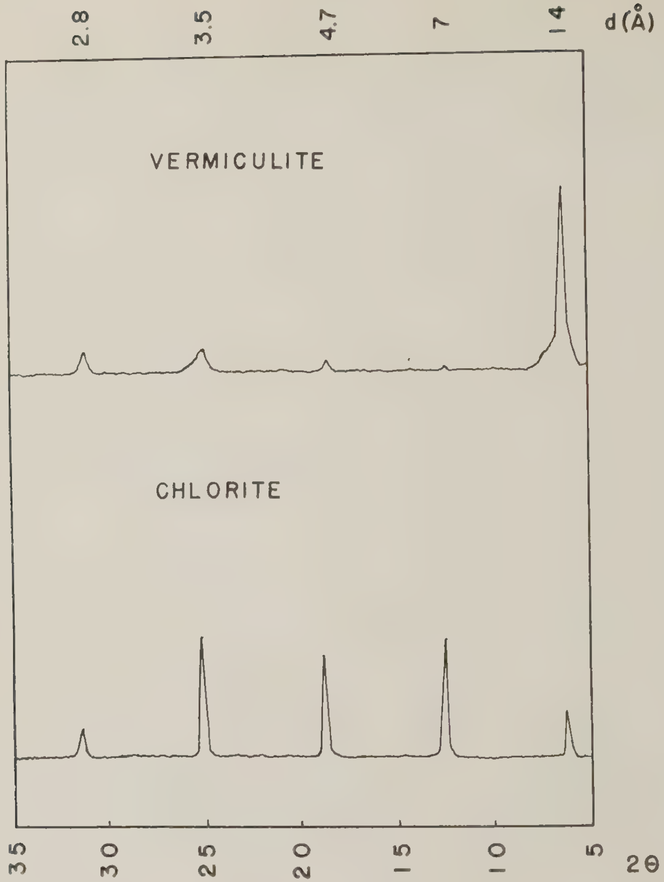

FIG. 3. *X*-ray diffraction diagrams of vermiculite and chlorite.

2. Mixed layer vermiculite-chlorite, (Weaver, 1956; Weiss and Rowland, 1956).
3. The presence of $Mg(OH)_2$ among $Mg \cdot H_2O$ in a chloritic vermiculite.
4. The presence of a high atomic number element (e.g., copper) in the intersilicate layer of a vermiculite.

Thus, the intermediate distribution of intensities observed in the diffraction patterns of the samples from Africa may result from either copper substitution in the exchange position of the vermiculite or the coexistence of chlorite and vermiculite. The problem of ascertaining the location of the copper in the samples becomes one of determining the rela-

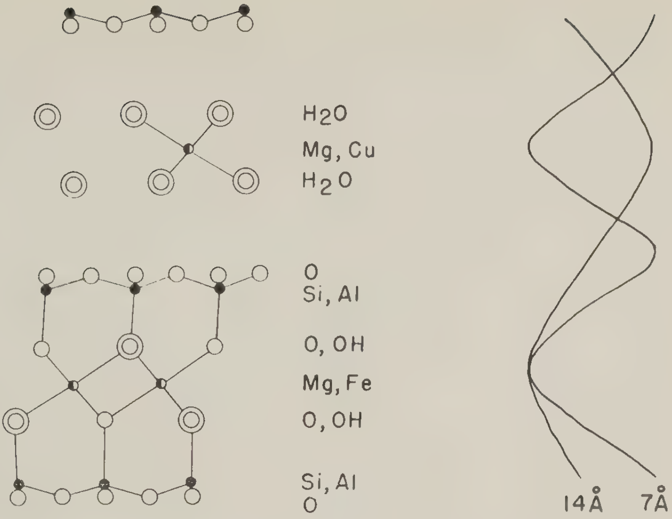

FIG. 4. Vermiculite structure and phase diagram.

tive amounts of chlorite and vermiculite, and of determining the effect on the diffraction pattern of copper substitution in the vermiculite exchange position. The former has been accomplished by various dehydration techniques; the latter, by the synthesis of copper vermiculite.

SYNTHESIS OF COPPER VERMICULITE

Copper vermiculite has been produced in the laboratory by two different procedures. First, by immersing a normal magnesium vermiculite from Corundum Hill, North Carolinia in a molar solution of ammonium acetate for 72 hours at 100° C., and then a molar cupric chloride for 120 hours at 100° C. The first stage reduced the lattice from 14 Å to 10 Å (Gruner, 1939). The second stage caused the lattice to expand to 14 Å again. The distribution of intensities in the x-ray pattern of the final product is quite different from the distribution observed in the x-ray pattern of the original material (Fig. 5). The intensities of the 7 Å, 4.7 Å, and 3.5 Å reflections have increased while those of the 14 Å and 2.8 Å reflections have decreased. Structure factor calculations show that this change represents an increased electron density in the exchange position which in this case can be attributed only to the substitution of copper for magnesium in the exchange position.

The second method for the preparation of copper vermiculite consisted of placing a normal biotite from Peekskill, New York in a molar solution of cupric chloride for 144 hours at 100° C. A hundredth of a gram of the

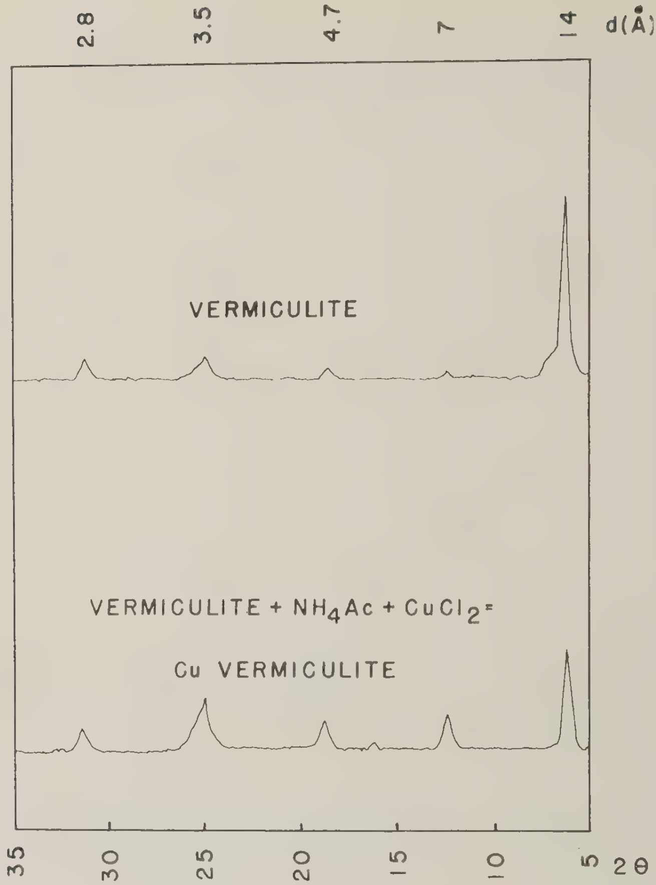

FIG. 5. *X*-ray diffraction diagrams of vermiculite and copper vermiculite synthesized from vermiculite.

biotite was used. At the end of the 144 hour period the biotite had turned from a vitreous black typical of biotite to a pearly, golden brown typical of vermiculite. It gave an *x*-ray pattern (Fig. 6) similar to that given by the material derived from the magnesium vermiculite by the method described above. Some residual biotite remained unaltered creating a pattern with striking similarity to G1 (Vermiculite and biotite from Roan Antelope).

When an attempt was made to repeat the synthesis of copper vermiculite from biotite using larger quantities of biotite, mixed layer biotite-vermiculite resulted giving an *x*-ray diffraction pattern (Fig. 6) with the broad hydrobiotite peaks mentioned earlier. When more biotite was used,

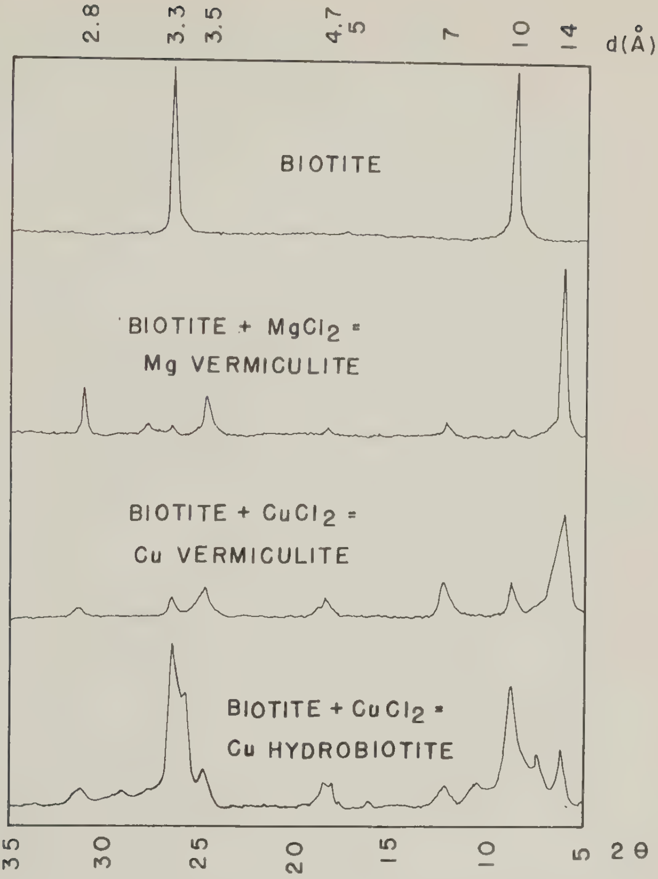

FIG. 6. *X*-ray diffraction diagrams of biotite and materials synthesized from biotite.

even more interstratified material formed at the expense of the discrete biotite and vermiculite. The formation of copper hydrobiotite, i.e., the interstratification of copper vermiculite with biotite seems to take place as readily as the formation of pure copper vermiculite from biotite. The resemblance between this mixed layer material and the natural mixed layer specimens, Nchanga and RA7, is also striking.

At the same time that the copper vermiculite was being prepared from the biotite, a magnesium vermiculite was synthesized from the same biotite for comparison with the copper vermiculite. The synthesized magnesium vermiculite gives a diffraction pattern (Fig. 6) with a 7 Å reflection only slightly more intense than the one observed in the natural magnesium vermiculite but a great deal less intense than the 7 Å reflections observed for copper vermiculites, either natural or synthesized.

Because the synthesized copper vermiculites were formed under closely controlled laboratory conditions from pure materials and give x-ray diffraction patterns completely reconcilable with the emplacement of the copper in the exchange position, they provide reference specimens against which the other materials may be compared.

DEHYDRATION STUDIES

As has been shown above, intensity distributions in x-ray diffraction patterns indicate merely the relative electron density of the intersilicate position $z=0.5$. It does not indicate whether the differences in electron density may be attributed to the presence of chloritic material, $Mg(OH)_2$, or to the presence of ions of high atomic number hydrated with H_2O. Because of the different bond strength with which the water is held in each case, one may distinguish the two types by studying dehydration characteristics. The following techniques were applied to the problem:

1. Exfoliation on rapid heating
2. Differential thermal analysis
3. Direct measurement of weight loss at 260° C.
4. X-ray diffraction during heating on the thermal increment diffractometer
5. Exchange of large univalent ions for small bivalent ions.

While this last method is carried out with the material entirely submerged in aqueous solution, it is considered a dehydration method here because the replaced small bivalent ions take with them the envelopes of H_2O molecules which accompany them in the vermiculite lattice.

Exfoliation

Perhaps the best known characteristic of vermiculite is its ability to exfoliate when rapidly heated to several hundred degrees. This exfoliation results from the puffing action of water vapor trapped between the layers. The water which is vaporized belongs to the H_2O hydration envelopes which surround the magnesium ions in the exchange position. The OH^- ions surrounding the magnesium in the brucite layer of the chlorite lattice are not driven off as readily and hence do not cause exfoliation. Thus, exfoliation may be used as an approximate indication of the amount of vermiculite and chlorite present in a sample.

A cubic centimeter of each sample from Africa was measured out and heated rapidly to red heat. The volumes of the samples were then remeasured. Table 3 gives the per cent increase in volume for each of the samples.

TABLE 3. VOLUME INCREASE ON HEATING

Nchanga	50%
RA5	70%
RA6	60%
RA7	100%
Gl	100%

It is not unusual for commercial vermiculites and hydrobiotites to expand to 20 times their volume or 1900%. When the heated samples were examined under the binocular microscope, long vermicules were observed indicating that the volume increase of some individual fragments had been far greater than the increase exhibited by the bulk samples.

Differential thermal analysis

Loss of either H_2O or OH^- is indicated on the differential thermal analysis apparatus as an endothermic reaction. Because the H_2O is held in the lattice by its polarity, while the OH^- is held by ionic bonding, there is a large difference in the temperature at which each is driven off. H_2O is lost from the vermiculite lattice in two stages at temperatures between 50° C. and 250° C. The first stage represents the removal of the hydration envelopes surrounding the magnesium ions in the exchange position and gives an endothermic peak between 150° C. and 200° C. The second stage represents the loss of a residual monomolecular layer of H_2O occupying space between the magnesium ions in the exchange position and gives an endothermic peak between 250° C. and 275° C. (Grim, 1953, p. 231). Removal of OH^- from the chlorite lattice requires a temperature of about 600° C. Both vermiculite and chlorite lose OH^- from the talc layer and decompose in the vicinity of 800° C. giving an endothermic reaction (Grim, 1953, pp. 231, 238).

The Roan Antelope specimens, G1, RA5, RA6, and RA7 give endothermic peaks at 150° C., 250° C., and 840° C. (Fig. 7) indicating vermiculite. RA5, RA6, and RA7 also show small peaks at 580° C. indicating the presence of some chlorite along with the vermiculite. G1, however, shows no peak at 580° C. and gives strong vermiculite reactions. The Nchanga specimen gives endothermic peaks at 300° C., 580° C., and 840° C. The endothermic peak at 300°–320° C. is pronounced in four of the samples but does not correspond with data that the author was able to find in the literature. Possibly this peak represents the loss of H_2O which is more tightly bound due to a high concentration of OH^- in the intersilicate layer. A high concentration of OH^- in this position would hold H_2O molecules entrapped making a higher temperature necessary for their removal.

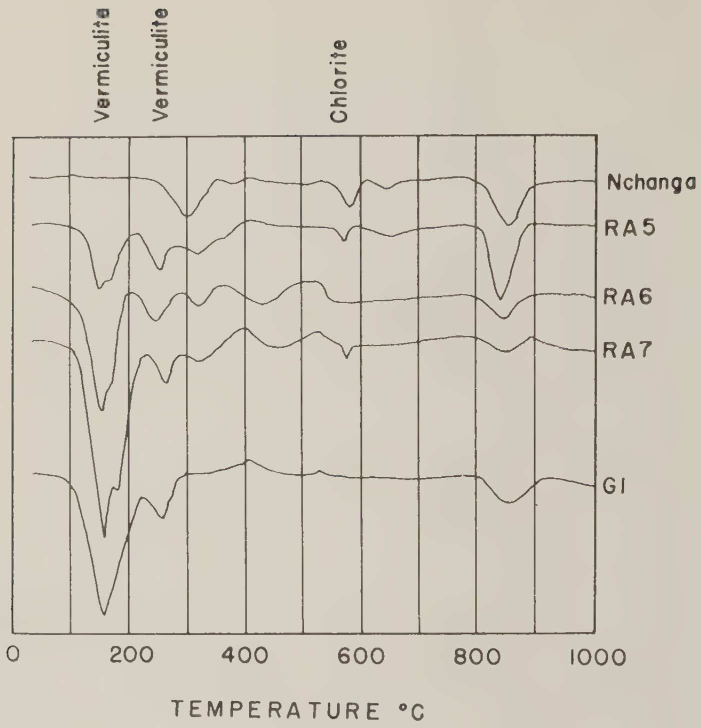

Fig. 7. Differential thermal analysis curves of five copper vermiculites from Northern Rhodesia.

Direct measurements of weight loss on drying

Table 4 shows the percentage weight loss of drying for each of the copper vermiculites and for a typical magnesium vermiculite from Corundum Hill, North Carolina. While the specimens from Roan Antelope lose from 3.85 to 5.90 per cent of their weight on drying at 260° C., the Nchanga specimen loses only 0.75 per cent. When the Nchanga specimen is heated just over 300° C. (exceeding the DTA peak at 300° C.), the

Table 4. Weight Loss on Drying

Sample	At 260° C.	At 300° C.
Nchanga	0.75%	1.2%
RA5	4.75%	
RA6	4.85%	
RA7	3.85%	
G1	5.90%	
Corundum Hill	13.5 %	

weight loss becomes 1.2 per cent which indicates that the material contains far less H_2O and more OH^- than the other samples and that the H_2O is lost at a higher temperature presumably because the greater OH^- content impedes the removal of the H_2O as suggested in the preceding section.

Thermal increment diffractometer

The thermal increment diffractometer (Bassett and Lapham, 1957) is designed to raise the temperature of a powdered sample while it is continuously subject to *x*-ray diffraction on a Norelco goniometer. The instrument makes it possible to chart the collapse of the vermiculite lattice as a function of temperature. A typical vermiculite from North Carolina shows two stages of dehydration, one just below 100° C and the other at about 200° C. (Fig. 8). Weiss and Rowland (1956) show a similar graph for jefferisite from West Chester, Pennsylvania. Walker recognizes six different stages of dehydration in vermiculite specimens from Kenya and from West Chester, Pennsylvania. They are 14.91 Å, 14.36 Å, 13.82 Å, 11.59 Å, 20.6 Å, and 9.02 Å. The shifts from 14.36 Å to 11.59 Å and from 11.59 Å to 9.02 Å are the most pronounced and unless the material is very pure and a great deal of care taken in its study, the other stages are difficult to observe. The two stages will suffice for the present purpose of distinguishing vermiculite from chlorite and recognizing mixed layer materials.

The Nchanga specimen shows no collapse during heating on the thermal increment diffractometer (Fig. 9). The 14 Å, 12 Å, and 10 Å reflections persist to nearly 500 ° C. with a gradual decline in intensity for the 14 Å and 12 Å peaks between 400° C. and 500° C. There is no change in either intensity or spacing at 300° C. to correspond with the DTA peak at that temperature. Apparently so much of the material is chlorite and mixed layer chlorite-biotite that no collapse is permitted.

The collapse in RA5 during heating from 25° C. to 200° C. is only from 14.48 Å to 14.13 Å. The intensity falls rapidly below 100° C., then gradually between 100° C. and 200° C. The fact that the 14 Å spacing does not collapse significantly but simply loses its intensity indicates the presence of a large amount of chlorite.

The 14 Å reflection of RA6 shows an immediate decrease in intensity and a rapid collapse of the 14 Å spacing indicating that the material is largely vermiculite. Unfortunately, the intensity decreases so fast that there is no opportunity to see if there is a second stage of dehydration.

RA7, also, has a 14 Å reflection which readily collapses and loses its intensity. The 12 Å reflection of the mixed layer material collapses also but its intensity increases and persists long enough to show a collapse be-

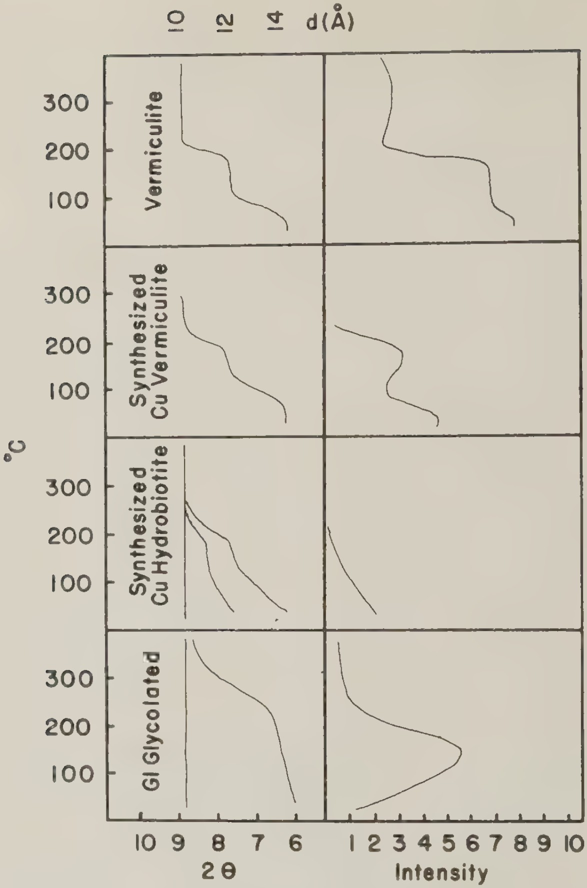

FIG. 8. Lattice collapse caused by dehydration on the thermal increment diffractometer.

low 100° C. and a leveling off at a constant spacing between 100° C. and 200° C. This is the behavior one should expect from vermiculite and hydrobiotite.

G1 gives the most satisfactory results on the thermal increment diffractometer. Its reflections persist to 200° C. and show the two stages of collapse found in the North Carolina specimen, the only difference being that the two stages of collapse seem to take place 20° C. or 30° C. lower in G1 than in the normal vermiculite. Also, the breaks are not as sharp as those in the normal vermiculite.

Because G1 gave reasonably good results, it was selected to be glycolated to determine if its behavior after glycolation would be similar to

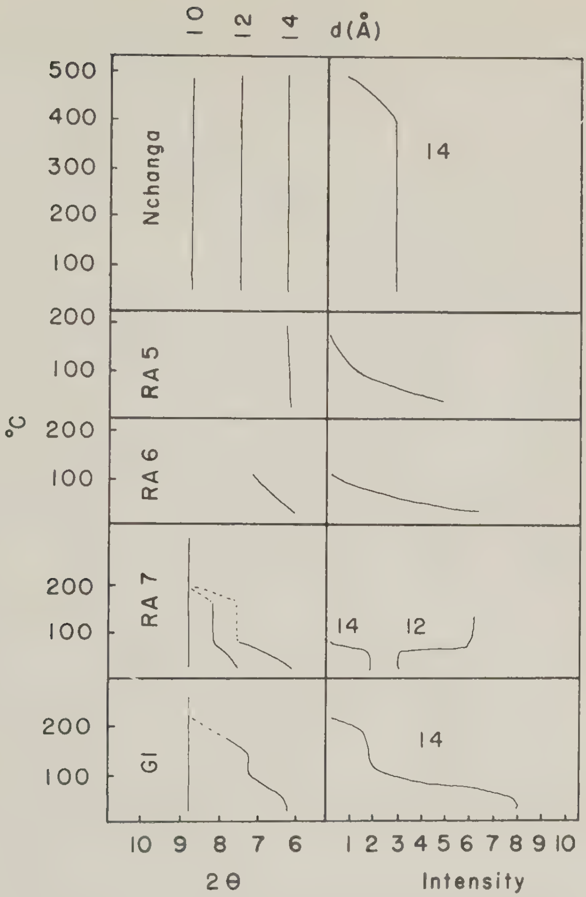

FIG. 9. Lattice collapse caused by dehydration on the thermal increment diffractometer.

that of abnormal vermiculite. According to Dr. Richards A. Rowland (personal communication), the glycolated material, if it is a true vermiculite, should have a more stable 14 Å spacing representing a single layer of glycol (in the place of two layers of H_2O) which should persist to a temperature well above 100° C. When G1 was glycolated and run on the thermal increment diffractometer, the 14 Å spacing shifted only slightly between room temperature and 230° C. (Fig. 8). Between these temperatures, the intensity rose and then fell. Between 230° C. and 400 °C., the 14 Å spacing collapsed to nearly 10 Å and the intensity fell to a low level.

Both copper vermiculite and copper hydrobiotite synthesized from biotite were run on the thermal increment diffractometer. The collapse exhibited in each case is very similar to the collapse observed in G1 and RA7 respectively (Fig. 8, 9).

Exchange of large univalent ions for small bivalent ions

When a pure vermiculite is placed in a potassium chloride or ammonium acetate solution and boiled for 80 hours, the potassium or ammonium enters the exchange position of the vermiculite and replaces the hydrated magnesium ions (Gruner, 1939). Since the hydrated magnesium ion is considerably larger than the unhydrated potassium or ammonium (they do not enter the exchange position in the hydrated form because they are too large to octahedrally coordinate six water molecules around them), the exchange causes a collapse of considerable proportions (14 Å to 10 Å). When potassium is used, the resultant material is a biotite.

When chlorite is submerged in potassium choride, there is no change in the spacing. The magnesium in the brucite layer is so tightly bound by the hydroxyl ions that no substitution can take place.

Mixed layer vermiculite-chlorite boiled in molar potassium chloride yields mixed layer biotite-chlorite which has a 12 Å spacing (Weaver, 1956). If a mechanical mixture of chlorite and vermiculite is boiled in molar potassium chloride, the vermiculite collapses leaving the chlorite pattern intact.

Each of the African specimens was boiled in molar potassium chloride for 80 hours. After this treatment they were run on the diffractometer (Fig. 10). Nchanga shows no sign of collapse indicating that the material is dominantly chlorite as was concluded from some of the other techniques. RA5, after treatment with potassium chloride shows a 14 Å reflection of diminished intensity but it shows no 10 Å reflection. Perhaps the 10 Å reflection is missing because the vermiculite does not collapse nicely to 10 Å, but instead collapses to a number of spacings in the vicinity of 10 Å. The pattern remaining after the potassium chloride treatment is that of chlorite.

After treatment with potassium chloride RA6 gives a far weaker chlorite pattern than the one encountered in RA5. A weak 10 Å peak appears indicating that at least some of the vermiculite was present as a mechanical mixture. The 14 Å and 12 Å reflections of RA7 both readily shift to 10 Å. Weak reflections at 7Å, 4.7 Å, and 3.5 Å indicate the presence of some chlorite in the original sample.

The potassium treatment causes the greatest change in G1. No 14 Å reflection remains and only weak ones persist at 7 Å, 4.7 Å, and 3.5 Å representing a minor amount of chlorite mechanically mixed with the vermiculite and biotite. The increased intensity of the 10 Å reflection results from nicely collapsed vermiculite indicating that there was no mixed layer structure in the original sample. The most interesting peak appearing in this run is at 17.52° 2*θ* (5.057 Å). Most normal biotites have a 5 Å reflection of zero or nearly zero intensity. In this run the intensity is 11 ($I_{10Å}$ =100). The author has attributed this to the presence of copper ions in the intersilicate position among the potassium ions. A 5 Å peak of 6 intensity appears in the diffraction pattern of RA7 after potassium chloride treatment suggesting a similar situation for that sample.

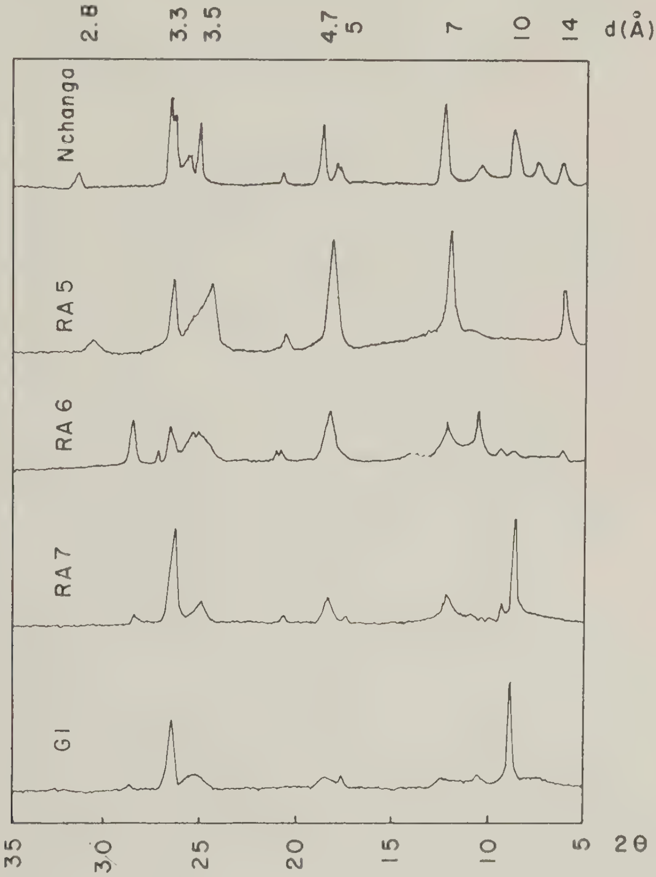

FIG. 10. *X*-ray diffraction diagrams of five copper vermiculites from Northern Rhodesia after treatment with potassium chloride.

When synthesized copper vermiculite was treated with molar potassium chloride at 100° C., the potassium did not replace the copper and no collapse took place. It is believed that some magnesium must be present along with the copper before potassium can enter the lattice and cause collapse. The synthesized copper vermiculite formed in a solution containing no cations but copper. Therefore, the material which resulted was a pure copper vermiculite with no magnesium. The natural copper vermiculites had access to magnesium and seem to have assimilated enough magnesium to permit collapse when subjected to the potassium chloride treatment.

COMPOSITION OF COPPER VERMICULITE

There are three specimens of copper vermiculite which are uncomplicated by chlorite or interstratification. They are the two synthesized copper vermiculites and G1. These three specimens have 7 Å reflections which are about one third the intensity of the 14 Å reflections (Table 5).

TABLE 5

Specimen	I_7/I_{14}
Mg Vermiculite	0.080
Vermiculite+Cu	0.346
G1	0.377
Biotite+Cu	0.380
RA6	0.625
RA5	0.877
Chlorite	2.500

According to structure factor calculations (Fig. 11), these three specimens have about 0.8 copper ions per ten oxygen atoms. This is corroborated by the 10% copper analysis for the synthesized copper vermiculites. G1 would probably have a comparable copper content were it not diluted by biotite.

Previous workers (Barshad, 1948; Walker, 1956) have found less than 0.5 magnesium ions per ten oxygen atoms in the vermiculite exchange position. One should expect 0.5 or less if magnesium or cupric copper is substituting stoichiometrically for potassium in biotite which has one potassium ion per ten oxygen atoms.

The high copper content of the specimens mentioned above is accounted for by the influx of hydroxyl ions with the cupric ions as they enter the exchange position. The hydroxyl ions attach themselves to the cupric ions leaving the solution acid. The molar cupric chloride used in the synthesis of copper vermiculite has a pH of 3.0 while the molar magnesium chloride has a pH of 6.1 (the pH of the distilled water used in the preparation of the solutions). The tenacity of the copper in the vermiculite lattice which makes the commercial recovery of the copper so dif-

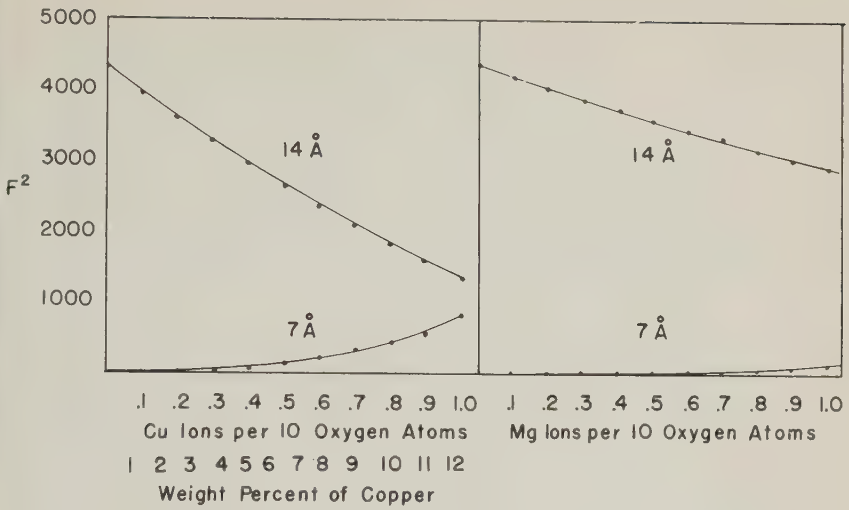

FIG. 11. F^2 (theoretical intensity) as a function of the copper and magnesium content of the exchange position of vermiculite.

ficult may be attributed to the presence of the hydroxyl ions.

The following general formula for simple copper vermiculite is suggested:

$$Cu_{0.8}(Mg, Fe)_3(Al, Si_3)O_{10}(OH)_2 \cdot xH_2O(OH)_{0.6}$$

It differs significantly from the general formula for magnesium vermiculite:

$$Mg_{0.5}(Mg, Fe)_3(Al, Si_3)O_{10}(OH)_2 \cdot xH_2O$$

Although it can be shown by differential thermal analysis, exfoliation, and direct weight measurements that both RA5 and Nchanga contain considerable amounts of H_2O, the other dehydration techniques indicate a large percentage of OH^- in the intersilicate position. In these samples the copper ions must be hydrated to a large degree by OH^- ions rather than H_2O, in which case they verge on being copper chlorites. Thus, there appears to exist a complete series from copper vermiculite which contains no more OH^- than is indicated by the formula given above to copper chlorite, in which the copper is hydrated by OH^- to the exclusion of H_2O. The samples dealt with have been termed copper vermiculites because they all contain significant quantities of loosely bound intersilicate water molecules.

CONCLUSIONS

X-ray diffraction studies and dehydration procedures have shown that the copper bearing micaceous materials from Africa contain vermiculite.

The flakes of vermiculite contain microscopic red and yellow inclusions which have been identified as hematite and goethite. The paucity of recognizable copper minerals even among the microscopic inclusions in the vermiculite flakes suggests that the copper is contained within the vermiculite lattice. Ion exchange experiments show that copper enters the exchange position of vermiculite. *X*-ray diffraction diagrams reveal certain similarities between synthesized copper vermiculite and the copper bearing micaceous materials from Africa which indicate that the samples from Africa contain copper within the exchange position of the vermiculite.

The ion exchange procedures used to synthesize copper vermiculite were carried out in molar solutions at 100° C. so that the reaction would take place in a reasonable length of time. These processes, however, would take place in more dilute solutions and at lower temperatures over longer periods of time. This and the fact that copper vermiculites are found in the oxidation zone suggest a low temperature supergene origin. Roy and Romo (1957) have indicated that vermiculite can form only under conditions of low temperature and pressure.

The samples of copper vermiculite from Northern Rhodesia are believed to have formed when copper solutions percolating through the oxidation zone encountered mixtures of biotite, chlorite, quartz, and tremolite reacting with the biotite to form copper vermiculite in varying mixtures with the other minerals.

ACKNOWLEDGMENTS

This paper represents a study conducted in the mineralogical laboratory of Columbia University, and was written at the suggestion and with the advice of Professor Paul F. Kerr, who has provided assistance and encouragement. The author is indebted to the Roan Antelope Copper Jenny Mines, Ltd. and to the Anglo American Corporation for samples and for permission to publish this report. He also wishes to acknowledge the efforts of Dr. Marc W. Bodine and Mr. Arnold J. Silverman in preliminary studies of the copper bearing micaceous materials from Africa. Dr. Richards A. Rowland of the Shell Research and Development Laboratory, Houston, Texas, provided advice and criticism on the work involving the application of the thermal increment diffractometer. These forms of assistance are greatly appreciated.

REFERENCES

BARSHAD, I. (1948), Vermiculite and its relation to biotite as revealed by base exchange reactions, *x*-ray analysis, differential thermal curves and water content: *Am. Mineral.*, **33,** 655–678.

Bassett, W. A. and Lapham, D. M. (1957), A thermal increment diffractometer: *Am. Mineral.*, **42,** 548–555.

Grim, R. E. (1953), Clay mineralogy: McGraw-Hill.

Gruner, J. W. (1934), The structure of vermiculites and their collapse by dehydration: *Am. Mineral.*, **19,** 557–575.

Gruner, J. W. (1939), Ammonium mica synthesized from vermiculite: *Am. Mineral.*, **24,** 428–433.

Roy, R. and Romo, L. A. (1957), Weathering studies 1. New data on vermiculite: *Journal of Geology*, **65,** 603–610.

Walker, G. F. (1956), The mechanism of dehydration of magnesium vermiculite: Proceedings of Fourth National Conference on Clay and Clay Minerals—National Academy of Sciences—National Research Council, 101–115.

Weaver, C. E. (1956), The distribution and identification of mixed layer clays in sedimentary rocks: *Am. Mineral.*, **41,** 202–221.

Weiss, E. J. and Rowland, R. A. (1956), Effect of heat on vermiculite and mixed-layered vermiculite-chlorite: *Am. Mineral.*, **41,** 899–914.

Manuscript received March 17, 1958.

THE AMERICAN MINERALOGIST, VOL. 43, NOVEMBER-DECEMBER, 1958

HEINRICHITE AND METAHEINRICHITE, HYDRATED BARIUM URANYL ARSENATE MINERALS

EUGENE B. GROSS* AND ALICE S. COREY,** *U. S. Atomic Energy Commission, Grand Junction, Colorado*
RICHARD S. MITCHELL, *University of Virginia, Charlottesville, Virginia*
AND
KURT WALENTA, *Institut für Mineralogie und Kristallchemie, Stuttgart, Germany.*

ABSTRACT

Heinrichite, $Ba(UO_2)_2(AsO_4)_2 \cdot 10\text{–}12H_2O$, and metaheinrichite, $Ba(UO_2)_2(AsO_4)_2 \cdot 8H_2O$, occur as tabular, yellow to green, fluorescent, transparent to translucent crystals belonging in the tetragonal system. Optically the minerals are uniaxial (−), sometimes anomalously biaxial with 2V up to 20°. The refractive indices of heinrichite are: $\omega = 1.605 \pm 0.002$ and $\epsilon = 1.573 \pm 0.002$. Those for metaheinrichite are: $\omega = 1.637 \pm 0.001$ (1.641 ± 0.002 for the mineral from the Black Forest, Germany) and $\epsilon = 1.609 \pm 0.002$. The calculated specific gravity of metaheinrichite is 4.09 and the measured specific gravity is 4.04. The space group of metaheinrichite is $P4_2$, $P4_2/m$, or $P4_222$; $a_0 = 7.07$ Å, $c_0 = 17.74$ Å, and $a_0 : c_0 = 1:2.509$, $Z = 2$.

The minerals have thus far been found near Lakeview, Oregon, and in the Black Forest of Germany. They are named for Professor E. William Heinrich, University of Michigan.

INTRODUCTION

In his description of the uranium deposits of the central Black Forest, Germany, Kirchheimer (1952, p. 56) mentioned a yellow secondary uranium mineral which he called meta-uranocircite or a similar barium uranyl arsenate. Bültemann (1954, p. 160) confirmed this, stating that he found small crystals of a secondary uranium mineral containing barium, uranium, arsenic, and water on specimens from the Anton mine. Walenta made a more thorough investigation of the Black Forest material which he described in an unpublished, preliminary report (Walenta, 1958).

In 1956 specimens of a mineral from the White King mine, Lakeview, Oregon, originally believed to be novacekite, were sent to the Mineralogy Laboratory, U. S. Atomic Energy Commission, Grand Junction, Colorado, by E. K. Thurlow, Salt Lake Exploration Branch, Atomic Energy Commission, and H. B. Wood, Geologic Branch, Atomic Energy Commission, Grand Junction. A spectrographic analysis of this mineral showed the presence of major amounts of barium, uranium, and arsenic. The material studied in the Atomic Energy Commission Mineralogy Laboratory was taken from ore shipped to Climax Uranium Company, Grand Junction.

---

* Present address: 755—15th St., Boulder, Colorado.

** Present address: Box 17, Ouray, Colorado.

In his preliminary report Walenta called the minerals sandbergerite and metasandbergerite (Walenta 1958, pp. 4–7, Guillemin and Permingeat, 1958, pp. 68–69). Simultaneously Gross, Corey, and Mitchell named the minerals heinrichite and metaheinrichite, for Professor E. William Heinrich, Department of Mineralogy, University of Michigan. The names heinrichite for $Ba(UO_2)_2(AsO_4)_2 \cdot 10\text{-}12H_2O$ and metaheinrichite for the lower hydrate with $8H_2O$ have since been accepted by all the authors.

Both hydrates are common in the Black Forest material. Only traces of the higher hydrate were found during the study of the minerals from Oregon because heinrichite dehydrates readily to metaheinrichite and the laboratory investigations took place under conditions of low relative humidity. Only freshly broken crystals showed the lower refractive indices and these fragments very shortly dehydrated.

OCCURRENCE

Heinrichite and metaheinrichite are found in the White King mine, sec. 30, T. 37 S., R. 19 E., approximately 14 miles northwest of Lakeview, Lake County, Oregon (Fig. 1). The minerals coat fractures and line vugs in light gray, altered, silicified rhyolite tuff. They are present at or near the surface, while at greater depth the uranium mineral is coffinite, which is associated with orpiment and realgar.

In the central Black Forest, heinrichite and metaheinrichite have thus far been discovered at three different localities: Wittichen (Sophia mine), Anton mine near Schiltach, and Reinerzau. They occur as small crystals and coatings of scaly aggregates on granite and on the gangue minerals, barite and quartz. They are formed from the alteration of pitchblende, a primary constituent of the Co-Ni-Bi-Ag-U veins of the region, and are

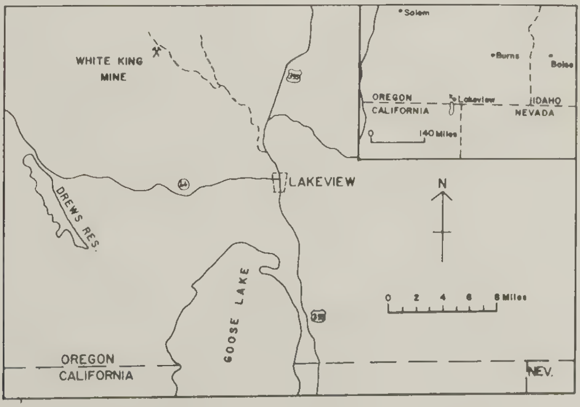

FIG. 1. Map of Lakeview, Oregon, and vicinity, showing location of the White King mine.

associated with other secondary uranium minerals, mainly zeunerite and novacekite, and with erythrite, arseniosiderite, and pitticite.

Physical and Optical Properties

The physical appearance of heinrichite and metaheinrichite crystals (Fig. 2) is identical. The crystals are transparent to translucent and yellow to green in color and have a vitreous to pearly luster. The minerals fluoresce bright green to greenish yellow under short and long wave ultraviolet light.

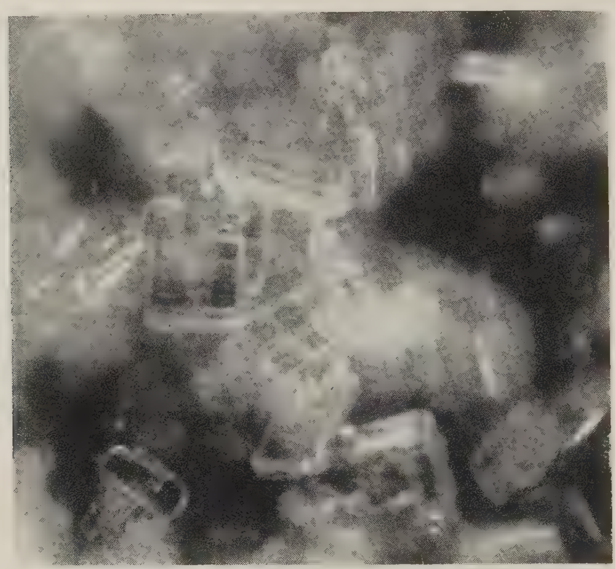

Fig. 2. Tabular crystals of metaheinrichite in vug from Oregon. ×50.

The crystals from Oregon are tabular {001} and are up to one mm. on a side, and not more than 0.1 mm. thick. Cleavage is perfect on {001} and distinct on {100} (Fig. 3). The forms observed are {001}, {100}, and {110}. Crystals from the Black Forest show the same cleavage and the same forms, but in part are elongated along a horizontal axis so that in their aspect they resemble the monoclinic bassetite crystals described by Frondel (1954, p. 348).

The hardness is 2.5. The calculated specific gravity of metaheinrichite is 4.09. A specific gravity of 4.04 was measured on material from Oregon dried at 110° C. using kerosene and a 10 ml. Leach pycnometer. Repeated grindings and separations using acetylene tetrabromide failed to eliminate a small percentage of host rock so that the measured value is slightly lower than the calculated one. Attempts to measure the specific gravity of

TABLE I. OPTICAL PROPERTIES OF HEINRICHITE AND METAHEINRICHITE

Black Forest	Oregon
Heinrichite	
Refractive indices Pleochroism	Refractive indices Pleochroism
$\omega=1.605\pm0.002$, pale yellow $\epsilon=1.573\pm0.002$, colorless Uniaxial (−), sometimes anomalously biaxial with 2V up to 20°.	$\omega=$- - - - - - - - - - - $\epsilon=1.574\pm0.001$, colorless Uniaxial (−), sometimes anomalously biaxial.
Metaheinrichite	
$\omega=1.641\pm0.002$, pale yellow $\epsilon=1.609\pm0.002$, colorless Uniaxial (−), sometimes anomalously biaxial with 2V up to 18°.	$\omega=1.637\pm0.001$, pale yellow $\epsilon=1.609\pm0.001$, colorless Uniaxial (−), sometimes anomalously biaxial with 2V up to 10°.

the Black Forest minerals failed because of the small amount of material available.

The optical properties of heinrichite and metaheinrichite are given in Table I.

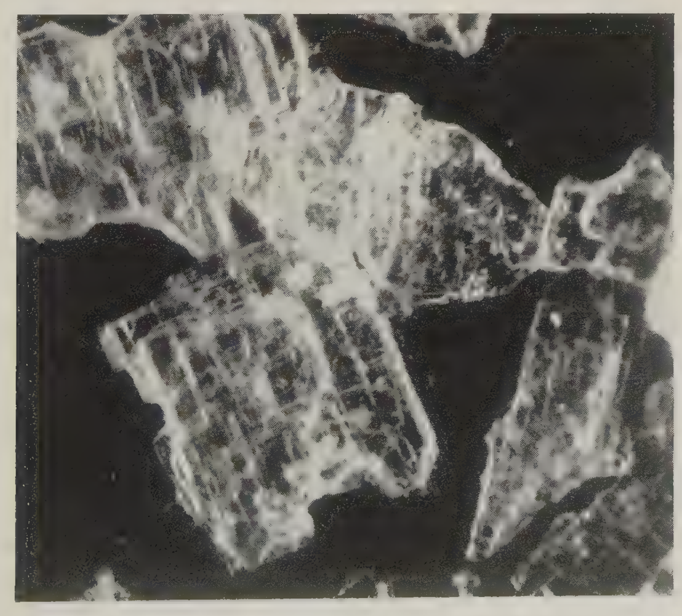

FIG. 3. Cleavage fragments of metaheinrichite from Oregon lying on (001), showing traces of (100) and (010) cleavages. ×100.

COMPOSITION

Two semi-quantitative spectrographic analyses of metaheinrichite from Oregon are given in Table II. The results agree closely with those of the chemical analysis (Table III). No phosphorus was detected in the heinrichite and metaheinrichite from the Black Forest, but a small quantity of copper was detected in some crystals.

The ideal formula for metaheinrichite, $Ba(UO_2)_2(AsO_4)_2 \cdot 8H_2O$, was derived from the recalculated chemical analysis given in Table IV. It

TABLE II. SEMI-QUANTITATIVE SPECTROGRAPHIC ANALYSES OF METAHEINRICHITE FROM OREGON

Element	(1) %	(2) %
Si	.3	.3
Al	.3	.3
Fe	.15	.1
Mg	.03	.003
Ca	.07	.1
P	1.5	1.0
Na	—	<.01
K	—	.003
Ti	—	.001
Mn	—	.003
As	M	M
Ba	M	M
Bi	<.1	—
Cu	.07	.003
Pb	.7	1.0
Sb	<.1	—
Sr	—	.003
U	M	M

M: Major constituent, greater than 10%.

—: Not looked for.

Looked for, but not detected: Ag, Au, B, Be, Cd, Ce, Co, Cr, Cs, Dy, Er, Eu, Ga, Gd, Ge, Hf, Hg, Ho, In, Ir, La, Li, Lu, Mo, Nb, Nd, Ni, Os, Pd, Pr, Pt, Rb, Re, Ru, Sc, Sn, Sm, Ta, Tb, Te, Th, Tl, Tm, V, W, Y, Yb, Zn, Zr.

(1) Analyst, Nancy Conklin: U. S. Geological Survey, Denver, Colorado. Figures are reported to the nearest number in the series 7, 3, 1.5, 0.7, 0.3, 0.15, etc. in per cent. Sixty per cent of the reported results may be expected to agree with the results of quantitative methods.

(2) Analyst: Katherine V. Hazel, U. S. Geological Survey, Washington, D. C. Figures are reported to the nearest number in the series 10, 3, 1, .3, etc. in per cent. Eighty per cent of the reported results may be expected to agree with the results of quantitative methods.

was assumed that some phosphorus has substituted for arsenic, and calcium for barium. The phosphorus and calcium were therefore recalculated as arsenic and barium respectively.

The portion insoluble in (1+3)HCl is rhyolite tuff carried down by metaheinrichite in the heavy separation. The role of lead and carbon dioxide is not known and they were also eliminated in the calculation of the ideal formula. It is assumed that most, if not all, of the $H_2O(-)$ (Table III) is zeolitic or adsorbed water since the material dried at 110° C. gives an *x*-ray powder pattern identical to that of the undried material.

TABLE III. CHEMICAL ANALYSIS OF METAHEINRICHITE FROM OREGON
Analyst: Robert Meyrowitz, U. S. Geological Survey

Constituent	%	Note
BaO	13.3	*e, h*
UO_3	52.5	*d, h*
As_2O_5	15.8	*i*
P_2O_5	2.4	*f, h*
PbO	0.9	*c, h*
CaO	0.1	*g, h*
CO_2	0.6	*j*
H_2O	12.2	*j*
Insoluble, (1+3) HCl	2.4	*b, h*
Total	100.2	
$H_2O(-)$	10.6	*a, h*

Notes:

a. Dried to constant weight at 110±5 degrees C.

b. Insoluble determined by dissolving sample with cold (1+3) HCl. Residue filtered, washed with dilute HCl and water, and weighed to constant weight at 110±5 degrees C.

c. Lead determined as sulfate following separation as PbS after removal of arsenic.

d. Uranium determined spectrophotometrically by ammonium thiocyanate procedure in acetone-water medium.

e. Barium separated and determined as sulfate.

f. Phosphorus determined spectrophotometrically by molybdenum-blue procedure using stannous chloride as reducing agent.

g. Calcium determined by flame photometry (wave length = 554 mμ).

h. Sample size for $H_2O(-)$, (1+3) HCl Insoluble, PbO, UO_3, BaO, P_2O_5, and CaO determinations was approximately 52 mg.

i. Arsenic separated by distillation as $AsCl_3$, following reduction by hydrazine sulfate and potassium bromide, and determined by titration with potassium bromate using p-ethoxychrysoidine as indicator. Sample size was approximately 29 mg.

j. CO_2 and H_2O determined by use of a microcombustion train, after decomposition of sample by ignition at 900 degrees C. in a stream of oxygen. Sample size was approximately 30 mg.

The procedures used were selected on the basis of the semiquantitative spectrographic analysis by Katherine V. Hazel, given in Table II.

TABLE IV. CORRECTED ANALYSIS OF METAHEINRICHITE FROM OREGON

Constituent	I Corrected Analysis[1] %	II Analysis I corrected to 100% %	III $Ba(UO_2)_2(AsO_4)_2 \cdot 8H_2O$ %
BaO	13.6	13.9	13.94
UO_3	52.5	53.5	52.05
As_2O_5	19.7	20.1	20.90
H_2O	12.2	12.5	13.11
Total	98.0	100.0	100.00

[1] Analysis of Meyrowitz (Table III), after elimination of PbO, CO_2, and Insoluble, with P_2O_5 calculated as As_2O_5 and CaO calculated as BaO.

Metaheinrichite is a member of the torbernite group. Table V gives a comparison of metaheinrichite and its analog meta-uranocircite, another member of the group.

No chemical analysis was carried out on heinrichite. The formula, $Ba(UO_2)_2(AsO_4)_2 \cdot 10\text{–}12H_2O$, is assumed on the basis of the similarity of its x-ray powder pattern to that of zeunerite, $Cu(UO_2)_2(AsO_4)_2 \cdot 10\text{–}12H_2O$.

TABLE V. COMPARISON OF DATA FOR METAHEINRICHITE AND META-URANOCIRCITE

	Metaheinrichite	Meta-uranocircite
Composition	$Ba(UO_2)_2(AsO_4)_2 \cdot 8H_2O$	$Ba(UO_2)_2(PO_4)_2 \cdot 8H_2O$[1]
Specific gravity	4.09 (calc.) 4.04 (meas.)	4.10 (calc.)[2] 4.08 (meas.)[3]
Optical	Uniaxial (−)	Uniaxial (−)
Space group	$P4_2$, $P4_2/m$, or $P4_222$	$P4_222$
Cell values	$a_0 = 7.07$ Å $c_0 = 17.74$ Å	$a_0 = 6.98$ Å[4] $c_0 = 16.85$ Å
$a_0:c_0$	1:2.509	1:2.416[4]
Z	2	2[4]

[1] Called "meta-uranocircite" by Strunz (1957).

[2] Data from Donnay and Donnay (1955).

[3] Data from Nuffield and Milne (1953).

[4] Data from Strunz (1957).

X-RAY DATA

Fragments of Oregon metaheinrichite exhibiting {001} and {100} cleavages were easily oriented for x-ray study. Good a axis rotation photographs as well as 0-l, 1-l, 2-l, and 3-l Weissenberg photographs were made using a camera of 5.73 cm. diameter and unfiltered Cu radiation. In addition to these, c axis 0-l, 1-l, and 2-l precession photographs were made using the same radiation. A study of these films showed that the system is tetragonal. The space group appears to be either $P4_2$, $P4_2m$, or $P4_222$, since the only characteristic missing reflections are $00l$ when $l \neq 2n$. At

TABLE VI. X-RAY POWDER DATA ON METAHEINRICHITE FROM OREGON

hkl	d(calc.) Å	d(obs.) Å	I	hkl	d(calc.) Å	d(obs.) Å	I
002	8.87	8.90	vs	118	2.03	2.02	mw
100	7.07	7.08	w	127	1.98	1.97	vw
101	6.57	6.56	mw	305, 230	1.96		
102	5.53	5.54	ms	231	1.95	1.95	vw
110	5.00	4.99	m	232, 226	1.91	1.92	vw
111	4.81	4.81	w	233	1.86	1.86	w
004	4.44	4.42	ms	234	1.79	1.79	vw
104	3.76	3.75	s	00·10, 400	1.77		
200	3.54	3.55	ms	401	1.76	1.76	w
201	3.47	3.47	mw			1.72	w
202	3.28	3.28	ms			1.67	mw
105	3.17	3.17	vw			1.64	vw
203	3.03	3.05	w			1.60	vvw
122	2.98	2.98	m			1.58	mw
115	2.89	2.89	vvw			1.55	vw
123	2.79	2.79	mw			1.53	vvw
106	2.73	2.72	mw			1.48	w
124	2.57	2.57	w			1.45	w
205, 220	2.50	2.49	mw			1.42	w
222	2.41	2.41	mw			1.39	vw
125, 300	2.36	2.35	vvw			1.38	vw
301	2.34					1.36	vvw
302	2.28	2.28	vvw			1.34	vvw
131, 008	2.22	2.22	m			1.31	w
224	2.18					1.28	vvw
132	2.17	2.17	mw			1.27	vw
126	2.16					1.25	w
108	2.12	2.12	vw			1.23	w
133	2.09					1.22	vw
304	2.08	2.08	vw				

vs very strong, s strong, ms medium strong, m medium, mw medium weak, w weak, vw very weak, vvw very very weak.

first the *hk*0 reflections also appeared to be missing when $h+k\neq 2n$, but closer inspection revealed that some of these reflections are present, though weak. Approximate unit cell values, which were of great value in the initial indexing of powder films, were also obtained from these single crystal films.

TABLE VII. *X*-RAY POWDER DATA ON HEINRICHITE AND METAHEINRICHITE FROM THE BLACK FOREST

Heinrichite

d(obs.) Å	I	*d*(obs.) Å	I	*d*(obs). Å	I
8.89	8	2.25	5	1.593	2
5.03	8	2.11	5	1.534	2
4.50	1	1.94	1	1.204	2
3.57	10	1.868	1	1.164	2
3.38	7	1.802	1	1.150	2
2.77	1	1.733	1	1.126	2
2.53	2	1.679	1		

Except for the strongest lines in the first part of the photographs, the lines are rather diffuse.

Metaheinrichite

9.26	4	2.70	4	1.481	3
8.55	10	2.57	2	1.449	2
5.41	9	2.48	1	1.422	3
4.96	2	2.41	4	1.385	2
4.36	9	2.22	5	1.316	1
3.71	10	2.15	4	1.276	1
3.52	5	2.10	1	1.253	2
3.45	1	2.02	5	1.237	2
3.27	6	1.966	1	1.218	1
3.15	1	1.763	3	1.179	2
3.01	1	1.709	2	1.121	2
2.96	3	1.676	5	1.110	2
2.75	1	1.579	5	1.098	2

The measured *x*-ray powder data on Oregon metaheinrichite, listed in Table VI, represent the average of values obtained from three films made with CuKα radiation in three different cameras, each with a diameter of 11.46 cm. After the films were partly indexed, using approximate unit cell values determined from single crystal data, the c_0 and a_0 constants were further refined using the powder data. The final values obtained are $a_0=7.07$ Å and $c_0=17.74$ Å, with $a_0:c_0=1:2.509$. Using these values an excellent correlation was obtained between the observed and calculated *d* spacings. In the study all possible *d* values down to 1.21 Å were calculated. This resulted in a list of 192 *hkl* reflections. In Table VI only calculated values down to 1.76 Å are included. Beyond this point the number of calculated values which corresponds to any one observed value is so large that the inclusion of these data seems pointless. All values observed for the films have their corresponding calculated values except for an extremely weak reflection at 4.09 Å which was not on all the films and which is probably due to an impurity. Using a molecular weight of 1099.32 for $Ba(UO_2)_2(AsO_4)_2 \cdot 8H_2O$ and a measured specific gravity of 4.04, with the unit cell dimensions determined by *x*-ray study, it was determined that $Z=2$ (calculated value, 1.96).

X-ray powder data for heinrichite and metaheinrichite from the Black Forest are given in Table VII. These films were obtained using FeKα radiation and a camera of 5.73 cm. diameter. Most of the differences between the data for metaheinrichite from the Black Forest and that from Oregon are smaller than possible error in line measurement.

The similarity between the *x*-ray data for metaheinrichite and its analog meta-uranocircite is illustrated in Table V.

ACKNOWLEDGMENTS

The writers wish to express their appreciation for the assistance in this study of Howard Dutro, Lakeview Mining Company (Thornburg Brothers), Lakeview, Oregon; Robert Meyrowitz, U. S. Geological Survey, Washington, D.C.; and William F. Giannini, University of Virginia, Charlottesville, Virginia.

REFERENCES

BÜLTEMANN, H. W. (1954), Fluoreszenzanalytische Untersuchungen an sekundären Uran mineralien: *Neues Jb. Mineral.*, **86,** 155–162.

DONNAY, J. D. H. AND DONNAY, G. (1955), Contributions to the crystallography of uranium minerals: *U. S. Geological Survey Trace Elements Inv. Rept.* **507.**

FRONDEL, C. (1954), Bassetite and uranospathite: *Mineral. Mag.*, **30,** 343–353.

GUILLEMIN, C. AND PERMINGEAT, F. (1958), Revue des espèces minérales nouvelles: *Bull. Soc. fran. Mineral. Cristal.*, **81,** 68–69.

KIRCHHEIMER, F. (1952), Die Uranerzvorkommen des mittleren Schwarzwaldes: *Mittlg.-Bl. Bad. Geol. Landesanstalt f.*, **1951,** 1–74.

NUFFIELD, E. W. AND MILNE, I. H. (1953), Studies of radioactive compounds: VI -Meta-uranocircite: *Am. Mineral.*, **38,** 476–488.

STRUNZ, H. (1957), Mineralogische Tabellen, 3rd ed., Leipzig.

WALENTA, K. (1958), Die sekundären Uranmineralien des Schwartzwaldes: *Vorl. Mittlg. aus dem Inst. f. Mineralogie und Kristallchemie,* Technische Hochschule, Stuttgart (unpublished manuscript).

Manuscript received March 24, 1958.

THE AMERICAN MINERALOGIST, VOL. 43, NOVEMBER–DECEMBER, 1958

FIRST KNOWN OCCURRENCE OF INYOITE IN A PLAYA, AT LAGUNA SALINAS, PERU[1]

Siegfried Muessig *U. S. Geological Survey, Spokane, Washington.*

Abstract

Inyoite ($Ca_2B_6O_{11} \cdot 13H_2O$) is here reported from near the surface of the borate playa, *Laguna Salinas*, Peru. The mineral occurs as crystal aggregates in a discontinuous bed up to 15 cm thick beneath a ulexite-bearing bed near the edge of the playa. The inyoite is the first established occurrence of a calcium borate in a playa. The mineral is primary at this place and was probably formed at about the same time as the enclosing muds.

The first known occurrence of the borate mineral, inyoite ($Ca_2B_6O_{11} \cdot 13H_2O$), in a playa is in the *Laguna Salinas*, Peru. The inyoite was probably formed at about the same time as the enclosing playa muds and is primary rather than being an alteration product of another borate.

*Laguna Salinas** is a borate playa, or *salar*, that lies at an altitude of about 14,000 feet, about 40 miles east of Arequipa, Peru. The playa occupies an enclosed basin that is underlain by young volcanic rocks of andesitic and dacitic composition (Jochamowitz, 1907). The black and olive-brown muds at the playa surface are covered during much of the year by an efflorescence, which according to Jochamowitz is composed of halite and thenardite. At depths of 5 to 15 cm. below much or all the playa surface there is a white volcanic ash bed as much as 15 cm. thick. The bed is probably part of the ash that was deposited during the explosive eruption of one of the neighboring volcanoes in 1600 and covers much of the surface of the Arequipa region (Jenks, 1948). Under the ash bed are layers of sandy black mud that contain nodules and irregular layers of ulexite ($NaCaB_5O_9 \cdot 8H_2O$), the common mineral of the South American borate playas. The ulexite layers range from a few centimeters to 2.5 m. in thickness. So far as I know, no other ulexite-bearing beds have been found at greater depth in the playa. The inyoite lies below the ulexite-bearing bed near one edge of the playa; elsewhere the ulexite beds are underlain by olive-brown mud.

The inyoite occurs predominantly as crystal aggregates in a discontinuous but compact layer up to 15 cm. thick near the eastern edge of the playa near the Tusca hot spring. Some of the inyoite also occurs as tiny clear pseudorhombs disseminated in the mud accompanying the bed of crystal aggregates. The bed has an extent of a few acreas and lies about a meter below the surface in structureless black mud; within the mud and above the inyoite bed are irregularly shaped and unevenly distributed lenses and masses of ulexite. The volcanic ash lies above, interspersed with black mud, and covered by efflorescent salts. No inyoite occurs along the extreme edge of the playa.

---

[1] Publication authorized by the Director, U. S. Geological Survey.

* The following stratigraphic description of the playa is based on the detailed logs of regularly spaced exploration pits and on maps obtained by me from private sources.

Figure 1 shows one of the inyoite crystal aggregates. They are clouded by inclusions of the mud in which they lie. The crystals are well-formed pseudorhombohedrons, intergrown in cockscomb-like fashion. The basal pinacoid (001) and the prism (110) are the dominant forms, modified in some crystals by small but perfectly developed pyramids (111). In form, the crystals are identical with those described by Schaller (1916) from the type locality in Death Valley. The indices of refraction (in white light), compared with those reported by Schaller, are:

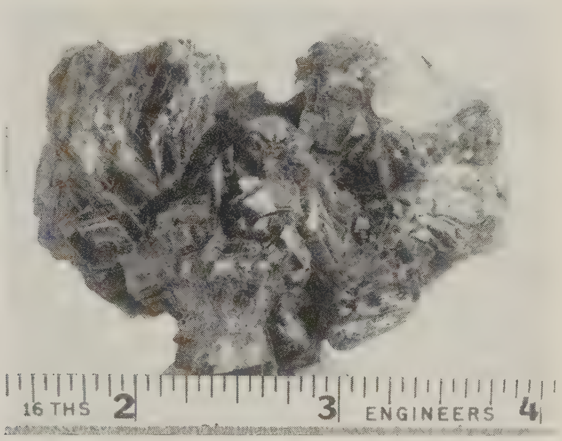

FIG. 1. Crystal aggregates of inyoite from Laguna Salinas, Peru.

	Peru	*California*
X	1.492±0.003	1.495
Y	1.505±0.003	1.51
Z	1.517±0.003	1.520
2V	Est. 70°–80°	70°
	Biaxial negative (−)	Biaxial negative (−)

Inyoite and ulexite have essentially the same indices of refraction; however, ulexite is biaxial positive (+) and has a distinctive fibrous habit.

The occurrence of inyoite is significant in two respects: (1) It is the only known occurrence of inyoite in a recent playa. Inyoite is the high hydrate of the colemanite series and it is therefore now known in an occurrence analogous to that of ulexite and borax, both the high hydrates of their respective mineral series. (2) This may be the first established occurrence of any calcium borate in a recent playa. Colemanite

($Ca_2B_6O_{11} \cdot 5H_2O$) has been reported from *Salar Cauchari*, Argentina, (Catalano, 1926) but more recent work in the same area by Ahlfeld and Angelelli (1948) and the writer suggests that the reported occurrence did not come from the *salar* but rather from the folded bedrock deposits in the same area. Foshag (1921), in a discussion of the physical and chemical conditions existing in playas, concluded that no calcium borates will form in them, as any calcium in solution will be fixed in the sodium-calcium borate, ulexite; the Peruvian occurrence of inyoite shows, however, that a calcium borate can form in playas, under surface or near-surface conditions of temperature and pressure.

The inyoite of the Salinas occurrence is primary, rather than being an alteration of an earlier borate mineral. This cannot be proved, of course, short of seeing the mineral actually growing in place. However, the facts that the inyoite has its own crystal habit rather than being pseudomorphous, and that so far no relicts of other borates have been recognized in the crystals convince me that the inyoite is the first-formed (primary) borate at this place. There seems no question that the crystals grew in the mud, and are therefore epigenetic if considered on a strict time scale, but on a grosser time scale the mud and the crystals formed at about the same time and in that sense can be considered syngenetic. That the inyoite is found only near a hot spring suggests that the constituents of the spring water were responsible at this place for the fixing of boron as inyoite rather than as ulexite. Moreover, if the ash bed is correctly dated, the inyoite could be very young.

The inyoite occurrence seems analogous to that of natron ($Na_2CO_3 \cdot 10H_2O$) in the alkaline lakes (wet playas) of British Columbia (Goudge, 1926). In these lakes natron occurs as surficial crusts and layers, which form during the winter and are called "winter crystal," and also as tiny euhedral crystals in the muds. According to Goudge the surficial natron dissolves in the spring, whereas the crystals do not. It seems obvious that the natron crystals in the mud are primary, as are the natron crusts, which form annually, and hence can almost be seen "actually growing in place."

REFERENCES

AHLFELD, F. AND ANGELELLI, V. (1948), Las especies minerales de la Republica Argentina: *Univ. Nac. de Tucuman, Instit. Geol. y Minería (Jujuy)*, Pub. no. **548,** 168.

CATALANO, L. R. (1926), Geología económica de los yacimientos de boratos y materiales de las cuencas—Salar Cauchari: *Dir. Gen. de Minas, Geol. e Hidrolog.*, Pub. no. **23,** 110 p., Buenos Aires.

FOSHAG, W. F. (1921), The origin of the colemanite deposits of California: *Econ. Geol.*, **16,** 199–214.

GOUDGE, M. F. (1926), Sodium carbonate in British Columbia: *Canada Dept. Mines, Mines Branch, Investigations of Mineral Resources . . .* **1924,** 81–102.

JENKS, W. F. (1948), Geology of the Arequipa quadrangle: *Instit. Geol. del Perú, Bol.*, **9,** 155–156.

JOCHAMOWITZ, A. (1907), The borax deposit of Salinas, near Arequipa, Peru: *The Mining Jour.*, **82,** 247.

SCHALLER, W. T. (1916), Inyoite and meyerhofferite, two new calcium borates: *U. S. Geol. Survey Bull.*, **610,** 35–55.

Manuscript received April 4, 1958.

THE AMERICAN MINERALOGIST, VOL. 43, NOVEMBER-DECEMBER, 1958

PHOSPHATE MINERALS OF THE BORBOREMA PEGMATITES: II—BOQUEIRÃO

JOSEPH MURDOCH, *University of California at Los Angeles.*

ABSTRACT

The "alto" Boqueirão is a typical zoned pegmatite of the heterogeneous type, which carries some unusual minerals besides those of the normal beryl-tantalite assemblage. Among them are minor amounts of uraninite, altered in part to uranophane and other secondary compounds; native bismuth. Lithiophilite and many secondary phosphates appear as usual in the general inner portion of the pegmatite near the quartz core. Among these phosphates appear a pink variscite (carrying minor beryllium); metastrengite as sometimes showy blue coatings of minute crystals; huréaulite and minor tavorite as coatings on fractures of lithiophilite; stewartite, massive or in rare crystals; mitridatite (a hydrous calcium iron phosphate), in deep red blades, or very fine grained masses yellowish to greenish in color. A new mineral, chavesite is described. It is a hydrous calcium manganese phosphate, occurring as thin platy crystals coating lithiophilite, and associated with huréaulite and tavorite. Triclinic, a_0 5.49 b_0 13.07, c_0 5.79; α 91°18½′, β 108°3′, γ 99°44′. The powder pattern resembles that of monetite, with which it may be isostructural. The stronger powder lines have the following spacings and intensities: 3.35 Å-10, 3.023 Å-2, 2.945 Å-3, 2.74 Å-2.

INTRODUCTION

This is the second in a projected series of reports on the phosphates and associated minerals from the complex, lithium-bearing beryl-tantalite pegmatites of Northeastern Brazil. Their general position is shown on the key map (Fig. 1). The first report was on the "alto" Patrimonio, Murdoch (1955) and the present one describes the occurrence at the "alto" Boqueirão. The general geologic setting, described in some detail by Johnston (1945) and others, is the same for both deposits: complex pegmatites intruded into a pre-Cambrian complex and exposed by erosion of the rock cover to form the Borborema "planalto"—a more or less well developed peneplane of possibly Cretaceous age, standing now at an elevation of 500 to 550 meters above sea level. In the States of Paraíba and Rio Grande do Norte, later erosion has lowered the earlier surface so that the pegmatites stand up in relief on it, hence the name "alto" given to their outcrops. Even in Ceará, where there has been no such differential erosion, the name is still applied. The Pre-Cambrian rocks are largely gneisses and mica schists (the Seridó schist), which shows no pronounced regional trend, striking sometimes northwesterly, sometimes northeasterly.

BOQUEIRÃO

The "alto" Boqueirão lies at the northern summit of a ridge reaching an elevation of about 300 meters above the surrounding territory, some three kilometers southeast of the town of Parelhas, in the State of Rio Grande do Norte (see index map, Fig. 2). The following description is taken largely from Johnston (1945). Exposed contracts are nearly everywhere practically vertical. The outcrop is some 240 by 25 meters, pinching out to the west, and cut off sharply by the steep slope of the ridge to the east. Johnston's zone II (coarse textured quartz-feldspar) with considerable black tourmaline, composed about half the outcrop. His zone III (very large crystals), has huge microclines, partially kaolinized The quartz core is multiple, and the various patches are made up largely of milky quartz, with occasional vugs carrying euhedral quartz crystals up to 200 kilograms in weight. The occasional phosphates occur, as is normal, in the third zone, and often close to the core. The following minerals are reported: arrojadite, vivianite, spodumene, lepidolite, rhodonite (?), pitchblende and its alteration products, metallic bismuth with bismutite, and some chalcocite. These are in addition to the usual quartz-feldspar mixture, with beryl, tantalite, muscovite, etc. Of these no arrojadite, rhodonite or chalcocite were observed by the writer. The "arrojadite" is presumably represented by lithiophilite and its alteration products (sicklerite etc.); the "vivianite" is apparently metastrengite, and the rhodonite (?) is probably a pink variscite which was observed in some of the alteration products. Several other minerals were observed

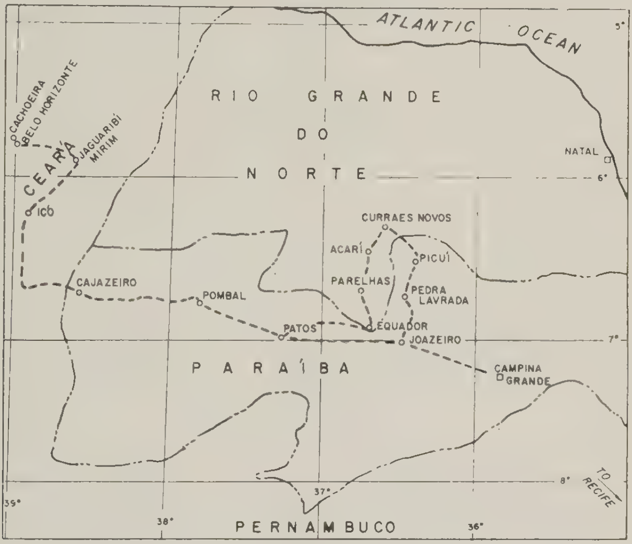

FIG. 1. General map of area.

by the writer, and are included in the descriptive list. The series of alteration products of lithiophilite form an interesting group, essentially the same as that described from Patrimonio.

Spodumene is not abundant, and is commonly altered to a fine grained mica (probably muscovite), associated with fine grained botryoidal growths of cookeite.

Lepidolite is sparingly present as rather fine grained aggregates, occasionally forming masses with curved surfaces, and associated with platy albite. Small prismatic grains of apatite have been seen in this association.

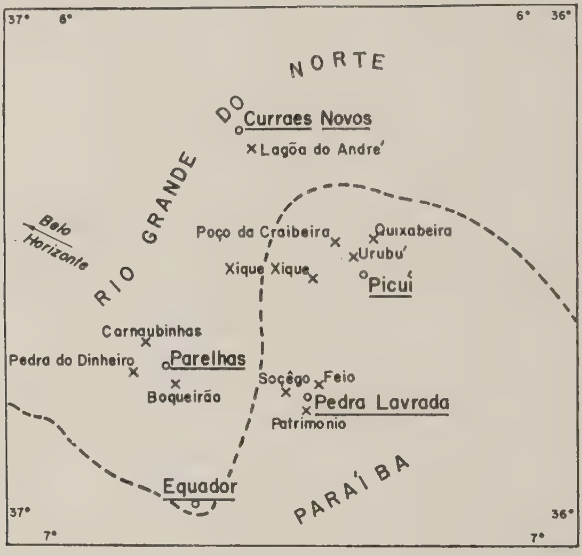

Fig. 2. Detailed map of area.

Tantalite, apart from the commercially large masses, is occasionally found in the quartz-feldspar aggregate as small crystals of mangano-tantalite. A few tabular crystals of columbite appear in a similar matrix.

Bismuth, as the native metal, has been found sparingly as grains or occasionally fair sized rough crystals interstitial to quartz, and associated with coatings and patches of secondary bismutite.

Uraninite. This has been reported as pitchblende, but one rough octahedral crystal was collected by the writer. This crystal is encrusted by a series of secondary minerals in thin concentric layers, and showing roughly three distinct zones. The outermost of these is uranophane, the next an undetermined uranium mineral, or perhaps a mixture, in a number of thin, slightly varied layers, and the innermost perhaps meta-torbernite, although the powder pattern does not match too closely. In addition, a dark red mineral appears in thin veins in the uraninite, and is possibly soddyite. An analysis of the uraninite is given in Table I. Other oxidized uranium minerals, mainly meta-torbernite and meta-autunite, were found in minor amount, usually as powdery or poorly crystallized coatings on columbite.

Table 1. Chemical Analyses

1		2		3	
U_3O_8	91.40	Fe_2O_3	1.00	FeO	1.97
PbO	5.92	FeO	13.23	Fe_2O_3	40.38
CuO	.04	MgO	1.11	Al_2O_3	1.20
Bi_2O_3	.015	CaO	.14	P_2O_5	39.18
FeO	.026	MnO	29.80	Mn_2O_3	—
Al_2O_3	.30	P_2O_5	45.00	H_2O-	17.42
TiO_2	.005	Li_2O	8.68	H_2O+	.198
CaO	.02		98.96		100.35
Na_2O	.03				
SiO_2	.31				
MnO	tr.				
H_2O+	1.76				
H_2O-	.54				
	100.37				

1. Uraninite, analysts, Johnson, Mathey & Co. Ltd. (Zn, Ni, Co, P_2O_5, As, Sb, Sn not detected). 2. Lithiophilite, analyst L. C. Peck. 3. Metastrengite, analyst E. L. Martin.

Variscite. One group of specimens shows a great variety of minerals apparently derived from the complete alteration of lithiophilite crystals (as shown by the outlines of the aggregates). These occur in a matrix of mixed albite, amblygonite and quartz. One of these minerals is variscite, in the form of a transparent crystalline crust, coating fracture surfaces and lining cavities. It was identified by optical properties, x-ray powder pattern, and crystal form. It varies from colorless through pale pink to raspberry red. Spectroscopic tests show the presence of a small amount of beryllium. This is in agreement with the findings on the pink variscite of the Sapucaia pegmatite (Mrose, priv. commun.)

Mitridatite. This rare mineral occurs in these same specimens in clear, red bladed grains: also probably fine-grained, massive, yellowish brown; and also perhaps in compact, almost earthy form, khaki colored. (This is somewhat doubtful, but the powder pattern is at least in moderate agreement with that of mitridatite.)

METASTRENGITE occurs as crusts, finely crystalline, and ranging in color from nearly white through pink to pale blue in this series of specimens. It also occurs in considerable amount, deep purplish blue, and often quite spectacular, as a late product of alteration of lithiophilite in other specimens. See Table I for analysis of this mineral.

BERAUNITE. An orange colored mineral occurring as blade-like grains in the variscite specimens, may perhaps be assigned to this species on the basis of a closely matching powder pattern.

ROCKBRIDGEITE. This mineral was found in small amount in dark green patches associated with alteration products of lithiophilite, and also in the variscite specimens as olive green, minute spherical clusters (probably partly altered).

MANGANITE and CRYPTOMELANE. The end-product of weathering besides some limonitic powders, is manganese oxide, which is sometimes crystalline, with powder pattern matching manganite, or in compact, steely masses which seem to be cryptomelane.

HURÉAULITE. This mineral is rather abundant as colorless or reddish brown crystalline crusts on fracture surfaces and in open spaces, in lithiophilite. It not infrequently has small, rather well developed crystals.

TAVORITE. Associated with some of the huréaulite, and approximately contemporaneous with it, tavorite occurs in yellowish green films or clusters of minute radiating crystals. This occurrence is identical with that at Patrimonio (Murdoch 1955).

STEWARTITE. Stewartite is rare, occurring in the outer zone of alteration of the lithiophilite. Rather poorly developed single crystals enabled the writer to make determinations of cell-size and symmetry which agree closely with those of this mineral from the Palermo Mine, New Hampshire, which is in process of study by Miss Mary Mrose. Powder patterns of stewartite made by the writer of material from Pala (the original locality), Palermo, Boqueirão and (quoted from Tennyson, 1956) from Hagendorf, are in good agreement with each other (see Table 2), and confirm the identity of the mineral from all four localities.

LITHIOPHILITE. This is the principal primary phosphate of the deposit (see Table 1 for analysis), and occurs as very coarse-grained aggregates, usually more or less altered to a considerable variety of secondary minerals, in general under oxidizing and hydrating conditions. Occasional small grains of green gahnite are associated with it, and rarely a little pyrite. Surrounding unaltered cores of lithiophilite are successive zones of sicklerite and purpurite, derived from the successive oxidation of the original mineral, accompanied by hydration and loss of lithium. This occurrence shows again the typical sequence which has been observed at Varuträsk, at Patrimonio, Pala and other localities. It is prob-

Table 2. *X*-ray Powder Patterns of Stewartite
Fe Radiation, Mn Filter. λ = 1.9373 Å

Pala		Boqueirão		Hagendorf		Palermo	
d	I	*d*	I	*d*	I	*d*	I
10.04	10	10.10	10	9.926	10	10.08	10
8.39	½	—		—		8.35	½
—		7.44	½	—		7.47	½
6.73	7	6.75	4	6.751	6	6.75	5
5.88	3	5.93	2	5.869	3	5.91	2
5.035	5	5.03	2	—		5.02	3
4.877	2	4.85	½	4.817	4b	4.84	2
4.75	3	4.75	½	—		—	
4.65	1	4.64	½	—		4.63	2
4.345	½	—		—		—	
3.925	5	3.94	3	3.935	4	3.96	4
3.83	½	—		—		3.84	½
—		—		—		3.77	½
3.59	1	3.59	½	3.602	1	3.618	½
3.48	½	—		—		3.453	½
3.384	2	3.40	1	3.351	2	3.392	2
3.318	3	3.315	1	—		3.313	3
3.246	½	3.238	½	—		3.247	½
—		3.156	1	—		—	
3.115	3	3.117	1	3.118	2	3.128	3
3.03	4	3.045	2	3.021	3	3.045	5
2.96	2	2.963	1	2.945	2	2.966	3
—		2.913	½	—		2.916	½
2.87	3	2.866	1	2.860	2	2.870	3
—		2.812	½	—		2.813	½
2.80	½	—		—		—	
—		2.775	½	—		—	
2.743	1	2.737	½	2.734	2	2.740	½
2.60	4	2.595	2	2.586	3	2.593	4
2.556	½	—		—		—	
2.489	4	2.491	2	2.484	2	2.492	4
2.44	½	2.443	½	2.420	2	—	
—		—		—		2.398	½
2.365	1	2.374	½	1.363	2	2.380	½
—		2.342	½	—		2.337	½
2.26	1	2.254	1	2.250	2	2.262	1
—		2.222	½	—		2.227	½
—		2.182	½	—		2.194	½
2.148	½	2.148	½	2.137	2	2.155	½
2.103	½	2.113	½	—		—	
2.075	½	2.080	½	2.077	2	2.086	½
2.039	½	2.039	½	—		2.052	½
2.003	2	2.005	1	—		2.008	1
1.984	2	1.989	1	1.986	3	1.982	1
1.956	½	1.934	½	1.923	1	1.933	½
1.904	½	1.892	½	1.881	1	1.886	½
1.841	2	1.844	½	1.838	1	1.844	½
1.826	½	1.828	½			1.824	½
1.812	½	1.804	½			—	
1.785	½	1.776	½			1.774	½

able that this sequence precedes the formation of huréaulite, since the latter is not uncommonly found intimately associated with the alteration products of sicklerite and purpurite as well as in cracks in the relatively fresh lithiophilite.

Chavesite. One specimen of lithiophilite shows, on fracture surfaces with huréaulite and tavorite, an intermittent thin colorless crystalline coating which sometimes shows poorly formed individual crystals. This appears to be a new mineral, tentatively named "chavesite" (pronounced shav-ez-ite), after Dr. Onofre Chaves, an engineer of the Brazilian Departamento Nacional da Producão Mineral. It is a hydrated calcium manganese phosphate, but not enough material is available for a chemical analysis. Hardness is near 3, cleavages, two good, in the prism zone, and nearly perpendicular to each other. Optically, biaxial positive, with 2V large, and indices $\alpha 1.60$, $\beta 1.62$, $\gamma 1.65$. Multiple twinning, with twin plane parallel to elongation of crystals. Extinction about 30° to the twin plane. A cleavage sliver which proved to be a single individual was used to determine the symmetry and cell-dimensions. Rotation, and Weissenberg equator, first and second layer lines about c show it to be triclinic with the following values:

$a_0=5.49$ $b_0=13.07$ $c_0=5.79$
$\alpha\ 91°\ 18\frac{1}{2}'$ $\beta\ 108°\ 3'$ $\gamma\ 99°\ 44'$
$\lambda\ 84°\ 58'$ $\mu\ 71°\ 20'$ $\nu\ 78°\ 00'$ $x_0'=0.325$ $y_0'=0.093$
$a{:}b{:}c=1.4200{:}1{:}0.4438$

The powder pattern (see Table 3) closely resembles that of monetite, and it has been suggested (Mrose, priv. commun.) that chavesite and monetite may be isostructural. The x-ray powder pattern can be adequately indexed using the above values for the elements.

Mineral A. One of the variscite specimens shows an unidentified mineral, chestnut brown in color, occurring in radiating blades, and with one good cleavage. Qualitative tests show it to be an anhydrous (?) iron phosphate, with index well over 1.74; extinction parallel to elongation; biaxial negative, with 2V large; pleochroic pale to amber brown. The powder pattern gives the following spacings and intensities for the stronger lines: 3.145–10, 2.405–6, 3.57–5, 3.36–5, 4.74–4.

Mineral B. Associated with tavorite are small, spherulitic aggregates, greenish white in color, of a calcium manganese phosphate with very high index of refraction. It is too fine-grained to make further optical determinations. The powder pattern does not appear to match that of any published mineral. Spacings and intensities of the stronger lines are as follows: 4.67–10, 3.42–5, 3.01–5, 2.52–2.

Table 3. *X*-ray Powder Pattern of Chavesite

Fe Radiation, Mn Filter, $\lambda = 1.9373$ Å

Chavesite			Monetite[1]	
d	I	*hkl*	*d*	I
6.33	1	0.20		
5.03	½	100, 011		
4.56	½	$\bar{1}11, 120$		
4.35	½	030		
3.89	½	$\bar{1}21$		
3.69	1	$1\bar{3}0$	3.72	1
3.54	½	120	—	
3.48	½	$1\bar{2}1$	3.47	1
3.35	10	$0\bar{3}1, \bar{1}31$	3.38	10
3.24	½	$1\bar{1}1$	—	
3.18	½	040	—	
3.13	½	$1\bar{2}1$	3.13	3
3.076?	½	—	—	
3.023	2	111	2.99	9
2.945	3	$\bar{1}\bar{3}0$	—	
2.87	½	$1\bar{3}1$	—	
2.81	½	131	—	
2.74	2	$002, 0\bar{4}1$	2.76	8
2.72	2	121	—	
2.66	½	$\bar{2}01, 0\bar{1}2$	—	
2.63	½	$2\bar{1}0, 012$		
2.56	½	$2\bar{2}0, 050$	—	
2.489	1	$140, 1\bar{4}1$	2.50	5
2.305	1	$0\bar{5}1, \bar{2}\bar{2}1$	2.32	1
2.23	3	$2\bar{4}0, 141$	2.26	6
2.198	1	220	2.21	2
2.155	½	$1\bar{5}1, 1\bar{6}0$	2.16	2
2.124	½	060, 150	—	
2.087	1	$201, 2\bar{2}1$	2.10	2
2.034	1 b	$2\bar{5}0$	2.04	1
1.978	1	$230, 0\bar{6}1$	2.00	2
1.918	2	$2\bar{4}1$	1.93	4
1.85	2	151, 003	1.86	6
1.79	2	$\bar{3}01, 240$	1.80	2
1.75	½	071	—	
1.725	3	$3\bar{1}0, \bar{3}\bar{1}1$	1.73	7
1.685	1	$3\bar{3}0$	1.69	3
1.657	½	$3\bar{4}0, 161$	1.65	2

[1] Comparative list of spacings for monetite from Prien & Frondel (1947), p. 949.

ACKNOWLEDGMENTS

A grant from the Research Funds of the University of California was of material assistance in allowing the collecting of minerals. Miss Mary Mrose of the U. S. Geological Survey has been very helpful in the identification of minerals, and in other advice.

Manuscript received April 10, 1958.

REFERENCES

JOHNSTON, W. D., JR. (1945), Beryl-Tantalite pegmatites of Northeastern Brazil, *Geol. Soc. Am. Bull.*, **56**, 1015–1070.

MURDOCH, J. (1955), Phosphate minerals of the Borborema pegmatites: I—Patrimonio, *Am. Mineral.*, **40**, 50–63.

PRIEN, E. L. AND FRONDEL, C. (1947), Studies in Urolithiasis: I. The composition of urinary calculi, *Jour. Urology*, **57**, 949–991.

TENNYSON, CHR. (1956), Das Stewartit-Problem, *Die Naturwissenschaften*, **6**, 128–129.

THE AMERICAN MINERALOGIST, VOL. 43, NOVEMBER-DECEMBER, 1958

MINERALOGICAL APPLICATIONS OF ELECTRON DIFFRACTION

I. THEORY AND TECHNIQUES*

MALCOLM ROSS AND C. L. CHRIST, *U. S. Geological Survey, Washington, D. C.*

ABSTRACT

The small wave lengths used in electron-diffraction experiments and the thinness of the crystals necessary for the transmission of the electron beam combine to require a somewhat different diffraction geometry for the interpretation of electron-diffraction patterns than is used in the interpretation of *x*-ray diffraction patterns. This geometry, based on the reciprocal lattice concept and geometrical construction of Ewald, needed for the interpretation of transmission electron-diffraction single-crystal patterns is here reviewed.

Transmission electron-diffraction single-crystal patterns of two monoclinic substances, colemanite [$CaB_3O_4(OH)_3 \cdot H_2O$] and potassium chlorate ($KClO_3$), are examined and the theory necessary for their interpretation is given in detail. The study of these patterns furnishes a basis for the interpretation of single-crystal patterns of materials belonging to any crystal system. It is shown that useful unit cell data, accurate to a few tenths of a per cent, can be obtained from the patterns of colemanite and $KClO_3$. A method of evaluating unit cell data from measurements of such single-crystal patterns is given.

The transmission electron-diffraction powder pattern obtained from an oriented aggregate of thin crystals gives the same unit cell data as is given by the electron-diffraction single-crystal pattern obtained from one crystal of the aggregate. A graphical method is given for precisely evaluating unit cell constants from measurements of such a powder pattern.

INTRODUCTION

Mineralogical applications of electron-diffraction techniques have been somewhat limited, partly because not all minerals are amenable to study by this method, and partly because of the extensive use of the *x*-ray diffraction method. Of particular interest to the mineralogist is the fact that symmetry-true, indexable single-crystal diffraction patterns can be obtained with electrons from very minute crystals contained within a sample which will give only a Debye-Scherrer pattern with *x*-rays. Because very small, individual crystals can be studied in this way, a given sample can be analyzed very thoroughly for crystalline components present in minor amounts, in contrast to the *x*-ray method which is relatively insensitive in this regard.

During the past few years, much experience has been gained in this laboratory in the application of the combined techniques of electron diffraction and electron microscopy to the study of mineralogical problems. This paper gives a description of the techniques developed, and the results obtained from a number of mineralogical studies. Part I of the

---

* Publication authorized by the Director, U. S. Geological Survey.

paper contains a discussion of the experimental methods used in the work and a description of the theory used in the interpretation of single-crystal electron-diffraction patterns. The methods of interpreting and measuring single-crystal patterns of the monoclinic substances colemanite, $CaB_3O_4(OH)_3 \cdot H_2O$, and potassium chlorate, $KClO_3$, are treated in detail. Part II of the paper (Ross, 1959) gives partial unit cell data for a number of fine-grained vanadium minerals.

This work is part of a program being conducted by the U. S. Geological Survey on behalf of the Division of Research of the U. S. Atomic Energy Commission.

THEORY OF INTERPRETATION OF SINGLE-CRYSTAL PATTERNS

In the present study, only transmission electron-diffraction patterns are considered. The experimental arrangement for obtaining such patterns is shown schematically in Fig. 1. If only one crystal lies in the path of the beam a spot pattern is obtained whereas if a large number of crystals lie in the path of the beam a powder pattern is obtained. The powder pattern will show a number of continuous rings and is similar to the x-ray Debye-Scherrer pattern.

The most powerful method for the interpretation of single-crystal patterns is based on the reciprocal lattice concept. The reciprocal lattice is treated at length in James (1954). In the present paper his notation is followed with the exception that $\mathbf{H}$ (present paper) $= \mathbf{r}^*$ (James). It is useful to recall here the differences in the interference geometry for the diffraction of electrons and the diffraction of x-rays. The Ewald sphere has a radius of the order of 1 $Å^{-1}$ for the wave lengths ordinarily used in x-ray diffraction. In electron-diffraction experiments much smaller wave lengths are used. For example, for electrons accelerated under a potential of 50 kv, $\lambda = 0.0534$ Å. Corresponding to this case the Ewald sphere has a radius of 18.7 $Å^{-1}$, and its surface approximates a plane relative to the reciprocal lattice. The nodes of the reciprocal lattice have the properties of mathematical points only for crystals that are ideally triperiodic. In the real crystal these nodes must be replaced by appropriate small volumes (rods, parallelepipeds, etc.) whose size and shape reflect the size and shape of the periodic continuum. For the case of interest in this paper, i.e. the very thin crystal, the reciprocal lattice points are replaced by rods having their lengths parallel to the thin direction of the crystal, with the total length p of each rod given by the relationship $p = 2/t$, where t is the thickness of the crystal. It can be seen from Fig. 2 that when the direction of the incident beam of electrons is parallel to the long direction of the reciprocal lattice rods (parallel to the thin direction of the crystal) the chances are greatly increased that some portion of the rod will intersect the Ewald sphere with ensuing diffraction. It can also be seen from Fig. 2 that the smaller the spacing of the reciprocal lattice in the thin direction of the crystal the greater are the chances that reciprocal lattice rods in the upper levels of the reciprocal lattice will intersect the sphere.

There are other factors that increase the possibility of meeting the interference condition. Lack of exact homogeneity in the wave length of the electrons results in the transformation of the Ewald surface into a thin slab having a thickness determined by the spread in wave lengths. Variations in the direction of the incident beam and distortion in the lattice planes normal to the beam will also contribute to an increase in the number of diffraction spots observed.

Description of Instruments

The electron microscope used in this study (RCA, type EMU2B, 50 kv) is designed for study of particles in the range of 0.001 to 10 microns. This instrument is equipped with a selected area diffraction attachment which can be used to obtain diffraction patterns from specific areas of the sample. Hall (1953) gives a complete description of the electron microscope and Picard and Reisner (1946) discuss the use of the electron microscope as a diffraction camera.

A separate diffraction unit (RCA, type EMD) was used to obtain many of the patterns for this study. The unit is specifically designed for work with powder and single-crystal mounts using either reflection or transmission methods. The diffraction patterns are recorded on a 4 by 5 inch photographic plate and yield more precise measurements than the smaller patterns obtained with the electron microscope. A disadvantage of the electron-diffraction unit is that the crystals from which the diffraction patterns are obtained can not be seen as they can be with the electron microscope. The diffraction unit is operated at a potential of 50 kv, d-c; the direct current is regulated to 1 part in 50,000 with a ripple of less than 2 volts peak-to-peak. The upper pole piece aperture has a diameter of 1/1000 inch. The specimen-to-plate distance for most of the patterns taken with this instrument is approximately 50 cm.

Sample Preparation and Examination

Samples are usually prepared by dispersing or dissolving the experimental material in distilled water. A droplet of the liquid is then placed on a 200-mesh stainless steel screen which has been previously covered by a collodion film, 50 to 150 Å thick. When an internal standard is desired aluminum or β-tin is vaporized in vacuum onto the collodion film prior to mounting the sample. A description of sample preparation techniques useful for this type of work was edited by Drumond (1950).

A preliminary examination of most samples is made with the electron microscope. The samples are checked for particle size, purity, orientation, and crystallinity. In general, single-crystal diffraction patterns ("spot" patterns) are obtained from individual crystals within the sample by converting the microscope into a diffraction camera. Usually an electron micrograph is made of the crystal or crystals producing the pattern. An example of this *selected area diffraction* technique, referred to as "SAD" in the following, can be seen in Fig. 6a.

After examination with the microscope the specimen mounts are transferred to the electron-diffraction unit and placed so that the collodion film is approximately normal to the electron beam. The mount is then traversed in a horizontal plane until a suitable spot or powder pattern is obtained. For spot patterns, adjustments in tilt of the specimen are made so that the intensities of spots related by a center of symmetry appear to be equal.

A second method of examining crystals with the electron-diffraction unit is sometimes used. A cleavage fragment, which must be thin enough in some areas to permit the transmission of the weakly penetrating electrons, is mounted on a holder that allows considerable freedom in the adjustment of the sample plane. The fragment is oriented so that the cleavage plane is approximately normal to the electron beam, and final adjustment is then made so that the resulting spot pattern appears symmetrical and spots related by a center of symmetry have approximately equal intensities. Hereafter we shall refer to patterns taken with the *electron-diffraction unit* as "EDU" patterns. In Part I all values given for unit cell constants are obtained from measurements of EDU patterns.

STANDARDIZATION OF ELECTRON-DIFFRACTION PATTERNS

Evaluation of direct lattice spacings from EDU spot or powder patterns may be accomplished with fair accuracy provided the specimen-to-photographic plate distance and wave length of the electrons are known. Referring to Fig. 1 we see that

$$\tan 2\theta' = \frac{D}{2L}$$

or

$$\frac{2 \sin \theta' \cos \theta'}{\cos 2\theta'} = \frac{D}{2L} \tag{1}$$

where D is the ring diameter (or the distance between spots related by a center of symmetry), L is the specimen-to-plate distance and θ' is the

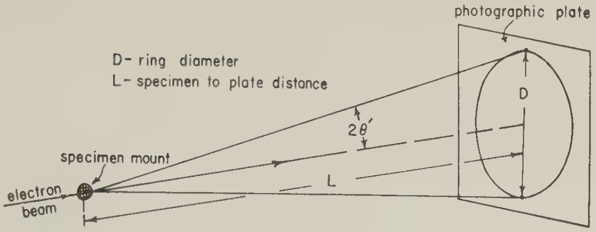

FIG. 1. Experimental arrangement for obtaining transmission electron diffraction patterns.

Bragg angle for the electron diffraction case. For small angles*

$$\frac{\cos \theta'}{\cos 2\theta'} \cong 1. \tag{2}$$

On combining (1) and (2) we then have

$$\sin \theta' = \frac{D}{4L} \cdot \tag{3}$$

Substituting (3) into Bragg's law gives

$$d' = \frac{2L\lambda}{D} \tag{4}$$

where d' is the direct lattice spacing given by the diffraction pattern.

Since it is inconvenient to measure λ and L with high accuracy, another method is used in this laboratory to evaluate direct lattice spacings. This is done by comparing the electron diffraction pattern of a standard material to that of the experimental material. This "standardization" of diffraction patterns can be accomplished in two ways. Collodion mounts previously coated with a thin layer of aluminum or β-tin are used for some specimen mounts. These yield photographs that show the diffraction pattern of the experimental material superimposed on the powder pattern of the standard substance. An example of this type of pattern may be seen in Fig. 11*a*. The second method of standardizing a pattern is to photograph the diffraction pattern of the experimental material and then to immediately photograph a pattern of the standard substance on another plate. This is done by traversing the specimen stage horizontally to bring a screen containing the standard directly under the beam. This operation involves no change in specimen-to-plate distance. The wave length is assumed to be constant over the brief period required to make the two photographs.

---

* Using 50 kv radiation ($\lambda = 0.0534$Å) $\cos \theta'$ never reaches a value smaller than 0.993 for d-spacings greater than 0.7 Å.

As will be shown later, the direct lattice spacings of the standard and experimental materials are very nearly inversely proportional to the ring diameters provided that the standard and experimental materials are photographed at constant wave length and specimen-to-plate distance - that is,

$$\frac{d_x}{d_s} \cong \frac{D_s}{D_x} \tag{5}$$

where d_x and d_s refer to the direct lattice spacings of the experimental and standard materials respectively and D_x and D_s refer to the ring diameters. Knowing d_s it is only necessary to measure D_x and D_s by some suitable means in order to calculate d_x.

Measurement of the spot or powder patterns is usually done with a measuring microscope. Another method of measurement found to be quite useful in evaluating parameters from single-crystal patterns is accomplished by enlarging the patterns of the standard and experimental materials photographically to about 5 times the original size and measuring the enlargement with a millimeter scale. This method has been found to give lattice parameters almost as precise as those evaluated from measurements obtained with a measuring microscope. Due to the appearance of a slight ellipticity in the diffraction patterns, care is taken to measure both the standard and experimental patterns over the same diameter.

ANALYSIS OF SINGLE CRYSTAL PATTERNS OF COLEMANITE

Interpretation of patterns

Colemanite, $CaB_3O_4(OH)_3 \cdot H_2O$, is monoclinic and has perfect cleavage parallel to (010). Single-crystal patterns of this mineral were obtained with the electron-diffraction unit by mounting a thin cleavage fragment so that the cleavage plane was approximately normal to the electron beam. Figures 3*a* and 4*a* show spot patterns of colemanite obtained in this manner; the patterns are indexed as shown in Figs. 3*b* and 4*b*.

One method of interpreting these spot patterns, as previously discussed, is based on the reciprocal lattice concept. In Fig. 5, a portion of the section of the colemanite reciprocal lattice through the origin and perpendicular to the *c*-axis, is represented. It can be seen that the trace of the sphere of reflection departs only slightly from the reciprocal lattice row [*h*00]. If the crystal is thin in the $\mathbf{b}^*$ direction the reciprocal lattice points become essentially rods elongated parallel to the $\mathbf{b}^*$ direction. Whenever one of these rods intersects the sphere of reflection a diffracted beam is developed. Inspection of Fig. 5 shows that if the *h*00 reciprocal lattice points are extended as rods it is highly probable

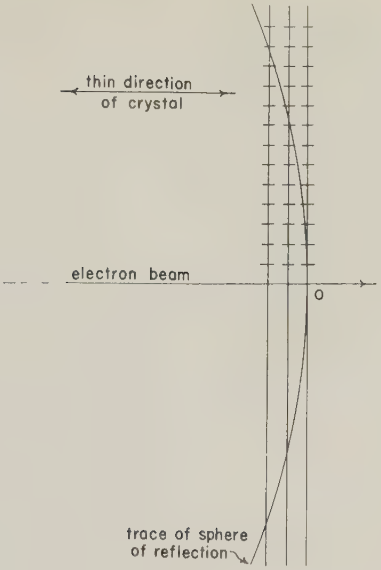

FIG. 2. The Ewald construction for the diffraction of electrons, showing the reciprocal lattice points extended into rods.

that they will penetrate the sphere since these points are nearly coincident with the trace of the sphere. If we consider the colemanite reciprocal lattice in three dimensions it can be easily seen that with a sufficiently thin crystal a large number of rods will penetrate the sphere and give a

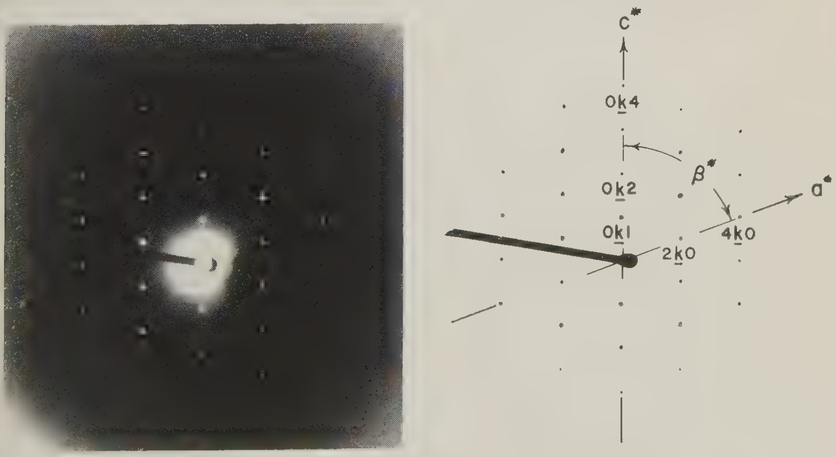

(*a*) (*b*)

FIG. 3*a*. EDU spot pattern of colemanite. 3*b*. Indexed reproduction of the EDU spot pattern shown in Fig. 3*a*.

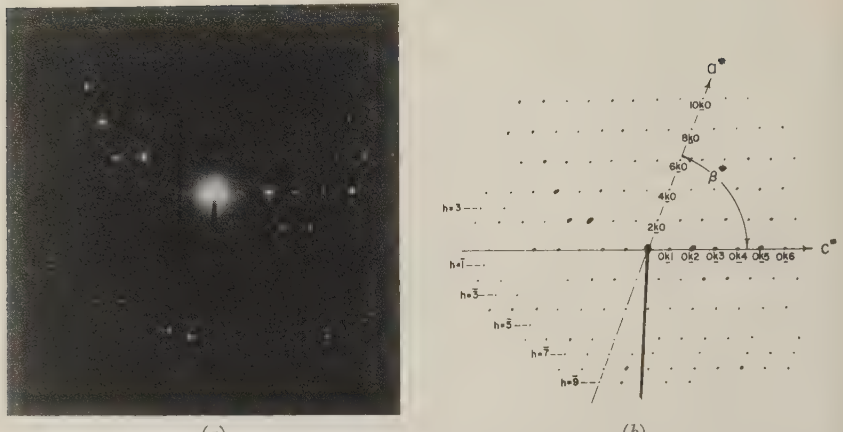

(a) (b)

FIG. 4a. EDU spot pattern of colemanite. 4b. Indexed reproduction of the EDU spot pattern shown in Fig. 4a.

diffraction pattern showing an extensive network of spots. Except for scale this network of spots will, geometrically, correspond very closely to the network of points in the $(h0l)$ reciprocal net of an ideally triperiodic colemanite crystal.

The spot patterns of colemanite are indexed with the k parameter as a variable: for example 2$\underline{k}$0, where $\underline{k}$ is equal to 0, 1, $\bar{1}$, etc. This is done because it is possible that the reciprocal lattice rods in the upper levels may also extend into the sphere. The geometry of the spot pattern is not altered by extension of upper level rods into the sphere for these rods

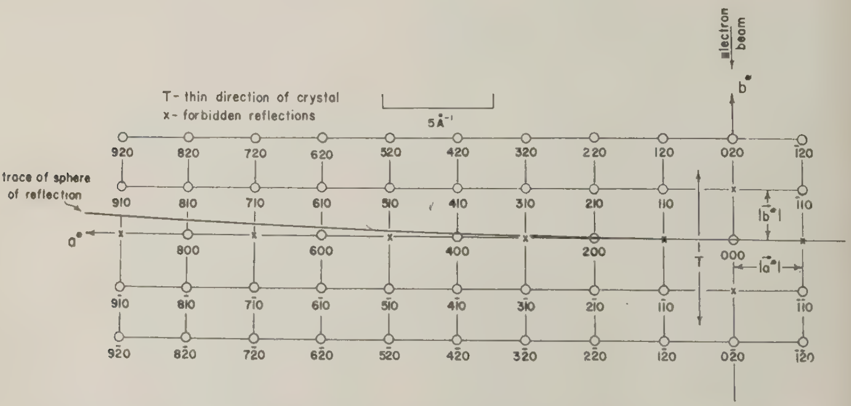
electron beam
b^*
T- thin direction of crystal
x- forbidden reflections
5Å^{-1}
920 820 720 620 520 420 320 220 120 020 $\bar{1}20$
trace of sphere of reflection
910 810 710 610 510 410 310 210 110 $\bar{1}10$
$|b^*|$
a^*
800 600 400 200 000
T
$|a^*|$
$9\bar{1}0$ $8\bar{1}0$ $7\bar{1}0$ $6\bar{1}0$ $5\bar{1}0$ $4\bar{1}0$ $3\bar{1}0$ $2\bar{1}0$ $1\bar{1}0$ $\bar{1}\bar{1}0$
$9\bar{2}0$ $8\bar{2}0$ $7\bar{2}0$ $6\bar{2}0$ $5\bar{2}0$ $4\bar{2}0$ $3\bar{2}0$ $2\bar{2}0$ $1\bar{2}0$ $0\bar{2}0$ $\bar{1}\bar{2}0$

FIG. 5. Ewald construction showing a portion of the section of the colemanite reciprocal lattice through the origin and perpendicular to the c axis ($\lambda = 0.0534$ Å).

are coincident in projection with those of the zero level. In fact, with an extremely thin crystal the reciprocal lattice points in the rows parallel to the thin direction of the crystal become continuous lines. In such a case we have pure two-dimensional diffraction.

The space group of colemanite is $P2_1/a$-(C_{2h}^5), $h0l$ and $0k0$ reflections being absent when h and k are odd, respectively (Christ, 1953). Some of the higher order spots in Fig. 4*a* appear to represent "forbidden" $h0l$ reflections. The appearance of such reflections where h is odd can be expected if upper level rods extend into the sphere. When a colemanite crystal is extremely thin in the **b*** direction all $h\underline{k}l$ reflections can be expected to appear. This is shown in Fig. 6*a*, which is an SAD spot pattern of colemanite internally standardized with aluminum. The pattern shows complete rows of spots for which h is odd. The SAD pattern is indexed as shown in Fig. 6*b*. Fig. 7 shows an electron micrograph of the crystal from which the SAD pattern was obtained.

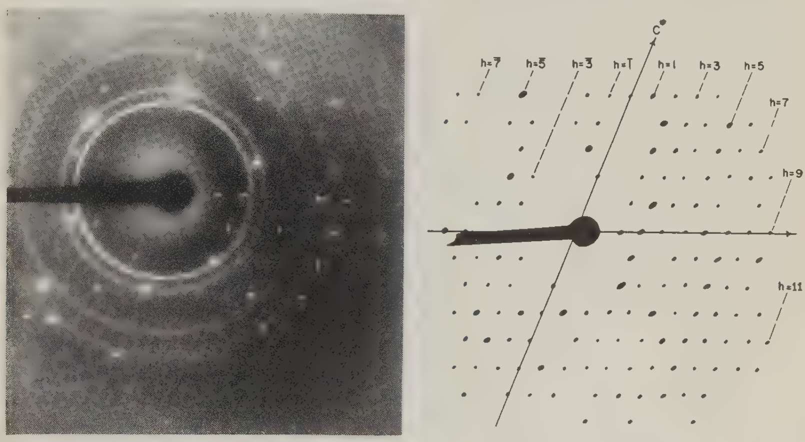

(*a*) (*b*)

FIG. 6*a*. SAD spot pattern of colemanite superimposed upon the powder pattern of the internal aluminum standard. 6*b*. Indexed reproduction of the SAD spot pattern shown in Fig. 6*a*.

Ideally these colemanite patterns should show a center of symmetry such that $I_{hkl}=I_{hkl}$; however in practice this symmetry is not always observed. The pattern shown in Fig. 3*a* very nearly shows a center of symmetry whereas the pattern shown in Fig. 4*a* definitely does not. This lack of symmetry is attributed mainly to the variation in thickness of the cleavage fragment and to departure of the (010) face from being normal to the electron beam.

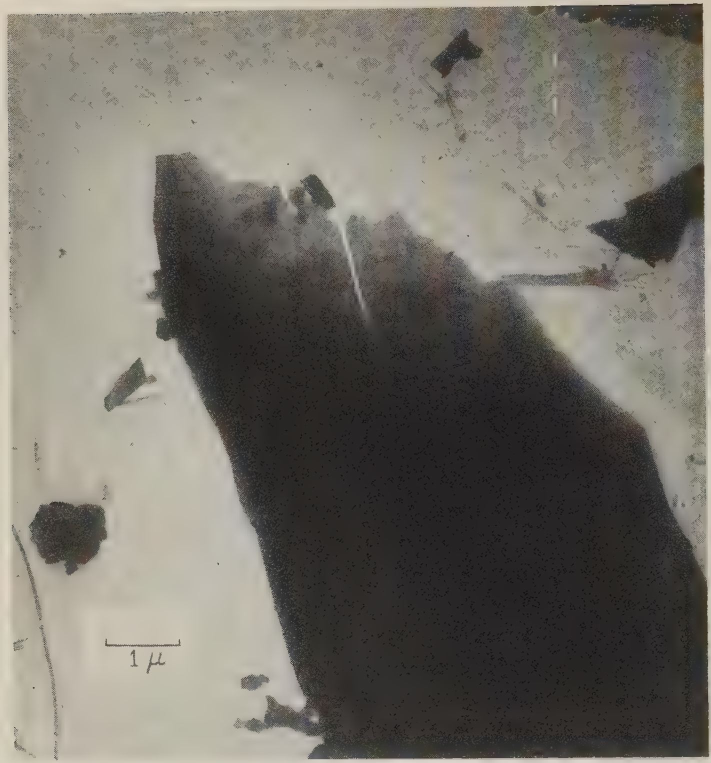

FIG. 7. Electron micrograph of the colemanite crystal from which the SAD spot pattern shown in Fig. 6*a* was made.

Measurement of patterns

Inasmuch as the sphere of reflection does not coincide exactly with the ($h0l$) reciprocal net a slight distortion will be introduced into the spot pattern of colemanite. This distortion in terms of error in reciprocal lattice spacings may be evaluated with the aid of Fig. 8. The ($h0l$) reciprocal lattice rod of the thin colemanite crystal will intersect the sphere at P′ giving a Bragg angle of θ_{h0l}' corresponding to a reciprocal lattice vector $\mathbf{H}_{h0l}'$. Ideally the reciprocal lattice point ($h0l$) should intersect the sphere at P giving a Bragg angle of θ_{h0l} corresponding to a true reciprocal lattice vector $\mathbf{H}_{h0l}$. The relation between the vectors $\mathbf{H}_{h0l}'$ and $\mathbf{H}_{h0l}$ is given by

$$\sin (90° - \theta_{h0l}') = \frac{|\mathbf{H}_{h0l}|}{|\mathbf{H}_{h0l}'|}$$

or

$$\cos \theta_{h0l}' = \frac{|\mathbf{H}_{h0l}|}{|\mathbf{H}_{h0l}'|}\,. \tag{6}$$

However

$$\cos \theta_{h0l}' \cong \cos \theta_{h0l} \tag{7}$$

(within a few parts per million), thus (6) on rearrangement becomes

$$|\mathbf{H}_{h0l}'| = \frac{|\mathbf{H}_{h0l}|}{\cos \theta_{h0l}}\,. \tag{8}$$

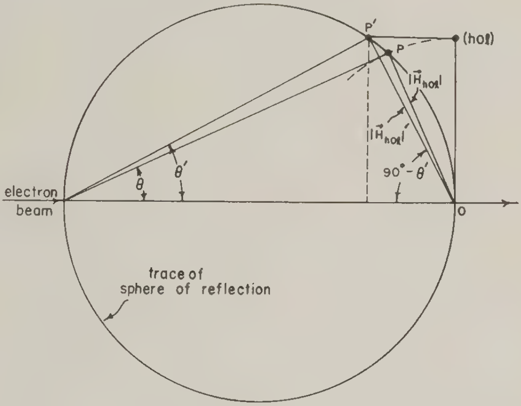

FIG. 8. The Ewald construction used to evaluate the error in reciprocal lattice spacings given by electron diffraction patterns. The curvature of the sphere of reflection is greatly exaggerated.

Relation (8) in terms of the direct lattice spacings is

$$d_{h0l}' = d_{h0l} \cos \theta_{h0l} \tag{9}$$

where d_{h0l}' is the direct lattice spacing given by the spot pattern and d_{h0l} is the true direct lattice spacing.

Evaluation of direct lattice spacings from standardized EDU spot or powder patterns may be accomplished with high accuracy provided the ring diameters can be precisely measured. Rearranging (1) we have

$$\sin \theta' = \frac{D}{4L}\,\frac{\cos 2\theta'}{\cos \theta'}\,. \tag{10}$$

According to Bragg's law

$$\lambda = 2d_s' \sin \theta_s' \tag{11}$$

and

$$\lambda = 2d_x' \sin \theta_x'. \tag{12}$$

Since λ is constant we may equate (11) and (12) giving

$$d_x' = \frac{d_s' \sin \theta_s'}{\sin \theta_x'} \cdot \tag{13}$$

Substitution into (13) of the value of $\sin \theta_s'$ and $\sin \theta_x'$ given by (10) gives

$$d_x' = \frac{d_s'\mathrm{D}_s}{\mathrm{D}_x} \frac{\cos 2\theta_s' \cos \theta_x'}{\cos 2\theta_x' \cos \theta_s'} \tag{14}$$

or for the special case of colemanite

$$d_{h0l}' = \frac{d_s'\mathrm{D}_s \cos 2\theta_s' \cos \theta_{h0l}'}{\mathrm{D}_{h0l} \cos 2\theta_{h0l}' \cos \theta_s'} \tag{15}$$

where D_{h0l} is the distance between the $h\underline{k}l$ and $\bar{h}\underline{k}\bar{l}$ spots of the colemanite pattern.

But

$$\cos \theta_{h0l}' \cong \cos \theta_{h0l} \tag{7}$$

and

$$d_{h0l}' = d_{h0l} \cos \theta_{h0l}. \tag{9}$$

Also for the small Bragg angles

$$\cos 2\theta_{h0l}' \cong \cos 2\theta_{h0l}. \tag{16}$$

Most of the standard materials used in electron diffraction -for example, aluminum and β-tin—are composed of very small randomly oriented equidimensional crystals. The reciprocal lattice points of such crystals will not elongate into rods; thus the reciprocal lattice lengths $|\mathbf{H}_{hkl}'|$ and $|\mathbf{H}_{hkl}|$ of the standard material will be identical (Fig. 8). Consequently,

$$\theta_s' \equiv \theta_s, \tag{17}$$

$$\cos \theta_s' \equiv \cos \theta_s, \tag{18}$$

$$\cos 2\theta_s' \equiv \cos 2\theta_s \tag{19}$$

and

$$d_s' \equiv d_s. \tag{20}$$

By (7), (9), (16), (18), (19), and (20), relation (15) reduces to

$$d_{h0l} = \frac{d_s\mathrm{D}_s \cos 2\theta_s}{\mathrm{D}_{h0l} \cos 2\theta_{hcl} \cos \theta_s} \tag{21}$$

or for the general case

$$d_x = \frac{d_s\mathrm{D}_s \cos 2\theta_s}{D_x \cos 2\theta_x \cos \theta_s} \tag{22}$$

where the subscript x now refers to a material composed of crystals so thin in one direction that the reciprocal lattice points elongate into rods.

The factor $(\cos 2\theta_s)/(\cos 2\theta_x \cos \theta_s)$ in (22) usually may be disregarded since it is nearly equal to unity (within 0.2 per cent) for the small θ angles encountered in the electron diffraction method; thus (22) reduces to

$$d_x \cong \frac{d_s \mathrm{D}_s}{\mathrm{D}_x}. \tag{23}$$

Relation (23) was used to evaluate the direct lattice spacings given by an EDU spot pattern of colemanite similar to the one shown in Fig. 3*a*. Table 1 is a comparison of the unit cell data obtained from the EDU pattern to those obtained by *x*-ray methods (Christ, 1953). The β angle for the electron-diffraction value was determined by triangulation.

TABLE 1. SINGLE CRYSTAL DATA: COLEMANITE, $CaB_3O_4(OH)_3 \cdot H_2O$, MONOCLINIC

X-ray diffraction[1]	Electron diffraction[2]
$a= 8.743\pm0.004$ Å	$a=8.71_5$ Å
$b=11.264\pm0.002$	—
$c= 6.102\pm0.003$	$c=6.09_3$
$d_{200}=$ 4.105 Å (calc.)	$d_{200}=4.09_4$ Å (meas.)
$d_{001}=$ 5.730 (calc.)	$d_{001}=5.72_6$ (meas.)
$d_{20\bar{1}}=$ 4.063 (calc.)	$d_{20\bar{1}}=4.05_0$ (meas.)
$\beta=110°07'\pm05'$	$\beta=110°00'$
Space group $P2_1/a$-(C_{2h}^5)	

[1] Christ, 1953.

[2] Measurements are taken from an EDU spot pattern similar to the one shown in Fig. 3*a*.

If accuracy of better than 0.2 per cent is desired d_x must be calculated using relation (22). The factor $(\cos 2\theta_s)/(\cos 2\theta_x \cos \theta_s)$ for a given direct lattice spacing may be routinely determined from a graph made by plotting the value of $(\cos 2\theta_s)/(\cos 2\theta_x \cos \theta_s)$ for several direct lattice spacings against the direct lattice spacings. Fig. 9 shows such a graph which is computed for use with electron diffraction patterns that are photographed at a potential of 50 kv ($\lambda=0.0534$ Å) and standardized with the (501) reflection of β-tin ($d_{501}=1.0950$ Å, Swanson and Tatge, 1953, p. 25). The graph is used in the following way. A $(d_x)_{\text{approx.}}$ is calculated using relation (23). For this value the corresponding value of $(\cos 2\theta_s)/\cos 2\theta_x \cos \theta_s)$ is found on the graph and then multiplied into $(d_x)_{\text{approx.}}$ to give a more accurate value of d_x. By this means it is possible to calculate d_x with an accuracy of better than 0.01 per cent assuming, of course, that d_s, D_s and D_x are as accurately known. Usually spot patterns cannot be measured with sufficient precision to warrant use of

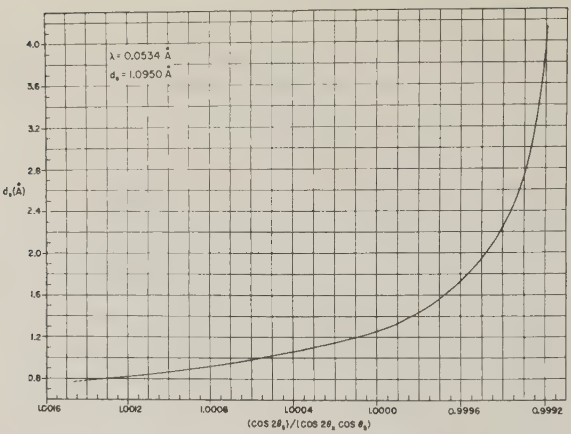

FIG. 9. Graph for evaluating the factor $(\cos 2\theta_s)/(\cos 2\theta_x \cos \theta_s)$ for a given direct lattice spacing. The graph is computed for electron diffraction patterns that are photographed at a potential of 50 kv ($\lambda = 0.0534$ Å) and standardized with the (501) reflection of β-tin ($d_{501} = 1.0950$ Å).

the graph. Powder patterns on the other hand, can sometimes be measured with great precision, thus the need for the more accurate evaluation of d_x furnished by the graph is apparent.

ANALYSIS OF SINGLE CRYSTAL PATTERNS OF $KClO_3$

Interpretations of patterns

$KClO_3$ is monoclinic and in its pure form crystallizes from solution as thin tablets on (001) (See Buckley 1951, p. 544). Specimens of this material were prepared by placing a drop of very dilute aqueous $KClO_3$ solution on a collodion mount which had been previously coated with aluminum or with β-tin. After the mounts were air-dried, they were oriented in the electron diffraction unit so that (001) was approximately normal to the electron beam. The position of the specimen mount and the $KClO_3$ crystal in relation to the electron beam is shown in Fig. 10.

Ten internally standardized EDU spot patterns were made of this material, eight of which were suitable for measurement. One of these patterns is shown in Fig. 11*a*; the pattern is indexed as shown in Fig. 11*b*.

The method of interpreting the $KClO_3$ patterns can be visualized with the aid of Fig. 12 which represents a portion of the $KClO_3$ reciprocal lattice through the origin and perpendicular to the *b*-axis. If the crystal is sufficiently thin in the $\mathbf{c}^*$ direction the reciprocal lattice rods will be elongated parallel to $\mathbf{c}^*$ and many of them will penetrate the sphere of

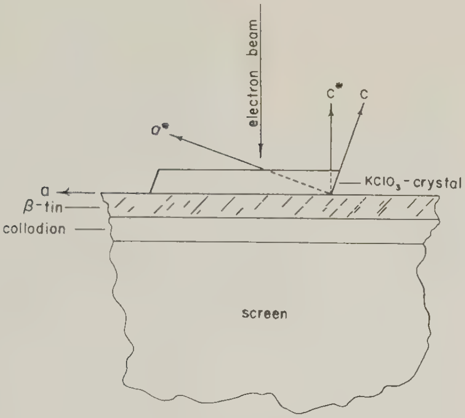

FIG. 10. The position of the specimen mount and the $KClO_3$ crystal in relation to the electron beam.

reflection. It can be seen with the aid of Fig. 12 that dimensions of the spot pattern obtained from the $KClO_3$ crystal will be very nearly proportional to those of a projection of the ($hk0$) reciprocal net onto the a-b plane of the crystal. The deviation from true proportionality arises becauses the sphere of reflection does not quite coincide with the a-b plane.

The spots along the positive $(\mathbf{a})^*_p$ direction (projected $\mathbf{a}^*$ direction) in the $KClO_3$ spot pattern (Fig. 11a) are indexed as $20\underline{l}$, $30\underline{l}$, and $40\underline{l}$ (Fig.

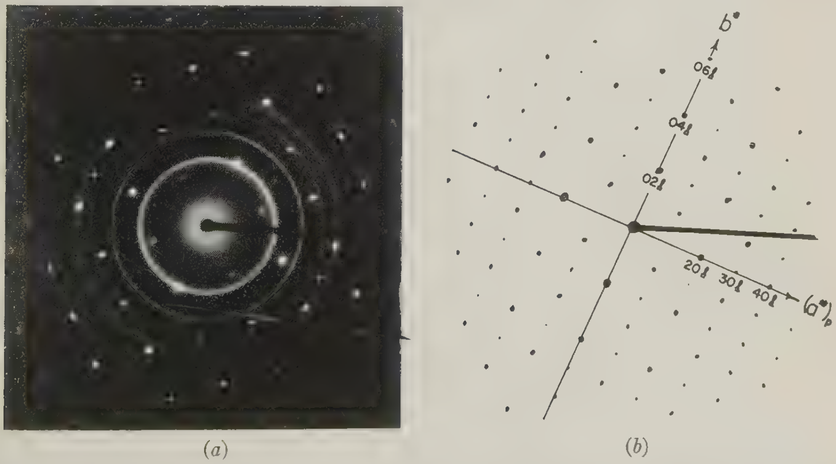

(a) (b)

FIG. 11a. EDU spot pattern of $KClO_3$ superimposed upon the powder pattern of the internal β-tin standard. 11b. Index reproduction of the EDU spot pattern shown in Fig. 11a.

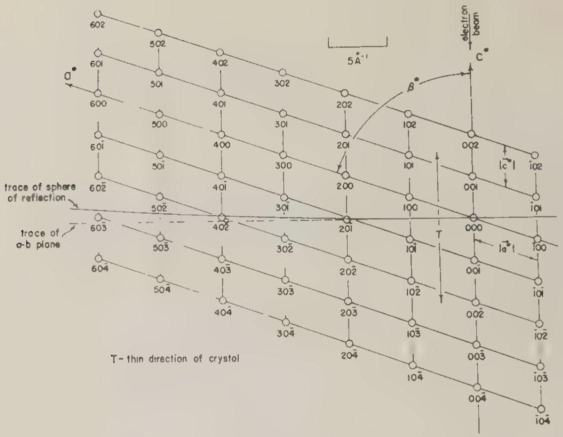

FIG. 12. Ewald construction showing a portion of the section of the $KClO_3$ reciprocal lattice through the origin and perpendicular to the *b*-axis ($\lambda = 0.0534$ Å).

11*b*); and correspond to the intersection of the sphere by one or more rods in the reciprocal lattice rows [20*l*], [30*l*] and [40*l*], respectively. Spots having the indices 10*l* and 50*l* do not appear in the spot pattern indicating that none of the rods in the reciprocal lattice rows [10*l*] and [50*l*] penetrate the sphere.

The space group of $KClO_3$ is $P2_1/m-(C_{2h}^2)$, $0k0$ reflections being absent when k is odd (Zachariasen, 1929, p. 501). The very weak spots indexed as $01l$, $03l$ and $05l$ (Figs. 13*a* and 13*b*) arise because reciprocal lattice rods from the upper $0kl$ levels penetrate the sphere. This can be readily understood from Fig. 14 which shows a portion of the section of the $KClO_3$ reciprocal lattice, through the origin and perpendicular to the *a*-axis.

Measurement of patterns

The lattice spacings given by the $KClO_3$ spot pattern may be evaluated with the aid of Fig. 15 which shows a projection of the $(hk0)$ reciprocal net of $KClO_3$ onto the *a*-*b* plane. Consider the reciprocal lattice vector $\mathbf{H}_{hk0}$ to any point $hk0$. The length of its projection onto the *a*-*b* plane is given by

$$|\mathbf{H}_{hk0}|_p^2 = [ha^* \cos(90° - \beta^*)]^2 + [kb^*]^2$$

or

$$|\mathbf{H}_{hk0}|_p = \left(\frac{\sin^2\beta}{d_{h00}^2} + \frac{1}{d_{0k0}^2}\right)^{1/2} \tag{24}$$

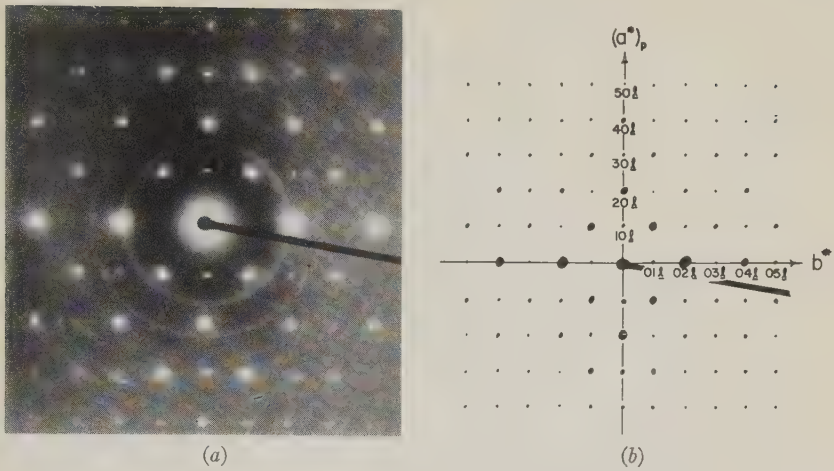

(*a*) (*b*)

FIG. 13*a*. EDU spot pattern of $KClO_3$ superimposed upon the powder pattern of the internal β-tin standard. 13*b*. Indexed reproduction of the EDU spot pattern shown in Fig. 13*a*.

where $|\mathbf{H}_{hk0}|_p$ is the reciprocal lattice spacing given by projection of the vector $\mathbf{H}_{hk0}$. In terms of the direct lattice (24) becomes

$$(d_{hk0})_p = \frac{1}{\left(\dfrac{\sin^2\beta}{d_{h00}{}^2} + \dfrac{1}{d_{0k0}{}^2}\right)^{1/2}} \tag{25}$$

where $(d_{hk0})_p$ is the projection of d_{hk0} and is very nearly equal to the spacing given by the spot pattern. If $h=1$ and $k=0$, (25) reduces to

$$(d_{100})_p = a. \tag{26}$$

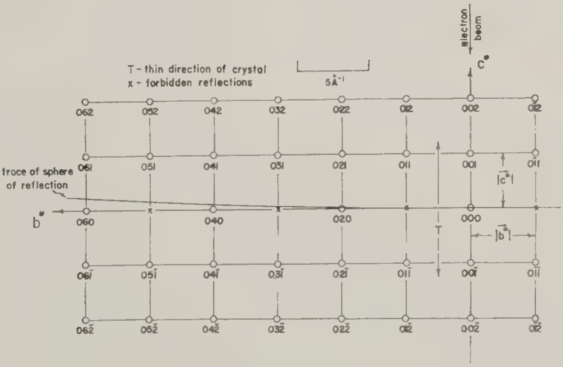

FIG. 14. Ewald construction showing a portion of the section of the $KClO_3$ reciprocal lattice through the origin and perpendicular to the *a*-axis (λ=0.0534 Å).

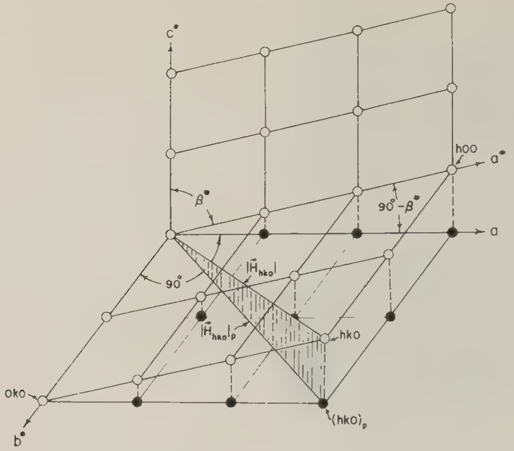

FIG. 15. Geometrical construction used to evaluate the projection of the (*hk*0) reciprocal net of $KClO_3$ onto the *a-b* plane.

TABLE 2. VALUES OF THE *a* AND *b* UNIT CELL CONSTANTS OBTAINED FROM MEASUREMENT OF THE HIGHER ORDER REFLECTIONS OF EIGHT $KClO_3$ EDU SINGLE-CRYSTAL PATTERNS

a	Pattern No.	*b*	Pattern No.
4.64_8 Å	233	5.54_2 Å	233
4.66_4	233	5.54_8	233
4.66_0	234	5.54_8	234
4.67_2	234	5.56_8	234
4.66_6	235	5.55_6	235
4.67_2	235	5.56_6	237
4.65_6	237	5.56_8	237
4.65_6	237	5.58_2	245
4.63_8	245	5.57_2	245
4.65_4	246	5.57_0	245
4.66_4	246	5.49_0[1]	246
4.65_0	402	5.57_0	402
4.67_2	404	5.55_6	404
Average 4.659 Å Average deviation 0.008 Å		Average 5.562 Å Average deviation 0.010 Å	

[1] This low value is not included in the average. It probably arises because the *a-b* plane of the crystal deviates appreciably from being normal to the electron beam. Average values for *a* and *b* are taken as being closer approximations to the truth than maximum values of *a* and *b*. It is considered that the errors are due principally to causes other than deviation of the *a-b* plane from the ideal position (except in Pattern No. 246).

If $h=0$ and $k=1$ (25) reduces to

$$(d_{010})_p = b. \tag{27}$$

Relation (23) gives a satisfactory method of evaluating direct lattice spacings from measurements of spot patterns. Applying this relation specifically to the $KClO_3$ case we have

$$(d_{hk0})_p \cong \frac{d_s D_s}{D_{(hk0)p}} \tag{28}$$

where $D_{(hk0)p}$ is the distance between the $hk\underline{l}$ and $\bar{h}\bar{k}\underline{l}$ spots.

Planes of symmetry appear in all the $KClO_3$ spot patterns showing that the γ^* angle is 90°. Table 2 gives the values of the a and b unit cell constants of $KClO_3$ obtained from measurement of the higher order $h0\underline{l}$ and $0k\underline{l}$ reflections of eight spot patterns. One pattern (No. 246) gives an exceptionally low value for b. This was probably the result of a large deviation of the a-b plane of the $KClO_3$ crystal from being normal to the electron beam. Table 3 compares the average values of a and b obtained from the EDU spot patterns to the x-ray values (Zachariasen, 1929).

No diffraction patterns of $KClO_3$ were obtained with the electron microscope because the heat generated by the beam decomposed the crystals. Some decomposition also occurred in the electron-diffraction unit. The pattern shown in Fig. 13*a* shows some effects of decomposition including broadening of the spots. The EDU pattern shown in Fig. 16*a* was taken after a $KClO_3$ single crystal had been centered in the beam for ten minutes. This pattern shows an almost complete decomposition of $KClO_3$ to KCl and represents a large number of KCl crystals oriented with a cube face parallel to the collodion film (arbitrarily assigned as the (001) face in Fig. 16*b*). The spots are more or less extended arcs having the most intense blackening in the centers and a sharp decrease in blackening towards their extremities. This shows that the KCl crystals

TABLE 3. SINGLE-CRYSTAL DATA: $KClO_3$, MONOCLINIC

X-ray diffraction[1]	Electron diffraction[2]
$a=4.656\pm0.004$ Å	$a=4.659\pm0.008$ Å
$b=5.596\pm0.005$	$b=5.562\pm0.010$
$c=7.099\pm0.007$	
$d_{100}=4.386$ Å (calc.)	
$d_{10\bar{1}}=4.409$ (calc.)	
$\beta=109°38'\pm05'$	
Space group$-P2_1/m-(C_{2h}^2)$	

[1] Zachariasen (1929), spacings have been converted from kX units to angstrom units.

[2] Average of eight EDU spot patterns.

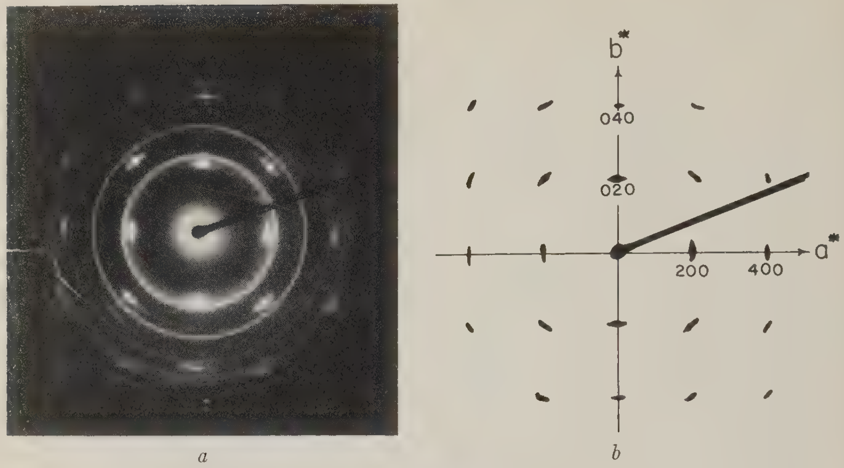

FIG. 16*a*. EDU pattern taken after a single crystal of $KClO_3$ had been centered in the electron beam for ten minutes. The rings are those of β-tin. 16*b*. Indexed reproduction of the EDU pattern shown in Fig. 16*a*.

are also oriented in azimuth—that is, in the plane of the film. The $hk0$ reflections with h and/or k odd do not appear in the KCl pattern shown in Fig. 16*a*. This is because the scattering powers of the potassium and chloride ions are almost exactly equal and therefore only hkl reflections where h, k, and $l=2n$ appear. The single crystal pattern of KCl thus appears to be that of a primitive cell with $a(\text{apparent}) = a/2(\text{real})$. Measurement of the KCl pattern yields a value of $d_{200} = 3.15$ Å. Swanson and Tatge (1953, p. 66) find d_{200} for KCl to be 3.146 Å.

Discussion

It is clear that useful crystallographic data can be obtained from the electron-diffraction study of single crystals, as shown by the results obtained on colemanite and $KClO_3$. For these substances unit cell constants accurate to a few parts per thousand were obtained.

It is to be emphasized that we have been here dealing with an experimental arrangement in which the electron beam is normal to a crystal lying on a cleavage or natural face. From reciprocal lattice theory this means that if the crystal is lying on the face (hkl) the beam is parallel to the reciprocal lattice vector $\mathbf{H}_{hkl}$. The vectors normal to $\mathbf{H}_{hkl}$, and lying in the plane of the face, are, in the general case, direct lattice vectors. The principal reciprocal lattice vectors may or may not lie in this plane, depending upon the crystal system, a fact which must be taken into account in the interpretation of the diffraction patterns. A thin monoclinic crystal lying on the (001) face is an example of a case for which the principal direct lattice and reciprocal lattice vectors do not lie in the same plane. We have treated this case in some detail for $KClO_3$. The interpretation given for this substance may be readily expanded for the most general case, the triclinic.

The electron-diffraction single-crystal experiment is to be contrasted with the x-ray diffraction single-crystal experiment. With the former the diffraction spots give directly the projected quantities $|\mathbf{H}_{hkl}|_p$ whereas with the latter the diffraction spots give directly the quantities $|\mathbf{H}_{hkl}|$. In the case of orthogonal crystals $|\mathbf{H}_{hkl}|_p \equiv |\mathbf{H}_{hkl}|$.

The procedures used to interpret the single crystal patterns of colemanite and $KClO_3$ may be applied to the interpretation of patterns obtained from crystals belonging to any crystal system. Table 4 gives the crystallographic data that may be obtained directly from spot patterns of crystals belonging to the six crystal systems. Spot patterns obtained from crystals which orient other than on (100), (010) or (001) would have to be indexed assuming orientation upon a pinacoidal face and then if possible a suitable transformation could be made to give the proper unit cell. The spot patterns obtained from triclinic crystals represent projections of the $hk0$, $h0l$, or $0kl$ reciprocal nets upon the plane of orientation.

Commonly only those crystals that have perfect cleavage or which crystallize as thin pates or tablets of constant thickness give single-crystal patterns suitable for measurement. Although spot patterns can be obtained from crystals that vary in thickness, the patterns are usually so distorted that they cannot be measured with any accuracy.

The main sources of error in evaluation of cell parameters from EDU single crystal patterns arise from: 1) limitations in the precision of meas-

TABLE 4. CRYSTALLOGRAPHIC DATA OBTAINED DIRECTLY FROM SPOT PATTERNS OF CRYSTALS BELONGING TO THE SIX CRYSTAL SYSTEMS

Crystal System	Plane of Orientation	Crystallographic data
Cubic	(100)	d_{100}
Tetragonal	(100)	d_{100}, d_{001}
Tetragonal	(001)	d_{100}
Orthorhombic	(100)	d_{010}, d_{001}
Orthorhombic	(010)	d_{100}, d_{001}
Orthorhombic	(001)	d_{100}, d_{010}
Hexagonal	(001)	d_{100}
Monoclinic	(100)	d_{010}, $(d_{001})_p$, $[(d_{001})_p = c]$
Monoclinic	(010)	d_{100}, d_{001}, β
Monoclinic	(001)	$(d_{100})_p$, d_{010}, $[(d_{100})_p = a]$
Triclinic	(100)	$(d_{010})_p$, $(d_{001})_p$, α, $[(d_{010})_p/\sin\alpha = b]$, $[(d_{001})_p/\sin\alpha = c]$
Triclinic	(010)	$(d_{100})_p$, $(d_{001})_p$, β, $[(d_{100})_p/\sin\beta = a]$, $[(d_{001})_p/\sin\beta = c]$
Triclinic	(001)	$(d_{100})_p$, $({}_{010})_p$, γ, $[(d_{100})_p/\sin\gamma = a]$, $[(d_{010})_p/\sin\gamma = b]$

urement, and 2) deviation of the crystal face from the horizontal. The precision of measurement is governed by the shape, size and intensity of the spots and varies according to the particular substance under examination. The deviation of a crystal from the ideal orientation can introduce very large errors if care is not taken to orient the crystal so that one face is approximately normal to the beam. For small deviations (within 5°), the error introduced into the spot pattern will be only a few parts per thousand.

The peculiarities of the electron-diffraction technique must be taken into account in the interpretation of electron-diffraction powder patterns. Consider an aggregate of crystals which are small thin plates or flakes oriented with the basal pinacoid parallel to the substrate of the specimen mount but with all possible orientations in the plane of the substrate. The electron-diffraction powder pattern obtained from these crystals will show a number of evenly blackened rings. Measurement of these rings will yield for the most part the projected quantities $|\mathbf{H}_{hkl}|_p$ of one net, i.e. the same data given by the spot pattern of one crystal of the aggregate. The projected quantities $|\mathbf{H}_{hkl}|_p$ are obtained from the oriented powder pattern because the reciprocal lattice points of each crystal in the aggregate are extended into rods. If an electron diffraction powder pattern were obtained from an aggregate of small, equidimensional, randomly oriented crystals where there is no extension of reciprocal lattice points into rods, measurement of the rings would yield the quantities $|\mathbf{H}_{hkl}|$, i.e. the same quantities that are given by an x-ray diffraction powder pattern. In Part II of this paper a method of indexing oriented electron-diffraction powder patterns will be given.

REFERENCES

Buckley, H. E. (1951), Crystal Growth, John Wiley and Sons, New York.

Christ, C. L. (1953), Studies of borate minerals: I. X-ray crystallography of colemanite: *Am. Mineral.*, **38**, 411–415.

Drumond, D. G. (1950), The practice of electron microscopy: *J. Roy. Microscopical Soc.*, **70**, 1–158.

Hall, C. E. (1953), Introduction to Electron Microscopy, McGraw-Hill, N. Y.

James, R. W. (1954), The Optical Principles of the Diffraction of X-Rays, G. Bell and Sons, Ltd., London.

Picard, R. G., and Reisner, J. H. (1946), Universal electron microscope as a high resolution diffraction camera: *Rev. Sci. Instr.*, **17**, 484–489.

Ross, Malcolm (1959), Mineralogical applications of electron diffraction: II. Results of studies of some vanadium minerals of the Colorado Plateau: *Am. Mineral.* (in press).

Swanson, H. E. and Tatge, E. (1953). Standard x-ray diffraction powder patterns: National Bureau of Standards Circular 539, Vol. I.

Zachariasen, W. H. (1929), The crystal structure of $KClO_3$: *Zeit. f. Krist.*, **71**, 501–516.

Manuscript received April 14, 1958

THE AMERICAN MINERALOGIST, VOL. 43, NOVEMBER–DECEMBER, 1958

THE OPTICAL PROPERTIES OF HEATED PLAGIOCLASES

J. R. SMITH,* *Geophysical Laboratory, Carnegie Institution of Washington, Washington, D. C.*

ABSTRACT

The optical properties of nine chemically analyzed samples of natural plagioclases have been accurately determined before and after changing them to high-temperature modifications by heat treatment. The change in Nx accompanying the structural change is slight in the composition range An 0 to An 20 and negligible from An 20 to An 100. Ny and Nz change measurably in the composition range An 0 to An 20, but negligibly in the remainder of the composition range. Measurements of principal refractive indices can therefore give a reliable estimate of the composition of a plagioclase regardless of its structural state.

The changes in optic axial angle accompanying the structural changes are such that, given composition, measurements of optic axial angle serve to distinguish low-temperature and high-temperature plagioclases in the composition ranges An 0 to about An 40 and An 60 to about An 90.

INTRODUCTION

Differences between the optical properties of feldspars at low and at high temperatures were reported by Merwin in 1911. Since then, Kohler (1949) has found that the orientation of the optical indicatrix in plagioclases from volcanic rocks is different from that in plagioclases from plutonic rocks. Tuttle and Bowen (1950) were able to distinguish high-temperature and low-temperature modifications of sodic plagioclases by means of optics and x-rays; they found that the low-temperature modifications could be changed to the high by heating at temperatures near those at which melting begins. The x-ray techniques used by Tuttle and Bowen to distinguish between low- and high-temperature plagioclases have been expanded and applied to more extensive groups of samples by Goodyear and Duffin (1954, 1955), J. R. Smith and Yoder (1956), and J. V. Smith (1956). The results of these studies indicate structural differences between low- and high-temperature plagioclases in the composition range An 0 to An 80;† many natural plagioclases are intermediate between the "maximum" low- and high-temperature states so far found. In the composition range An 80 to An 100, Gay (1954) and Laves and Goldsmith (1954) have found structural differences between low- and high-temperature plagioclases by single-crystal x-ray methods. In view of these facts, it is important that carefully controlled tests be made of the differences between the optical properties of low- and high-temperature plagioclases throughout the composition range, partly to determine the applicability of presently available refractive index determinative curves to high-temperature plagioclases, and partly to investigate further the optical methods of distinguishing between low- and high-temperature plagioclases. This has been done in the present study by making accurate measurements of the optical properties of chemically analyzed natural plagioclases before and after changing them to the high-temperature forms by heat treatment. This method has the distinct advantage of using the same samples for the measurements in the low- and high-temperature states; observed differences in optical properties cannot therefore be attributed to possible errors in the chemical analyses.

---

* Present address: Department of Geology, University of Saskatchewan, Saskatoon, Sask., Canada.

† Compositions are stated as mole per cent anorthite, calculated as $100(Ca^{++}/Ca^{++}+Na^{+}+K^{+})$.

The object of the study was to determine the direction and magnitude of the optical changes in different parts of the composition range rather than to establish accurate determinative curves for maximum high-temperature plagioclases, because such plagioclases appear to be rare in nature, and the curves would be of little practical value.

METHODS

Carefully purified and chemically analyzed samples of natural plagioclases ranging in composition from pure albite to almost pure anorthite were available at the Geophysical Laboratory, thanks to many contributors; the samples selected for study are listed and described in Table 1. The optical properties of most of these samples had previously been measured by the writer using techniques developed in cooperation with H. H. Hess. These techniques are described in detail in a memoir of the Geological Society of America (Smith, in Hess, in press). Briefly, total birefringence was determined on the universal stage by accurate comparison with the total birefringence of quartz, which is known to the fifth decimal place. Optic axial angles (2V) were measured by the standard orthoscopic procedure (Fairbairn and Podolsky, 1951) in thin sections of grains mounted in bakelite. Refractive indices were determined by a controlled-temperature universal stage technique, in which a grain, illuminated in sodium light, is rotated from a principal orientation toward another principal orientation until the refractive index of the grain exactly matches that of the oil in which it is immersed, at which point it disappears if it is colorless and transparent. Knowing the index of the oil, the angle of rotation from the principal orientation, and the birefrigence of the section of the mineral perpendicular to the axis of rotation, two principal refractive indices of the grain can be calculated. If 2V is also known, the third principal index can be calculated. In determining each of the optical properties, measurements were made on several different grains in each sample and averaged. The estimated accuracy of the average values of refractive indices is ±0.0003, of total birefringence ±0.0001, and of 2V ±0.5°. The optical properties of the plagioclase samples selected for study were measured by these methods

TABLE 1. DESCRIPTION OF PLAGIOCLASE SAMPLES

Sample No.	Composition (mole %)			Analyst	Occurrence and Locality	Contributor
	An	Ab	Or			
D761-1	0.2	98.7	1.1	R. E. Stevens*	Pegmatite, Ramona, Calif.	C. S. Ross
D761-3	0.4	98.2	1.4	R. E. Stevens*	Pegmatite, Amelia, Va.	C. S. Ross
80165	21.6	74.5	3.9	E. Chadbourn**	Pegmatite, Hawk Mine, Bakersville, N. C.	F. C. Kracek
D638	29.8	69.7	0.5	R. E. Stevens*	Pegmatitic vein in dunite, Macon Co., N.C.	C. S. Ross
1963	44.2	53.7	2.1	E. H. Oslund*	Ferrogabbro, Skaergaard Intrusion, East Greenland.	L. R. Wager
GD29	51.8	46.3	1.9	E. H. Oslund*	Dolerite, Great Dyke, S. Rhodesia.	H. H. Hess
BV63	59.2	38.6	2.2	E. H. Oslund*	Gabbro, Bushveld Igneous Complex, South Africa.	H. H. Hess
EB41	62.5	36.8	0.7	E. H. Oslund*	Gabbro, Stillwater Igneous Complex, Montana.	H. H. Hess
EB38	80.0	19.5	0.5	A. H. Phillips*	Norite, Stillwater Igneous Complex, Montana.	H. H. Hess
Synthetic anorthite	100	0	0	—	Crystallized from anhydrous glass at 1500° C. and cooled very quickly to room temperature.	J. F. Schairer

* Analysis quoted in Smith (in Hess, in press).

** Analysis quoted in Kracek and Neuvonen (1952).

before and after changing them to high-temperature modifications by heat treatment. The samples (100- to 200-mesh in grain size) were heated in platinum crucibles in platinum-wound electric resistance furnaces; temperatures were measured with Pt-Pt10Rh thermocouples, and were controlled and recorded continuously, the recorded variations being less than ±5° C. The progress of the structural changes was checked by removing the samples from the furnaces at intervals and measuring $2\theta(131)$–$2\theta(1\bar{3}1)$ in x-ray powder diffraction patterns, using the same techniques and instruments as those described by J. R. Smith and Yoder (1956). Many grains in some of the samples heated in this way were found to contain blebs and sheets of glass, even though the maximum temperatures at which they were heated were somewhat lower than the temperatures of beginning of melting for the compositions concerned (see Table 2 and Bowen, 1913). This was undoubtedly a result of the lowering of the melting temperature by foreign inclusions in the grains of plagioclase. Four samples in the composition range An 0 to An 30, which contain very few inclusions, contained very little glass after heating. Five samples in the composition range An 44 to An 80, which contain rather abundant solid inclusions, contained enough blebs of glass after heating to make the material unsuitable for refractive index determinations. In order to obtain material in the high-temperature form suitable for refractive index measurements, six samples were held for one week at 990°±5° C. in water at a pressure of 1000 psi. This was done in cold-seal type pressure vessels (Tuttle, 1949), the samples being contained in small unsealed platinum tubes. Some grains in the samples subjected to this hydrothermal treatment were found to contain blebs of glass, but not in sufficient amount to hinder refractive index measurements; many grains contained no visible glass.

Discussion of Results

1. *Structural state of samples*

The values of $2\theta(131)$–$2\theta(1\bar{3}1)$ before and after heating the samples are listed in Table 2; the initial and final values are plotted in Fig. 1. The curve in Fig. 1 represents $2\theta(131)$–$2\theta(1\bar{3}1)$ for plagioclases synthesized in the dry way, and is taken from J. R. Smith and Yoder (1956). These plagioclases are probably the highest temperature modifications which can exist metastably at room temperature, because they were crystallized at temperatures near those at which melting begins in the anhydrous binary system $NaAlSi_3O_8$-$CaAl_2Si_2O_8$, and were quenched quickly to room temperature. The curve in Fig. 1 therefore represents *maximum* high-temperature plagioclases. The values of $2\theta(131)$–$2\theta(1\bar{3}1)$

Table 2. Heat Treatment and *X*-ray Measurements

Sample No.	Heat Treatment*	$2\theta(131)-2\theta(1\bar{3}1)$** (CuK$\alpha$)
D761-1 (An 0.2)	(1) None	1.08°
	(2) $24\frac{1}{2}$ days—1080° C. dry	1.98
D761-3 (An 0.4)	(1) None	1.09
	(2) $24\frac{1}{2}$ days—1080° C. dry	1.98
	(H) 1 day—975° C., 3700 psi H_2O	1.95
80165 (An 21.6)	(1) None	1.52
	(2) 14 days—1100° C. dry	1.91
	(3) 28 days—1120° C. dry	1.92
D638 (An 29.8)	(1) None	1.74
	(2) 14 days—1100° C. dry	1.98
	(3) 28 days—1160° C. dry	1.98
	(H) 7 days—990° C., 1000 psi H_2O	1.94
1963 (An 44.2)	(1) None	1.79
	(2) 7 days—1150° C. dry	1.97
	(3) 4 days—1200° C. dry	1.99
	(4) 28 days—1230° C. dry	2.00
	(H) 7 days—990° C., 1000 psi H_2O	1.95
GD29 (An 51.8)	(1) None	1.82
	(2) 7 days—1150° C. dry	2.00
	(3) 4 days—1200° C. dry	2.01
	(4) 28 days—1270° C. dry	2.00
	(H) 7 days—990° C., 1000 psi H_2O	1.99
BV63 (An 59.2)	(1) None	1.87
	(2) 7 days—1150° C. dry	2.05
	(3) 4 days—1200° C. dry	2.04
	(4) 28 days—1310° C. dry	2.05
	(H) 7 days—990° C., 1000 psi H_2O	2.02
EB41 (An 62.5)	(1) None	1.91
	(2) 8 days—1150° C. dry	2.07
	(3) 14 days—1200° C. dry	2.08
	(4) 28 days—1310° C. dry	2.05
	(H) 7 days—990° C., 1000 psi H_2O	2.06
ED38 (An 80.0)	(1) None	2.12
	(2) 8 days—1150° C. dry	2.18
	(3) 14 days—1200° C. dry	2.19
	(4) 28 days—1420° C. dry	2.17
	(H) 7 days—990° C., 1000 psi H_2O	2.19
Synthetic anorthite (An 100)	Crystallized from anhydrous glass at 1500° C., cooled very quickly to room temperature.	2.28

* Numbers in parentheses indicate successive heatings of *same* sample. (H) indicates hydrothermal treatment of a *different* sample.

** Values listed are averages of three or more measurements.

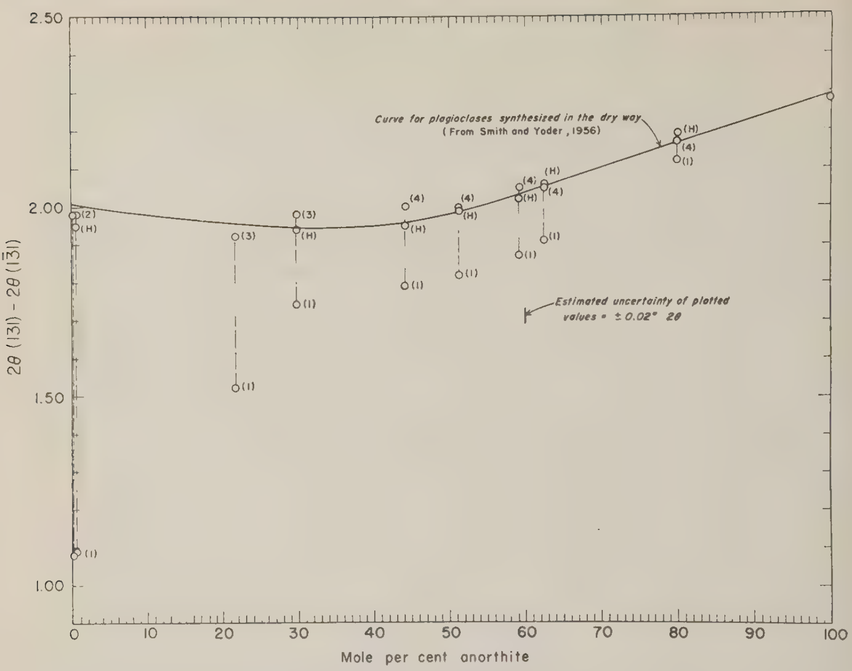

Fig. 1. $2\theta(131)$–$2\theta(131)$ for plagioclase samples before and after heating. Numbers and letters in parentheses refer to heat treatment of samples described in Table 2.

plotted in Fig. 1 show that the samples studied optically, whether heated in air or hydrothermally, were changed nearly or quite completely to maximum high-temperature plagioclases. Synthetic anorthite (An 100) was not reheated, but it is assumed to be in the high-temperature form because it was crystallized at 1500° C. and quenched quickly to room temperature. The assumption is supported by the fact that in single-crystal x-ray photographs of grains from this sample, "c"-type reflections are very diffuse and "d"-type reflections are apparently absent (cf. Gay, 1954).

2. *Changes in optical properties*

The measurements of optical properties before and after heating are listed in Table 3. Except for the values of Ny and Nz, each of the measurements listed was determined on a different grain in the heated or unheated samples. Because of the method of determination, individual determinations of Ny and Nz have the same range of values as do the individual determinations of Nx, so that for convenience only the mean values of Ny and Nz are listed.

TABLE 3. OPTICAL PROPERTIES BEFORE AND AFTER HEATING

NOTE: All measurements before heating except for samples D761-3, 80165, and synthetic anorthite are taken from Smith (in Hess, in press).
Numbers in parentheses and (H) refer to heat treatment of samples described in Table 2.

Sample No.	N_x		N_y (Means)		N_z (Means)		N_z–N_x		$2V_z$	
	Before heating	After heating	Before heating	After heating	Before heating	After heating	Before heating	After heating	Before heating	After heating
D761-1	1.5285	(2)					.01003	(2)	76.4°	(2)
(An 0.2)	1.5285	1.5270					.01008	.00839	76.4	129.8°
	1.5286	1.5271					.01018	.00842	77.0	132.4
	1.5286	1.5271		(2)		(2)	.01022	.00846	77.2	133.2
	1.5286	1.5271	1.5326	1.5341	1.5388	1.5357	.01023		77.3	133.5
	1.5287	1.5276					.01026	Mean	77.7	133.7
	1.5290	1.5278					.01033	.00842	77.8	133.8
							.01037		78.0	134.3
	Mean	Mean								134.4
	1.5286	1.5273					Mean		Mean	
							.01021		77.2	Mean
										133.1
D761-3	1.5286	(2)					.00983	(2)	75.9°	(2)
(An 0.4)	1.5286	1.5268		(2)		(2)	.00989	.00840	76.3	133.8°
	1.5286	1.5269	1.5326	1.5343	1.5387	1.5356	.00989	.00848	76.5	134.2
	1.5287	1.5273					.00994	.00849	76.6	134.6
	1.5288	1.5274					.01007	.00851	76.7	134.7
	1.5289									135.3
	1.5294	Mean					Mean	Mean	Mean	135.3
		1.5271					.00992	.00847	76.4	
	Mean									Mean
	1.5288									134.7
		(H)						(H)		
		1.5266						.00845		
		1.5268		(H)		(H)		.00852		(H)
		1.5268		1.5340		1.5354		.00859		132.1°
		1.5269						.00862		132.3
		1.5270						.00869		133.7
										133.9
		Mean						Mean		134.5
		1.5268						.00857		
										Mean
										133.3
80165	1.5388	(3)					.00763	(3)	92.8°	(3)
(An 21.6)	1.5388	1.5383		(3)		(3)	.00764	.00721	93.0	116.5°
	1.5390	1.5386	1.5431	1.5440	1.5467	1.5459	.00764	.00728	93.4	117.1
	1.5391	1.5387					.00768	.00732	93.6	117.7
	1.5392	1.5389					.00782	.00743	93.9	118.7
	1.5392							.00745	94.2	119.3
		Mean					Mean			
	Mean	1.5386					.00768	Mean	Mean	Mean
	1.5390							.00734	93.5	117.9
D638	1.5433	(3)					.00733	(3)	91.4°	(3)
(An 29.8)	1.5433	1.5433					.00735	.00723	91.9	104.8°
	1.5433	1.5436		(3)		(3)	.00739	.00732	92.0	105.1
	1.5435	1.5436	1.5479	1.5483	1.5514	1.5510	.00752	.00752	94.0	105.2
	1.5437	1.5437					.00756	.00761	94.4	105.4
	1.5439	1.5438					.00777		94.5	105.4
	1.5442						.00778	Mean	94.6	

TABLE 3. (*Continued*)

Sample No.	Nx		Ny (Means)		Nz (Means)		Nz−Nx		2V$_z$	
	Before heating	After heating	Before heating	After heating	Before heating	After heating	Before heating	After heating	Before heating	After heating
	1.5444 1.5444 1.5450 Mean 1.5439	Mean 1.5436 (H) 1.5437 1.5437 1.5438 1.5440 1.5440 Mean 1.5438		(H) 1.5483		(H) 1.5510	Mean .00753	.00744 (H) .00714 .00715 .00716 .00716 Mean .00715	94.7 94.7 94.8 95.1 Mean 93.6	Mean 105.2 (H) 103.6° 104.3 104.4 105.2 Mean 104.4
1963 (An 44.2)	1.5506 1.5506 1.5506 1.5506 1.5517 1.5519 1.5520 1.5520 1.5520 1.5521 1.5525 1.5525 Mean 1.5516	(H) 1.5520 1.5520 1.5522 1.5523 1.5525 Mean 1.5522	1.5547	—	1.5590	(H) 1.5595	.00721 .00722 .00736 .00739 .00750 .00754 .00757 Mean .00740	(H) .00719 .00730 .00733 .00736 Mean .00730	Variable	Variable
GD29 (An 51.8)	1.5540 1.5541 1.5542 1.5545 1.5548 1.5548 1.5549 1.5550 1.5558 Mean 1.5547	(H) 1.5539 1.5545 1.5547 1.5549 1.5550 1.5553 Mean 1.5547	1.5575	(H) 1.5576	1.5621	(H) 1.5621	.00738 .00740 .00748 .00751 .00752 Mean .00746	(4) .00736 .00738 .00753 .00753 Mean .00745	75.0° 75.0 75.7 75.7 76.0 76.0 76.3 76.5 76.6 76.6 77.0 77.0 77.7 78.1 78.2 Mean 76.4	(4) 76.0° 76.6 76.6 76.7 76.8 78.0 Mean 76.8
BV63 (An 59.2)	1.5579 1.5580 1.5581 1.5581 1.5581 1.5583 1.5586 Mean 1.5582	(H) 1.5577 1.5579 1.5581 1.5586 1.5587 Mean 1.5582	1.5615	(H) 1.5611	1.5662	(H) 1.5662	.00776 .00794 .00796 .00813 .00814 .00814 Mean .00801	(4) .00792 .00793 .00799 .00806 Mean .00797	78.8° 79.0 79.0 79.3 79.4 81.6 Mean 79.5	(4) 73.0° 73.3 73.6 74.0 74.7 74.8 Mean 73.9

TABLE 3. (*Continued*)

Sample No.	Nx		Ny (Means)		Nz (Means)		Nz−Nx		2V_z	
	Before heating	After heating	Before heating	After heating	Before heating	After heating	Before heating	After heating	Before heating	After heating
EB41	1.5589	(H)					.00791	(4)	78.5°	(4)
(An 62.5)	1.5598	1.5599					.00812	.00792	79.0	74.8°
	1.5599	1.5600					.00821	.00796	79.7	75.1
	1.5600	1.5602		(H)		(H)	.00823	.00817	80.6	75.5
	1.5603	1.5604	1.5640	1.5634	1.5687	1.5684	.00823	.00826	81.5	75.8
	1.5604	1.5605					.00825	.00827	81.8	76.0
	1.5605	1.5611					.00826	.00834	82.0	76.3
	1.5607	———					.00830	———	82.2	———
	1.5607	Mean					.00831	Mean	82.2	Mean
	1.5615	1.5603					.00832	.00815	82.2	75.6
	1.5615						.00837		82.6	
	———						.00850		82.6	
	Mean						.00852		82.6	
	1.5604						.00853		82.7	
							.00871		82.8	
							———		82.9	
							Mean		83.1	
							.00832		83.3	
									83.4	
									84.5	
									84.5	
									—	
									Mean	
									82.1	
EB38	1.5664	(H)					.01046	(4)	93.7°	(4)
(An 80.0)	1.5668	1.5667					.01058	.00888	93.7	86.1°
	1.5668	1.5668					.01061	.00896	94.2	87.2
	1.5669	1.5670		(H)		(H)	.01066	.00910	94.4	87.7
	1.5669	1.5671	1.5729	1.5716	1.5778	1.5765	.01070	.00955	94.5	88.1
	1.5669	1.5677					.01076	.00963	95.1	88.1
	1.5670	———					.01081	.00983	96.0	———
	1.5670	Mean					.01088	.00993	96.1	Mean
	1.5671	1.5671					.01090	———	96.2	87.5
	1.5671						———	Mean	96.6	
	1.5671						Mean	.00941	———	
	1.5672						.01071		Mean	
	1.5673								95.0	
	1.5673									
	1.5673									
	1.5679									
	———									
	Mean									
	1.5671									
Synthetic	1.5746						.01307		104.2°	
anorthite	1.5748						.01326		104.7	
(An 100)	1.5749						.01328		104.8	
	1.5750		1.5834		1.5883		.01334		104.9	
	1.5752						.01343		105.3	
	1.5754						.01352			
	1.5754						———		Mean	
	———						Mean		104.8	
	Mean						.01331			
	1.5750									

As stated previously, some of the samples studied were heated in air and some were heated hydrothermally at lower temperatures in order to avoid the formation of glass around inclusions in the grains, which hinders refractive index measurements. Refractive indices of the five samples in the composition range An 44 to An 80 were determined only on material heated hydrothermally. In order to be sure that plagioclase heated hydrothermally has the same optical properties as that heated in air, two samples, D761-3 (An 0.4) and D638 (An 29.8), were changed to the high-temperature forms in both ways, and the optical properties of both products were measured. The measurements are listed in Table 3, and they show that no significant differences in any of the optical properties result from the difference in the method of heating.

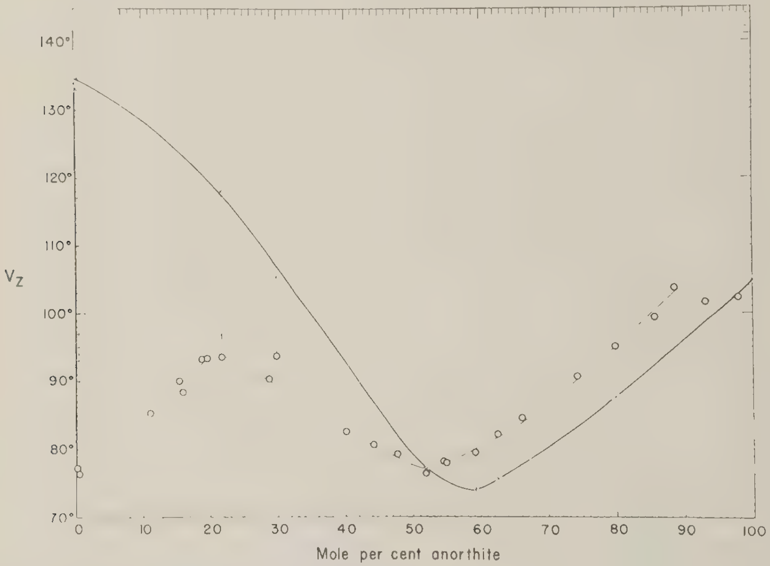

FIG. 2. Optic axial angle of plagioclase samples before (open circles) and after (crosses) heating. Light curve is for low-temperature plagioclases, taken from Smith (in Hess, in press). Heavy curve is tentative curve for maximum high-temperature plagioclases.

The average values of $2V_z$ before and after heating are plotted in Fig. 2. In this figure the curve for low-temperature plagioclases (light-line curve) is essentially the same as that in Smith (in Hess, in press), with a few additional determinations which are listed in an appendix to the present paper. All the samples on which it is based have been studied by x-ray methods (J. R. Smith and Yoder, 1956, and unpublished single-crystal studies); by comparison with other natural plagioclases, they are known to be the lowest temperature plagioclases so far found. The changes in $2V_z$ caused by heating suggest that the curve for maximum high-temperature plagioclases has the shape of the heavy line in Fig. 2. From this it may be seen that, knowing composition, high-temperature and low-temperature plagioclases in the composition ranges An 0 to about An 40 and An 60 to about An 90 can be distinguished by accurate 2V measurements. Relations in the range An 90 to An 100 remain somewhat ambiguous, and require further study.

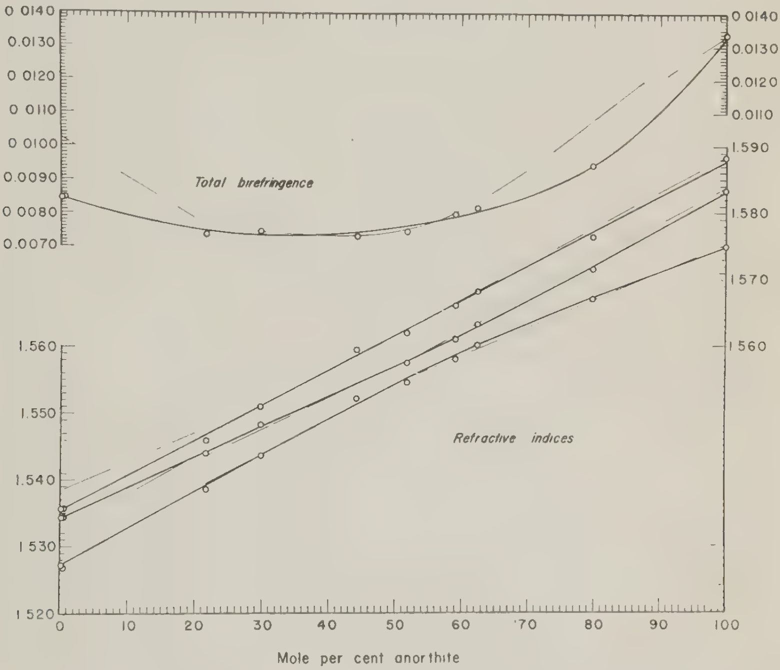

FIG. 3. Total birefringence and refractive indices for maximum high-temperature plagioclases (open circles and heavy curves). Light curves are for low-temperature plagioclases, taken from Smith (in Hess, in press).

The average values of total birefringence and refractive indices after final heat treatment are plotted in Fig. 3, and tentative curves are drawn for maximum high-temperature plagioclases. The curves shown for low-temperature plagioclases are from Smith (in Hess, in press); they are based on the same samples as those on which the 2V curve for low-temperature plagioclases in Fig. 2 is based, but to avoid confusion the determined values are not plotted. The significant fact here is that the difference in Nx between the low- and high-temperature modifications appears to be very slight in the composition range An 0 to An 20, and negligible throughout the remainder of the range. Measurements of Nx therefore provide a reliable estimate of the composition of a plagioclase regardless of its structural state. In the composition range An 20 to An 100, any of the three principal indices provides a reliable composition estimate regardless of structural state.

3. *The temperature of the change from low- to high-temperature plagioclases*

The hydrothermal experiments of the present study show that plagioclases in the composition range An 30 to An 80 can be changed to maximum high-temperature modifications at temperatures as low as 990° C. In other experiments not reported here, it was found that slight, but measurable changes toward the high-temperature forms take place in natural plagioclases of composition An 20 and An 30 after long hydrothermal treatment at 690° C.; whether the changes would ever go to completion at this temperature is not known. Apart from these isolated observations, little was learned of the nature of the change from low- to high-temperature plagioclases or of the temperature at which it takes place under conditions of equilibrium.

4. *Comparison with results of others*

The present results compare well with those of Tuttle and Bowen (1950) as far as 2V of high-temperature sodic plagioclases is concerned, but differ from their tentative curve for 2V of high-temperature calcic plagioclases (cf. their Fig. 4 and present Fig. 2).

Kano (1955) has measured the refractive indices and 2V's of many sodic plagioclases from lavas. Following a suggestion by Chayes (1952), he assumed that Nx and Ny of high-temperature sodic plagioclases are not different from Nx and Ny of low-temperature sodic plagioclases, and determined the compositions of his samples by refractive index measurements. This assumption of course prevented him from discovering the small but real differences in Nx and Ny, and probably contributed some bias to his curve for Nz. However, the results of the present study in general agree well with Kano's.

Schwarzmann (1956) measured the optical properties of plagioclases in inclusions and ejecta in Tertiary volcanic rocks. Her determinations of Nx and Nz in the composition range An 20 to An 50 are lower by as much as 0.005 than the values determined here for high-temperature plagioclases of the same compositions; this represents a difference of as much as 6 per cent anorthite if the curves are used for composition determinations. The reason for the discrepancy is not apparent. It may be that the refractive indices of plagioclases which have been heated as inclusions in lavas differ from those of plagioclases heated under laboratory conditions; this seems unlikely, because by other optical and structural criteria, sodic plagioclases from volcanic rocks are similar to those either made or heated in the laboratory (see, for example, Tuttle and Bowen, 1950, and Tuttle and Keith, 1954). Part of the discrepancy may result from the fact that Schwarzmann determined the compositions of most of her samples by optical methods, which is somewhat circuitous in a study aimed at discovering differences in optical properties.

Summary and Conclusions

The change in Nx accompanying the structural change from low- to high-temperature plagioclase is slight in the composition range An 0 to An 20 and negligible from An 20 to An 100. Ny and Nz change measurably in the composition range An 0 to An 20, but negligibly in the remainder of the composition range. Measurements of the principal refractive indices can therefore give a reliable estimate of the composition of a plagioclase regardless of its structural state.

The changes in 2V accompanying the structural changes are such that it may be used to distinguish low-temperature and high-temperature plagioclases of known composition in the composition ranges An 0 to about An 40 and An 60 to about An 90. This fact will be of use to the petrographer who does not have access to an x-ray diffractometer, by means of which a more rapid determination of the structural state of a plagioclase of known composition can be made.

Acknowledgments

The writer is indebted to F. Chayes, H. H. Hess, D. B. Stewart, and H. S. Yoder, Jr., who offered helpful criticism of the manuscript.

References

Bowen, N. L. (1913), The melting phenomena of the plagioclase feldspars: *Am. Jour. Sci.*, **35,** 577–599.

Chayes, F. (1952), Relation between composition and indices of refraction in natural plagioclase: *Am. Jour. Sci.*, **Bowen Vol.,** 85–105.

Fairbairn, H. W. and Podolsky, T. (1951), Notes on precision and accuracy of optic angle determination with the universal stage: *Am. Mineral.*, **36,** 823–832.

Gay, P. (1954), The structure of the plagioclase feldspars. V. The heat treatment of lime-rich plagioclases: *Min. Mag.*, **30,** 428–438.

Goodyear, J. and Duffin, W. J. (1954), The identification and determination of plagioclase feldspars by the x-ray powder method: *Min. Mag.*, **30,** 306–326.

——— and ——— (1955), The determination of composition and thermal history of plagioclase by the x-ray powder method: *Min. Mag.*, **30,** 648–656.

Hess, H. H. (in press), Stillwater Igneous Complex: A quantitative mineralogical study, with an appendix on the optical properties of low-temperature plagioclase, by J. R. Smith: *Geol. Soc. Am. Memoir.*

KANO, H. (1955), High-temperature optics of natural sodic plagioclases: *Japanese Mineral. Jour.*, **1**, 255–277.

KOHLER, A. (1949), Recent results of investigations of the feldspars: *Jour. Geol.*, **57**, 592–599.

KRACEK, F. C. AND NEUVONEN, K. J. (1952), Thermochemistry of plagioclase and alkali feldspars: *Am. Jour. Sci.*, Bowen Vol., 293–318.

LAVES, F. AND GOLDSMITH, J. R. (1954), Long-range—short-range order in calcic plagioclase as a continuous and reversible function of temperature: *Acta Cryst.*, **7**, 465–472.

MERWIN, H. E. (1911), The temperature, stability ranges, density, chemical composition and optical and crystallographic properties of the alkali feldspars: *Jour. Wash. Acad. Sci.*, **1**, 59–60 (Abstract).

SCHWARZMANN, S. (1956), Über die Lichtbrechung und die Achsenwinkel von Hochtemperatur-plagioklasen und ihre Entstehungsbedingunen: *Heidelberger Beit. zur Min. und Pet.*, **5**, 105–112.

SMITH, J. R. AND YODER, H. S., JR. (1956), Variations in x-ray powder diffraction patterns of plagioclase feldspars: *Am. Mineral.*, **41**, 632–647.

SMITH, J. V. (1956), The powder patterns and lattice parameters of plagioclase feldspars. I. The soda-rich plagioclases: *Min. Mag.*, **31**, 47–68.

TUTTLE, O. F. (1949), Two pressure vessels for silicate-water studies: *Geol. Soc. Am. Bull.*, **60**, 1727–1729.

——— AND BOWEN, N. L. (1950), High-temperature albite and contiguous feldspars *Jour. Geol.*, **58**, 489–511.

——— AND KEITH, M. L. (1954), The granite problem: Evidence from the quartz and feldspar of a Tertiary granite: *Geol. Mag.*, **91**, 61–72.

APPENDIX

ADDITIONAL OPTICAL DATA FOR LOW-TEMPERATURE PLAGIOCLASES

Measured values of 2V for low-temperature plagioclases are plotted in Fig. 2 of this paper. The optical measurements on all but four of these plagioclase samples have been published by the writer, either in Hess (in press) or in Table 3 of this paper. The writer's measurements of the optical properties of the remaining four samples have not previously been published, and do not appear in Table 3 because the samples in question were not heated. In the belief that accurate optical and x-ray data for chemically analyzed plagioclases will be of use in future studies, these four samples are described and the measurements are listed here. Unless otherwise noted, each value listed for optical properties was determined on a different grain by the methods referred to in the text. By the following x-ray criteria, the four samples are judged to be low-temperature plagioclases: (*a*) Values of $2\theta(131)-2\theta(1\bar{3}1)$ for samples 9(24), 12(97) and 13(92) are similar to those of Bushveld-type plagioclases (J. R. Smith and Yoder, 1956); (*b*) "c"-type reflections are diffuse but relatively intense in single-crystal oscillation photographs of grains from sample HGIF-AN-53 (cf. Gay, 1954).

(*See tables A and B on following pages*)

TABLE A. DESCRIPTION OF PLAGIOCLASE SAMPLES

Sample No.	Composition (mole %)*			Analyst	Occurrence and Locality	Contributor
	An	Ab	Or			
9(24)	47.7	48.8	3.5	L. C. Peck**	Anorthosite, Essex Co., N. Y.	R. C. Emmons
12(97)	54.5	43.3	2.2	L. C. Peck**	Plagioclase-rich rock of metamorphic origin, Eland, Wis.	R. C. Emmons
13(92)	54.9	42.8	2.3	L. C. Peck**	Same as 12(97), Tigerton, Wis.	R. C. Emmons
HGIF-AN-53	88.7	8.8	2.5	E. H. Oslund***	Large single crystal in vein-like mass in hornblende-actin olite schist, Olricksfjord Area, N.W. Greenland.	Allan H. Nicol

$$* \text{An}=100\left(\frac{\text{Ca}^{++}}{\text{Ca}^{++}+\text{Na}^{+}+\text{K}^{+}}\right); \qquad \text{Ab}=100\left(\frac{\text{Na}^{+}}{\text{Ca}^{++}+\text{Na}^{+}+\text{K}^{+}}\right);$$

$$\text{Or}=100\left(\frac{\text{K}^{+}}{\text{Ca}^{++}+\text{Na}^{+}+\text{K}^{+}}\right).$$

** Analysis in Emmons, R. C., et al. (1953), Selected Petrogenic Relationships of Plagioclase; Geol. Soc. Am. Memoir 52, Table 2, pp. 18–19.

*** Analysis in Smith, J. R. and Yoder, H. S., Jr. (1956), Variations in *X*-ray Powder Diffraction Patterns of Plagioclase Feldspars; Am. Min. 41, Table 3, p. 639.

TABLE B. OPTICAL AND *X*-RAY DATA

Sample	N_x	N_y and N_z means	$N_z - N_x$	$2V_z$	$2\theta(131) - 2\theta(1\bar{3}1)$ CuKα
	1.5515		0.00737	77.7°	1.79°
	1.5519		0.00745	78.5	1.79
	1.5524		0.00745	78.8	1.80
	1.5525		0.00754	79.0	1.80
	1.5526	N_y	0.00760	79.4	——
	1.5526	1.5558	0.00762	79.8	
	1.5527		0.00764	80.0	
9(24)	1.5529	N_z	———	80.6	
	1.5529	1.5602		——	
(An 47.7)	1.5531				
	1.5531				
	1.5534				
	1.5539				

TABLE B. *(Continued)*

Sample	Nx	Ny and Nz means	Nz−Nx	$2V_z$	$2\theta(131)$ $-2\theta(1\bar{3}1)$ CuKα
9(24)	Mean 1.5527		Mean 0.00752	Mean 79.2°	Mean 1.79°
(An 47.7)	Range 0.0024		Range 0.00027	Range 2.9°	Range 0.01°
	1.5562		0.00740	77.5°	1.82°
	1.5562	Ny	0.00742	77.6	1.82
	1.5562	1.5593	0.00748	77.7	1.82
	1.5563		0.00758	77.7	1.83
	1.5563	Nz	0.00758	78.4	
	1.5563	1.5638	0.00762	78.5	
12(97)	1.5568		0.00778	78.9	
				79.1	
(An 54.5)					
	Mean 1.5563		Mean 0.00755	Mean 78.2°	Mean 1.82°
	Range 0.0006		Range 0.00038	Range 1.6°	Range 0.01°
	1.5563		0.00756	77.2°	1.80°
	1.5564	Ny	0.00760	77.3	1.80
	1.5564	1.5595	0.00761	77.7	1.81
13(92)	1.5566		0.00777	78.0	1.82
	1.5566	Nz	0.00786	78.1	
		1.5642		78.5	
(An 54.9)				78.6	
	Mean 1.5565		Mean 0.00768	Mean 77.9°	Mean 1.81°
	Range 0.0003		Range 0.00030	Range 1.4°	Range 0.02°
	1.5714		0.01213	102.8°	2.22°
	1.5718		0.01213	103.6	2.23
	1.5719		0.01217	103.9	2.23
	1.5720	Ny	0.01224	104.6	
HGIF-AN-53	1.5720	1.5794			
	1.5720				
	1.5722	Nz			
(An 88.7)	1.5722	1.5841			
	Mean 1.5719		Mean 0.01217	Mean 103.7°	Mean 2.23°
	Range 0.0008		Range 0.00011	Range 1.8°	Range 0.01°

Manuscript received April 16, 1958.

THE AMERICAN MINERALOGIST, VOL. 43, NOVEMBER–DECEMBER, 1958

SYNTHETIC CUSPIDINE

A. VAN VALKENBURG AND G. F. RYNDERS, *National Bureau of Standards, Washington, D. C.*

ABSTRACT

Cuspidine ($3CaO \cdot 2SiO_2 \cdot CaF_2$) can be synthesized hydrothermally, from crystallizing melts, and by solid state reactions. Efforts to substitute hydroxyl for fluoride ions in the cuspidine structure were not successful, and this suggested that custerite, $3CaO \cdot 2SiO_2 \cdot Ca(F,OH)_2$ may not exist as a mineral. Synthetic cuspidine is monoclinic, optically positive with indices of refraction of $\alpha = 1.591$, $\beta = 1.596$, and $\gamma = 1.602$ ($\pm .003$). The extinction angle measured from the c axis is 7°. The specific gravity was determined as 3.05. Cuspidine melts congruently at approximately 1410° C. at atmospheric pressure. On prolonged heating cuspidine alters to γ-$2CaO \cdot SiO_2$ with the escape of silicon tetrafluoride. Powder x-ray data, a differential thermal curve and an infrared spectrogram are given.

INTRODUCTION

Cuspidine ($3CaO \cdot 2SiO_2 \cdot CaF_2$) was obtained as a hydrothermal reaction product in experiments designed to substitute fluoride for hydroxyl ions in a calcium hydro-garnet. The optical properties of this synthetic cuspidine corresponded to the natural mineral described by Scacchi in 1876. The material was found in ejected blocks of metamorphosed limestone at Vesuvius [1]. The natural crystals had a characteristic spear-shape and were referred to by Scacchi as cuspis, the Latin word for spear, hence the name cuspidine. Figure 1 shows natural cuspidine crystals from Vesuvius having the characteristic spear outline. Cuspidine has been synthesized by V. V. Lapin [2] in 1944, who identified the material from reaction products formed in electric welding slags; by C. E. Tilley [3] in 1947, who sintered $CaCO_3$, SiO_2 and excess CaF_2 at 1140° C.; and by McCaughey, Kautz and Wells [4] in 1948, from melts consisting of CaO, CaF_2 and SiO_2.

In 1913 Umpleby, Schaller and Larsen [5] described a mineral with essentially the same composition as cuspidine except that it contained some hydroxyl groups, and they named the mineral custerite. The optical indices reported for custerite were significantly lower than those found for cuspidine, and this seemed strange, for it is well-known with silicates that the indices of refraction increase when a hydroxyl replaces a fluoride ion. Tilley [3], in his excellent work on cuspidine, seriously doubted the existence of a hydroxyl-bearing cuspidine (custerite) as described by Umpleby et al., and he showed quite conclusively from x-ray, optical and chemical data that cuspidine and custerite were one and the same mineral. Through the courtesy of Dr. George Switzer of the U. S. National Museum, the authors obtained a specimen of custerite from Custer County, Idaho, and found that it had essentially the same x-ray

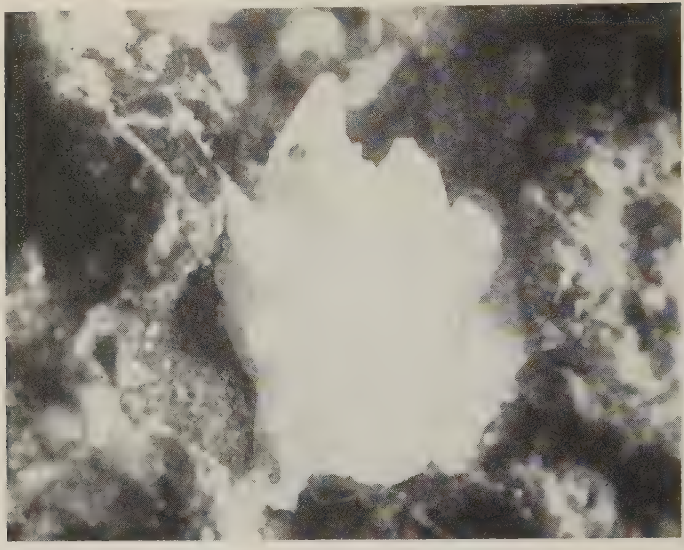

FIG. 1. Natural cuspidine from Vesuvius. Magnification 50×.

and optical properties as cuspidine. Since no one had attempetd experimentally to replace fluorine by hydroxyl in the cuspidine structure, it was decided to study the hydrothermal reactions of mixes corresponding to cuspidine, with and without fluorine. The investigation was carried on at the National Bureau of Standards as part of a larger program of fluorine substitution in hydroxyl silicates under the sponsorship of the Office of Naval Research.

EXPERIMENTAL WORK

Crystallizations from Melt

Cuspidine can be readily synthesized from a melt having the composition in weight per cent of $CaO = 45.9$, $SiO_2 = 32.8$ and $CaF_2 = 21.3$. This composition corresponds to the formula proportions and it melts congruently under a vapor pressure of fluorine. Platinum crucibles were used in all experiments to avoid contamination of the charge as fluoride melts are quite corrosive with refractory materials. For practical considerations cuspidine can be crystallized from a melt in air, as the vapor pressure of the fluorine melt is quite low at elevated temperatures. Usually a platinum cover is placed over the crucible to lessen the escape of volatile constituents. Synthetic cuspidine melts at 1410° C. ± 10° as determined by the well-known quench technique. A variation of this technique was employed to obtain reproducible results. The quench technique requires the use of small samples of 0.1 gram or less to ensure quick freezing when the sample is dropped from the furnace into the quenching medium. This technique does not work well when a volatile constituent is present, as slight losses greatly change the bulk composition of small samples. Consequently, large errors are introduced in determining the melting temperature. With the use of large samples of a gram, or more, one can minimize this difficulty and slight losses do not appear to alter the bulk composition. The quenching of a large sample, however, will not produce uniform conditions of freezing within the charge. For example, a melt when quenched will form a glass at the interface of the container and the glass will grade to crystalline material towards the center, where cooling is slower. Quenching at successively lower temperatures will decrease the proportion of glass to crystalline material, and by carefully analyzing the frozen surface adjacent to the container wall by means of a petrographic microscope, one can establish the temperature of crystallization within one or two degrees centigrade.

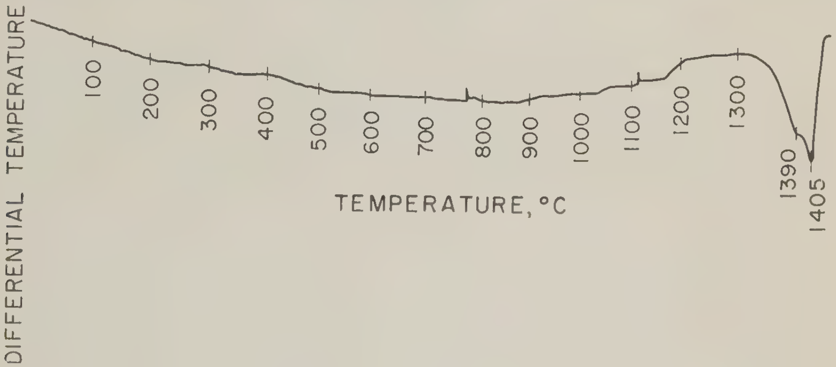

FIG. 2. Differential thermal curve of synthetic cuspidine.

A differential thermal analysis of synthetic cuspidine crystallized from a melt was made to determine the possible existence of high temperature polymorphic forms. Figure 2 is the differential thermal curve which was made at a heating rate of 12° per minute in a conventional apparatus. The temperatures indicated in this figure and elsewhere are all given in degrees centigrade. There is no indication of a phase change occurring before the endothermic break at 1405°, which agrees satisfactorily with the melting temperature obtained by quenching.

Figure 3 is an infrared transmission spectrogram of synthetic cuspidine crystallized from a melt. The spectrogram was made by pressing powdered cuspidine with powdered potassium bromide into a clear

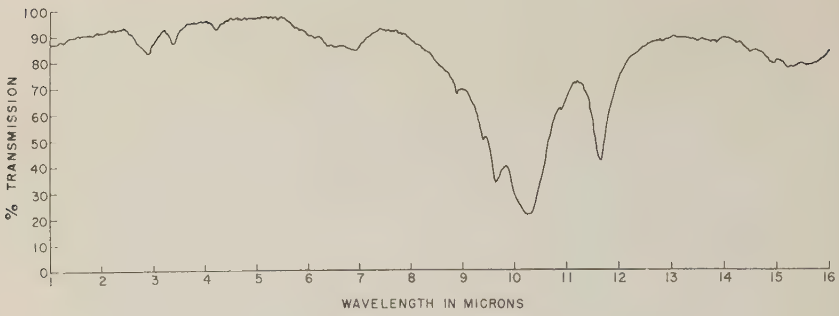

FIG. 3. Infrared spectrogram of synthetic cuspidine.

transparent pellet. The scanning instrument was a double beam spectrometer. The major absorption peak occurs at a wavelength of 10.3 microns and it is attributed to the stretching moments of the Si-O bonds. The second absorption peak occurring at 11.7 microns has not been identified.

Hydrothermal Synthesis

A series of hydrothermal experiments were made to synthesize cuspidine in the presence of water vapor to determine the possibility of substituting hydroxyl for fluoride ions. The apparatus used in these experiments was of the "cold seal type" developed by personnel of the Geophysical Laboratory. The reaction products were identified by *x*-ray and microscopic techniques. The raw batch materials consisted of calcium carbonate, silicic acid and calcium fluoride of reagent grade compounded in formula proportions. Compositions corresponding to cuspidine were prepared by mixing and grinding together the above constituents in stoichiometric proportions. Cuspidine has the molar ratio of Ca:Si:F=8:4:4. The ratios were 8:4:4, 8:4:3, 8:4:2, 8:4:1, and 8:4:0, with the last being equivalent to a hypothetical hydrous end member of the series. These mixtures were treated in the presence of five to ten per cent of water in sealed platinum capsules at temperatures from 500° to 700° C. at 20,000 psi. The experiments lasted from 3 to 7 days. The results are summarized in Table 1. The major phase in compositions 8:4:4, 8:4:3, and 8:4:2 was cuspidine with secondary phases of β-$CaO \cdot SiO_2$ and $6CaO \cdot 3SiO_2 \cdot 2H_2O$. Small amounts of calcite were observed in the composition 8:4:2 at 500° and 600°C. and probably represent uncombined material. The major phase in composition 8:4:1 was $6CaO \cdot 3SiO_2 \cdot 2H_2O$ with cuspidine next in abundance. Small amounts of CaF_2 were also observed in this composition. In composition 8:4:0 the compound $6CaO \cdot 3SiO_2 \cdot 2H_2O$ constituted the major phase with minor amounts of γ-$2CaO \cdot SiO_2$ present. It was observed that when the fluorine content of the batches was reduced, as in compositions 8:4:3, 8:4:2 and 8:4:1, there was a reduction in the amount of cuspidine and β-$CaO \cdot SiO_2$ and a corresponding increase in the amounts of $6CaO \cdot 3SiO_2 \cdot 2H_2O$. A synthetic cuspidine prepared from a melt, when treated at 800° C. and 20,000 psi in the presence of water vapor for four days, produced a large percentage of $CaO \cdot SiO_2$ and CaF_2. This indicates that the upper hydrothermal stability range is near 800° C. at 20,000 psi. In all the experiments where cuspidine formed in the presence of water vapor, the *x*-ray powder patterns and the indices of refraction for this compound remained constant and were identical to cuspidine crystallized from melts. These results appear to confirm Tilley's observations that hydroxyl groups are not a constituent part of the cuspidine structure; and the authors wish to join with him in discrediting the mineral name custerite, and they suggest the name be dropped from the literature.

Table 1. Hydrothermal Cuspidine Experiments at 20,000 psi for 3–7 Days

Composition	Temperatures		
Ca:Si:F	500°	600°	700°
8:4:4	*Cuspidine** β $CaO \cdot SiO_2$ $6CaO \cdot 3SiO_2 \cdot 2H_2O$	*Cuspidine* β $CaO \cdot SiO_2$	*Cuspidine* β $CaO \cdot SiO_2$
8:4:3	*Cuspidine* β $CaO \cdot SiO_2$ $6CaO \cdot 3SiO_2 \cdot 2H_2O$	*Cuspidine* β $CaO \cdot SiO_2$	*Cuspidine* β $CaO \cdot SiO_2$
8:4:2	*Cuspidine* β $CaO \cdot SiO_2$ $CaCO_3$	*Cuspidine* β $CaO \cdot SiO_2$ $CaCO_3$	*Cuspidine* β $CaO \cdot SiO_2$ $6CaO \cdot 3SiO_2 \cdot 2H_2O$
8:4:1	*$6CaO \cdot 3SiO_2 \cdot 2H_2O$* Unidentified Phase CaF_2	*$6CaO \cdot 3SiO_2 \cdot 2H_2O$* Cuspidine β $CaO \cdot SiO_2$ CaF_2	*$6CaO \cdot 3SiO_2 \cdot 2H_2O$* Cuspidine CaF_2
8:4:0	*$6CaO \cdot 3SiO_2 \cdot 2H_2O$* γ-$2CaO \cdot SiO_2$	*$6CaO \cdot 3SiO_2 \cdot 2H_2O$* γ-$2CaO \cdot SiO_2$	*$6CaO \cdot 3SiO_2 \cdot 2H_2O$* γ-$2CaO \cdot SiO_2$

* Underlined item indicates major phase.

Solid State Synthesis

Three compositions, 8:4:4, 8:4:3, and 8:4:2, were heated in a crimped platinum envelope in the absence of water at 1000° C. and atmospheric pressure for 22 days. Solid state reactions occurred. The 8:4:4 composition resulted in the formation of cuspidine with minor amounts of β-CaO$\cdot$SiO$_2$ and γ-2CaO$\cdot$SiO$_2$. Decreasing the amount of fluorine in these experiments resulted in increased formation of γ-2CaO$\cdot$SiO$_2$. Cuspidine was also synthesized by solid state reactions using a hot press technique. The raw ingredients were first compressed into a wafer of about 1″ in diameter by $\frac{1}{4}$″ thick. The wafer was then placed between two opposing carbon pistons enclosed in a carbon cylinder. Heat was obtained by the internal electrical resistance of the carbon cylinder. Cuspidine formed readily at 900° C. and 2,000 psi when left for $\frac{1}{2}$ hour. At 1150° C. and 2,000 psi, the cuspidine batch extruded along the cylinder walls acting as if it were a fluid phase. When synthetic cuspidine is heated in air at 1200° C. for 12 hours or longer, it is converted into fine polycrystalline aggregates of γ-2CaO$\cdot$SiO$_2$.

PROPERTIES OF SYNTHETIC CUSPIDINE

The optical properties of the synthetic cuspidine were measured by oil immersion techniques on crystals grown hydrothermally, from melts, and by solid state reactions. The mineral has monoclinic symmetry and is biaxially positive in character. The extinction angle, measured from the *c* axis, is about 7°. The indices of refraction are $\alpha = 1.591$, $\beta = 1.595$ and $\gamma = 1.602 \pm 0.003$. The optic angle $2V = 76°$ (estimated).

Density measurements were made on a Berman Torsion Balance using toluene as the immersing medium, and an average value of 3.05 g/cm$^3 \pm 1\%$ was obtained. This was thought to be high as the values reported in the literature were 2.9 or less. To check the accuracy of the density measurement against other known constants of cuspidine, the principle of Gladstone and Dale was employed. This principle is stated in the formula $K = n - 1/d$, where n = mean index of refraction, d = density and K = the specific refraction of any substance. K was calculated for cuspidine from Larsen and Berman's table of specific refraction of the chief constituents of minerals [6]. Cuspidine's mean index of refraction was calculated using $d = 3.05$ and it was found to be 1.596, which is the same as the observed value of 1.596. If the value 2.9 is used for d, the mean index is found to be 1.586. The principle of Gladstone and Dale is an excellent tool for checking the accuracy of optical data and densities when the formula of a compound is known. The recent article by Jaffe [7] is an excellent example of the usefulness of this principle.

Table 2 contains the *x*-ray powder pattern data obtained from synthetic cuspidine made from a crystallizing melt. For comparison a natural cuspidine from Monte Somma, Italy, has been included. The patterns were made on an *x*-ray diffractometer using copper K$_\alpha$ radiation.

TABLE 2. CUSPIDINE

NBS Synthetic		Specimen from Monte Somma, Italy	
d	I	*d*	I
A		A	
—	—	10.11	13
7.36	4	7.36	9
7.11	3	7.12	3
5.27	3	5.28	3
5.13[d]	4	5.14[d]	4
4.62[d]	3	4.62[d]	1
4.55[d]	3	4.55[d]	4
4.23	3	4.23	3
3.68	7	3.68	9
3.42	4	3.43	4
3.361	21	3.363	14
3.257	7	3.259	32
3.064	100	3.062	100
—	—	3.034	26
2.944	16	2.943	37
2.930	14	—	—
2.898	17	2.900	28
2.871	40	2.873	29
2.819[d]	4	—	—
2.568	4	2.569	6
2.550	7	2.550	7
2.520	1	2.521	4
2.493	8	2.493	8
2.477	<1	2.479	4
2.452	4	2.451	3
2.435	<1	2.435	<1
2.420	<1	2.421	2
2.307	8	2.307	6
2.292	14	2.289	10
2.159	3	2.158	3
2.089	3	2.089	4
2.063	8	2.063	9
2.047	7	2.047	7
2.016	16	2.018	17
1.995	4	1.994	4
1.985	4	1.984	4
1.959	1	1.959	8
1.884	27	1.883	9
1.832	7	1.832	14
1.821	10	1.821	11
1.809	6	1.809	8
1.787	3	1.787	3
1.770	1	1.770	2
1.733	7	1.733	11
1.691	3	1.691	4
1.658	1	1.658	3

[d] Indicates diffused.

TABLE 3. VALUES OF DIELECTRIC CONSTANT (K) AND THE QUALITY FACTOR (Q) WITH TEMPERATURE AT 1 MEGACYCLE

° C.	K	Q
25	5.8	160
50	5.8	400
75	5.8	310
100	5.9	270
125	5.9	210
150	5.9	170
200	6.0	110
300	6.3	53
400	6.7	19
500	7.3	10

Preliminary work on the electrical properties of synthetic cuspidine formed by solid state reactions indicate that the dielectric constant K increases with a rise in temperature, while the quality factor Q decreases. It was also found that with increasing frequency Q and K decrease in value. Table 3 gives the variation of K and Q at one megacycle with temperatures up to 500° C. The test specimen was not previously dried and the low Q value of 160 at 25° C. is probably the result of moisture contaminating the specimen surfaces.

ACKNOWLEDGEMENTS

The authors wish to acknowledge the help and assistance rendered by Mr. Robert Pike, Mr. George Ugrinic, Dr. Elmer Bunting and Dr. Ellis Lippincott.

REFERENCES

[1] ARZRUNI, A. (1877), *Zeits. Krust. Min.*, **1,** 398.

[2] LAPIN, V. V. (1941), *Compt. Rend. Acad. Sci. URSS*, **31,** 694–696 [*Min. Abstracts*, **9,** 1944].

[3] TILLEY, C. E. (1947), *Min. Mag.*, **28,** No. 197, 90–95.

[4] MCCAUGHEY, KAUTZ AND WELLS (1948), *Am. Mineral.*, **33,** 200–201.

[5] UMPLEBY, J. B., SCHALLER, W. T., LARSEN, E. S. (1913), *Am. Jour. Sci.*, **186,** 358.

[6] LARSEN, E. S. AND BERMAN, H. (1934), *Geol. Surv., Bull.* **848,** 31.

[7] JAFFE, H. W. (1956), *Am. Mineral.*, **41,** 757.

Manuscript received April 18, 1958.

THE AMERICAN MINERALOGIST, VOL. 43, NOVEMBER-DECEMBER, 1958

NOTES AND NEWS

ESKOLAITE, Cr_2O_3, IN "MERUMITE" FROM BRITISH GUIANA*

Charles Milton and Edward C. T. Chao, *U. S. Geological Survey, Washington 25, D. C.*

The account by Kuovo and Vuorelainen on page 1098 of this issue of the discovery in Finland of eskolaite, chromic oxide, makes it of interest to report that the same mineral is a major constituent of black pebbles found in the bed of the Merume River, British Guiana. The pebbles, normally under a centimeter in size, but occasionally ten times as large, were described by Bracewell (1946) as a new mineral, merumite. Actually, merumite is not a simple mineral, or even an essentially single though impure species, but rather an aggregate of eskolaite and possibly two new chromium oxide minerals with quartz, pyrophyllite, and perhaps other substances. We are now studying merumite, and at a later date will present our findings.

Eskolaite from British Guiana has not been analyzed—only various specimens of merumite. One analysis of merumite is given by Bracewell, and others have since been made by commercial firms. Cr_2O_3 generally exceeds 75%, alumina and water 7% or 8% each, and silica, iron, titania from about 1% to 5%. Vanadium is less than 0.2%. The *x*-ray diffraction patterns of the British Guiana eskolaite (which has a characteristic green streak by which it may be recognized) and that of commercial reagent anhydrous chromic oxide, Cr_2O_3, are identical.

At present little is known of the provenance of the British Guiana merumite. All the specimens studied were free from any matrix rock, and the material has been found only in the stream gravels. None of the minerals listed by Kuovo and Vuorelainen as associated with the eskolaite in Finland has been found in our samples of merumite.

We are indebted to Dr. R. B. McConnell, Director of the Geological Survey of British Guiana, and to Murray R. Director, President of the Director International Corporation, New York City, who have generously given us noteworthy specimens of merumite for study.

Reference

Bracewell, Smith (1946), The geology and mineral resources of British Guiana. Handbook of natural resources of British Guiana, Georgetown, 1946. Sec. 4, p. 18–40; Mineralogical Abstracts **10**,, p. 292 (1948).

---

* Publication authorized by the Director, U. S. Geological Survey.

THE AMERICAN MINERALOGIST, VOL. 43, NOVEMBER-DECEMBER, 1958

SOME NEW OCCURRENCES OF SASSOLITE IN THE UNITED STATES*

ROBERT L. SMITH, *U. S. Geological Survey, Washington 25, D. C.*

Recent finds of sassolite ($B_2O_3 \cdot 3H_2O$) in southern California, Allen and Kramer (1957) and Smith, Almond, and Sawyer (1958) have prompted the author to place on record three heretofore unpublished localities. These sassolite finds, although not as well documented as could be desired, seem worth recording in the literature because of the present widespread interest in boron minerals and relative rarity of sassolite.

STEAMBOAT SPRINGS, WASHOE COUNTY, NEVADA

In 1941, the author made a study of the minerals of the Steamboat Springs hot spring area. Sassolite was found in crystalline incrustations on the roof and walls of a partly enclosed large hole in a siliceous sinter terrace. The hole was 8 or 9 feet deep and perhaps 10 to 12 feet in inside diameter. The walls were curved over to form a domelike roof. A hole in the roof gave access to the interior. The hole had formerly been filled with hot water and was perhaps an extinct geyser pool. Lowering of the water table had drained the pool so that in 1941, it was relatively dry, but steam issued from small vents in the floor. The sassolite seemed to be forming at the time by evaporation of droplets of water condensed from the steam. The mineral occurred in very thin, transparent, curved, cellophanelike flakes of small size. Perhaps some were as large as 2 millimeters in diameter. The mineral was determined to be sassolite on the basis of optical properties, presence of boron (flame test), and its solubility in water and alcohol. The indices of refraction were not precisely determined but were judged to be consistent with the values for sassolite given by Larsen and Berman (1934). As determined, the optical properties were:

$\alpha >$ water (1.33) $<$ ethyl alcohol (1.36), β and $\gamma > 1.45 < 1.46$, Biaxial ($-$), very small 2v.

This material was compared optically and by chemical tests with type sassolite from Sasso, Italy, and the two seemed to be identical minerals. The specimens were left with the Geology Department of the University of Nevada.

THE GEYSERS, SONOMA COUNTY, CALIFORNIA

In 1942, the author was asked to identify some minerals from the collection of the late J. B. Nichols of Sacramento, California. Among these minerals was a group from the well known geyser area, Sonoma County, California. These specimens were collected by J. B. Nichols and the late M. Vonsen from Petaluma, California. One specimen consisted of a matte of tiny transparent flakes that had the same optical properties as the Steamboat Springs sassolite. The presence of boron was confirmed by flame test. The same group of specimens contained boussingaltite and mascagnite and other minerals well known from the Sonoma County locality. The specimen of sassolite was retained as part of Mr. Nichols' collection. The disposition of the collection after Mr. Nichols' death a few years ago, is not known to the author.

---

* Publication authorized by the Director, U. S. Geological Survey.

Norris Geyser Basin, Yellowstone National Park

In 1954, the author examined a number of mineral specimens submitted by the National Park Service to the Geological Survey for identification. These specimens were collected in the Norris Geyser Basin and consisted predominantly of water soluble sulphates and other solfataric and hot spring deposits. One sample consisted of small nodular growths of halite intimately intergrown with at least three unidentified minerals. Sassolite occurred in tiny, curved, transparent flakes coating the other minerals. The optical properties, presence of boron, and its solubility in water and alcohol serve to identify the mineral as sassolite. This material has been retained by the author pending identification of the unidentified minerals.

These three localities, and the presence of boron-bearing waters in each, are of interest in that they are all areas of geyser activity.

References

Allen, R. D. and Kramer, Henry (1957), Ginorite and sassolite from Death Valley, California: *Am. Mineral.*, **42,** 56–61.

Larsen, E. S., Jr. and Berman, Harry (1934), Microscopic determination of the non-opaque minerals, 2d ed.: *U. S. Geol. Survey Bull.*, **848,** 149.

Smith, George I., Almond, Hy and Sawyer, Dwight L. (1958), Sassolite from the Kramer Borate District, California: *Am. Mineral.*, **43,** 1068.

THE AMERICAN MINERALOGIST, VOL. 43, NOVEMBER–DECEMBER, 1958

NATROJAROSITE FROM NEAR THE MONTANA-WYOMING LINE

Richard S. Mitchell and William F. Giannini,
University of Virginia, Charlottesville, Virginia

The purpose of this paper is to report an occurrence of natrojarosite, $NaFe_3(SO_4)_2(OH)_6$, near the Montana-Wyoming line. The senior writer first noticed this material in August of 1954, but was not able to study it adequately until more material was collected in September of 1957. Other American localities of this relatively uncommon mineral are Lawrence County, South Dakota (Headden, 1893), Soda Springs Valley, Nevada (Hillebrand and Penfield, 1902), Kingman, Arizona (Shannon and Gonyer, 1927), and Luna County, New Mexico (Ford, 1932).

The natrojarosite occurs in sediments of the Gypsum Spring anticline in an exposure in Sec. 21, T. 9 S., R. 27 E., Carbon County, Montana, about 3 miles north of the Montana-Wyoming line (Fig. 1). Natrojarosite is associated with fragments of carbonized wood and gypsum in a fine-grained gray sandstone which is about 2½ feet thick and is in sequence with other sandstones. The beds here dip eastward and have been transected by an intermittent creek. The specimens were collected several yards downstream from where the road crosses the creek. Sediments containing the natrojarosite apparently belong to the Morrison formation of the Upper Jurassic. This material is overlain by other sandstones and greenish-gray shales containing dinosaur (?) bones. The stratum is underlain by sandstones, including a greenish-gray cross-bedded glauconitic type characteristic of the Upper Sundance formation of the Jurassic. Numerous belemnite remains are found immediately below this glauconitic sandstone. The general stratigraphy and structure of this area have been outlined by Blackstone (1940).

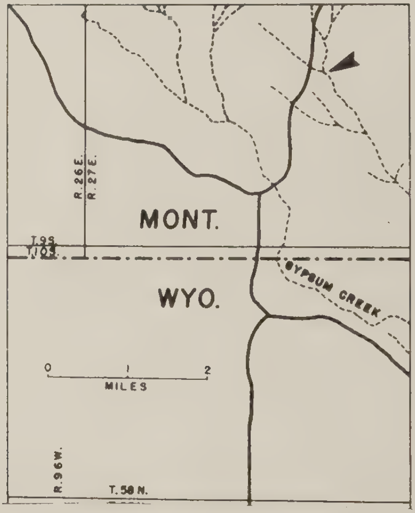

FIG. 1. Map showing natrojarosite locality. Chevron points to area where mineral is exposed. The town of Cowley (on U.S. 310) lies about 8 miles south of the Montana-Wyoming line on the road shown.

The natrojarosite occurs as a very fine-grained bright-yellow powder.

For a tentative identification some simple chemical tests were performed. The powder readily dissolved in warm hydrochloric acid to give a yellow solution. The addition of barium chloride to this solution formed a white cloudy precipitate indicating the presence of sulfate. When fused with charcoal and sodium carbonate and placed on a clean silver coin a dark stain resulted, thus indicating the presence of sulfur. An excellent test for ferric iron was obtained upon the addition of potassium ferrocyanide to a solution in hydrochloric acid. A flame test showed the intense persistent yellow coloration for sodium. In boiling water the mineral was apparently insoluble.

A semiquantitative spectrographic analysis* confirmed the fact that sodium is the major alkali metal present. The ratio of sodium to potassium determined by this method is 3 to 1. This analysis also detected the presence of considerable silica (up to 25%). That silica is present as an intermixed impurity was shown by a study of insoluble residues and by *x*-ray diffraction patterns. Small amounts of the following elements were also detected by the spectrographic analysis: Al, Ca, Sr, Ba, Ti, Mg, Zr, Mn and Cu. Although these elements are probably due to impurity compounds, it should be noted that Al (1.75% Al_2O_3 was detected) could substitute isomorphously for some of the Fe, and Ca, Sr and Ba could substitute for Na (Kulp and Adler, 1950).

For a final check on the identification of this substance six samples, taken from different specimens and associations, were studied by the *x*-ray powder method. The measured *x*-ray data listed in Table 1, represent an average of values obtained for these six films made with FeK_α radiation in cameras with a diameter of 11.46 cm. Using data available in the literature the films were partially indexed using the Davey charts (Davey, 1922). From the powder data the unit cell values obtained are $a_0 = 7.34$ Å and $c_0 = 16.72$ Å, with $a_0 : c_0 = 1 : 2.278$. Using these values all possible *d* spacings down to 1.35 Å were calculated. The excellent correlation obtained between these calculated values and the observed values is presented in Table 1. Observed values correspond only with *d* values for reflections which are allowed by an $R3m$ space group and this is the reported space group for natrojarosite. The structure cell dimensions for the Montana natrojarosite are slightly larger than those reported by Hendricks (1937) for this mineral. Perhaps the slight isomorphous replacement of sodium by potassium would contribute to this difference.

Because of the intimate association of the natrojarosite powder with other minerals, occasional impurity lines were noticed on some of the *x*-ray films. The most consistent impurity lines were from the quartz

---

* This analysis was performed by the American Spectrographic Laboratories, Inc., San Francisco, California.

Table 1. *X*-ray Powder Data on Natrojarosite from Carbon County, Montana. $a_0=7.34$ Å; $c_0=16.72$ Å; $a_0:c_0=1:2.278$. FeKα Radiation

hk·l	$d_{(\text{calc.})}$ Å	$d_{(\text{obs.})}$ Å	$I_{(\text{obs.})}$
10·1	5.94	5.94	w
00·3	5.57	5.57	mw
01·2	5.06	5.06	vs
11·0	3.67	3.67	vw
10·4	3.49	3.49	vw
02·1	3.12	3.12	ms
11·3	3.07	3.06	s
20·2	2.97		
01·5	2.96	2.96	vw
00·6	2.79	2.78	vw
02·4	2.53	2.53	w
21·1	2.38		
12·2	2.31		
20·5	2.30		
10·7	2.24	2.24	m
11·6	2.22		
30·0	2.12	2.13	vw
21·4	2.08		
01·8, 30·3	1.98	1.98	m
12·5	1.95		
02·7	1.91	1.91	vvw
00·9	1.86		
22·0	1.84	1.83	mw
13·1, 20·8	1.75		
22·3	1.74	1.74	vvw
31·2	1.73	1.72	vvw
21·7, 30·6	1.69		
11·9	1.66		
13·4, 10·10	1.62		
12·8	1.58	1.57	vw
31·5	1.56		
22·6	1.53	1.54	vw
02·10, 01·11	1.48	1.48	vw
13·7	1.42		
30·9	1.40		
00·12, 14·0	1.39		
21·10, 20·11	1.37		
31·8, 41·3	1.35	1.34	vvw

10·0 (4.26 Å) and 10·1 (3.34 Å) reflections. The intensities of these, relative to natrojarosite, varied on five of the films and on a sixth one they were completely missing.

Because microscopic examination revealed no evidence of single crystals, it was virtually impossible to obtain optical data.

The matrix rock with which the natrojarosite is associated is a gray to buff fine-grained sandstone showing an apparently ripple-marked structure. An *x*-ray study of the sandstone revealed a composition of quartz and illite. Scattered throughout the rock are irregularly shaped fragments of black carbonaceous matter averaging about an inch or less across. Most of these black fragments resemble common charcoal, but a few were noted with a brilliant pitchy luster and good conchoidal fracture. Small splinters of each type of carbonaceous matter were *x*-rayed using the powder method. In addition to the broad diffuse bands typical of amorphous solids, lines for natrojarosite were observed. A light-brown earthy powder in small cavities and crusts is associated with the rock. An excellent correlation was obtained between *x*-ray powder data for this earthy powder and goethite. Also brown stains streak the gray sandstone. Selenite gypsum commonly occurs in the specimens as thin crusts. Two fossil bone fragments, the largest measuring three by four inches, were noted in the deposit. These are cellular, and vary in color from yellow-brown to dark red-gray. A typical apatite pattern was obtained from these by the diffraction method, but an exact categorization of the apatite mineral was not achieved.

Natrojarosite is associated with all the minerals in the deposit. Cavity fillings and discontinuous crusts rarely thicker than 1/16 inch were found in the sandstone. The yellow powder commonly surrounds the carbonaceous fragments and frequently veins them. In one specimen natrojarosite has almost completely replaced the carbonaceous material leaving only a woody structure and a few black streaks in a yellow irregular patch. *X*-ray study revealed natrojarosite even in apparently pure black splinters of the carbonaceous material. The relationship between goethite powder and natrojarosite suggests that goethite may result from the alteration of this sulfate. Crusts of the two minerals seem to grade into each other and most of the natrojarosite has some brown stains. Natrojarosite fills some cavities between crystals in the selenite crusts, but an intimate relationship between these sulfates, like one might expect, does not seem to exist. The bone fragments also contain thin coatings of natrojarosite on their outer surfaces. This association was verified by *x*-ray data. Of all these minerals it appears that natrojarosite is most intimately associated with the carbonaceous material of the rock.

After the completion of this study the writers received samples of a yellow mineral collected in Big Horn County, Wyoming, about 40 miles from the locality described above. This material is identical to that already described. *X*-ray films have identical *d* values and show the material is of exceptional purity. Crusts up to $\frac{1}{2}$ an inch wide are associated with a gray-brown sandstone. Much carbonized wood and gypsum are also present. The total thickness of these sediments, which belong to the

Morrison formation, is about 6 feet. The material described is from a uranium claim, owned by Mr. Irvin Asay, which is located 4 miles east of U. S. 310 on a turn-off about $13\frac{1}{4}$ miles southeast of Lovell, Wyoming.

The discovery of this second locality suggests that natrojarosite may be of widespread occurrence in the Morrison formation within and around the Big Horn Basin.

The writers wish to express their gratitude to Mr. C. F. Mitchell, of Lovell, Wyoming, for his assistance in checking certain field data included in this paper, and for collecting specimens from the Asay property.

References

Blackstone, D. L., Jr. (1940), Structure of the Pryor Mountains, Montana: *Jour. Geol.*, **48,** 590–618.

Davey, W. P. (1922), A New *X*-ray Diffraction Apparatus: *Gen. Elect. Rev.*, **25,** 565–580.

Ford, W. E. (1932), *Dana's Textbook of Mineralogy*, 4th ed., New York, p. 769.

Headden, W. P. (1893), Kehoeite, a New Phosphate from Galena, Lawrence Co., S. D.: *Am. Jour. Sci.*, **46**(3), 22–25.

Hendricks, S. B. (1937), The Crystal Structure of Alunite and the Jarosites: *Am. Mineral.*, **22,** 773–784.

Hillebrand, W. F. and Penfield, S. L. (1902), Some Additions to the Alunite-Jarosite Group of Minerals: *Am. Jour. Sci.*, **14**(4), 211–221.

Kulp, J. L. and Adler, H. H. (1950), Thermal Study of Jarosite: *Am. Jour. Sci.*, **248,** 475–487.

Shannon, E. V. and Gonyer, F. A. (1927), Natrojarosite from Kingman, Arizona: *Wash. Acad. Sci., Jour.*, **17,** 536–537.

THE AMERICAN MINERALOGIST, VOL. 43, NOVEMBER-DECEMBER, 1958

X-RAY DATA FOR DOLOMITE AND ANKERITE

R. A. Howie and F. M. Broadhurst, *Geology Department, The University, Manchester, England.*

Although the structure of dolomite was determined by Wyckoff and Merwin (1924) and by Wasatjerna (1924), the effect of the replacement of magnesium by iron on the cell parameters has remained in doubt. Wyckoff and Merwin examined various specimens of dolomite, two of them having over 10% FeO by weight, and using single crystal photographs they found that the cell sizes were identical within experimental error. Schoklitsch (1935), however, using the powder method, gave values for dolomite with 1.17% FeO of a_{rh} 6.007 Å,* α 47°32′ or a 4.843, c 15.95 Å on hexagonal axes and for ankerite with 16.43% FeO a_{rh} 6.062 Å, α 46°58′ or a 4.832, c 16.14 Å; these results indicating that the

---

* Original values given in kX units have been converted to Å.

c dimension increased with the substitution of the larger ferrous ion for magnesium but that the *a* dimension decreased.

Two analysed specimens available for study were the Haley dolomite (Harker and Tuttle, 1955) which shows an almost negligible iron content, and an ankerite from the British Coal Measures with a composition approaching $Ca_3(Mg_2Fe)(CO_3)_6$ (Broadhurst and Howie, 1958): the analyses of these minerals are given in Table 1, the specific gravity for the dolomite being quoted from Zen (1956). The more iron-rich of these two minerals has been called ankerite following the nomenclature of Smythe and Dunham (1947, p. 66) and of Hey (1955). Palache et al. (1951) recommended that the names dolomite and ankerite should depend on the ratio of Mg to Fe^{+2} in the Mg positions, but arbitrarily divided the series at Mg:Fe = 1:1, referring material with Mg > Fe to the species dolomite and material with Fe > Mg to the species ankerite. With their nomenclature, the material of analysis 2 would be termed ferroan dolomite. A

TABLE 1. ANALYSES AND PROPERTIES OF DOLOMITE AND ANKERITE

	1	2		1A	2A
SiO_2	0.12	0.15	Fe^{+3}		.002
TiO_2	nil	tr.	Fe^{+2}	.006	.330
Al_2O_3	nil	0.28	Mn		.022
Fe_2O_3	tr.	0.10	Mg	.973	.626
FeO	0.22	12.06	Ca	1.036	1.024
MnO	nil	0.77	Na		.002
MgO	21.12	12.85	CO_2	1.993	1.995
CaO	31.27	29.23			
Na_2O	n.d.	0.06		Atomic percentages	
K_2O	n.d.	0.01			
CO_2	47.22	44.70	Mg	48.3	31.2
H_2O^-	0.02	0.02	Fe	0.3	16.6
			Mn		1.1
Total	99.97	100.23	Ca	51.4	51.1
D	2.86	2.97			
ϵ	1.503	1.515			
ω	1.680	1.710			

1. White dolomite, Ross Township, Haley, Ontario (Harker and Tuttle, 1955). Analyst: R. A. Howie.

2. Yellow ankerite, Bed OC 8, Oak Victoria Colliery, Oldham, Lancashire (Broadhurst and Howie, 1958).

1A and 2A. Analyses recalculated to show the number of metal ions on the basis of 6 oxygen ions.

disadvantage of this nomenclature is that the term ferroan dolomite is used for material relatively poor in iron whilst the term ferrodolomite has previously been used for the iron end-member $FeMg(CO_3)_2$, confusion in terminology may therefore easily arise. A plot of carbonate analyses in the series $CaMg(CO_3)_2$-$CaFe(CO_3)_2$, e.g. Hügi (1945), Smythe and Dunham (1947), shows a grouping around the centre of the series in line with the accustomed use of the term ankerite. Dolomites with only moderate amounts of ferrous iron are less common, while carbonates with greater than 70% of the $CaFe(CO_3)_2$ molecule are rare: thus to split the series arbitrarily at 50% $CaFe(CO_3)_2$ obscures the prevalence of material of this intermediate composition. Accordingly for the material of composition $Ca_3(Mg_2Fe)(CO_3)_6$ here discussed the name ankerite is preferred.

TABLE 2. *X*-RAY SPACINGS, INDICES AND INTENSITIES

hkil	*hkl*	Dolomite		Ankerite	
		d(Å)	I	*d*(Å)	I
$10\bar{1}1$	100	4.025	15		
$01\bar{1}2$	110	3.690	25	3.704	15
$10\bar{1}4$	211	2.886	500	2.899	500
0006	222	2.670	50	2.685	15
$01\bar{1}5$	221	2.540	40	2.552	10
$11\bar{2}0$	$10\bar{1}$	2.405	50	2.411	15
$11\bar{2}3$	210	2.192	150	2.199	30
$02\bar{2}1$	$11\bar{1}$	2.066	25	2.067	5
$20\bar{2}2$	200	2.015	75	2.020	15
$02\bar{2}4$	220	1.848	25	1.852	5
$01\bar{1}8$	332	1.804	100	1.812	30
$11\bar{2}6$	321	1.786	150	1.792	30
0009	333	1.781			
$21\bar{3}1$	$20\bar{1}$	1.567	40	1.569	5
$12\bar{3}2$	$21\bar{1}$	1.545	50	1.548	10
$10\bar{1},10$	433	1.496	10	1.501	2
$21\bar{3}4$	310	1.465	25	1.468	10
$02\bar{2}8$	224	1.445	20	1.449	15
$11\bar{2}9$	432	1.431	50	1.436	5
$12\bar{3}5$	320	1.413	20	1.416	2
$03\bar{3}0$	$11\bar{2}$	1.389	75	1.391	5
000,12	444	1.335	40	1.341	5
$21\bar{3}7$	421	1.297	20	1.300	2
$02\bar{2},10$	442	1.269	20	1.273	2
$12\bar{3}8$	431	1.238	25	1.241	5
$22\bar{4}0$	$20\bar{2}$	1.202	15	1.205	2
$11\bar{2},12$	543	1.168	20	1.171	3
$31\bar{4}2$	$30\bar{1}$	1.144	10	1.144	2
$21\bar{3},10$	532	1.123	25	1.126	3
$13\bar{4}4$	$32\bar{1}$	—*		1.112	3
$22\bar{4}6$	420	1.096	15	1.099	3
$30\bar{3}9$	522				
000,15	555	1.068	5	1.066	1
$40\bar{4}4$	400	1.008	20	1.010	2
$31\bar{4}8$	521	1.001	25	1.003	3
$10\bar{1},16$	655	$.973_5$	15	.976	1
$30\bar{3},12$	633	.962	25	.966	3
$32\bar{5}2$	$2\bar{1}\bar{3}$	.949	5	.953	1
$32\bar{5}4$	$41\bar{1}$	.930	5		
$\bar{2}\bar{1}3,14$	356	.926	15		
$\bar{4}048$	044	.923	15		
$32\bar{5}\bar{5}$	$1\bar{2}\bar{4}$	.913	5		
$41\bar{5}0$	$3\bar{1}\bar{2}$	.909	10		
$\bar{2}02,16$	466	.903	5		
$31\bar{4},11$	632				
$22\bar{4},12$	642	.894	10		
$21\bar{3},16$	754	.845	15		
$11\bar{2},18$	765	.835	20		
$32\bar{5},10$	631	.821	10		

* For dolomite this line was obscured by a line of the Si standard.

The *x*-ray powder data were obtained on the Philips high-angle *x*-ray diffractometer with CuK_α radiation, using a scanning speed of 0.25° 2θ per minute and chart speed of 2.67 cm. per 1° 2θ. Silicon was mixed with the powdered carbonate as an internal standard and linearly interpolated corrections were applied to the 2θ values measured from the carbonate peaks. The reproducibility of the *d*-spacings finally determined was ±0.001 Å. The diffraction pattern obtained was indexed on hexagonal axes using the approximate cell dimensions: after the cell dimensions had been accurately determined from the $11\bar{2}0$, $03\bar{3}0$, $22\bar{4}0$, and 0006, 000,12 and 000,15 reflections for *a* and *c* respectively the *d*-spacings of all possible reflections up to $2\theta = 140°$ were tabulated and compared with those observed, leading to the complete indexing of the pattern (Table 2). The relative intensities of the reflections are given in terms of peak heights, that of the strong $10\bar{1}4$ reflection being arbitrarily assigned an intensity of 500 in each case to avoid giving fractional values for the high angle reflections. The indices assigned differ in some details from those given to the dolomite-type powder patterns by Bradley et al. (1953).

The accurate cell parameters obtained from the powder data are:

	a(Å)	c(Å)	c/a	a_{rh}(Å)	α
Dolomite, Haley, Ontario	4.810±0.002	16.02±0.001	3.330	6.020	47°07′
Ankerite, Oldham, Lancashire	4.819	16.10	3.341	6.045	47°00′

Space group $R\bar{3}$.

The values for dolomite are thus comparable with the results of previous workers. The effect of the substitution of roughly one third of the magnesium ions by the larger ferrous iron ion in the ankerite examined is seen to be an increase in both the *a* and *c* dimensions, as might be expected from the structure, but contrary to the results earlier reported by Schoklitsch (1935); the axial ratio *c/a* also increases.

References

Bradley, W. F., Burst, J. F. and Graf, D. L. (1953), Crystal chemistry and differential thermal effects of dolomite: *Am. Mineral.*, **38,** 207–217.

Broadhurst, F. M. and Howie, R. A. (1958), On the occurrence of ankerite in a band of non-marine lamellibranchs from the Lancashire Coal Measures: *Geol. Mag.* **95,** 397–402.

Harker, R. I. and Tuttle, O. F. (1955), Studies in the system CaO-MgO-CO_2. Part I, The thermal dissociation of calcite, dolomite and magnesite: *Amer. Journ. Sci.*, **253,** 209 224.

Hey, M. H. (1955), An index of mineral species and varieties arranged chemically. 2nd edition, London (British Museum).

Hügi, Th. (1945), Gesteinsbildend wichtige Karbonate und deren Nachweis mittels Färbmethoden: *Schweiz. Min. Petr. Mitt.*, **25,** 114 140.

Palache, C., Berman, H. and Frondel, C. (1951), Dana's System of Mineralogy. 7th edition, p. 211.

Schoklitsch, K. (1935), Beitrag zur Physiographie steirischer Karbonspäte Gitterkonstanten, physikalische Angaben und Chemische Zusammensetzung: *Zeits. Krist.*, **90,** 433–445.

Smythe, J. A. and Dunham, K. C. (1947), Ankerites and chalybites from the northern Pennine orefield and the northeast coalfield: *Min. Mag.*, **28,** 53–74.

Wasastjerna, J. A. (1924), The crystal structure of dolomite: *Soc. Scient. Fennica Comm. Phys-Math.*, **2,** No. 14.

Wyckoff, W. G. and Merwin, H. E. (1924), The crystal structure of dolomite: *Amer. Journ. Sci.*, ser. 5, **8,** 447–461.

Zen, E-An (1956), Correlation of chemical composition and physical properties of dolomite: *Amer. Jour. Sci.*, **254,** 51–60.

International Mineralogical Association

This association was started with a motion by Professor Buerger at the Minneapolis meeting of the Mineralogical Society of America, November 1, 1956 (*Am. Mineral.*, **42,** 1957, 270). A pre-organization meeting was held at Montreal July 16, 1957, in connection with the sessions of the International Union of Crystallography (*Am. Mineral.*, **43,** 1958, 352). The inaugural meeting took place at Madrid in the week of April 6, 1958. Here officers were elected, a constitution was adopted, and commissions were set up. All this is described in detail in the Sept. 1958 GeoTimes, a copy of which may be obtained from the American Geological Institute or the writer. A similar description is given (in English) in a Beilage of the *Schweizerische Mineralogische und Petrographische Mitteilungen*, **38** (1), 1958. Professor Grigoriev of Leningrad has written (in Russian, with five half-tones) about the Madrid meetings and the accompanying field trips (*Akad. Nauk, U.S.S.R.*, Memoirs of the All-Union Mineralogical Society, **87** (4), 1958, 518–525.

The chief object of the I.M.A. is to further international cooperation in the mineralogical sciences. Its members are not individuals, but are the various national mineralogical societies or corresponding bodies. In addition to the work of the various commissions, an important function of the I.M.A. is to see that arrangements are made for programs, including field trips of interest to mineralogists at the International Meetings of the geologists, crystallographers and other scientific groups at which there will be a significant attendance of mineralogists and petrologists.

A meeting of the Executive Committee of the I.M.A. is scheduled for Zurich, January 19–21, 1959. This committee consists of the five officers and four councilors. In addition the members of the four commissions (abstracts, data, new minerals, and museums) will be in attendance. It is requested that anyone with suggestions for consideration at this meeting send them to President Parker at Zurich, Professor Amoros (Secretary) at Madrid, or the writer (Treasurer).

The next meeting of the association is to be held at Zurich, August 29–September 6, 1959. At this session, besides meetings of the Executive Committee and Delegates and the various Commissions, there will be two symposia and a field trip (Sept. 4–6).

D. Jerome Fisher
University of Chicago

The Geochemical Society is undertaking the project of issuing an English translation of the Russian journal *Geokhimiya*, which appears eight times yearly. It is being aided by a grant from the National Science Foundation. The translation of the first issue of 1958 has already appeared.

The success of this venture will depend in large part on the response, in the form of subscriptions, from individual scientists. The subscription price is $20 per year (8 issues); $10 to educational institutions and to members of the Geochemical Society. Send subscriptions to E. Wm. Heinrich, Managing Editor, Mineralogical Laboratory, University of Michigan, Ann Arbor, Mich.

BIBLIOGRAPHY AND INDEX OF LITERATURE ON URANIUM AND THORIUM AND RADIOACTIVE OCCURRENCES IN THE UNITED STATES. PARTS 1–5

The Geological Society of America has published as its Special Paper No. 67 "Bibliography and Index of Literature on Uranium and Thorium and Radioactive Occurrences in the United States. Part 5: Connecticut, Delaware, Illinois, Indiana, Maine, Maryland, Massachusetts, Michigan, New Hampshire, New Jersey, New York, Ohio, Pennsylvania, Rhode Island, Vermont, and Wisconsin," prepared by Margaret Cooper of the U. S. Geological Survey on behalf of the Division of Raw Materials of the U. S. Atomic Energy Commission, September 1958, 472 pages (paper cover), and priced at $6.75 a copy.

This book contains a section on bibliography (26 pages), a gazetteer for the States (38 pages), a geographical index (243 pages), and a subject index (165 pages). Factually it is a key to the literature on deposits in which uranium, thorium, and radioactive minerals are found in the northeastern United States. For many of the States there is also much detailed information in the indexes on the geology and the general mineralogy of the pegmatites, coal beds, sandstones, shales, beach sands, and other formations in which the uranium and thorium have been repoted.

Parts 1 to 4 of this bibliography were prepared by Margaret Cooper in the Division of Raw Materials of the U. S. Atomic Energy Commission and published in the Bulletin of the Society. These sections, which also include a bibliography, gazetteer, geographical index, and subject index, with detailed geological information for each area covered, are available as reprints for public sale, as follows:

Part 1:	Arizona, Nevada, and New Mexico. February 1953, 38 pp.	25 cents
Part 2:	California, Idaho, Montana, Oregon, Washington, and Wyoming. October 1953. 70 pp.	25 cents
Part 3:	Colorado and Utah. June 1954, 124 pp.	50 cents
Part 4:	Arkansas, Iowa, Kansas, Louisiana, Minnesota, Missouri, Nebraska North Dakota, Oklahoma, South Dakota, and Texas. March 1955, 70 pp.	50 cents

All five parts of the bibliography may be purchased from the Geological Society of America at the prices indicated above. Remittance must accompany orders, which should be sent to:

Geological Society of America
419 West 117 Street
New York 27, New York

MINERALOGICAL ABSTRACTS

The councils of the Mineralogical Society of America and the Mineralogical Society (Great Britain and Ireland) have agreed to jointly sponsor the publication of *Mineralogical Abstracts* as a separate publication, commencing with volume 14 for 1959.

The new journal will have a two-column format with a page size of $(10\frac{3}{8}'' \times 7\frac{7}{8}'')$ and will contain at the outset about twice the number of abstracts in the present issues. The journal will be published quarterly.

Mineralogical Abstracts will be grouped under the following headings:

Age-determination
Apparatus and techniques
Bibliographies
Clay minerals
Crystal structure of minerals

Experimental mineralogy
Geochemistry
Gemstones
History and biography
Meteorites and tektites
Mineral data
New minerals
Notices of books
Ore deposits and economic mineralogy
Petrology
Physical properties of minerals
Topographical mineralogy
Various topics

The price of the new journal to subscribers other than personal members of the two sponsoring societies will be \$9. U. S. per calendar year issue of 4 numbers. There will be a special price of \$6. for educational institutions.*

It is proposed to make the journal available to personal members of the Mineralogical Society of America at \$3. per calendar year. Those who are now members of the Mineralogical Society of Great Britain and Ireland, who already receive the abstracts as part of their privileges of membership, will continue to receive Mineralogical Abstracts for an increase in the annual membership fee of 10s.

* The price of the Mineralogical Magazine when separated from Mineralogical Abstracts will be reduced to £2 10s. 0d. per calendar year issue of 4 numbers.

ANNUAL MEETING

The fourth annual meeting of the Mineralogical Association of Canada will be held in Toronto, Ontario, Canada, March 1 4, 1959. It is to be held in conjunction with the annual meetings of the Prospectors and Developers Association and the Geological Association of Canada. For further information write to:

S. Kaiman, Secretary,
Mineralogical Association of Canada,
c/o Mines Branch,
552 Booth Street,
Ottawa, Canada.

BOOK REVIEWS

GETTING ACQUAINTED WITH MINERALS, 2d ed., by George Letchworth English and David E. Jensen. 363 pages. McGraw-Hill Book Company, Inc., New York, N. Y. $6.95.

"Getting Acquainted with Minerals," first published twenty-four years ago by George Letchworth English, and long out of print, has been superbly brought up to date in this second edition by David E. Jensen, of Ward's Scientific Establishment, Rochester, New York.

Part 1, about one-third of the book, is an excellent elementary introduction to mineralogy, with clearly written sections on crystallography, chemistry, and physics. Part II, descriptions of minerals, arranged alphabetically, includes all the common minerals, and takes up another third; it is followed by a section on Dana's Classification, and a listing of the elements as represented by their more important minerals. Part III includes a brief but adequate account of rocks, and a table for identification of minerals by luster, hardness, color, and other characteristics. Finally, an index of some 1,200 entries makes the immense amount of information in this book immediately accessible. Three hundred and fifty-five excellent illustrations—photographs of minerals, drawings of crystals, and scenes of mineralogical activity—embellish the text.

It is stated in the preface that within the last twenty years mineral collecting has become the third among so-called hobbies in this country, with some three million amateur mineralogists. It is indeed gratifying that there is available for their guidance and instruction a book that is both scientifically accurate and a pleasure to read.

Charles Milton
U. S. Geological Survey
Washington 25, D. C.

NENDO-KOBUTSO (CLAY MINERALS) by Toshio Sudo. No. 178 of the Iwanami Series, 4th edition, 273 pages plus 4 fold-in tables, and 1 fold-in plate, $4\frac{1}{2}\times 6\frac{3}{4}''$, cloth bound. Publisher: Iwanami-Shoten, Tokyo, Japan. 1958 (in Japanese). Price 340 yen; about $1.00.

This little volume is essentially another reprint of the first edition (1953) with an additional chapter of 31 pages summarizing briefly the important recent developments in clay mineralogy. The new references are appended to the bibliography.

The author plans a revision of the work that will provide a much more comprehensive summary of the current status of clay mineralogy and its problems. For an outline of subject matter of chapters 1 to 6 see the review of the first edition, *Am. Mineral.*, **39**, p. 685, 1954.

Earl Ingerson
University of Texas

CONSTITUTION OF BINARY ALLOYS, by Max Hansen. Prepared with the cooperation of Kurt Anderko. 1305 pages plus 40 diagrams. McGraw-Hill Book Company, New York, 1958. Price: $32.50.

A first edition of this appeared as "Aufbau der Zweistofflegierungen" in the late thirties. The book would have been more aptly titled "Handbook and Constitution of Binary Alloys" since it served as a reference work for 20 years for metallurgists, solid state physicists, crystallographers and others interested in the constitution of binary alloys. Even without translation the original work was deemed valuable enough to be off-set printed in the early forties and distributed in the United States.

The revised edition has added all the material of the last twenty years and critically evaluated all earlier diagrams as well in view of later findings. This has resulted in almost a doubling of the size of the book so that the present edition includes 1382 systems and 740 diagrams. Dr. Hansen spent several years at Armour Research Foundation following World War II and in the reviewer's opinion added clarity to the book in the translation. The sponsorship by the United States Air Force through the Wright Air Development Center made possible the publication of the book in its present form.

The thoroughness with which the German or English compile such a volume is well demonstrated in this book. About 9800 literature references are cited and the reviewer knows from personal experience that these references were not simply added to the bibliography but were critically examined before drawing the final diagram which appears in the book. As examples, the system Ag-Al has 35 references, the Fe-C has 135 and the last one in the book Zn-Zr has two references.

All diagrams have been re-drawn so that temperature is plotted versus atomic per cent rather than weight per cent as in the first edition. Also, "The presentation of data concerning the constitution of binary alloys system would be incomplete if crystallographic data were not considered systematically. As compared with the older work, not only the symmetry of the intermediate phases is given but their lattice spacings as well. Furthermore the literature dealing with the variation of lattice parameters of primary solid solutions has also been considered."

This book has far more exhaustive treatment of subject matter than its mineralogical counterpart—Phrase Diagrams for Ceramists (The American Ceramic Society, 1956). It is a monumental work and destined to be on every technical reference book shelf for the next 25 years.

Earl T. Hayes
Bureau of Mines
Washington, D. C.

MINÉRAUX D'URANIUM DU HAUT KATANGA. Introduction by J. F. Vaes; mineral descriptions by C. Guillemin; and photographs by A. Destas. 81 pp. Published by "Les Amis du Musée Royal du Congo Belge," 13, Chausée de Louvain, Tervuren, Belgium. 1958. Price 240 francs.

This paper bound book has 16 pages on the mode of formation and the associations of the secondary uranium minerals at Haut Katanga, followed by descriptions of these minerals, including optical and *x*-ray data. However, the most remarkable feature is the inclusion of 27 color plates (10×15 cm.). These photographs are beautifully reproduced, and anyone interested in minerals will be delighted with this feature.

Lewis S. Ramsdell
University of Michigan

SELECTED ELECTRON MICROGRAPHS OF CLAYS AND OTHER FINE-GRAINED MINERALS, by Thomas F. Bates. Circular No. 51, Mineral Industries Experiment Station, College of Mineral Industries, The Pennsylvania State University. 61 pages, $8\frac{1}{2}\times 11$ inches. Price $2.00.

This circular contains 101 reproductions of electron micrographs, with brief descriptions and comments, as follows: Kaolin group, 1–31; serpentine group, 32–44; illite group, 45–58; montmorillonite group, 59–77; vanadium minerals, 78–88; others, 89–101. A list of references is included.

These excellent reproductions should be of value to all who are working on clay minerals, and any mineralogist will find them of interest.

Lewis S. Ramsdell
University of Michigan

NEW MINERAL NAMES

Idaite

GERHARD FRENZEL. Ein neues Mineral: Idait. *Neues Jahrb. Mineral., Monatsh.*, **1958**, No. 6, 142.

A preliminary note. Chemical composition Cu_5FeS_6 (in part with a small excess of Cu). Hexagonal, in very fine plates, D_{6h} (?), a_0 3.90, c_0 16.95A, Z=1. Closely related crystallographically to covellite. H. $2\frac{1}{2}$, G. (*x*-ray) 4.21. Luster metallic, color similar to that of bornite, but not tarnished. Strongly birefringent. In reflected light resembles freshly polished bornite. In air, R_o reddish-orange to reddish-brown, R_e yellowish bright gray.

A lamellar decomposition product of bornite, commonly associated with fine spindles of chalcopyrite. Apparently the first product of weathering. Apparently widely distributed; noted from the Ida Mine, Khan, S. W. Africa and 30 other localities.

The name is for the Ida Mine.

MICHAEL FLEISCHER

Gelbertrandite, Spherobertrandite

E. I. SEMENOV. New hydrous silicates of beryllium-gelbertrandite and spherobertrandite. *Inst. mineral., geokhim., and crystallokhim. redkikh elementov, Trudy*, **1**, 64–66 (1957) (in Russian).

Gelbertrandite

Occurs in irregular masses in fibrous beryllite. Color pale violet (fades to yellowish-white), luster vitreous, H. 4, G. 2.176 (by hydrostatic suspension). Optically isotropic, *n* 1.525 (range 1.511–1.530). Analysis by M. E. Kazakova gave SiO_2 38.70, Al_2O_3 1.20, BeO 34.16, CaO 1.93, $(Na, K)_2O$ 0.33, H_2O^+ 15.62, H_2O^- 8.17, sum 100.11%, corresponding to $Be_4Si_2O_7(OH)_2 \cdot 3H_2O$ (i.e. a hydrated bertrandite). Spectrographic analysis by N. V. Lizunov showed the presence of Mn, Pb, Zn, Mg, Cu, and Ba (weak lines). A dehydration curve by A. S. Skripkin showed continual loss of weight to 700°.

X-ray powder data by N. N. Sludsko are given. Fifteen lines are given; the strongest are 4.31 (10), 3.15 (10), 2.53 (10), 2.31 and 2.20 (8), 1.467 (6).

Occurs in pegmatites in nepheline syenites at Mt. Karnasurt and Mt. Mannepakhk, Lovozero massif, Kola Peninsula; formed by the epithermal alteration of epididymite.

DISCUSSION.—Each of the *x*-ray lines corresponds closely to a line of bertrandite, but with lower intensity, and many lines of bertrandite are missing. This therefore seems to be a poorly crystallized bertrandite, and the name is unnecessary.

Spherobertrandite

The mineral occurs in spherulites in drusy cavities in epididymite in pegmatite at Mt. Mannepakhk, also at Kuftny and Sengischorr, Lovozero massif, and Yukspor, Khibina massif. The mineral is yellow to colorless, luster vitreous, H. 5, G about 2.5. Optically biaxial, neg., 2V about 70°, α 1.595, γ 1.612, $Y=c$. The colored variety is weakly pleochroic with X yellow, Z colorless. Absorption $X>Z$.

Analysis by M. E. Kazakova gave SiO_2 41.03, Al_2O_3 1.40, Fe_2O_3 0.07, BeO 45.20, H_2O^+ 11.70, H_2O^- 0.30, sum 99.70%, corresponding to $Be_5Si_2O_7(OH)_4$, whereas bertrandite is $Be_4Si_2O_7(OH)_2$. Spectrographic analysis showed Na, Ca, and Ba (weak lines). A dehydration curve showed that all the water is lost between 600° and 800°.

X-ray powder data (38 lines) are given. The strongest lines (and in parentheses the nearest line of bertrandite) are: 3.15-10 (3.14-10), 2.32-10 (2.28-9), 2.17-10 (2.20-9), 4.89-9 (4.81-3), 1.250-9 (1.250-8), 3.80-8 (3.81-3), 2.73-8 (2.78-4), 1.352-8 (1.362-2), 1.140-8 (1.150-2), 1.970-7 (1.973-8), 1.525-7 (1.495-1), 1.411-7 (———).

DISCUSSION.—The close correspondence of the optical properties (except the orientation) and of the x-ray powder diagram (despite a few missing lines and differences in intensities) makes one wonder whether the analysis can be correct. Could beryllite have been present? The mineral cannot be accepted as a valid species without further study.

M.F.

Gerasimovskite (Niobobelyankinite), Mangano-belyankinite

E. I. SEMENOV. Oxides and hydroxides of titanium and niobium in the Lovozero alkalic massif. *Inst. mineral., geokhim., and crystallokhim. redkikh elementov, Trudy,* **1,** 41–59 (1957) (in Russian).

The mineral belyankinite was described in 1950 (see *Am. Mineral.,* **37,** 882 (1952)). New data are now given for it, for its Mn-analogue (Mn-belyankinite), and for its Nb analogue (gerasimovskite). New analyses are given of gerasimovskite (1 and 2) and of Mn-balyankinite (3).

The minerals are considered to be substituted $Ti(OH)_4$ ranging to the end member $Nb(OH)_5$ (gerasimovskite), and the formulas are calculated to be:

Belyankinite—$(Ti_{0.70}Zr_{0.06}Nb_{0.07}Fe_{0.03}Ca_{0.13})(OH)_{3.78}$
Mn-belyankinite—$(Ti_{0.60}Nb_{0.06}Fe_{0.05}Mn_{0.18}Ca_{0.11})O_{0.55}(OH)_{2.70}$
Gerasimovskite—$(Ti_{0.42}Nb_{0542}Mn_{0.14}Ca_{0.13})O_{0.76}(OH)_{2.83}$

(Note—The atomic ratios of gerasimovskites no. 1 and no. 2 are Nb 0.33, Ti 0.305; Nb 0.34, Ti 0.29. A different method of calculation gives:

Belyankinite—$Ca_1(Ti, Nb, Zr, Si)_6O_{13} \cdot 11H_2O$ or $Ca_{0.9}(Ti, Nb, Zr, Si)_{5.5}O_{12} \cdot 10H_2O$
Mn-belyankinite—$(Mn, Ca)_{1.9}(Ti, Nb)_5O_{12} \cdot 9H_2O$

Analyses

	(1)	(2)	(3)
Nb_2O_5	43.91	44.90	7.42
Ta_2O_5	0.38	0.50	—
TiO_2	24.37	23.44	44.30
SiO_2	1.83	2.30	1.51
Fe_2O_3	tr.	0.21	3.77
Al_2O_3	—	0.65	—
MnO	7.85	2.65	14.03[c]
MgO	—	0.30	—
CaO	1.37	1.95	5.77
Na_2O	—	0.10	—
K_2O	—	0.21	—
CO_2	—	0.20	—
H_2O^+	3.95	3.78	22.36
H_2O^-	16.55	14.77[b]	
Total	100.21[a]	95.96[b]	99.16
Analyst	T. A. Burova	M. E. Kazakova	T. A. Kapitonova

[a] Given as 100.11 in original.

[b] Sum given as 99.91 in original, but the atomic ratio given for total H_2O is exactly that obtained by taking H_2O^+ as 18.77%.

[c] $= MnO_2$.

Gerasimovskite no. 1—$(Mn, Ca)_{1.0}(Nb, Ti, Si)_5O_{12} \cdot 8H_2O$
Gerasimovskite no. 2—$(Mn, Ca)_{0.6}(Nb, Ti, Si)_5O_{12} \cdot 9H_2O$ M. F.)

The minerals are amorphous and give no x-ray lines except that gerasimovskite gives diffuse lines at 2.60, 1.85, and 1.64 Å. When heated at 900°, all give sharp patterns that resemble that of rutile or the high-temperature modification of Nb_2O_5. Belyankinite gave (d and I): 3.21 (8), 2.90 (3), 2.48 (6), 2.18 (3), 1.690 (10), 1.633 (2), 1.361 (5), 1.259 (2). Mn-belyankinite gave 3.21 (2), 2.89 (2), 2.48 (3), 2.17 (1), 1.880 (1), 1.692 (4). Gerasimovskite gave lines at 3.04, 2.49, 2.05, 1.736, 1.706, 1.666 Å.

D.T.A. curves are given. Belyankinite has a large endothermal break at 170°, a small exothermal break at about 410°, and a larger exothermic break at 740°. Gerasimovskite shows an endothermal break at about 150° and an exothermal one at about 730°.

Gerasimovskite is brown to gray or light gray, luster pearly. Perfect cleavage in one direction. H. 2, G. 2.52–2.58. Optically biaxial, negative, 2V 18°, α about 1.74, $\beta\sim\gamma$ about 1.81. Extinction parallel, elongation positive. Manganobelyankinite is brownish-black, luster resinous, color and pleochroism "more intense than those of belyankinite," optically biaxial, neg., 2V 29°.

Gerasimovskite occurs in platy masses up to $1.5\times1\times0.3$ cm. in ussingite-bearing pegmatites of Punkarua Mt., Mt. Nepkha, and Mt. Allua, Lovozero, Kola Peninsula. It is believed to have formed by the hydrothermal alteration of minerals of the murmanite-lomonosovite series. Manganobelyankinite occurs in pegmatite at Mt. Kedykverpakh.

The name is for V. I. Gerasimovskii, Russian mineralogist.

M.F.

D'Ansite

H. Autenrieth and G. Braune. Ein neues Salzmineral, seine Eigenschaften, Sein Auftreten und seine Existenzbedingungen im System der Salze ozeanischer Salzablagerungen. *Naturwissenschaften*, **45**, No. 15, 362–363 (1958).

Study of the system $Na\text{-}Mg\text{-}SO_4\text{-}Cl\text{-}H_2O$ shows the existence of a new phase $MgSO_4\cdot3NaCl\cdot9Na_2SO_4$, which may be written as $MgNa_{21}(Cl_3SO_4)(SO_4)_9$ for comparison with hanksite $KNa_{22}(Cl(CO_3)_2)(SO_4)_9$. At 46°, the lower limit of stability, it co-exists with thenardite and bloedite; at higher temperatures its field is between those of thenardite and vanthoffite. Crystals are tetrahedral with {211} dominant, and {2$\bar{1}$1} and {110} noted. G. 2.655. Isotropic, n Na 1.489. Melts in the Bunsen burner flame. An x-ray diagram, with no measurements of lines is given. a_0 15.90 Å, Z=4.

The compound would be expected to be formed in close association with vanthoffite. No such material was found by the authors, but they believe that it was probably the mineral described by Görgey, *Mineralog. petrog. Mitt.*, **28**, 341 (1909), from Hall, Tyrol. Görgey described the material as closely associated with vanthoffite, enclosed in bloedite, isotropic with n (Na) 1.503, G. 2.590, contains Mg, Na, Cl, SO_3, melts easily without giving water.

The name is for Professor Jean D'Ans, Kali-forschungsanstalt, Berlin, who has published many papers on equilibrium in salt systems.

M.F.

Bonchevite

Ivan Kostov. Bonchevite, $PbBi_4S_7$, a new mineral. *Mineralog. Mag.*, **31**, 821–828 (1958).

Analysis by N. Yordanov gave Bi 66.62, Pb 15.50, Cu 0.85, S 16.71, sum 99.68%, corresponding closely to $PbBi_4S_7$. Spectrographic tests detected also Ag, Zn, Cd, Sb, and Te.

The mineral occurs in acicular or long prismatic, apparently orthorhombic crystals up to 2 cm. The forms m{110} (dominant), e{011}, a{100}, and b{010} were observed. Goniometric measurements on 4 crystals gave $a:b:c=0.9004:1:0.3249$, intermediate between the ratios for bismuthinite and galenobismutite. The {110} faces are commonly striated along the c-axis. Cleavage {100} perfect, fracture uneven to subconchoidal, very brittle. Luster metallic, color lead- to steel-gray. In polished section homogeneous with rare minute inclusions, perhaps native bismuth. Weakly pleochroic, distinctly to strongly anisotropic. H. $2\frac{1}{2}$, G. (av. of 5) 6.92.

X-ray powder data are given for bonchevite, 2 samples of bismuthinite, and galenobismutite. The strongest lines of bonchevite are 3.50 (10), 3.08 (8), 1.939 (8), 2.78 (6), 1.733 (6), 2.50 (5). The bismuthinites gave 3.44, 3.46 (10), 3.03, 3.06 (5), 1.910, 1.915 (8), 2.76, 2.76 (3), 1.722 (4) and 1.726 (2), and 2.48, 2.47 (7). The galenobismutite gave 3.48 (10), 3.05 (3), 1.929 (5), 2.77 (4), 1.726 (3), and 2.49 (8).

The mineral occurs in quartz veins cutting gneisses and amphibolites close to the so-called Yugovo granite, Central Rhodopian Mts. Associated minerals are scheelite, pyrite, and sparse sphalerite and molybdenite. The gangue is milky quartz, locally enriched in calcite.

The name is for Georghi Bonchev, former professor and founder of the Institute of Mineralogy and Petrography, University of Sofia.

Discussion.—The differences in the x-ray patterns given for bonchevite, bismuthinite, and galenobismutite are not convincing, and the validity of the mineral must be substantiated by single crystal x-ray study.

M.F.

Ordite

Yu. M. Ambramovich. Pseudomorphism in sedimentary mineral formation. *Voprosy Mineral. Osadoch. Obrazovanii Lvov Univ.* **1956,** No. 3-4, 80-86; *Chem. Abstracts* **52,** 13549 (1958).

The name ordite, for the locality Orda village, Molotov Oblast, is given to pseudomorphs of crystalline gypsum after fibrous gypsum.

Discussion.—There is no excuse for naming such material.

M. F.

Hydroparagonite

J. Erdelyi, V. Koblencz, and V. Tolnay. Über hydroparagonit, ein neues Glimmermineral, sowie über Beziehungen zum Hydromuskovit, Natronillit, und Brammallit. *Acta Geol. Sci. Hung.* **5,** 169–186 (1958).

In this paper new analyses are given of hydromuscovite from Nagybörzsöny. The analysis, x-ray, and optical data are essentially identical with those of illites, but the authors consider hydromuscovite to be a distinct mineral on the basis of (1) grain size (b) the DTA curve shows the main endothermic break at a temperature 100° higher than illite does. For the same reasons, plus the fact that the x-ray pattern does not change when the mineral is heated, the authors consider that brammallite, described by Bannister (*Am. Mineral.* **29,** 73 (1944) as a sodium-illite, is actually a hydroparagonite, and suggest this name.

Discussion.—The name hydroparagonite (=brammallite) was used by Strunz (Mineralogische Tabellen, 3rd Ed., 1957), but there is no valid reason for discarding brammallite, which has priority. Grain size is not a valid criterion for giving a new name to the same mineral.

M. F.

Kêsterite (Kosterite)

Z. V. Orlova. *Trudy Vses. Magadansk Nauchno-Issled. Inst. Magadan,* **2,** 76 (1956), from an abstract by E. M. Bonshtedt-Kupletskaya in *Zapiski Vses. Mineral. Obshch.,* **87,** 76 (1958).

The name kêsterite (pronunciation nearly that of German form kösterite) is given, with no description, to a mineral, analysis of which gave Cu 30.56, Ag 0.005, Zn 11.16, Mn 0.09, Fe 1.68, Ni tr., Sn. 25.25, Sb 0.90, S 28.40, Se 0.01, sum 98.05%, corresponding to (Cu, Sn, Zn) S with ratio Cu:Sn:Zn about 54:24:19:3. Occurs in quartz-sulfide veinlets in the Kêster deposit in the Yano-Adychansk region. (The name is for the locality.)

Discussion.—A name should not be given without proof of homogeneity. This name also is easily confused with custerite.

M. F.

Giulekhite

Ch. M. Khalifa-Zade, *Doklady Akad. Nauk Azerbaidjan S.S.R.*, **13,** 647–653 (1957), from an abstract by E. M. Bonshtedt-Kupletskaya in *Zapiski Vses. Mineral Obshch*, **87,** 83 (1958).

The mineral is a hydromica occurring in the fraction <0.001 mm. in argillites of southeastern Caucasus. Analysis of the entire dispersed fraction gave SiO_2 31.14, Al_2O_3 14.50, Fe_2O_3 29.88, FeO 3.52, MgO 4.00, K_2O 3.71, Na_2O 0.15, H_2O^+ 8.07, H_2O^- 3.31, sum 98.28%. The D.T.A. curve shows endothermic breaks at 130°, 390°, and 560°. Gives no reaction with benzidine, turns blue with methylene blue, gives a yellow color with brownish tint with chrysoidine. Elongation positive, n'_p 1.543, n'_g 1.552. The strongest x-ray lines are 1.699 (9, broad), 4.32, 3.59, 2.50 (8), 4.93, 1.52 (7).

The name is for the locality near the village of Giulekh (suggested transliterations in the abstract are Gewlekhite for English, Gülechite for German).

Discussion.—The abstractor states, "The mineral is insufficiently characterized and the name was given prematurely." I agree.

M. F.

Bismutomicrolite

N. E. Zalashkova and M. V. Kukharchik, Bismutomicrolite—a new variety of microlite. *Akad. Nauk S.S.S.R., Inst. mineral, geokhim., and Kristallokhim. redkikh elementov, Trudy*, **1,** 77–79 (1957).

Analysis by M. V. K. gave Ta_2O_5 79.72, Nb_2O_5 0.08, TiO_2 0.05, Al_2O_3 0.45, Fe_2O_3, 0.32, MnO 0.08, CaO 8.60, K_2 0.08, Na_2O 5.27, rare earth oxides 0.18, Bi_2O_3 3.25, H_2O 0.60, F 2.00, sum 100.68% (given as 100.70)—$(O=F_2)$ 0.84=99.84 (given as 99.92). Isotropic with n 2.044, G. 6.426, a_0 10.51A. The formula is $(Na, Ca, Bi)_2Ta_2O_6(O, OH, F)$.

Discussion.—Unnecessary name for bismuthian microlite.

M. F.

Stibiotellurobismuthite

I. G. Magak'Yan. *Zapiski Vses. Mineral Obshch.* **86,** 343–346 (1957).

The name is given to a tellurobismuthite containing Sb 2.7%.

Discussion.—Unnecessary name for antimonian tellurobismuthite.

M. F.

NEW DATA

Stainierite

Jean Orcel, Stéphane Hénin, and Simonne Caillère. Sur la presence de stainierite á Bou Azzer et les propriétés de cet hydroxyde. *Compt. rend.*, **246,** No. 5, 792–795 (1958).

Stainierite (heterogenite) has been considered to be $Co_2O_3 \cdot H_2O$ or CoO(OH), analogous to goethite. (See Dana's System, 7th Ed., Vol. I, p. 650–653). Material from a new locality, Bou Azzer, Morocco, gave CoO 70.00, SiO_2 1.35, Al_2O_3 1.0, Fe_2O_3 3.30, Cr_2O_3 0.20. MnO 0.35, TiO_2 0.05, CuO 0.10, MgO 1.40, CaO 0.85, H_2O^- 4.00, H_2O^+ 17.00, sum 99.60%. A dehydration curve showed a loss in weight, corrected for impurities, of about 13.5% at

250–275° and another loss in weight of about 3.5% at about 900°. The DTA curves (not given) of the Bou Azzer and Katanga material showed endothermal breaks at 260–300° and a very intense one at 900–960°.

X-ray study of the two samples gave very similar patterns (no data given) which are similar to those of brucite and pyrochroite. The *x*-ray pattern of a sample heated at 550° is of the spinel type (Co_3O_4?), that obtained at 1000° and cooled in air was similar, but that of material heated at 1000° and cooled in a closed container resembles the pattern of periclase. It is concluded that stainierite is $Co(OH)_2$.

M.F.

Coeruleolactite (=Ca analogue of Turquois)
Planerite (=cuprian Coeruleolactite and calcian Turquois)
Alumochalcosiderite (=aluminian Chalcosiderite)

Emil Fischer. Über die Beziehungen zwischen Coeruleolactit, Planerit, Turkis, Alumochalkosiderit, und Chalkosiderit. *Beitr. Mineral. u. Petrog.*, **6,** 182–189 (1958).

New microchemical analyses and *x*-ray powder data are given for 2 samples of turquois and one of "alumochalcosiderite." These show that there is a continuous series from turquois to chalcosiderite with a corresponding change in *d*-spacings. Microchemical analyses are also given of coeruleolactite from the Rindsberg mine, Nassau, Germany (type locality) (no. 1) and for 2 samples of planerite labelled Tschornaya River near Syssert, Urals, (no. 2) and Mt. Tschernovskaya near Syssert (no. 3); these probably represent type material. The analyses gave:

	CaO	CuO	FeO	MgO	Al_2O_3	Fe_2O_3	P_2O_5	H_2O	Sum
1.	5.09	0.24	—	0.40	40.3	—	30.1	23.4	99.5
2.	2.88	3.48	0.8	—	37.1	—	35.5	20.4	100.2
3.	1.15	6.31	tr.	0.09	37.7	—	35.0	19.4	99.7

X-ray powder data are given for these samples; they agree closely with those for turquois, but some differences in spacing and intensities are noted. The minerals are considered to be members of the same group with the general formula $(Cu, Ca, Fe'', Mg)(Al, Fe''')_6((P, As)O_4)_4 \cdot 4\text{–}5H_2O$. The analyses of planerite show a deficiency in the RO group, that of coeruleolactite an excess of Al_2O_3, ascribed to the presence of an unidentified aluminum hydroxide. No optical data are given and much of the pertinent literature is not mentioned.

Discussion.—The data indicate that coeruleolactite is a member of the turquois group, but the isomorphous relationships and possible substitutions have not yet been worked out satisfactorily. The names planerite and alumochalcosiderite are superfluous and should be dropped.

M.F.

DISCREDITED MINERALS

Ptilolite, Flokite, Arduinite (all = Mordenite)

R. J. Davis. Mordenite, ptilolite, flokite, and arduinite. *Mineralog. Mag.*, **31,** 887–888 (1958).

These minerals had previously been considered by various investigators to be identical, but mordenite and ptilolite from the type localities had not been re-examined. *X*-ray powder diagrams of the four minerals, each from the type locality, show them to be identical.

M.F.

Comuccite (=Jamesonite)

Carlo Garavelli. Identita fra "comuccite" e jamesonite. *Periodico Mineralogia*, **27**, 207–210 (1958).

Comuccite was described as a lead antimony sulfide from San Giorgio, Sardinia, by Comucci in 1916 and was named by Doelter in 1926. Short (1931) and Rodolico (1940) believed it to be jamesonite from optical data. *X*-ray powder data on type material proves the identity.

M. F.

Alumian (=Natroalunite)

A. A. Moss. Alumian and natroalunite. *Mineralog. Mag.*, **31**, 884–885 (1958).

Alumian, described by Breithaupt in 1858 as $Al_2(SO_4)_2O$, has been guessed to be alunite or natroalunite (Dana's System, 7th Ed., Vol. II, p. 560). A complete analysis and *x*-ray study of type material from the Sierra Almagrera, Spain, show it to be nearly the natroalunite end member (Na_2O 7.6, K_2O 0.1%), with ω 1.574, ϵ 1.590, G. 2.78.

M.F.

Arsenolamprite (=Arsenic+Arsenolite)

Karel Padera and Emil Fischer. Does the modification of arsenic, arsenolamprite, exist as a mineral? *Mineralog. Sbornik Lvov Geol. Obshch.* No. 10, 160–167 (**1956**) (in Russian).

X-ray powder data on arsenolamprite from Copiapo, Chile, show it to be a mixture of rhombohedral arsenic with arsenolite. The type material from Marienberg, Saxony, had previously been reported to have the same *x*-ray pattern as the Copiapo material (see Dana's System, 7th Ed., Vol. I, p. 130).

M.F.

INDEX TO VOLUME 43

Leading articles are in **bold face** type; notes, abstracts and reviews are in ordinary type. Only minerals for which definite data are given are indexed.

Absorption for rod-shaped single crystals, correction for (Buerger, Niizeki) 726
Adsorption and retention of an organic material by montmorillonite in the presence of water (Brindley, Rustom) 627
Ajoite, a new hydrous aluminum copper silicate (Schaller, Vlisidis) 1107
Alkali amphiboles, classification of (Miyashiro, Iwasaki) (Andreev) 797
Alkali feldspars: IV. The cooling history of high-temperature sodium-rich feldspars (Smith, MacKenzie) 872
Allen, R. D., and Almond, H., Nonfibrous ulexite from the Kramer District, California . 169
Almond, H., with Smith, G. L., and Sawyer, D. L. Sassolite from the Kramer borate district, California 1068
———, with Allen, R. D. Nonfibrous ulexite from the Kramer District, California . 169
Alumian (=natroalunite) (Moss) . 1225
Aluminum boride monocrystals, microhardness of (Cotter) 781
Alumochalcosiderite (=aluminian chalcosiderite) (Fischer) . . . 1224
Ambramovich, Y. M. 1222
Ames, L. L., and Sand, L. B. Factors effecting maximum hydrothermal stability in montmorillonites 641
——— Hydrothermal synthesis in wairakite and calcium-mordenite 476
Amphibole paragenesis in the Bidwell Bar region, California, significance of (Compton) 890
Amstutz, G. C. (Book Review) . . 788
. . . . 794
Andradite-spessartite garnet from Pajsberg, Sweden (Lee) 208
Andreev, Y. K. 797
Ankerite and dolomite, x-ray data for (Howie, Broadhurst) 1210
Anthoinite (Niggli, Jäger) 384
Arduinite (=mordenite) (Davis) . . 1224
Argon and helium, excess, in beryl and other minerals (Damon, Kulp) 433
Arsenolamprite (=arsenic+arsenolite) (Padera, Fischer) 1225
Ashby, G. E., and Kellagher, R. C. Apparatus for the study of thermoluminescence from minerals 695
Atchley, F. W. Low-magnification thin-section photography 997
Atoms and ions in minerals, chart showing the sphere of influence of (Remick) 166
Autenrieth, H. 1221
Axelrod, J. M., with Milton, C., Carron, M. K., and MacNeil, F. S. Gorceixite from Dale County, Alabama 688
——— with Milton, C., and Ingram, B. Bismutoferrite, chapmanite and "hypochlorite" . . . 656

(β-MnS), unnamed (Baron, Debysser) 795
Barbierite (=microcline) (Schneider, Laves) 1008
Baron, G. 795
Barton, P. B., Jr. Synthesis and properties of carnotite and its alkali analogues 799
Bassett, W. A. Copper vermiculites from northern Rhodesia 1112
Bastiansen, O., with Vogt, T., and Skancke, P. Holmquistite as a rhombic amphibole 981
Batchelorite (=muscovite) (Bothwell, Moss) 1008
Bates, T. F. Selected electron micrographs of clays and other fine-grained minerals (Book Review) 1218

Bayerite (natural) = gibbsite (Sasvari, Zaiai) 626
Beamish, F. E., with Westland, A. D. Chemical analysis of iridosmines and other platinum-metal minerals 503
Bellite (Strunz) 798
Beryl and other minerals, excess helium and argon in (Damon, Kulp) 433
Beryllium content of roscherite from the Sapucaia pegmatite mine, Minas Gerais, Brazil (Lindberg) 824
Bikitaite additional data on (Hurlbut) 768
Biotite, chlorine-rich, from Lemhi County, Idaho (Lee) 107
Bismutoferrite, chapmanite and "hypochlorite" (Milton, Axelrod, Ingram) 626, 656
Bismutomicrolite (Zalashkova, Kukharchik) 1223
Blade, L. V. 1006
———, with Rose, H. J., Jr., and Ross, M. Earthy monazite at Magnet Cove, Arkansas 995
Blix, R. 387
Bonattite (Garavelli) 180
Bonchevite (Kostov) 1221
Bose, M. K. Goethite-hematite relation 989
Bothwell, D. I. 1008
Branche, G. 180
Braune, G. 1221
Breger, I. A. (Book Review) 788
Breislakite (= vonsenite) (Federico) 626
Brindley, G. W., and Rustom, M. Adsorption and retention of an organic material by montmorillonite in the presence of water 627
Broadhurst, F. M., with Howie, R. A. *X*-ray data for dolomite and ankerite 1210
Bruyerite (Tacnet) 624
Buckle, E. R., and Taylor, H. F. W. Calcium analogue of chondrodite 818
Buerger, M. J., and Kennedy, G. C. Improved specimen holder for the focusing-type *x*-ray spectrometer 756
——— **and Niizeki, N. Correction for adsorption for rod-shaped single crystals 726**
Bunting, E. N., and Van Valkenburg, A. Some properties of diamond 102
Burst, J. F. Mineral heterogeneity in "glauconite" pellets 481
Bur'yanova, E. Z. 623
Butkovich, T. R. Hardness of single ice crystals 48

Cadmoselite (Bur'yanova, Kovalev, Komkov) 623
Caillère, S. 1223
Calcite, melting of in the presence of water and carbon dioxide (Paterson) 603
Calcium-mordenite and wairakite, hydrothermal synthesis in (Ames, Sand) 476
Carnotite, synthesis and properties and its alkali analogues (Barton) 799
Carr, R. M., and Fyfe, W. S. Some observations on the crystallization of amorphous silica 908
Carron, M. K., with Glass, J. J., Evans, H. T., Jr., and Hildebrand, F. A. Cerite from Mountain Pass, San Bernardino County, California 460
——— **with Milton, C., MacNeil, F. S., and Axelrod, J. M. Gorceixite from Dale County, Alabama 688**
———, Mrose, M. E., and Murata, K. J. Relation of ionic radius to structures of rare-earth phosphates, arsenates and vanadates 985
Célébonovic, S. The Living Rocks (Book Review) 177
Cerite from Mountain Pass, San Bernardino County, California (Glass, Evans, Carron, Hilde-

brand) 460
Chalmers, R. A. 624
Chantret, F. 180
Chao, E. C. T., with Milton, C. Eskolaite in "merumite" from British Guiana 1203
Chapmanite, bismutoferrite, and "hypochlorite" (Milton, Axelrod, Ingram) 656
Chapmanite, bismutoferrite, hypochlorite (Milton, Axelrod, Ingram) 626
Chayes, F. Memorial of Samuel James Shand 317
Chemical Engineering in the Coal Industry (F. W. Sharpley, Ed.) (Book Review) 788
Chernikov, A. A. 383
Chondrodite, calcium analogue of (Buckle, Taylor) 818
Chlorine in serpentinized dunite (Earley) 148
Chlorite, chromium, structural and chemical variation in (Lapham) 921
Chlorite, white, from Cobargo, N.S.W. (Loughnan, See) 671
Chlorites, synthesis of, and their structural and chemical constitution (Nelson, Roy) 707
Christ, C. L., with Ross, M. Mineralogical applications of electron diffraction 1157
Chrome mica-clay, Temple Mountain, Utah (Kerr, Hamilton) . . 34
Chromian muscovite from Baker Mountain, Virginia (Dietrich) 162
Cipriani, C. 378
Clay-carbonate-soluble salt interaction during differential thermal analysis (Martin) 649
Coeruleolactite (=Ca analogue of turquois) (Fischer) 1224
Coffinite, thorite and uranothorites, synthetic, x-ray studies of (Fuchs, Gebert) 243
Cohen, A. J., and Rice, R. V. New method for orienting electron microscope replicas 25
——— and Sumner, G. G. Relationships among impurity contents, color centers and lattice constants in quartz 58
Combeite (Sahama, Hytönen) 791
Compton, R. R. Significance of amphibole paragenesis in the Bidwell Bar region, California 890
Comuccite (=jamesonite) (Garavelli) 1225
Concise International Dictionary of Mechanics and Geology (Book Review) 1004
Constitution of Binary Alloys. (Hansen) (Book Review) 1217
Copper vermiculites from northern Rhodesia (Bassett) 1112
Corey, A. S., with Gross, E. B., Mitchell, R. S., and Walenta, K. Heinrichite and metaheinrichite, hydrated barium uranyl arsenate minerals 1134
Corwin, J. F., with White, J. F., and Shaw, E. R. A chalcedony-like variety of germania, GeO_2 580
Cotter, P. G. Microhardness of aluminum boride monocrystals 781
Crandallite (pseudowavellite) from Gardner Mine Ridge, Lawrence County, Indiana (Greenberg, Elberty) 983
Cuspidine, synthetic (Van Valkenburg, Rynders) 1195

Dahhlite pseudomorphs after pyrite concretions (Mitchell, Sherwood) 600
Damon, P. E., and Kulp, J. L. Excess helium and argon in beryl and other minerals 433
D'Ansite (Autenrieth, Braune) 1221
Davis, R. J. 1224
Day, G., with Sabine, P. A., and Rowe, R. H. Device for precisely controlling an iris diaphragm 784
Debyser, J. 795
De Las Casas, F. 794
Denning, R. M. (Book Reviews) 618, 622
Diamond, some properties of (Bunting, Van Valkenburg) . . . 102

Dietrich, R. V. Chromian muscovite from Baker Mountain, Virginia 162
Differential Thermal Investigation of Clays (Mackenzie, Ed.) (Book Review) 617
Digenite, Cu$_9$S$_5$, crystal and twin structure of (Donnay, Donnay, Kullerud) 228
Discredited minerals 626, 1008, 1224
Dolomite and ankerite, x-ray data for (Howie, Broadhurst) 1210
Dolomonova, E. I. 386
Donnay, G. (Book Review) 376
———, **Donnay, J. D. H., and Kullerud, G. Crystal and twin structure of digenite, Cu$_9$S$_5$** 228
Donnay, J. D. H. (Book Review) 376
———, **with Donnay, G., and Kullerud, G. Crystal and twin structure of digenite Cu$_9$S$_5$** 228
Douglass, R. M. Crystal structure of sanbornite, BaSi$_2$O$_5$ 517
Duffin, W. J. 384

Earley, J. W. On chlorine in serpentinized dunite 148
Einführung in die Kristallographie (Kleber) (Book Review) 788
Eitel, W. 626
Elberty, W. T., with Greenberg, S. S. Crandallite (pseudowavellite) from Gardner Mine Ridge, Lawrence County, Indiana 983
Electron diffraction, mineralogical applications of (Ross, Christ) 1157
Electron microscope replicas, new method for orienting (Rice, Cohen) 25
Emerson, D. O. Stage for macro point counting 1000
English, G. L., and Jensen, D. E. Getting Acquainted with Minerals. 2d ed. (Book Review) 1217
Eosphorite-childrenite series, optics of (Winchell) 765
Erdelyi, J. 1222
Eskolaite, a new chromium mineral (Kouvo, Vuorelainen) 1098
Eskolaite in "merumite" from British Guiana (Milton, Chao) 1203
Evans, H. T., Jr. 385
——— (Book Review) 787
———, **with Glass, J. J., Carron, M. K., and Hildebrand, F. A. Cerite from Mountain Pass, San Bernardino County, California** 460

Fahey, J. J. 625
Faick, J. N., and Hildebrand, F. A. An occurrence of molybdenian stolzite in Arizona 156
Faust, G. T. (Book Reviews) 178, 616, 617
Federico, M. 626
Ferroelectricity in Crystals (Megaw) (Book Review) 787
Ferutite (Getseva, Savel'eva) 382
Fischer, E. 1224
Fisher, D. J. Pegmatite phosphates and their problems 181
——— Addendum to the pegmatite phosphates 609
——— Note on lithiophosphate 761
——— Refractometer perils 777
———, **and Runner, J. J. Morinite from the Black Hills** 585
Fleischer, M. Memorial of Benno Wasserstein 331
———, New mineral names 180, 378, 623, 790, 1006, 1219
——— (Book Review) 616
Flokite (=mordenite) (Davis) 1224
Foshagite: composition, unit cell and dehydration (Gard, Taylor) 1
Foster, L. M., Long, G., and Stumpf, H. S. Production of graphite single crystals by thermal decomposition of aluminum carbide 285
Francevillite (Branche, Ropert, Chantret, Morignat, Pouget) 180
Frenzel, G. 1219
Frolovite (Petrova) 385
Frondel, C. 793
Fuchs, L. H. Formation and properties of synthetic thorite crystals 367

———, and Gebert, E. *X*-ray studies of synthetic coffinite, thorite and uranothorites 243

Fyfe, W. S., with Carr, R. M. Some observations on the crystallization of amorphous silica .. 908

Gabrielson, O. 387

Garavelli, C. L. 180, 1225

Gard, J. A. 624

———, and Taylor, H. F. W. Foshagite: composition, unit cell and dehydration 1

Garnet, composition and physical properties of (Winchell) 595

Gebert, E., with Fuchs, L. H. *X*-ray studies of synthetic coffinite, thorite and uranothorites 243

Geffroy, J. 792

Geier, B. H. 1006

Gelbertrandite, spherobertrandite (Semenov) 1219

Gerasimovskite (niobobelyankinite), mangano-belyankinite (Semenov) 1220

Germania, GeO_2, a chalcedony-like variety (White, Shaw, Corwin) 580

Getseva, R. V. 378

Getting Acquainted with Minerals. 2d ed. (English, Jensen) (Book Review) 1217

Giannini, W. F., with Mitchell, R. S. Natrojarosite from near the Montana-Wyoming line .. 1205

Giardini, A. A. Double arc goniometer head for crystal orientation, sawing and grinding .. 370

——— Piezobirefringence in silicon 249

——— Study of the directional hardness in silicon 957

Gillespite, leached, a sheet silicate, structure of (Pabst) 970

Giulekhite (Khalifa-Zade) 1223

Glass, J. J., Evans, H. T., Jr., Carron, M. K., and Hildebrand, F. A. Cerite from Mountain Pass, San Bernardino County, California ... 460

———, Rose, H. J., Jr., and Over, E. Yttrium-bearing pegmatite body near Lake George, Park County, Colorado 991

"Glauconite" pellets, mineral heterogeneity in (Burst) 481

Goethite-hematite relation (Bose). 989

Goldsmith, J. R., and Graf, D. L. Relation between lattice constants and composition of the Ca-Mg carbonates 84

Goniometer head, double arc, for crystal orientation. sawing and grinding (Giardini) 370

Goodman, N. R. 791

Goodyear, J. 384

Gorceixite from Dale County, Alabama (Milton, Axelrod, Carron, MacNeil) 688

Gorceixite, occurrence in Arkansas (Young) 762

Gotman, Y. D. 1007

Götzenite (Sahama, Hytönen) 790

Gradwell, R. A simple fusion method for determination of plagioclase feldspar from thin section 368

Graf, D. L., with Goldsmith, J. R. Relation between lattice constants and composition of the Ca-Mg carbonates 84

Graphite single crystals, production of by thermal decomposition of aluminum carbide (Foster, Long, Stumpf) 285

Greenberg, S. S., and Elberty, W. T. Crandallite (pseudowavellite) from Gardner Mine Ridge, Lawrence County, Indiana 983

Grigor'ev, I. F. 386

Gross, E. B., Corey, A. S., Mitchell, R. S., and Walenta, K. Heinrichite and metaheinrichite, hydrated barium uranyl arsenate minerals 1134

Guillemin, C. 796

Guinier camera, multiple, application in clay mineral studies (Porrenga) 770

Häggite (Evans, Mrose)......... 385
Hallimond, A. F. Manual of the Polarizing Microscope (Book Review).................. 616
Hamilton, P. K., with Kerr, P. F. Chrome mica-clay, Temple Mountain, Utah............. 34
Hansen, M. Constitution of Binary Alloys. (Book Review)....... 1217
Hayase, K..................... 623
Hayes, E. T. (Book Review)..... 1218
Heating stage, liquid, a new low-temperature (Virgin, Massoni) 606
Heide, F. Kleine Meteoritekunde (Book Review)............. 177
Heinrich, E. Wm. (Book Reviews) 177, 1004
Heinrichite and metaheinrichite, hydrated barium uranyl arsenate minerals (Gross, Corey, Mitchell, Walenta).......... 1134
Helium and argon, excess, in beryl and other minerals (Damon, Kulp).................... 433
Hénin, S...................... 1223
Hessenbergite (=bertrandite) (Parker, Indergand)......... 1008
Hildebrand, F. A., with Faick, J. N. An occurrence of molybdenian stolzite in Arizona.... 156
———, **with Glass, J. J., Evans, H. T., Jr., and Carron, M. K. Cerite from Mountain Pass, San Bernardino County, California**..................... 460
Holmquistite as a rhombic amphibole (Vogt, Bastiansen, Skancke).................. 981
Hooker, M..................... 624
Horobetsuite (Hayase)........... 623
Howie, R. A., and Broadhurst, F. M. X-ray data for dolomite and ankerite................ 1210
Hunt, W. F. Acceptance of the Roebling Medal............ 336
Huntite from Tea Tree Gully, South Australia (Skinner)... 159
Hurlbut, C. S., Jr. Additional data on bikitaite............... 768
Hutton, C. O. Notes on tapiolite, with special reference to tapiolite from southern Westland, New Zealand............. 112
Hydroparagonite (Erdelyi, Koblencz, Tolnay)............. 1222
"Hypochlorite," bismutoferrite and chapmanite (Milton, Axelrod, Ingram).................. 656
Hypochlorite, bismutoferrite, chapmanite (Milton, Axelrod, Ingram)..................... 626
Hytönen, K..............790, 791, 795
———, **with Sahama, T. G. Calcium-bearing magnesium-iron olivines**................... 862

Ice crystals, single, hardness of (Butkovich)............... 48
Idaite (Frenzel)................. 1219
Indergand, P.................... 1008
Índice Alfabético Para el Diccionario Minero (Español, Francés, Alemán Y Ruso) (Novitzky) (Book Review).. 1004
Ingerson, E. (Book Reviews)..... ....176, 177, 376, 1004, 1217
Ingram, B., with Milton, C., and Axelrod, J. M. Bismutoferrite, chapmanite and "hypochlorite"....................... 656
Inyoite at Laguna Salinas, Peru, first known occurrence in a playa (Muessig)........... 1144
Ionic radius, relation to structures of rare-earth phosphates, arsenates and vanadates (Carron, Mrose, Murata)........... 985
Iridosmines and other platinum-metal minerals, chemical analysis of (Westland, Beamish).. 503
Iriginite (Soboleva, Pudovkina)... 379
Iris diaphragm, device for precisely controlling (Sabine, Rowe, Day)......................... 784
Iron-alabandite (Ramdohr)....... 378
Iron Ore Beneficiation (Roe) (Book Review).................. 376
Isogyres in interference figures (Kamb).................. 1029
Iwasaki, M.................... 797

Jäger, E. 384
Jagoite (Blix, Gabrielson, Wickman) 387
Jasmund, K. Die Silikatischen Tonminerale (Book Review) 178
Jensen, D. E., with English, G. L. Getting Acquainted with Minerals. 2d ed. (Book Review) 1217
Johan, Z. 794

Kalita, A. P. 797
Kamb, W. B. Isogyres in interference figures 1029
Kazakova, M. E. 792
Keith, M. L., with Van Hook, H. J. The system Fe_3O_4-Mn_3O_4 69
Kellagher, R. C., with Ashby, G. E. Apparatus for the study of thermoluminescence from minerals 695
Kelly, W. C. (Book Review) 178
Kennedy, G. C., with Buerger, M. J. Improved specimen holder for the focusing-type *x*-ray spectrometer 756
Kerr, P. F. Memorial of Austin Flint Rogers 310
———, and Hamilton, P. K. Chrome mica-clay, Temple Mountain, Utah 34
———, with Kopp, O. C. Differential thermal analysis of pyrite and marcasite 1079
——— Differential thermal analysis of sphalerite 732
Kesterite (Orlova) 1222
Kettnerite (Zak, Syneček) 385
Khalifa-Zade, Ch. M. 1223
Khapaev, I. A. 1007
Kimzeyite (Milton, Blade) 1006
Kirschsteinite (Sahama, Hytönen) 790
Kleber, W. Einfuhrung in die Kristallographie (Book Review) 788
Kleine Meteoritekunde. 2d ed. (Heide) (Book Review) 177
Koblencz, V. 1222
Kobokobite (Thoreau) 795
Kohn, J. A. Twinning in diamond-type structures: A proposed boundary-structure model 263
Komkov, A. I. 623
Kopchenova, E. V. 383
Kopp, O. C., and Kerr, P. F. Differential thermal analysis of pyrite and marcasite 1079
——— Differential thermal analysis of sphalerite 732
Kostov, I. 1221
Koutekite (Johan) 794
Kouvo, O., and Vuorelainen, Y. Eskolaite, a new chromium mineral 1098
Kovalev, G. A. 623
Krutetskaya, O. V. 383
Kukharchik, M. V. 1223
Kullerud, G., with Donnay, G., and Donnay, J. D. H. Crystal and twin structure of digenite, Cu_9S_5 228
Kulp, J. L., with Damon, P. E. Excess helium and argon in beryl and other minerals 433
Kupa, F. 792
Kutina, J. Memorial of František Slavík 325

Laboratory Manual of Crystallography for Students of Mineralogy and Geology (Tunell, Murdoch) (Book Review) 618
Lapham, D. M. Structural and chemical variation in chromium chlorite 921
Larsen, E. S., 3rd. Memorial of John Charles Rabbitt 307
Lattice constants and composition of the Ca-Mg carbonates, relation between (Goldsmith, Graf) 84
Laves, F. 1008
Lee, D. E. An andradite-spessartite garnet from Pajsberg, Sweden 208
——— A chlorine-rich biotite from Lemhi County, Idaho 107
Leonard, B. F. 793
Lermontovite (Soboleva, Pudovkina) 379

Leucite nepheline dolerite of Meiches, Vogelsberg, Hessen (Tilley)........ 758
Lindberg, M. L. Beryllium content of roscherite from the Sapucaia pegmatite mine, Minas Gerais, Brazil........ 824
Lithiophosphate, note on (Fisher). 761
Living Rocks (Célébonovic) (Book Review)........ 177
Lodochnikite (Gotman)........ 1007
Lodochnikite (Soboleva, Pudovkina)........ 380
Long, G., with Foster, L. M., and Stumpf, H. S. Production of graphite single crystals by thermal decomposition of aluminum carbide........ 285
Losert, J........ 792
Louderback, George Davis, memorial of (Pabst)........ 297
Loughnan, F. C., and See, G. T. White chlorite from Cobargo, N. S. W........ 671

MacKenzie, W. S., with Smith, J. V. Alkali feldspars: IV. The cooling history of high-temperature sodium-rich feldspars........ 872
MacNeil, F. S., with Milton, C., Axelrod, J. M., and Carron, M. K. Gorceixite from Dale County, Alabama........ 688
Macro point counting, stage for (Emerson)........ 1000
Magak'Yan, I. G........ 1223
Magnetic susceptibilities of minerals in the Frantz Isodynamic separator (Rosenblum)........ 170
Manganese silicate, unnamed (Smirnov)........ 793
Mangano-belyankinite (Semenov). 1220
Manual of the Polarizing Microscope (Hallimond) (Book Review)........ 616
Marcasite and pyrite, differential thermal analysis of (Kopp, Kerr)........ 1079
Martin, R. T. Clay-carbonate-soluble salt interaction during differential thermal analysis........ 649
Mason, B........ 1008
Massoni, C. J., with Virgin, W. W., Jr. A new low-temperature, liquid heating stage........ 606
Mathieson, A. M. Mg-vermiculite: a refinement and re-examination of the crystal structure of the 14.36 Å phase........ 216
McConnell, D. The so-called "oxygen excess"........ 786
——— (Book Review)........ 619
——— and Murdoch, J. Crystal chemistry of scawtite........ 498
McLachlan, D., Jr. *X*-ray Crystal Structure (Book Review)........ 620
Meen, V. B. Memorial of Arthur Leonard Parsons........ 302
Megaw, H. D. Ferroelectricity in Crystals (Book Review)........ 787
Melkov, V. G........ 1008
———, with Thompson, M. E., and Roach, C. H. Sherwoodite, a mixed vanadium(IV)-vanadium(V) mineral from the Colorado Plateau........ 749
——— Simplotite, a new quadrivalent vanadium mineral from the Colorado Plateau........ 16
Mg-Al oxides and silicates, physical properties and bond type in (Verhoogen)........ 552
Mg-vermiculite: a refinement and re-examination of the crystal structure of the 14.36 Å phase (Mathieson)........ 216
Milton, C........ 1006
——— (Book Review)........ 1217
———, Axelrod, J. M., Carron, M. K., and MacNeil, F. S. Gorceixite from Dale County, Alabama........ 688
———, Axelrod, J. M., and Ingram, B. Bismutoferrite, chapmanite and "hypochlorite"........ 656
———, and Chao, E. C. T. Eskolaite in "merumite" from British Guiana........ 1203
Mineralogical Society of America

Award, acceptance of (Roy) . . 346

Mineralogical Society of America Award, presentation to Rustum Roy (Osborn) 344

Mineralogical Society of America, proceedings of the thirty-eighth annual meeting at Atlantic City, New Jersey 349

List of papers of special mineralogical interest presented at annual meeting 362

List of fellows and members 388

Mineralogische Tabellen (Strunz) (Book Review) 619

Minéraux D'uranium du Haut Katanga (Vaes, Guillemin, Destas) (Book Review) 1218

Mitchell, R. S., and Giannini, W. F. Natrojarosite from near the Montana-Wyoming line 1205

———, **with Gross, E. B., Corey, A.S., and Walenta, K. Heinrichite and metaheinrichite, hydrated barium uranyl arsenate minerals** 1134

——— and Sherwood, W. C. Dahhlite pseudomorphs after pyrite concretions 600

Miyashiro, A. 797

Moluranite (Soboleva, Pudovkina) 380

Molybdenian stolzite, an occurrence in Arizona (Faick, Hildebrand) 156

Monazite, earthy, at Magnet Cove, Arkansas (Rose, Blade, Ross) . 995

Montmorillonites, factors effecting maximum hydrothermal stability in (Ames, Sand) 641

Morignat, B. 180

Morinite from the Black Hills (Fisher, Runner) 585

Moss, A. A. 1008, 1225

Mountain, E. D. 624

Mountainite, Rhodesite (Mountain) (Gard, Taylor, Chalmers) 624

Mrose, M. E. 385

———, with Carron, M. K., and Murata, K. J. Relation of ionic radius to structures of rare-earth phosphates, arsenates and vanadates 985

Muessig, S. First known occurrence of inyoite in a playa, at Laguna, Peru 1144

Murata, K. J., with Carron, M. K., and Mrose, M. E. Relation of ionic radius to structures of rare-earth phosphates, arsenates and vanadates 985

Murdoch, J. Phosphate minerals of the Borborema pegmatites. II. Boqueirão 1148

———, **with McConnell, D. Crystal chemistry of scawtite** 498

———, with Tunell, G. Laboratory Manual of Crystallography for Students of Mineralogy and Geology (Book Review) 618

Nakaya, U. Snow Crystals, Natural and Artificial (Book Review) 622

Natrojarosite from near the Montana-Wyoming line (Mitchell, Giannini) 1205

Nelson, B. W., and Roy, R. Synthesis of chlorites and their structural and chemical constitution 707

Nendo-Kobutso (Clay Minerals) (Sudo) (Book Review) 1217

Nepheline, natural, a complex form from Iivaara, Finland (Sahama) 165

New data 384, 626, 795, 1223

New mineral names 180, 378, 623, 790, 1006, 1219

Niggli, E. 384

Niizeki, N., with Buerger, M. J. Correction for absorption for rod-shaped single crystals 726

Nioboloparite (Tikhonenkov, Kazakova) 792

Novak, F. 792

Novitzky, A. Índice Alfabético Para el Diccionario Minero (Español, Francés, Alemán Y Ruso) (Book Review) 1004

——— Tables for the Microscopic

and *X*-ray Determination of the Opaque Minerals ("Tablas Para la Determinación Microscópica y Rayos X de Minerales Opacos") (Book Review) 176

Obruchevite (Getseva, Savel'eva) 380
Obruchevite (Kalita) 797
Olivine and orthopyroxene in basic lavas and shallow intrusions, alteration of (Wilshire) 120
Olivines, calcium-bearing magnesium-iron (Sahama, Hytönen) 862
Orcel, J. 1223
Ordite (Ambramovich) 1222
Organov, N. I. 383
Orlite (Soboleva, Pudovkina) 381
Orlova, Z. V. 1222
Orthochamosite (Novak, Vtelensky, Losert, Kupa, Valcha) 792
Osborn, E. F. Presentation of the Mineralogical Society of America Award to Rustum Roy 344
Over, E., with Glass, J. J., and Rose, H. J., Jr. Yttrium-bearing pegmatite body near Lake George, Park County, Colorado 991
"Oxygen excess," so-called (McConnell) 786

Pabst, A. Memorial of George Davis Louderback 297
——— **The structure of leached gillespite, a sheet silicate** 970
—— (Book Review) 620
Padera, K. 1225
Parapitchblende (Geffroy, Sarcia) 792
Parker, R. L. 1008
Parsons, Arthur Leonard, memorial of (Meen) 302
Paterson, M. S. Melting of calcite in the presence of water and carbon dioxide 603
Pegmatite phosphates, addendum to (Fisher) 609
Pegmatite phosphates and their problems (Fisher) 181
Petrova, E. S. 385
Phosphate minerals of the Borborema pegmatites. II. Boqueiro (Murdoch) 1148
Physics and Chemistry of the Earth (Book Review) 616
Pierrot, R. 796
Plagioclase, heated, optical properties of (Smith) 1179
Plagioclase feldspar, a simple fusion method for determination from thin section (Gradwell) 368
Plagioclase feldspars, effect of temperature, structural state and composition on the albite, pericline and acline-A twins of (Smith) 546
Planerite (=cuprian coeruleolactite and calcian turquois) (Fischer) 1224
Platinum-metal minerals, chemical analysis of (Westland, Beamish) 503
Porrenga, D. H. Application of multiple Guinier camera in clay mineral studies 770
Potassium "fixation" by expandable clay minerals derived from muscovite, biotite, chlorite and volcanic material, effects of geologic significance of (Weaver) 839
Pouget, R. 180
Przhevalskite (Soboleva, Pudovkina) 381
Ptilolite, Flokite, Arduinite (all =mordenite) (Davis) 1224
Pudovkina, I. A. 378
Pukhal'skii, L. C. 1008
Pyrite and marcasite, differential thermal analysis of (Kopp, Kerr) 1079

Quartz, relationships among impurity contents, color centers and lattice constants in (Cohen, Sumner) 58

Rabbitt, John Charles, memorial of (Larsen) 307

Ramdohr, P. 378, 794
Ramsdell, L. S. Presentation of the Roebling Medal to Walter F. Hunt 334
——, Book Reviews 1218
Ranite (=gonnardite) (Mason) ... 1008
Refractometer perils (Fisher) 777
Reinerite (Strunz, Söhnge, Geier). 1006
Remick, J. H. Chart showing the sphere of influence of atoms and ions in minerals 166
——— (Book Review) 622
Revoredite (Amstutz, Ramdohr, De Las Casas) 794
Rhodesite, Mountainite (Mountain) (Gard, Taylor, Chalmers) 624
Rice, R. V., and Cohen, A. J. New method for orienting electron microscope replicas 25
Rinkite, johnstrupite, rinkolite lovchorrite, and calcium rinkite (all = mosandrite) (Slepnev) (Sahama, Hytönen) 795
———, with Thompson, M. E., and Meyrowitz, R. Sherwoodite, a mixed vanadium(IV)-vanadium(V) mineral from the Colorado Plateau 749
——— Simplotite, a new quadrivalent vanadium mineral from the Colorado Plateau 16
Roe, L. A. Iron Ore Beneficiation (Book Review) 376
Roebling Medal, acceptance of (Hunt) 336
Roebling Medal, presentation to Walter F. Hunt (Ramsdell) .. 334
Rogers, Austin Flint, memorial of (Kerr) 310
Ropert, M. E. 180
Roscherite from the Sapucaia pegmatite mine, Minas Gerais, Brazil, beryllium content of (Lindberg) 824
Rose, A. J. Tables Permettant le Dépouillement des Diagrammes de Rayons X et Abaques de Réglage des Monochromateurs à Lame Courbe (Book Review) 376
Rose, H. J., Jr., Blade, L. V., and Ross, M. Earthy monazite at Magnet Cove, Arkansas 995
———, with Glass, J. J., and Over, E. Yttrium-bearing pegmatite body near Lake George, Park County, Colorado 991
Rosenblum, S. Magnetic susceptibilities of minerals in the Frantz Isodynamic magnetic separator 170
Ross, C. S. Welded tuff from deep-well cores from Clinch County, Georgia 537
Ross, M., and Christ, C. L. Mineralogical applications of electron diffraction 1157
———, with Rose, H. J., Jr., and Blade, L. V. Earthy monazite at Magnet Cove, Arkansas ... 995
Rowe, R. H., with Sabine, P. A., and Day, G. Device for precisely controlling an iris diaphragm 784
Roy, D. M. System $CaO-Al_2O_3-SiO_2-H_2O$ IV: Phase equilibria in the high lime portion of the system $CaO-SiO_2-H_2O$ 1009
Roy, H. Acceptance of the Mineralogical Society of America Award 346
———, with Nelson, B. W. Synthesis of chlorites and their structural and chemical constitution 707
Runner, J. J., with Fisher, D. J. Morinite from the Black Hills 585
Rustom, M., with Brindley, G. W. Adsorption and retention of an organic material by montmorillonite in the presence of water 627
Rynders, G. F., with Van Valkenburg, A. Synthetic cuspidine. 1195

Sabine, P. A., Rowe, R. H., and Day, G. Device for precisely controlling an iris diaphragm. 784
Saha, P., and Smith, J. B. The

structure and properties of natural and synthetic minerals 174
Sahama, T. G. A complex form of natural nepheline from Iivaara, Finland 165
—— – 790, 791, 795
———, and Hytönen, K. Calcium-bearing magnesium-iron olivines 862
Sanbornite, $BaSi_2O_5$, crystal structure of (Douglass) 517
Sand, L. B., with Ames, L. L. Factors effecting maximum hydrothermal stability in montmorillonites 641
——— Hydrothermal synthesis in wairakite and calcium-mordenite 476
Santafeite (Sun, Weber) 623
Santafeite, a new hydrated vanadate from New Mexico (Sun, Weber) 677
Sarcia, J. A. 792
Sassolite, new occurrences in the United States (Smith) 1204
Sassolite from the Kramer borate district, California (Smith, Almond, Sawyer) 1068
Sasvari, K. 626
Savel'eva, K. T. 378
Sawyer, D. L., with Smith, G. L., and Almond, H. Sassolite from the Kramer borate district, California 1068
Sborgite (Cipriani) 378
Scarbroite (Duffin, Goodyear) 384
Scawtite, crystal chemistry of (McConnell, Murdoch) 498
Schaller, W. T., and Vlisidas, A. C. Ajoite, a new hydrous aluminum copper silicate 1107
Schneider, T. R. 1008
Schuilingite (Guillemin, Pierrot) 796
See G. T., with Loughnan, F. C. White chlorite from Cobargo, N.S.W. 671
Semenov, E. I. 1219, 1220
Selected Electron Micrographs of Clays and Other Fine-grained Minerals. (Bates) (Book Review) 1218
Serpentine minerals, characterization of (Whittaker, Zussman) 917
S. James Shand Memorial Volume. (Taljaard, M. S., Editor.) (Book Review) 178
Shand, Samuel James, memorial of (Chayes) 317
Shaw, E. R., with White, J F., and Corwin, J. F. A chalcedony-like variety of germania, GeO_2 589
Sherwood W. C., with Mitchell, R. S. Dahhlite pseudomorphs after pyrite concretions 600
Sherwoodite, a mixed vanadium(IV)-vanadium(V) mineral from the Colorado Plateau (Thompson, Roach, Meyrowitz) 749
Silica, amorphous, some observations on the crystallization of (Carr, Fyfe) 908
Silicon, piezobirefringence in (Giardini) 249
Silicon, study of the directional hardness in (Giardini) 957
Silikatischen Tonminerale, 2d ed. (Jasmund) (Book Review) 178
Simplotite, a new quadrivalent vanadium mineral from the Colorado Plateau (Thompson, Roach, Meyrowitz) 16
Skancke, P., with Vogt, T., and Bastiansen, O. Holmquistite as a rhombic amphibole 981
Skinner, B. J. Huntite from Tea Tree Gully, South Australia 159
Skvortsova, K. V. 383
Slavík, František, memorial of (Kutina) 325
Slepnev, Y. S. 795
Smirnov, S. S. 793
Smirnovskite (Grivor'ev, Dolomonova) 386
Smith, G. L., Almond H., and Sawyer, D. L. Sassolite from the Kramer borate district, California 1068
Smith, J. B., with Saha, P. The structure and properties of

natural and synthetic minerals 174
Smith, J. R. Optical properties of heated plagioclases 1179
Smith, J. V. Effect of temperature, structural state and composition on the albite, pericline and acline-A twins of plagioclase feldspars 546
———, **and MacKenzie, W. S. Alkali feldspars: IV. The cooling history of high-temperature sodium-rich feldspars** ... 872
Smith, R. L. New occurrence of sassolite in the United States. 1204
Snow Crystals, Natural and Artificial (Nakaya) (Book Review). 622
Soboleva, M. V................. 378
Sodium autunite (Chernikov, Krutetskaya, Organov)...... 383
Sodium Uranospinite............ 383
Sogrenite (Soboleva, Pudovkina).. 382
Söhnge, G..................... 1006
Specimen holder, improved, for the focusing-type *X*-ray spectrometer (Buerger, Kennedy). 756
Sphalerite, differential thermal analysis of (Kopp, Kerr)..... 732
Spherobertrandite (Semenov)... 1219
Stainierite (Orcel, Hénin, Caillère). 1223
Steiner, A. Occurrence of wairakite at The Geysers, California... 781
Stibiotellurobismuthite (Magak'-Yan)...................... 1223
Stottite (Strunz, Söhnge, Geier).. 1006
Structure and properties of natural and synthetic minerals (Saha, Smith)..................... 174
Structure Reports for 1951 (Book Review).................... 622
Struktur und Eigenschaften der Kristalle (Winkler) (Book Review)........................ 177
Strunz, H. Mineralogische Tabellen (Book Review)............ 619
——— 798, 1006
Strunzite (Frondel)............. 793
Stumpf, H. S., with Foster, L. M., and Long, G. Production of graphite single crystals by thermal decomposition of aluminum carbide............ 285
Sudo, T. Nendo-Kubutso (Clay minerals) (Book Review)..... 1217
Sumner, G. G., and Cohen, A. J. Relation among impurity contents, color centers and lattice constants in quartz.......... 58
Sun, M. S...................... 623
———. **and Weber, R. H. Santafeite, a new hydrated vanadate from New Mexico**.......... 677
Syneček, V..................... 385
System CaO-Al_2O_3-SiO_2-H_2O IV: Phase equilibria in the high lime portion of the system CaO-SiO_2-H_2O (Roy)........ 1009
System Fe_3O_4-Mn_3O_4 (Van Hook, Keith)..................... 69

Tables for the Microscopic and X-ray Determination of the Opaque Minerals ("Tablas para la Determinación Microscópia y Rayos X de Minerales Opacos"), 2d ed. (Novitzky) (Book Review)............. 176
Tables Permettant le Dépouillement des Diagrammes de Rayons X et Abaques de Réglage des Monochromateurs à Lame Courbe (Rose) (Book Review) 376
Tacnet, G...................... 624
Tapiolite, notes on, with special reference to tapiolite from southern Westland, New Zealand (Hutton).............. 112
Taylor, H. F. W................ 624
———, **with Buckle, E. R. Calcium analogue of chondrodite**.. 818
———, **with Gard, J. A. Foshagite: composition, unit cell and dehydration**.................. 1
Thermoluminescence from minerals, apparatus for the study of (Ashby, Kellagher)........ 695
Thin-section photography, low-magnification (Atchley)...... 997
———, **Roach, C. H., and Mey-**

rowitz, R. Sherwoodite, a mixed vanadium(IV)-vanadium(V) mineral from the Colorado Plateau 749
———, Simplotite, a new quadrivalent vanadium mineral from the Colorado Plateau 16
Thoreau, J. 795
Thorite crystals, synthetic, formation and properties of (Fuchs) 367
Thorite, uranothorites, and coffinite, synthetic, *X*-ray studies of (Fuchs, Gebert) 243
Thorutite (smirnovite) (Gotman, Khapaev) 1007
Tikhonenkov, I. P. 792
Tilley, C. E. Leucite nepheline dolerite of Meiches, Vogelsberg, Hessen 758
Tolnay, V. 1222
Tunell, G., and Murdoch, J. Laboratory Manual of Crystallography for Students of Mineralogy and Geology (Book Review) 618
Twinning in diamond-type structures: A proposed boundary-structure model (Kohn) 263

Ufertite (Soboleva, Pudovkina) ... 378
Ulexite, nonfibrous, from the Kramer district, California (Allen) 169
Uranium minerals from U.S.S.R. (Soboleva, Pudovkina) (Getseva, Savel'eva) 378
Uranothorites, thorite and coffinite, synthetic, *X*-ray studies of (Fuchs, Gebert) 243
Usigite (usihyte) (Melkov, Pukhal'skii) 1008

Valcha, Z. 792
Van Hook, H. J., and Keith, M. L. The System Fe$_3$O$_4$-Mn$_3$O$_4$ 69
Van Valkenburg, A., with Bunting, E. N. Some properties of diamond 102
———, and Rynders, G. F. Synthetic cuspidine 1195
Verhoogen, J. Physical properties and bond type in Mg-Al oxides and silicates 552
Vibertite (Goodman) 791
Virgin, W. W., Jr., and Massoni, C. J. A new low-temperature, liquid heating stage 606
Vlisidis, A. C., with Schaller, W. T. Ajoite, a new hydrous aluminum copper silicate 1107
Vogt, T., Bastiansen, O., and Skancke, P. Holmquistite as a rhombic amphibole 981
Vtelensky, J. 792
Vuorelainen, Y., with Kouvo, O. Eskolaite, a new chromium mineral 1098

Wairakite, occurrence at The Geysers, California (Steiner) 781
Wairakite and calcium-mordenite, hydrothermal synthesis in (Ames, Sand) 476
Walenta, K., with Gross, E. B., Corey, A. S., and Mitchell, R. S. Heinrichite and metaheinrichite, hydrated barium uranyl arsenate minerals 1134
Walpurgite, unnamed phosphate analogue of (Soboleva, Pudovkina) 383
Wasserstein, Benno, memorial of (Fleischer) 331
Weathered sedimentary ironstones, mineralogical changes in (Youell) 774
Weaver, C. E. Effects of geologic significance of potassium "fixation" by expandable clay minerals derived from muscovite, biotite, chlorite and volcanic material 839
Weber, R. H. 623
———, with Sun, M. S. Santafeite, a new hydrated vanadate from New Mexico 677
Welded tuff from deep-well cores from Clinch County, Georgia (Ross) 537

Westland, A. D., and Beamish, F. E. Chemical analysis of iridosmines and other platinum-metal minerals 503
White, J. F., Shaw, E. R., and Corwin, J. F. A chalcedony-like variety of germania, GeO_2 . . . 580
Whittaker, E. J. W., and Zussman, J. Characterization of serpentine minerals 917
Wickman, F. E. 387
Wilshire, H. G. Alteration of olivine and orthopyroxene in basic lavas and shallow intrusions . . 120
Winchell, H. The composition and physical properties of garnet . . 595
——— Optics of the eosphorite-childrenite series 765
Winkler, H. G. F. Struktur und Eigenschaften der Kristalle (Book Review) 177

X-ray Crystal Structure (McLachlan) (Book Review) 620

Yagi, K. 624
Youell, R. F. Mineralogical changes in weathered sedimentary ironstones 774
Young, E. J. Occurrence of gorceixite in Arkansas 762
Yttrium-bearing pegmatite body near Lake George, Park County, Colorado (Glass, Rose, Over) 991

Zak, L. 385
Zalai, A. 626
Zalashkova, N. E. 1223
Zussman, J., with Whittaker, E. J. W. Characterization of serpentine minerals 917

AMERICAN MINERALOGIST

Price Information

Back issues of the AMERICAN MINERALOGIST can be purchased at the prices given below, but certain issues as listed are available only in microtext edition. The microtext edition is on 3 x 5 inch cards, each card containing 48 pages of text material, with a heading in regular type to indicate the volume, number, pages and date. Microtext will be furnished on all orders where necessary, unless specific instructions are received to the contrary. Prices apply to both the regular and microtext editions, and postage is charged except on indexes. Agents and dealers are allowed the usual 10% discount on orders. Subscriptions for the current volume (calendar year) are available to libraries, colleges, and other organizations at $6.00, postpaid. Individuals can receive the current volume by becoming members of the Mineralogical Society of America.

Volume	Year	Price per volume	Price per issue (except special issues)
1-9	1916-1924	$3.00	$ .50
10-19	1925-1934	4.00	.50
20-28	1935-1943	6.00	.80 (monthly issue)
29-42	1944-1957	6.00	1.60 (bimonthly issue)

Microtext Edition

Vol.	No.	Year	Vol.	No.	Year
1-5	Complete	1916-1920	27	1-12	1942
7	2	1922	28	1-8	1943
9	3	1924	29	1-8	1944
10	3	1925	30	1-4, 7-8	1945
11	3	1926	31	1-4	1946
25	5	1940	32	1-4	1947
26	1-3, 6-9, 12	1941			

Special Issues

Year	Issue	Vol.	No.	Price	Year	Issue	Vol.	No.	Price
1925	Michigan	10	9	$1.00	1945	Quartz Symposium	30	5-6	$3.00
1925	Harvard	10	11	1.00	1950	Larsen	35	9-10	2.50
1927	Harvard	12	4	1.00	1953	Hunt	38	1-2	2.00
1928	Harvard	13	7	1.00	1953	Ross-Schaller	38	11-12	3.00
1930	Harvard	15	8	1.00	1955	Kraus	40	11-12	2.00
1932	Harvard	17	7	1.00	1957	Harvard	42	11-12	2.00
1937	Palache	22	7	3.00					
1938	Harvard	23	11	1.50					

Indexes

Vols. 1-20 (1916-1935) $2.00; $1.00 to members; postpaid
21-30 (1936-1945) 3.00; 2.00 to members; postpaid
31-40 (1946-1955) 5.00; 3.00 to members; postpaid

Send all orders to

MINERALOGICAL SOCIETY OF AMERICA
Earl Ingerson, Treasurer
c/o U. S. Geological Survey, Washington 25, D.C.

RECENT ACQUISITIONS

Celestite, New York. Good quality blue crystals, medium to large, on limestone, some slightly stained. 2 x 2″, $1,00; 2 x 3″, $1.50; 3 x 4″, $2.50; 4 x 5″, $3.50.

Chrysoberyl. Madagascar. Very choice partly transparent greenish yellow flat twinned crystals. Average ½″ $1.50; ½″ to ¾″ $3.50, $5.00, $7.50.

Corundum, var. Ruby. Norway. (Not for cutting). Dark red crystals in gneiss (fluoresce red under long wave UV). 2 x 2″, $2.50; 2 x 3″, $5.00; 3 x 4″, $12.50; 4 x 5½″, $12.50, $15.00; $17.50; 5 x 7″, $35.00, $50.00.

Hackmanite. Ontario. Massive in nepheline. Bright orange yellow fluorescence under long wave UV. 2 x 2″, $1.00; 2 x 3″, $2.00; 3 x 4″, $4.00; 4 x 5″, $7.50. A few larger pieces are available.

Iron, meteoritic. A fine series of polished slices of the Brenham, Kansas pallasite are now available. They are described in the meteorite section of our FM 11 catalog. Ask for your free copy today.

Josephinite, Oregon. A terrestrial nickel-iron in waterworn placer nuggets. ½″ to ¾″ $2.50; ¾″ to 1″ $3.50, $5.00.

Millerite. Ontario. New—rare—unusual. Millerite is a relatively rare mineral, usually occurring as delicate acicular crystals or radial crusts. At this new Canadian occurrence, the millerite occurs in large cleavage masses associated with chalcopyrite and some gersdorffite, etc. Sizes are 2 x 3″ to 3 x 4″ at $5.00, $7.50, $10.00.

Prices are list at Rochester, N.Y.

NEW WARD CATALOG

583 Ward's Geology Catalog—The most comprehensive geology catalog ever published by Ward's. It contains a listing of mineral, rock and fossil collections; minerals, rocks and reference clay minerals in bulk or student specimens; color slides for geology (physical geology, mineralogy, paleontology, astronomy). The section on equipment for field and laboratory includes expanded listings of storage equipment, and an especially fine section on thin section equipment. There is an illustrated section on crystallographic aids including crystal models. If you are not on our mailing list to receive this catalog, write for it today.

WARD'S *NATURAL SCIENCE ESTABLISHMENT, INC.*
P.O. BOX 1712 **ROCHESTER 3, N.Y.**

GEORGE BANTA COMPANY, INC., MENASHA, WISCONSIN, U.S.A.